10.13147/SOE.2018.004

10.13147/SOE.2018.004

Soproni Egyetem
Kitaibel Pál Környezettudományi Doktori Iskola
„Biokörnyezet-tudomány” program

THE EFFECT OF VEGETATION ON THE WATER BALANCE IN CONTEXT OF CLIMATE CHANGE

A NÖVÉNYZET VÍZKÖRFORGALOMRA GYAKOROLT HATÁSA A KLÍMAVÁLTOZÁS TÜKRÉBEN

DOKTORI (PhD) ÉRTEKEZÉS

Készítette:

Herceg András

Témavezető:

Prof. Dr. Gribovszki Zoltán

Sopron
2017

10.13147/SOE.2018.004

The effect of vegetation on the water balance in context of climate change

A növényzet vízkörforgalomra gyakorolt hatása a klímaváltozás tükrében

Értekezés doktori (PhD) fokozat elnyerése érdekében készült

a Soproni Egyetem Kitaibel Pál Környezettudományi Doktori Iskolája Biokörnyezet-tudomány programja keretében.

Írta:
Herceg András

Témavezetők: Prof. Dr. Gribovszki Zoltán

Elfogadásra javaslom (igen / nem)

(aláírás)

A jelölt a doktori szigorlaton …..... % -ot ért el,
Sopron,

……..
a Szigorlati Bizottság elnöke

Az értekezést bírálóként elfogadásra javaslom (igen /nem)

Első bíráló: igen/nem

(aláírás)

Második bíráló igen/nem

(aláírás)

(Esetleg harmadik bíráló (Dr. .....) igen /nem

(aláírás)

A jelölt az értekezés nyilvános vitáján….....% - ot ért el

Sopron, ……..

a Bírálóbizottság elnöke

A doktori (PhD) oklevél minősítése….....

……..

Az EDHT elnöke

10.13147/SOE.2018.004

NYILATKOZAT

Alulírott ……**Herceg András**…..…, jelen nyilatkozat aláírásával kijelentem, hogy a(z) ……**The effect of vegetation on the water balance in context of climate change** …….. című PhD értekezésem önálló munkám, az értekezés készítése során betartottam a szerzői jogról szóló 1999. évi LXXVI. törvény szabályait, valamint a …**Kitaibel Pál Környezettudományi**… Doktori Iskola által előírt, a doktori értekezés készítésére vonatkozó szabályokat, különösen a hivatkozások és idézések tekintetében.[1]

Kijelentem továbbá, hogy az értekezés készítése során az önálló kutatómunka kitétel tekintetében témavezető(i)met, illetve a programvezetőt **nem tévesztettem meg.**

Jelen nyilatkozat aláírásával tudomásul veszem, hogy amennyiben bizonyítható, hogy az értekezést **nem magam készítettem**, vagy az értekezéssel kapcsolatban szerzői jogsértés ténye merül fel, a Soproni Egyetem **megtagadja a PhD értekezés befogadását és ellenem fegyelmi eljárást indíthat**.

Az értekezés befogadásának megtagadása nem érinti a szerzői jogsértés miatti egyéb (polgári jogi, szabálysértési jogi, büntetőjogi) jogkövetkezményeket.

Sopron, 2017…….

……..

doktorjelölt

[1] 1999. évi LXXVI. tv. **34. § (1) A mű részletét – az átvevő mű jellege és célja által indokolt terjedelemben és az eredetihez híven – a forrás, valamint az ott megjelölt szerző megnevezésével bárki idézheti.**
36. § (1) Nyilvánosan tartott előadások és más hasonló művek részletei, valamint politikai beszédek tájékoztatás céljára – a cél által indokolt terjedelemben – szabadon felhasználhatók. Ilyen felhasználás esetén a forrást – a szerző nevével együtt – fel kell tüntetni, hacsak ez lehetetlennek nem bizonyul.

10.13147/SOE.2018.004

Contents

Contents 5
List of symbols and abbreviations 7
Abstract 9
Kivonat 10
1. Introduction 10
1.1. Background and objective 11
1.2. Structure of the dissertation 12
2. Climate change and evapotranspiration 13
2.1. The climate change 13
2.2. Climate models 14
2.3. Hydrological effects of climate change 16
2.3.1. Floods, inland inundation and droughts 17
2.3.2. Climate change impacts on soil moisture, groundwater level and plants physiology 18
2.4. Water-balance approaches and the role of the evapotranspiration in them 22
2.5. Significance of evapotranspiration 24
2.6. Physical process of the evaporation and the turbulent energy exchange 24
2.6.1. Vapor-pressure relations 26
2.6.2. Latent heat exchange and sensible heat exchange 27
2.7. Categorization of evapotranspiration process 28
2.7.1. Free-water evaporation 29
2.7.2. Lake evaporation 29
2.7.3. Bare-soil evaporation 29
2.7.4. Transpiration 29
2.7.5. Interception and interception loss 30
2.8. Evapotranspiration 31
2.8.1. Lysimeters 33
2.8.2. Satellite or aircraft based remote sensing measurements 34
2.8.3. Potential evapotranspiration 35
2.9. Impact of climate changes on the hydrological cycle: results of water balance models 38
2.10. Discussion and research need 42
3. Objectives and research questions 44
4. Data and methods 45
4.1. Databases for calibration and validation 45
4.1.1. CREMAP 45
4.1.2. Weighing lysimeter 49
4.2. Study areas 52
4.2.1. Forested area 53
4.2.2. Mixed parcel 54
4.2.3. Marchfeld 55

4.3. The Thornthwaite-type hydrological model description 56
4.4. Model calibration and validation 59
4.5. Projection procedure 60
4.5.1. FORESEE database 60
4.5.2. Regional Climate Models 61
4.6. Water stress 63
4.7. Evaluating model performance 63
4.8. Rooting depth parameterisation of the Marchfeld 63
4.9. Summary of objectives and methods 64
5. Results 65
5.1. Methodical results 65
5.1.1. Calibration of the potential evapotranspiration 65
5.1.2. Calibration of the actual evapotranspiration 65
5.2. Results of calibration of potential evapotranspiration 66
5.3. Results of the calibration of actual evapotranspiration 67
5.4. Results of validation 67
5.5. Results of the model adjustments 68
5.6. Results and tendencies of the Regional Climate Models 70
5.7. Results of the projections for the 21st century 71
5.8. Results of the water stress analyses 77
5.9. Comparison of the static rooting depth and the adaptive rooting depth of the plants at Marchfeld 82
6. Discussion and Conclusions 86
7. Outlook 91
8. Theses of the dissertation 92
Acknowledgement 94
References 95
List of figures 110
List of tables 113
Annex 114
Annex 1. The identification numbers (ID) of the grid cells over Hungary with the involved areas (The IDs are illustrated on Figure 4.6.) 114
Annex 2. The original model with snowpacks and snowmelts 115
Annex 3. Input and results databases of study areas for present 116
Annex 4. The script of the model 133
Annex 5. Annual mean values of temperature and precipitation derived from the regional climate models at the 3 study area from 1985 to 2100 with standard deviations in parentheses 153

List of symbols and abbreviations

a	first parameters of the linear transformations (*dimensionless*)
AET	actual evapotranspiration (*mm*)
b	second parameters of the linear transformations (*dimensionless*)
c	Priestley-Taylor constant (*dimensionless*)
CRAN	Comprehensive R Archieve Network
CREMAP	Calibration-Free Evapotranspiration Mapping
D_W	drainage (*mm*)
D	daylenght (*hour*)
E	evaporation ($m \cdot s^{-1}$); ($mm \cdot month^{-1}$); ($kg \cdot m^{-2}\ s^{-1}$)
e_a	vapor pressure of overlaying air (*Pa*)
e_a^*	saturation vapor pressure at the air temperature (*kPa*)
e_s	vapor pressure of evaporating surface (*Pa*)
e^*_s	saturation vapor pressure at the surface temperature (*kPa*)
e_m*	saturation vapor pressure (*kPa*)
ET	evapotranspiration (*mm*)
ET_{CREMAP}	remote-sensing based actual evapotranspiration (*mm*)
$ET_{LYSIMETER}$	actual evapotranspiration values measured by weighing-lysimeter (*mm*)
E_s	simulated evapotranspiration (*mm*)
ET_{MSR_i}	time series of measured ET values (*mm*)
ET_M	monthly actual evapotranspiration ($mm \cdot month^{-1}$)
ET_{SIM_i}	time series of simulated values (*mm*)
ET_W	wet environment evaporation (*mm*)
EW_M	maximum extractable water (*mm*)
FAO	United Nations Food and Agricultural Organization
f(u)	wind function ($mm \cdot day^{-1} \cdot hPa^{-1}$)
GHG	greenhouse gas
GCM	general circulation model
G_{OUT}	groundwater outflow (*mm*)
H	upward rate of sensible heat exchange (*J*)
K_E	coefficient that reflects the efficiency of vertical transport of water vapor by the turbulent eddies of the wind ($1 \cdot Pa^{-1}$)
LE	latent heat exchange ($J \cdot s^{-1}\ m^{-2}$)
m_{MSR_i}	average value of ET measured in the study period (*mm*)
MODIS	Moderate Resolution Imaging Spectroradiometer
OMSZ	Országos Meteorológiai Szolgálat (Hungarian Meteorological Service)
P	precipitation (*mm*); ($mm \cdot year^{-1}$)
PAW	plant available water (*mm*)
PET	potential evapotranspiration (*mm*)
PET_{CREMAP}	remote-sensing PET based on actual evapotranspiration at well-watered conditions (*mm*)
$PET_{LYSIMETER}$	actual evapotranspiration values measured by weighing-lysimeter at well-watered conditions (*mm*)
PET_H	Hamon type potential evapotranspiration (*mm*)
PET_M	calibrated monthly potential evapotranspiration (*mm*)
PM	Penman-Monteith method
P_M	monthly summed precipitation (*mm*)
PT	potential transpiration ($mm \cdot day^{-1}$)

Q	runoff (*mm*)
Q_m	mean measured runoff ($mm \cdot year^{-1}$)
Q_n	available energy at the surface ($mm \cdot day^{-1}$)
R^2	coefficient of determination (*dimensionless*)
r_a	aerodynamic resistance ($s \cdot m^{-1}$)
RCM	regional climate model
REW	Relative Extractable Water (*dimensionless*)
R^2_{NS}	Nash-Sutcliffe coefficients (*dimensionless*)
$SOIL_M$	monthly soil moisture (*mm*)
$SOIL_{MAX}$	soil-water storage capacity (*mm*)
$SOIL_{M\_10Percentile}$	10^{th} percentile soil moisture minimum values (*mm*)
SWD	Soil Water Deficit (*mm*)
T	actual transpiration ($mm \cdot day^{-1}$)
T_a	air temperature ($^{\circ}C$)
T_M	monthly summed temperature ($^{\circ}C$)
T_s	temperature of the surface ($^{\circ}C$)
T_{sw}	temperature based on the spatial averaging of coldest pixel values ($^{\circ}C$)
T_w	water body temperature ($^{\circ}C$)
u^2	mean horizontal wind velocity ($m \cdot s^{-1}$)
v_a	wind speed ($m \cdot s^{-1}$)
VITUKI	Környezetvédelmi és Vízgazdálkodási Kutató Intézet Nonprofit kft. (Environment and Water Management Research Institute Nonprofit Ltd.)
W	relative humidity (*dimensionless*)
W_a	relative humidity of the air (*dimensionless*)
Y	psychrometric constant ($hPa \cdot °C^{-1}$)
z_i	i^{th} variable of segmented relationship (*dimensionless*)
z_{rz}	rooting depth (vertical extent of root zone (*mm*))
z_u; z_t	reference elevations (*m*)

Greek symbols:

β_1	left slope of segmented relationship (*dimensionless*)
β_2	right slope of segmented relationship (*dimensionless*)
β_e	annual bias ($mm \cdot year^{-1}$)
ΔW_{lys}	daily change of soil water ($mm \cdot day^{-1}$)
ΔW_{drain}	daily change of drainage water ($mm \cdot day^{-1}$)
ΔP_{lys}	daily change of precipitation ($mm \cdot day^{-1}$)
ΔI_{lys}	daily change of irrigation ($mm \cdot day^{-1}$)
ΔET_{lys}	daily change of evapotranspiration ($mm \cdot day^{-1}$)
ΔS	change in soil water content (*mm*)
$\Delta SOIL$	decrease in soil storage (*mm*)
δ	slope of e_s curve at the temperature of air ($hPa \cdot °C^{-1}$)
φ	latitude (°)
Γ	day angle (°)
σ	declination (°)
θ_{fc}	water content at field capacity (*dimensionless*)
θ_{pwp}	water content at permanent wilting point (*dimensionless*)
λ_v	latent heat vaporization ($MJ \cdot kg^{-1}$)
ψ	break-point of segmented regression (*dimensionless*)

10.13147/SOE.2018.004

Abstract

Aim: The main purposes of this dissertation are (1) to establish a monthly step water balance model; (2) and to project the components of the water balance for the 21st century.

Methods: A Thornthwaite type monthly step water balance model (that requires only temperature and precipitation time series as inputs) has been utilized. The base model was calibrated and validated using measured actual evapotranspiration data. The key parameter is the water storage capacity of the soil, which can be also calibrated using measured actual evapotranspiration data. The maximal rooting depth is determinable if the physical properties of the soil are available. For testing the model, I utilized 3 different surface cover types, which are located in the western part of the Pannonian Basin ('forested area', 'mixed parcel', and an agricultural field called 'Marchfeld'). Using the calibrated and validated model, projections were done for the 21st century for actual evapotranspiration and soil moisture. The projections are based on 4 bias-corrected regional climate models assuming on the A1B greenhouse gas emission scenario of the IPCC. I have done two model runs for the Marchfeld: the first is for the calibrated rooting depth situation, the second is with the assumption that the plants may try to adapt to the water stress by growing deeper roots.

Results: The base water balance model was successfully calibrated for the three different surface cover types. The determined relationship between the calculated and the measured actual evapotranspiration was tested on a validation data set, and it proved to be reliable for each study area. The projections demonstrate increasing actual evapotranspiration values in each case (forested area: +9%; mixed parcel: +6%; and Marchfeld: +8%) at the end of the 21st century. In the context of the 10th percentile minimum soil moisture values, I found an increasing trend for the forested area (+11%), whereas a strong decrease in case of Marchfeld (-41%) and the mixed parcel (-29%). The 30-year monthly means of evapotranspiration shows the maximum values in June and July, while in case of soil moisture, the minimum is in September. The water stress analysis indicates that water stress assumed to occur only in the Marchfeld during the 21st century. The comparison of the two run in the case of Marchfeld reveals that however the second run also projects increasing evapotranspiration values (+10%), and strongly decreasing soil moisture minimum values (10th percentile: -23%) for the 21st century, but calculation of the potential stress revealed that significant water stress may occur only in case of the first run.

Main conclusion: The developed model can estimate the soil-water storage capacity. According to the projections of the water balance model less water stress is assumed to occur in case of vegetation with deep rooting depth, than with shallow rooting depth.

10.13147/SOE.2018.004

Kivonat

Cél: A disszertáció fő céljai (1) egy Thornthwaite típusú vízmérleg-modell létrehozása; (2) és annak paramétereire való előrejelzés a 21. századra.

Módszer: Egy Thornthwaite-típusú, havi időlépcsős víz-mérleg modell (csak hőmérséklet és csapadék adatokat igényel bemeneti paraméterként) került felhasználásra. Az alap modellt mért aktuális párolgás adatokkal kalibráltam és validáltam. A kulcsparaméter a talaj maximális víztartó képessége, mely szintén az aktuális párolgás adatokkal kalibrálható. Ha a talaj fizikai paraméterei ismertek, a maximális gyökérmélység is meghatározható. Három különböző felszínborításon futattam a modellt, melyek a Kárpát-medence nyugati részén találhatóak (erdős terület, ”vegyes” parcella, és mezőgazdasági terület (Marchfeld)). A kalibrált és a validált modellt felhasználva, projekciókat végeztem a 21. századra, az aktuális párolgás és talaj-nedvesség paramétereire. A projekciókhoz 4 korrigált regionális klímamodell adatait használtam, melyek az A1B üvegházgáz kibocsátási forgatókönyvön alapulnak. Két külön modell-futtatást alkalmaztam a Marchfeld területén. Az első a kalibrált gyökérmélységre vonatkozik, míg a második azon a feltételezésen alapszik, hogy a növényzet próbál a vízhiányhoz alkalmazkodni a gyökérmélysége növelésével.

Eredmények: Az alap vízmérleg-modellt sikeresen kalibráltam a három különböző felszínborításra. A kalkulált és a mért aktuális párolgás között meghatározott kapcsolat a validációs időszakon került tesztelésre, és minden kutatási területen hiteles eredményt mutatott. Az előrejelzés mindhárom esetben emelkedő aktuális párolgás értékeket mutat (erdős terület: +9%; ’vegyes parcella’: +6%; Marchfeld: +8%), a 21. század végére. A talajnedvesség 10%-os percentilis minimumai esetén emelkedő tendencia várható az erdős területen (+11%), de erős csökkenés tapasztalható a „vegyes” parcella (-29%) és a Marchfeld esetén (-41%). A párolgás 30 éves havi dinamikája szerint június és július hónapokban jelentkezik a maximum, míg a talajnedvesség esetén a minimum értékek szeptemberben jelentkeznek. A víz stressz elemzés kimutatta, hogy egyedül a Marchfeld az a terület, ahol jelentős szárazság stressz prognosztizálható, a 21. század végére. A Marchfeld esetén, a két futtatás összehasonlításából kiderült, hogy a második futtatás is emelkedő aktuális párolgás értékeket (+10%), és erősen csökkenő talajnedvesség (10%-os percentilis) minimumokat (-23%) mutat, de a potenciális stressz számítások rámutattak, hogy szignifikáns vízhiány csak az első futtatás esetén várható.

Fő konklúzió: A kifejlesztett modell révén becsülhető a talaj víztározó kapacitása. A klímamodellek eredményeinek felhasználásával történt futtatások szerint a jövőben, a nagyobb gyökerezési mélységű vegetációformákat a víz stressz kevésbé súlyosan érinti, mint a sekély gyökérmélységgel rendelkező társulásokat.

1. Introduction

1.1. Background and objective

The current and ongoing climate change can be characterized by a global temperature rise (an increase of 3.7 °C to 4.8 °C until 2100 relative to the period 1850-1900, according to the baseline scenarios – those without additional mitigation) (*IPCC*, 2014). Larger temperatures also reflect larger energy potentials in the atmosphere, which will accelerate the hydrological cycle. This acceleration means changes of the temporal distribution of the precipitation, which often results in an increase of the amount within a single precipitation event; however, the annual rainfall amount shows no significant change (*Bartholy and Pongrácz*, 2006). Consequently, the most significant effect of climate change is its impact on the water cycle through altering precipitation patterns and the evapotranspiration processes at multiple scales (*Sun* et al., 2011a). The supposed changes in the distribution and amount of precipitation with the continuously increasing temperature may induce a higher rate in water consumption of the plants. In addition, this higher rate will generate changes in soil moisture, groundwater and after all in the water cycle.

Globally circa 62% of the precipitation that falls on the continents is evapotranspired and nevertheless, it exceeds runoff on all continents except of Antarctica (*Dingman*, 2002). In the Carpathian Basin 90% is evapotranspired, while the remaining 10% is runoff (*Kovács*, 2011). Therefore, evapotranspiration plays an important role in the water availability on the land surface, thereby controlling the large scale distribution of plants and primary production (*Vörösmarty* et al., 1998). Evapotranspiration also plays a key role in runoff and water availability in agriculture. Furthermore, most of the world's food supply is grown on irrigated land; thus, efficient irrigation requires reliable information on transpiration (*Dingman*, 2002).

Although evapotranspiration is a major component of the hydrologic water balance, it is not well understood (*Wilson and Brown*, 1992). Accordingly, the necessity of modeling and attaining a quantitative understanding of the evapotranspiration process is unquestionable, particularly in context of climate change projections. Consequently, further studies are required, especially on regional scale.

The overall objective of my dissertation is to reveal the impacts of climate change on water-cycle, considering the Carpathian Basin's special climatic attributes in case of the agrarian and forestry sectors in the 21st century. To achieve this purpose, a robust water balance model has to be established. The model have to be calibrated and validated with measured actual evapotranspiration data for the 3 chosen study areas, which represent three different surface covers in the North-western part of the Carpathian basin and therefore, they can be assured reliable basis for projections for the 21st century with the help of the simulation results of 4 bias corrected regional climate model. Nevertheless, different kinds of water stress indices have to be determined to quantify the impacts of climate change on the vegetation.

10.13147/SOE.2018.004

1.2. Structure of the dissertation

Chapter 1 focuses on the background and the main objective of my dissertation. After the Introduction in *Chapter 2* the processes and tendencies of climate change as well as its modeling possibilities, particularly for the future, are discussed. Furthermore, the physical process of evapotranspiration, its types and importance in context of water balance modeling as well as the recent studies and the required researches are described. Based on the main purpose of my dissertation, I formulated the objectives of my dissertation (*Chapter 3*). *Chapter 4* demonstrates the three case study areas, their input data and the used method in detail. After the model runs in *Chapter 5*, I introduce the methodical results and evaluate the concrete results of calibrations, validations and projections with comparison of the 3 study sites. In addition, another aspect of evaluation has been executed with taking into account the static rooting depth and the adaptive rooting depth of the plants in case of the Marchfeld, where water stress assumed to occur. *Chapter 6* is the discussion of the results of recently released similar studies and a comparison with our results. The final conclusions are given in *Chapter 6* as well. The outlook (*Chapter 7*) focuses on the potentials of the model development to a more accurate reliable phase, and the possible further utilization of it. Finally, the *Chapter 8* summarizes the theses of the dissertations.

2. Climate change and evapotranspiration

2.1. The climate change

There is a general agreement in regional climate change projections over Europe with the results of statistically significant warming in all seasons (*Christensen* et al., 2007; *Jacob* et al., 2008; *Linden van der and Mitchell*, 2009). *Vautard* et al. (2014) analyzed the changes in European regional climate associated with a 2 °C global warming relative to preindustrial climate. They used 30 years periods of an ensemble of global climate simulations of the SRES Scenario A1B, which downscaled at 25 km resolution using regional climate models (RCMs). In context of the temperature, the main feature of the changes in Europe expected for a 2 °C global warming relative to a reference period (1971–2000) is higher warming (more than 2 °C) than the global average; however, significant differences were found across Europe. This difference means slightly weaker amplitude than the global warming over Northwestern Europe, although a more intense warming (up to 3 °C) in Southern Europe in summer as well as in Northern and Eastern Europe in winter (*Vautard* et al., 2014).

It has to be noted that the European society is nevertheless particularly vulnerable to changes in the frequency and intensity of extreme events like heat waves, heavy precipitation, droughts, and wind storms (*Beniston*, 2007). The 2003 heat wave (*Beniston* 2004; *Schär* et al., 2004), the "1999 wind-storm of the century" (*Goyette* et al., 2003; *Ulbrich* et al., 2000) and the recurring flood events in numerous parts of Europe (e.g., *Christensen and Christensen*, 2003; *Kundzewicz* et al., 1999), are great examples of extremes and can be the cause for concern.

In Hungary, the warming process in question was the most intense in the last 30 years, and the most significant increase in temperatures occurred during the summer when temperature have risen by as much as 2 °C (*Bartholy* et al., 2011; *Lakatos* et al., 2012). This warming process induced the more frequent appearance of aridity as well as extreme weather events during 20th century (*Nováky and Bálint*, 2013).

Nonetheless, a consensus emerged on the climate projections, which indicated the further increase of temperature (expected in all of the seasons) and of climatic aridity for the 21st century in Hungary. The projected warming can be between 2-5 °C depending on the applied climate model and emission scenario (*Nováky and Bálint*, 2013; *Pongrácz* et al., 2011). Consequently, in our country in case of the largest projected change the annual average temperature can be equal with recent averages of south Mediterranean areas in the end of the 21st century (*Mika*, 1999; *URL1*).

In general, one of the most significant political, scientific and social challenges of the 21st century is the climate change (*IPCC*, 2014). To mitigate the intensity of this change, humanity has made many efforts to ease their anthropogenic greenhouse gas emissions down. However, it is not expected to be reduced to the desired level. In order to reduce the potential damages of the changing environmental conditions, the policy-makers has to evaluate the effects of the climate change as well as needs to apply adaptation strategies (*IPCC*, 2007). Nonetheless, when the policy-makers determine those adaptation and mitigation responses to climate

change, the uncertainty in the projections of future climate have to be considered and quantified (*Christensen and Christensen*, 2007). Furthermore, many natural and socio-economic systems are affected by the meteorological conditions, moreover there is an increasing demand on impact studies, and thus the requirement of a reliable climate database (especially in context of the future projections) is unquestionable.

2.2. Climate models

Climate models are mathematical representations of the climate, which divide the Earth's atmosphere and oceans into a grid. The models calculate every point's values of projected variables for the future over time - surface pressure, temperature, wind, humidity, rainfall. The best known climate models are the "atmospheric general circulation models" (GCMs) (*URL2*; *URL3*). Therefore, GCMs are the main tools that project future climate change information (*Chen* et al., 2013).

A main limitation of GCMs is the relatively rough horizontal resolution (run at coarse spatial resolution; from 250 to 600 km (*URL4*). Consequently, GCMs are unable to capture sub-grid cell features and fine scale, topography-induced local characteristics. Because of this, GCM results are not feasible to demonstrate and evaluate local-scale changes; consequently several downscaling methods were developed. In case of dynamical downscaling, higher spatial resolution models (so called regional climate models, RCMs) are run using GCM outputs as driver (*Giorgi*, 1990). The RCMs are able to simulate smaller-scale atmospheric processes, due to their higher resolution topography and physics (*Olsson*, 2014). RCMs typically cover a $10 \cdot 10$ km^2 area (*URL3*).

In context of the hydrological models in order to evaluating the hydrological impacts of climate change, the GCMs' outputs cannot be directly applied (*Sharma* et al., 2007; *Hansen* et al., 2006; *Feddersen and Andersen*, 2005; *Chen* et al., 2011a). The reason is that data provided by GCMs with spatial resolution below 200 km is not reliable for most hydrological-relevant variables (*Fowler* et al., 2007; *Grotch and MacCracken*, 1991; *IPCC*, 2007; *Salathé*, 2003). Therefore, when assessing the effects of climate change on a watershed scale, the use of RCMs instead of GCMs is recommended, because RCMs have proven to provide more reliable results for impact studies of climate change on regional water resources (*Buytaert* et al., 2010; *Elguindi* et al., 2011). RCMs are more consistent at reproducing relevant mesoscale patterns of local precipitation, thus they can much better represent the topographic effects on precipitation at a regional scale (*Frei* et al., 2003, 2006; *Intergovernmental Panel on Climate Change*, 2007; *Buonomo* et al., 2007).

It is important to note that all numerical models (as climate models) have systematic error (in varying extent), which means the difference between the simulated value and the observed (*Christensen* et al., 2008; *Teutschbein and Seibert*, 2010; *Varis* et al., 2004). These systematic errors are quite stable in time (e. g. equals in the past and in the future (*Maraun*, 2012)), consequently if just the projectable changes are studied, the caused problem by those errors are negligible. Nevertheless, problems arise if realistic data are needed for a climate change related impact study (*Dobor* et al., 2012). Consequently, the output of climate models cannot be applied in numerous hydrological simulations and in climate change impact studies

without any preprocessing in order to remove the occurring biases (*Chen* et al., 2013; *Haerter* et al. 2011; *Sharma* et al., 2007; *Hansen* et al., 2006; *Christensen* et al., 2008). Bias is defined as the time independent component of the mentioned systematic error (*Haerter* et al., 2010).

Nevertheless, RCMs may also have significant biases when comparing the simulated and the observed climate data at the same period (*Christensen* et al., 2008; *Teutschbein and Seibert*, 2010; *Varis* et al., 2004). The biases include systematic model errors caused by imperfect conceptualization, discretization and spatial averaging within grid cells. Besides, the observed precipitation and temperature data can be subjected to biases as well. The direct applying of RCMs for hydrological impact studies is possible, if a calibrated hydrological model (utilizing RCM outputs) is able to appropriately reproduce the observed data with realistic internal parameters. Hence, the temperature and precipitation of RCM are no more biased than observed data.

During the bias correction procedures, a transformation algorithm is utilized for adjusting RCM output. The main concept is the recognition of possible biases between observed and simulated climate variables, which is the basis for correcting control and scenario RCM runs as well (*Teutschbein and Seibert*, 2012). According to *Haerter* (2007), the sole purpose of bias correction is to eliminate the time independent component of the systematic error if it exists. Bias correction methods have to be stationary. This means that the correction algorithm and parameterization of it are valid for present climate conditions as well as for future conditions (*Teutschbein and Seibert*, 2012).

The inappropriate representations of dynamical and/or physical processes cannot be corrected by bias correction and model data must provide a suitable representation of the physical system from the outset, which ensure the applicability of the statistical bias correction (*Haerter* et al. 2011). Employ of uncorrected model output can lead to serious implications for various applications.

It is well known that several bias correction techniques have been developed to downscale meteorological variables from the RCMs, ranging from the simple scaling approach to sophisticated distribution mapping (*Teutschbein and Seibert*, 2012; *Sharma* et al., 2007; *Piani* et al., 2010; *Mpelasoka and Chiew*, 2009; *Ryu* et al., 2009; *Chen* et al., 2011b, 2013; *Salvi* et al., 2011; *Iizumi* et al., 2011; *Lafon* et al., 2012).

The most popular bias correction methods are the following:

- Linear scaling (for precipitation and temperature) (*Lenderink* et al., 2007).
- Local intensity scaling (for precipitation) (*Schmidli* et al., 2006).
- Power transformation (for precipitation) (*Teutschbein and Seibert*, 2012).
- Variance scaling (for temperature) (*Terink* et al., 2010; *Teutschbein and Seibert*, 2012).
- Distribution mapping (for precipitation and temperature) (*Themeßl* et al., 2012).
- Quantile mapping (for precipitation): (*Chen* et al., 2013; *Sun* et al., 2011b; *Themeßl* et al., 2012; *Wilcke* et al., 2013).

Considering the overall objective of this dissertation (evaluating the hydrological impacts of climate change), regional climate models were required with their fine scale as inputs for

projections. I have chosen a bias-corrected database as input to achieve reliable, realistic projections, namely 'FORESEE', which was established for Central Europe. The details about the FORESEE database can be found on *Chapter 4.5.1*.

2.3. Hydrological effects of climate change

In Europe the annual precipitation sum is projected to increase in the northern, and decrease in the southern regions towards the end of the 21st century (*Kjellström* et al., 2011). In context of the heavy precipitation there may be robust increase everywhere in Europe and in all seasons, except Southern Europe in summer (*Vautard* et al., 2014).

In the transition zone, where the Carpathian Basin is located, the changes are smaller and statistically insignificant. However, the mean annual precipitation for the whole country decreased during the 20th century by one average monthly precipitation (~7%) (*Szalai*, 2011). Projections show a northward shift of the transition zone in summer resulting in a decrease of the precipitation amount in the Carpathian Basin, while the southward shift of the transition zone in winter may results in increase of precipitation. The Carpathian Basin has nevertheless irregular precipitation distribution that may lead equally to more frequent heavy precipitation events or severe droughts (*Gálos* et al., 2015; *Nováky and Bálint*, 2013).

In Hungary, the extreme events have become more prevalent in the last 30 years and this tendency is expected to continue in the 21st century (*Gálos* et al., 2007; *Lakatos* et al., 2012).

Based on the special report of the IPCC (*IPCC*, 2012) it is very likely that natural disasters - floods, droughts, extreme precipitation events (intense rainfalls and severe droughts) etc. –, can be more frequent due to climate change, because these are influenced by the expected intensification of the hydrological cycle. Therefore, the most significant effect of climate change is its impact on the water cycle through altering precipitation patterns and the evapotranspiration processes at multiple scales (*Pongrácz* et al., 2014; *Sun* et al., 2011a). The water cycle has been becoming more intense, therefore the atmosphere contains more water at the same time and/or the retention time of the water vapor in atmosphere will be shorter. Either process will affect to ocean-land and meridional energy transfer, which might change the range and condition of climate. Thus, the climate change can cause changes in the water balance equations structure. In case of arid climates the hydrological balance can move to the direction of the evapotranspiration, while the more humid conditions may move to the direction of runoff (*Keve and Nováky*, 2010).

The most important hydrological effects of the climate change can be summarized as follows:

- The water quality can be worse, due to the higher water temperature and lower water level with constant water pollution (pollutant and thermal pollution).
- The dynamic groundwater storage might be decreased.
- Increasing probability of extremes (e.g. floods, droughts, inland inundation).
- The required water in agriculture and fishponds may strongly increase.
- The watercourses low-stage water resources can decrease in summer, as well as the low-water periods are expected to become more frequent (ponds and shallow water lakes may dry out) (*Somlyódy* et al., 2010).

Consequently, the climate change may cause a great impact on water management as fresh water demand for irrigation in summer (*Somlyódy* et al., 2010).

2.3.1. Floods, inland inundation and droughts

Management of the risk connected with hydrological extremes, i.e. droughts and floods are great challenges for the modern society in context of the changing climate (*Vörösmarty* et al., 2000; *Oki and Kanae*, 2006).

According to the IPCC SREX report (*IPCC*, 2012), floods are defined as: "the overflowing of the normal confines of a stream or other body of water or the accumulation of water over areas that are not normally submerged. Floods include river (fluvial) floods, flash floods, urban floods, pluvial floods, sewer floods, coastal floods, and glacial lake outburst floods."

Floods are affected by various characteristics of the climatic system, particularly the precipitation (intensity, duration, amount, timing, phase), but temperature patterns (responsible for such phenomena as soil freezing, snow and ice melt and ice jam formation) as well. In addition, floods are also affected by drainage basin conditions (pre-existing water levels in rivers, the snow and ice cover, the soil character and status (permeability, soil moisture content and its vertical distribution)), the rate of urbanization, and the presence of dikes, dams and reservoirs (*Bates* et al., 2008).

In Hungary the triggers and effects of the floods can be categorized to large, medium and small rivers, furthermore spring and summer transit times. In the case of large rivers the spring floods are determined by the thickness of the stored snow mass, its melting speed and greater precipitations in early spring (*Somlyódy* et al., 2010).

If the snow accumulation, sudden melting in large areas and significant precipitation appear in spring, there will be higher probability of the occurrence of the countrywide extreme inland inundations (exceeding 250.000 ha). Moreover, the drainage system capacity of the inland inundation is limited; therefore, a flood wave can be also an additional factor to the occurrence of the extreme inland inundations. Considering the climate change predictions for Hungary, the significant inland inundations mainly appear in the late of the winter or in the early spring. These periods generally related to floods. However, this process will be compensated somewhat with the drying up. The occurrence of years followed by each other with highly or moderate inland waters affections will probably decrease, but inland inundations generated by the intensive great precipitations in summer, may slightly increase (*Somlyódy* et al., 2010).

As a climate related natural hazard, drought is a frequent, widespread as well as recurring event. It can occur in all climate zones and impacts the local ecological and social environment (*Namias*, 1966; *Riebsame* et. al, 1991; *Wang* et al., 2003).

Drought is usually defined based on the degree of dryness, plus the duration of the dry period (*Palmer*, 1965). *Landsberg* (1982) considered drought as a shortage of precipitation over an extended period of time, which may results in a water deficiency for some activity, group or environmental sector (*Liu* et al., 2011).

In the future, the occurrence of drought periods can increase with high probability. The reasons as follows:

- Increase in temperature and therefore in evapotranspiration
- Decrease of summer precipitation
- Days without precipitation will increase (*Lakatos* et al., 2012).

Droughts are recurrent event in the climate of the Carpathian Basin, and might be more frequent and severe until the end of the century (*Gálos* et al., 2007, *Gálos* et al., 2015).

2.3.2. Climate change impacts on soil moisture, groundwater level and plants physiology

Revealing the potential effects of climate variability and change on groundwater is more difficult than on surface water, since the most noticeable impacts of climate change can be observed in surface water levels and quality (*Holman*, 2006; *Winter*, 1983; *Leith and Whitfield*, 1998). However, there are potential effects on the quantity and quality of groundwater as well (*Zektser and Loaiciga*, 1993; *Bear and Cheng*, 1999). Although, the groundwater-residence times can range from days to tens of thousands of years or even more, which delays and disperses the effects of climate and makes difficult to determine the responses in the groundwater to climate variability and change (*Chen* et al., 2004).

In the context of groundwater recharge, the precipitation and the evapotranspiration are especially important, since they have direct effect on it. Even small changes in precipitation may alter greatly the recharge in semiarid and arid regions (*Woldeamlak* et al., 2007).

During the 1990s, several studies on groundwater figured out that climate change will have a negative impact on groundwater reserves in many parts of the Earth (*Goderniaux* et al., 2009a, 2009b; *Van Roosmalen* et al., 2009; *Scibek* et al., 2007; *Serrat-Capdevila* et al., 2007; *Woldeamlak* et al., 2007; *Holman*, 2006; *Scibek and Allen*, 2006b, 2006a; *Allen* et al., 2004; *Brouye`re* et al., 2004a; *Chen* et al., 2004; *Loaiciga*, 2003; *Chen* et al., 2002; *Yusoff* et al., 2002; *Loaiciga* et al., 2000).

Nevertheless, the groundwater has some buffer capacity against extremes for short term, but if several extremely dry years follow each other, the buffer capacity may deplete (*Somlyódy* et al. 2010).

Soil moisture is stored water amount in the unsaturated soil zone/vadose zone (where the pores contain water and air as well) (*Seneviratne* et al., 2010). However, soil water (particularly in the recharge zone) is an essential component of the hydrologic cycle, especially in those climates where the available precipitation is insufficient to meet the demands of plants (*Keables and Mehta*, 2010). Plant available water (PAW) is the maximum amount of water that plants can extract from the soil, and nevertheless the water amount which is potentially available to the atmosphere through evapotranspiration. Furthermore, PAW is the function of soil texture, soil structure and rooting depth (*Nebo and Sumaya*, 2012). The plant available water is determined by hydraulic properties of soil, the nature of soil and the water retention capacity.

Precipitation, ground and surface water refill the water that stored in the soils under natural conditions (*Nebo and Sumaya*, 2012). Consequently, the recharge – induced mainly by the

infiltration from the precipitation – plays a key role not just in the condition of groundwater, but even in case of the available water for the plants. This recharge depends on the difference of winter half term's precipitation and potential evapotranspirations and on the soil moisture conditions in late autumn (*Simonffy*, 2003).

Moreover, in the dormancy, the ordinary refilled soil water level will also decrease due to climate change, therefore the water amount that moves up to the roots of the plants through the capillary zone can also decrease. This process may intensify the drought probability (*Somlyódy* et al. 2010).

The intense aridity in summer will decrease the soil moisture in the late of autumn; therefore higher rate of winter precipitation will be consumed to replenishment of the water that stored in the soil, and lower rate for infiltration remains to supply the groundwater (*Figure 2.1.*).

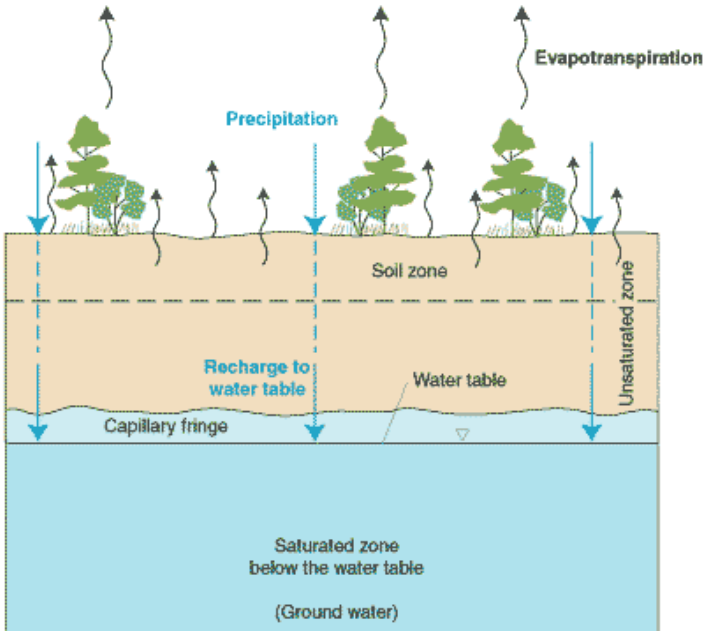

Figure 2.1. The saturated and the unsaturated zones (URL7)

The plant available water can be calculated as the difference between the field capacity and the permanent wilting point (*Figure 2.2.*).

The *Glossary of Soil Science Terms* (2008) defined field water or field capacity as "the content of water, on a mass or volume basis, remaining in a soil 2 or 3 days after having been wetted with water and after free drainage is negligible." Field capacity is the upper limit of the *available soil water* reservoir, from which water can be released, but not necessarily absorbed by plants, until the *permanent wilting point* is reached. The matric potential at the field capacity is around -1/10 to – 1/3 bar. In equilibrium, this potential would be applied on the soil capillaries at the soil surface when the water table is between 3 to about 10 feet below the soil surface, respectively. The larger pores drain first the gravity drainage, if not restricted, it may only take hours; while in clay soils (without macropores), gravity drainage may take even two to three days. The volumetric soil moisture content remaining at field capacity is about 15 to 25% for sandy soils, 35 to 45% for loam soils, and 45 to 55% for clay soils (*URL5*).

The permanent wilting point is the water content of a soil when most plants (corn, wheat, sunflowers) wilt and fail to recover their turgor upon rewetting. The matric potential at this soil moisture condition is commonly estimated at -15 bar. Most agricultural plants will generally show signs of wilting long before this moisture potential or water content is reached (more typically at around -2 to -5 bars) because the rate of water movement to the roots decreases and the stomata tend to lose their turgor pressure and begin to restrict transpiration. This water is strongly retained and trapped in the smaller pores and does not readily flow. The volumetric soil moisture content at the wilting point will have dropped to around 5 to 10% for sandy soils, 10 to 15% in loam soils, and 15 to 20% in clay soils (*URL6*).

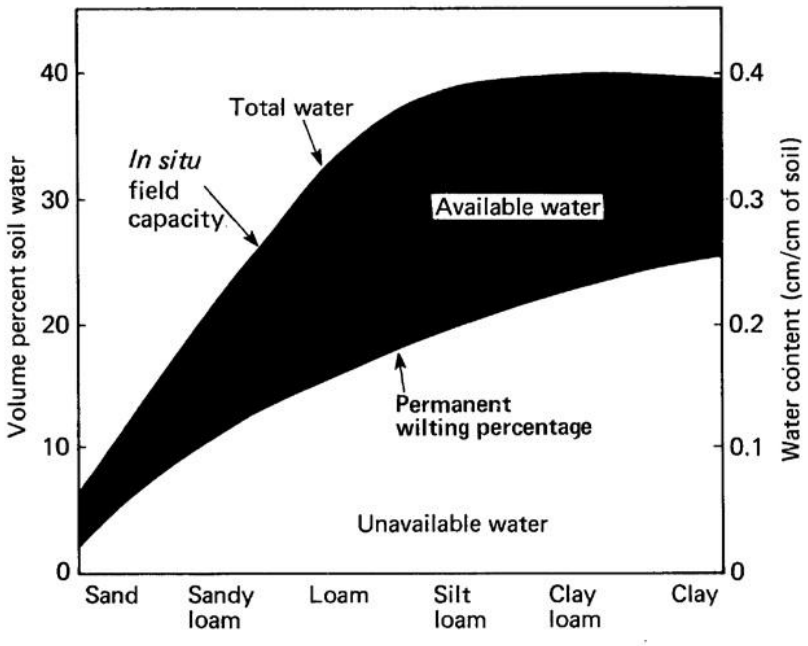

Figure 2.2. The available water in the different case of physical soil types (URL8)

In the soil-plant-atmosphere continuum water fluxes are controlled by atmospheric evaporative demand but limited by soil water supply. The ratio of actual transpiration (T) and potential transpiration (PT) and therefore relative transpiration (T/TP) is converging to 1, under wet soil condition (*Figure 2.3.*). That means the roots of plants can supply enough water into the canopy to maintain the evaporation generated by atmospheric demand, consequently the wilting of the plants is prevented. This is an atmospheric demand limited phase. The value of relative transpiration is starting to decrease below 1, when the soil dries beyond field capacity, therefore this process is water supply limited. Beyond the permanent wilting point, the relative transpiration value is equal to 0 and the transpiration discontinues (*Nebo and Sumaya*, 2012).

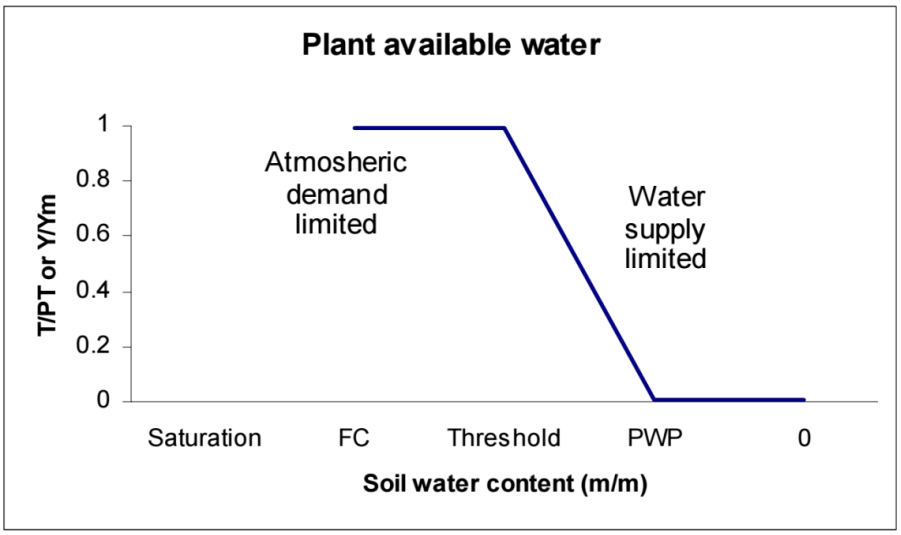

Figure 2.3. Actual yield/maximum yield (Nebo and Sumaya, 2012)

In regard to the previously written facts, the climate change also influences the plants physiology:

- By reason of the high temperature values in summer, the constraint of transpiration will increase, but the decreased amount of precipitation blocks the process simultaneously.
- For certain plants, the large amount of precipitation falls in winter cannot be utilized, because of its infiltration. That results in high soil water level.
- The combination of species will be changing that means there will be more frequent occurrence of heat tolerant species. In addition, they will change the water balance (runoff, soil water) through the altered transpiration conditions.

Consequently, climate change influences the richness and distribution of plants as well (*Sommer* et al., 2010).

Climate change is having significant and widespread impacts on the forest (as the most complex ecosystems on the Earth) worldwide and consequently, on the forest sector as well (*Moore and Allard*, 2008). These impacts of the climate change on the forest management can be studied analyzing interdependent processes. In Hungary climate change can lead to increasing temperature, decreasing precipitation amount for summer as well as to increasing probability of extreme events that affect the distribution, vitality and growth of forest ecosystems (*Mátyás and Czimber*, 2000, 2004; *Berki* et al., 2009; *Czúcz* et al., 2010; *Gálos* et al., 2015, *Mátyás*, 2010; *Mátyás* et al., 2010, *Molnár and Lakatos*, 2007, *Führer*, 1995; *Manninger*, 2004; *Solymos*, 2009; *Somogyi*, 2009; *Csáki* et al., 2014).

In addition, the vegetation is not just an indicator of the climate, but plays a key role in the weather and climate change. The reason is because in case of plant covered surfaces, the albedo is lower, but the roughness as well as the evaporating surface is higher than on a bare soil. Consequently, the plant covered surfaces affect to the atmosphere energy and hydrological cycle (*Bonan*, 2004). In Hungary the impact of vegetation on water balance was analyzed in the frame of small catchment research (*Gribovszki* et al., 2006) as well as paired plot analysis (*Móricz* et al., 2012).

As we have seen the climate change may strongly modify the water cycle through many different but connected processes. Considering the overall objective of my dissertation to reveal the impacts of climate change on water-cycle, a water balance model has to be established. Before the establishment, we have to introduce how a water balance equation is working.

2.4. Water-balance approaches and the role of the evapotranspiration in them

The water balance modeling is essential in the assessment and management of water resources, especially under the effects of human disturbed land use as well as in context of climate change. The quantification of water balance is basically a challenge, because of its complexity, variability of its spatial and temporal dimensions and uncertainties as well (*Nebo and Sumaya*, 2012).

In the case of a land surface the classic form of the long-term water-balance equation is what follows:

$$ET = P - Q - G_{OUT} \quad \text{(eq. 2.1.)}$$

Where:

ET: evapotranspiration
P: precipitation
Q: streamflow
G_{OUT}: groundwater outflow (*Dingman*, 2002)

Considering eq. 2.1., the measurement of water inputs, outputs and solving the water-balance equation for a given region and time period (ΔT) is a common way to determine the actual evapotranspiration. Nevertheless, it is essential to provide a reliable estimate of regional precipitation, measurement of liquid outflows (particularly if the groundwater flow is significant) as well as assuring that the changes in storage can be neglected in the given period. The changes in storage is negligible, if the given time period is only few years and the storage is in the form of soil water, hence this assumption leads to only small errors in estimating ET. Nonetheless, those errors can be minimized if one chooses a hydrological year that begins and ends during the dormant season, when soil moisture is near the soil-water storage capacity (*Dingman*, 2002).

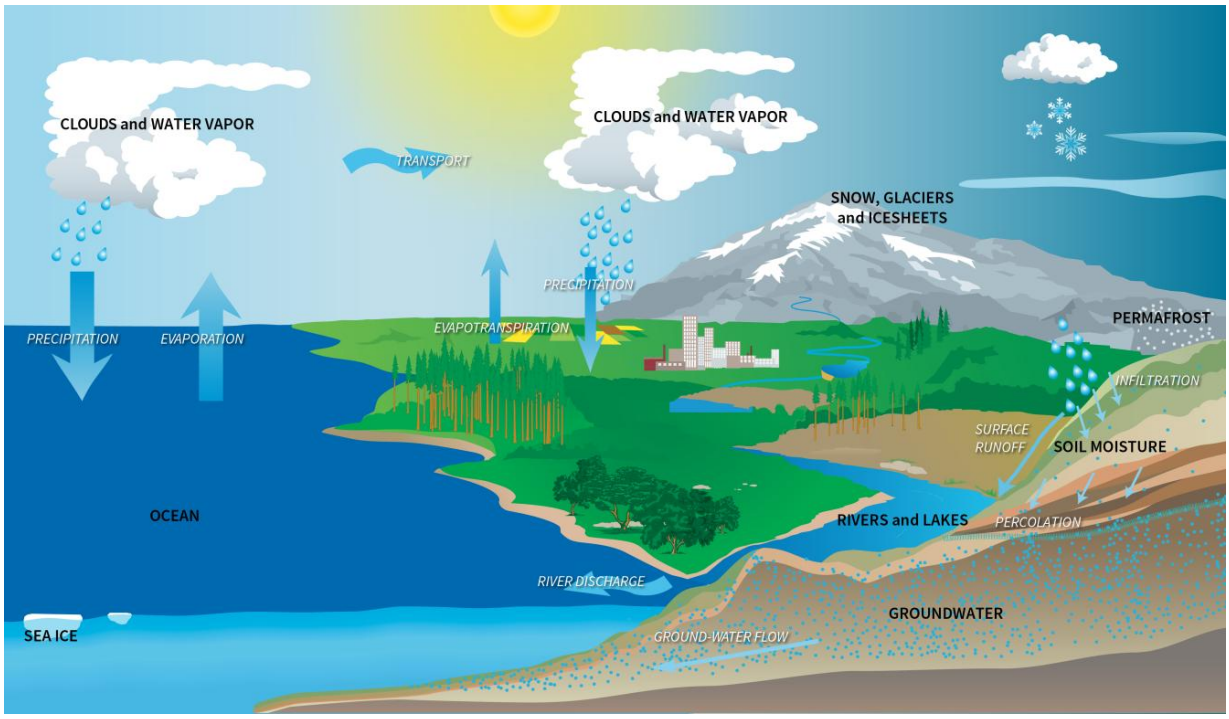

Figure 2.4. The water-cycle (URL9)

Based on the previously written facts and considering *Figure 2.4.*, it can be said that in the global hydrologic cycle between the atmosphere and land surface, the evapotranspiration is the primary link (*Dingman*, 2002). Nevertheless, 97% of the evapotranspiration is derived from land surfaces, and 3% from open-water evaporation. Although evapotranspiration is a major component of hydrologic water balance, it is not well understood (*Wilson and Brown*, 1992). In addition, evapotranspiration is a very effective vehicle for mass and energy transfer (due to the high latent heat of vaporization value of water) between the land- or vegetation surface and the ambient atmosphere (*Szilágyi and Józsa*, 2009; *Csáki* et al., 2014).

Here, the terms of evaporation, transpiration and evapotranspiration have to be defined.

Evaporation covers all processes in which liquid water is transferred to the atmosphere as water vapor. Considering that evaporation is a collective term, thus it includes: evaporation of water from reservoirs, lakes, soil surfaces and also from water intercepted by vegetative surfaces. Most of the time evaporation's dimension is depth per unit time, such as mm day^{-1}. It can be expressed as energy during a day and noting that the latent heat of water is 2.45 MJ · kg^{-1} (at 20 °C) it follows 1 mm · day^{-1} of evaporation equals 2.45 MJ · m^{-2} · day^{-1} (*McMahon* et al., 2013).

Transpiration means the evaporation from within the leaves of plants with water vapor flux through leaf stomata (*Maidment*, 1993).

The sum of the transpiration and evaporation can be defined as evapotranspiration (*Allen* et al. 1998). Nonetheless, evaporation and transpiration occur simultaneously.

2.5. Significance of evapotranspiration

Globally circa 62% of the precipitation that falls on the continents is evapotranspired (from over 90% in Australia to approximately 60% in Europe (*McMahon* et al., 2013)). In Hungary, the evapotranspired rate for fallen precipitation is 90% while the remaining 10% is runoff (*Dingman*, 2002; *Kovács*, 2011). The runoff is exceeded by evapotranspiration on all continent (except Antarctica) and most of the river basins. Consequently, the evapotranspiration determines the water availability at land surfaces and controls the large scale distribution of plant communities and primary production (*Vörösmarty*, 1998). Thus, the necessity of modelling and attaining a quantitative understanding of the evapotranspiration process is unquestionable in many practical contexts:

- Evapotranspiration is the main component of the energy and water-vapor exchange between the atmosphere and land surfaces, therefore climate change projections need to consider the related processes. Furthermore, impact assessments should relay on appropriate modeling of evapotranspiration.
- The difference between precipitation and evapotranspiration over long term means the availability of water for direct human use as well as for management. Hence, quantitative assessments of water resources and the effects of climate change and land use alteration on those resources require quantitative understanding of evapotranspiration.
- Most of the water that consumed by plants is a water "loss" through evapotranspiration. The plants that form the base of the earth's land ecosystem use this water to their growing process. Thus, comprehension of the relations between evapotranspiration and ecosystem type is necessary for prediction of the ecosystem's response to climate change.
- Irrigation means one of the highest water usage all over the world, and the world's food supply is grown mainly on irrigated lands, therefore efficient irrigation needs accurate information of crop water uses (transpiration).
- The yield of water-supply reservoirs and consequently the economics of building reservoirs of various sizes are significantly influenced by the evaporation.
- The "wetness" of the land determines considerably the fraction of water falling in a given rainstorm that contributes to streamflow and to groundwater. To quantify this wetness, the evapotranspiration has to be determined, which has occured since the previous storm (*Dingman*, 2002).

2.6. Physical process of the evaporation and the turbulent energy exchange

The exchange of water molecules between air and water surfaces includes two processes. First is condensation, which means the capturing process of molecules that move from the air towards the surface. The second is vaporization, which is the molecules movement away from surface. The vaporization rate is a function of temperature, while the condensation rate is a function of vapor pressure. The difference between those rates is the evaporation rate. The condensation and the evaporation occur simultaneously. They are dynamic process, but with increasing of the temperature (what also means greater molecular kinetic energy) the

evaporation dominates and with decreasing of the temperature the condensation dominates (*Maidment*, 1993).

The rate of evaporation from wet surfaces are determined by

- surrounding airs physical state,
- net available heat,
- wetness of the evaporating surface (*McMahon* et al., 2013).

The physical state of surrounding air is determined by its vapor pressure, temperature and velocity (Monteith, 1991).

Quantifying the available heat energy for evaporation requires the understanding of surface radiation balance (*Maidment*, 1993). Therefore, the available heat energy for evaporation is equal with the net incoming radiation plus net input of water advected energy (associated with inflows and outflows to a water body), minus net output of sensible heat exchange to the atmosphere minus net output with conduction to the ground and minus the change in heat storage in the water body. The incoming shortwave solar radiation minus outgoing shortwaves makes the net incoming radiation. Moreover, the outgoing shortwave radiation is a function of surface albedo and can be calculated by the incoming longwave less the outgoing longwave. Nonetheless, in case of the net incoming radiation, the heat for plant evaporation can be supplied by turbulent transfer by conduction from the soil as well as from the air (*McMahon* et al., 2013).

Besides the energy need for the latent heat, a process that removes the water vapor from the evaporating surface is required for the occurrence of evaporation. The atmospheric boundary layer is continually responding to large scale weather movements. That process sustain humidity deficit even over the oceans, and provide a sink for the water vapor (*McMahon* et al. 2013).

Directly above the surface there is thin non-turbulent layer, what generates the main resistance (called aerodynamic or atmospheric resistance) to evaporation flux (turbulent transfer) (*Penman*, 1948). In the case of leaves, the major resistance is the surface resistance, which is the function of stomatal opening in leaves (*Monteith*, 1991).

If air moves across the landscape, the water vapor is transported at the rate equal to the product of the water vapor content and the wind speed (*Figure 2.5.*). This transport is called advective flow. When air moves from a dry area to a wetter region, the concentration of water vapor increases at the transition to a higher value downwind. Furthermore, at the transition, the evaporation level immediately increases to a much higher level (because this originally dry air is unsaturated), and then slowly decreases to a value representative of the wetter region (*McMahon* et al., 2013). The low evaporation over the dryland means the overpassing air will be hotter and drier, thus increasing the available heat energy to increase evaporation in the downwind wetter (*Morton*, 1983).

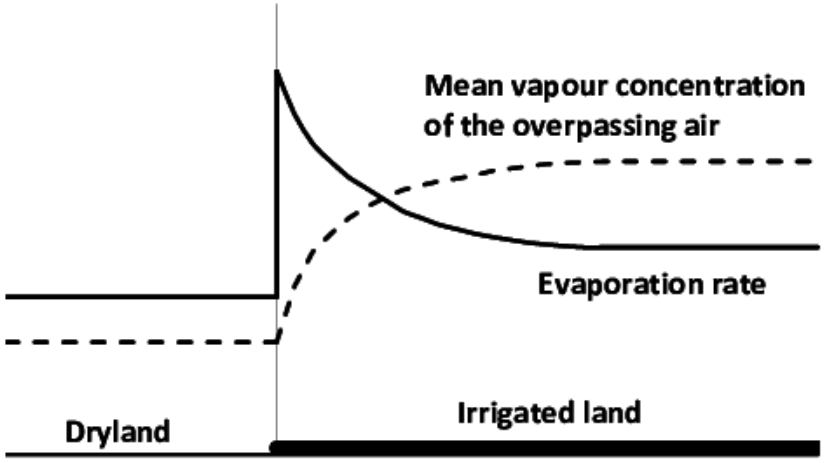

Figure 2.5. The effect of advected air that passing from dryland over an irrigated land (McMahon et al., 2013)

Evaporation is basically a diffusive process considering the Fick's first law.

$$E = K_E \cdot v_a \cdot (e_s - e_a) \quad \text{(eq. 2.2)}$$

Where:
E: evaporation rate [$m \cdot s^{-1}$]
v_a: wind speed [$m \cdot s^{-1}$]
K_E: coefficient that reflects the efficiency of vertical transport of water vapor by the turbulent eddies of the wind [$1 \cdot Pa^{-1}$]
e_s: vapor pressure of evaporating surface [Pa]
e_a: vapor pressure of overlaying air [Pa]

It should be noted that there is a vapor transfer from higher to lower concentration (the transfer is "down the gradient"), the gradient would become smaller and smaller with time, and finally go away. Thus, to sustain evaporation, a process is required in which the evaporated water molecules blown away, consequently a vertical gradient can be maintained. This explains why evaporation and the latent heat flux depend so critically on the turbulent wind field (*Dingman*, 2002).

2.6.1. Vapor-pressure relations

The vapor pressure of an evaporating surface (e_s) is equivalent to the saturation vapor pressure at the surface temperature (e^*_s) [kPa]. The saturation vapor pressure is a function of the temperature (*Allen*, 1998).

$$e_s = e^*_s \quad \text{(eq. 2.3.)}$$

$$e^*_s = 0.611 \cdot \exp\left(\frac{17.3 \cdot T_s}{T_s + 237.3}\right) \quad \text{(eq. 2.4.)}$$

Where:

T_s: temperature of the surface [˚C]

Nonetheless, the vapor pressure in the air is a function of air temperature (T_a) [˚C] and relative humidity of the air (W_a).

$$e_a = W_a \cdot e_a^* \quad \text{(eq. 2.5.)}$$

e_a^*: saturation vapor pressure at the air temperature [kPa]

If we divide the actual vapor pressure of the air with the saturation vapor pressure of the air ones get relative humidity of the air (*Bowen*, 1926).

$$W_a = \frac{e_a}{e_a^*} \quad \text{(eq. 2.6.)}$$

Another important definition is the dew point, which is a temperature T_D, where the air parcel is as cool as to become saturated. After further cooling down, condensation occurs (*URL10*).

2.6.2. Latent heat exchange and sensible heat exchange

The attractive intermolecular forces hold the molecules close together in liquid water. In this liquid phase, the molecules are circa 10 times closer to each other (and for that very reason the intermolecular forces are much more stronger) than in the water vapor. Latent heat of evaporation is the energy, which is needed to separate the molecules, or in other words, to work against the intermolecular forces.

Latent heat transfer from the evaporating body into the air is always accompanying the evaporation. This is a heat loss, which tends to reduce the surface temperature. However, this reduction partially or completely compensated by heat transfer to the surface from within the evaporating body or by radiative or sensible-heat transfer from the overlying air.

To calculate the latent heat exchange, the evaporation rate must be multiple by mass density of water (ρ_w) [$kg \cdot m^3$] and latent heat vaporization (λ_v [$MJ \cdot kg^{-1}$]; ($2.501 \cdot 106\ J \cdot kg^{-1}$)). The latter is the energy that is needed to break the hydrogen bonds.

$$LE = \lambda_v \cdot \rho_w \cdot E = \lambda_v \cdot \rho_w \cdot K_E \cdot v_a \cdot (e_s - e_a) \quad \text{(eq. 2.7.)}$$

$$LE\ [W \cdot m^{-2} = J \cdot s^{-1}\ m^{-2}] \text{ and } E\ [kg \cdot m^{-2}\ s^{-1}] \quad \text{(eq. 2.8.)}$$

When the temperature of evaporating surface increases, the latent heat of vaporization decreases.

The upward rate of sensible heat exchange (H) [J] by turbulent transfer can be expressed as:

$$H = K_H \cdot v_a \cdot (T_s - T_a) \quad \text{(eq. 2.9.)}$$

Normally, H is upward from the ground during the day, and downward at night to support radiant energy loss from the land surface (*Maidment*, 1993).

To enable and maintain evapotranspiration 4 basic conditions are needed:

- Accessible liquid water;
- Energy to break hydrogen bonds;
- Vertical vapor pressure gradient;
- Turbulence to blow out vapor molecules to sustain the vertical vapor pressure gradient (*Dingman*, 2002).

To understand the physics of evaporation, consider a body of water (for example a lake). To break the hydrogen bonds, which maintain the attraction between water molecules at the water surface, we have to add surplus energy. That is why the number of molecules with sufficient energy to break those hydrogen bonds is proportional to the water body temperature (T_w [°C]). Consequently, the mentioned surplus energy requires increased T_w. Directly above the water body an (almost) equilibrium occurs where molecules accumulate and the amount escaping and re-entering molecules are (nearly) equivalent. This equilibrium is a thin saturated layer with a vapor pressure e^*_s at temperature T_s. The rate of evaporation is the rate at which molecules move in above the unsaturated layer with a lower vapor pressure e_a at temperature T_a. Evaporation is proportional to $e_s - e_a$ (Dalton law). Thus, the drier the air mass above the surface, the greater the vertical vapor pressure gradient, and the greater the evaporation, while other factors being equal. Furthermore, the $e_s - e_a$ difference can be positive – evaporation is occurring –, negative – deposition is occurring – or even zero, when neither evaporation nor condensation are occurring in a net sense. The value of e_a can be less than or equal to the saturation vapor pressure at T_a. When they are equal, the relative humidity is 100%. Saturation at T_a does not mean that evaporation cannot occur; what counts is the vertical vapor pressure gradient. In the case of evaporation, the vertical gradient of vapor pressure is the requirement, but a saturated surface layer is unnecessary (*Maidment*, 1993).

2.7. Categorization of evapotranspiration process

The different approaches of evapotranspiration calculation have been created for specific surface and energy-exchange situations determined by the following conditions:

- Type of surface: open water, bare soil, leaf or leaf canopy, a specific reference crop or land region (commonly including vegetated surfaces, surface-water bodies, and bare soils as well)
- Water availability: unlimited water available for evaporation, or water supply to the air can be limited since water vapor must pass through plant openings or soil pores.
- Stored-energy use: may be significant, negligible, or nonexistent.
- Water-advected energy use: may be significant, negligible, or nonexistent similar to the previous condition. (Water-advected energy can be defined as the heat content of all water flows into and out of a given water body or a land parcel.) (*Dingman*, 2002)

Table 2.1. summarizes the various "types" of evapotranspirations in the context of the previous enumeration.

Table 2.1. Types of evapotranspirations and their main properties (after Dingman (2002; pp. 276, Table 7.1.)

Evapotranspiration type	Type of surface	Availability of water to surface	Stored energy use	Water-advected energy use
Free-water evaporation	Open water	Unlimited	None	None
Lake evaporation	Open water	Unlimited	May be involved	May be involved
Bare-soil evaporation	Bare soil	Limited to unlimited	Negligible	None

Transpiration	Leaf or leaf canopy	Limited	Negligible	None
Interception loss	Leaf or leaf canopy	Unlimited	Negligible	None
Potential evaporation	Reference crop	Limited to air unlimited to plants	None	None
Actual evaporation	Land area	Varies in space and time	Negligible	None

2.7.1. Free-water evaporation

Free-water evaporation is a theoretical concept developed by hydrometeorologist. Evaporation of an open-water surface that depends only on regionally continuous meteorological or climate condition and there is absence of advection and changes in heat storage (*McMahon* et al., 2013).

2.7.2. Lake evaporation

Adjustment of free-water evaporation to include heat-storage effect and advection in a given actual water body (*Finch and Calver*, 2008).

2.7.3. Bare-soil evaporation

More than one-third of land surface of our planet consist of Entisols, Inceptisols and Aridisols supporting insignificant or no vegetation. Furthermore, most agricultural fields have negligible vegetative cover much of the time. Hence, the understanding of the evaporation from a bare soil is globally significant in the context of irrigation. Evaporation from bare-soil (also called exfiltration) can basically be separated into two main stages. In stage one, what is an atmosphere-controlled stage, the evaporation is mainly determined by the surface energy balance and mass-transfer conditions (wind and humidity), but mostly independent of soil-water content. In this stage evaporation occurs at or near the rate of free-water evaporation. In stage two the evaporation rate is regulated by the rate at which water can be conducted to the surface in response to potential gradient. The potential gradient is generated by upward-decreasing soil water contents (*Dingman*, 2002).

2.7.4. Transpiration

Transpiration includes absorption of soil water by plant roots, translocation in liquid water through the vascular system of the roots, stem, and branches to the leaves and translocation through the vascular system of the leaf to the walls of tiny stomatal cavities. The evaporation takes place in the stomatal cavities from which water vapor moves into the ambient air through openings in the leaf surface named stomata (*Iturbe and Porporato*, 2004).

However, the basic function of stomatal cavities is to provide a place for CO_2 dissolution, but this process is necessarily accompanied by water evaporation. In addition, transpiration cools the plant, maintains the turgor of plant cells and delivers mineral nutrients from the soil to growing tissue. In stomatal cavities air is saturated at the temperature of the leaf, and water moves from cavities into the atmosphere, which forced by vapor-pressure difference, similar

to the open-water evaporation. The difference between the two processes is that the plants can physiologically regulate the size of the stomatal openings. Accordingly, transpiration is a physical process instead of metabolic. The vapor-pressure difference generates a movement of water vapor into the atmosphere through the stomata which is a potential-energy gradient. Water in the form transpiration stream is pulled through the plant by this potential-energy gradient. When vapor exits through the stomata, water evaporates from the walls of the stomatal cavity to replace the loss. The mentioned potential-energy decreases – produced by loss of liquid water – which generate the movement of replacement water up through the vascular system. This movement finally causes a water content gradient between the root and the soil, therefore a movement of soil water into the root is induced (*Baird and Wilby*, 1999).

2.7.5. Interception and interception loss

The precipitation falls on vegetative surface (canopy), from there it can evaporate without reaching the ground surface. This process is called interception (*Delfs*, 1955). The intercepted water that is evaporated is the interception loss, which can be divided into: canopy interception loss and litter interception loss. The latter is where water is evaporated from the litter on the ground (*Figure 2.6*.) (*Gash and Morton*, 1978).

The interception loss is determined by the followings:

- Vegetative type and stage of development (can be characterized by the leaf area index, which can be defined as the total area of leaf surface above ground area divided by the ground area)
- The duration, frequency, intensity, and form of precipitation (*Dingman*, 2002)

The interception loss is important, because it ranges from 5-40% of gross precipitation. The percentage differs in the various plant communities, but generally forests demonstrate higher rate (*Dingman*, 2002).

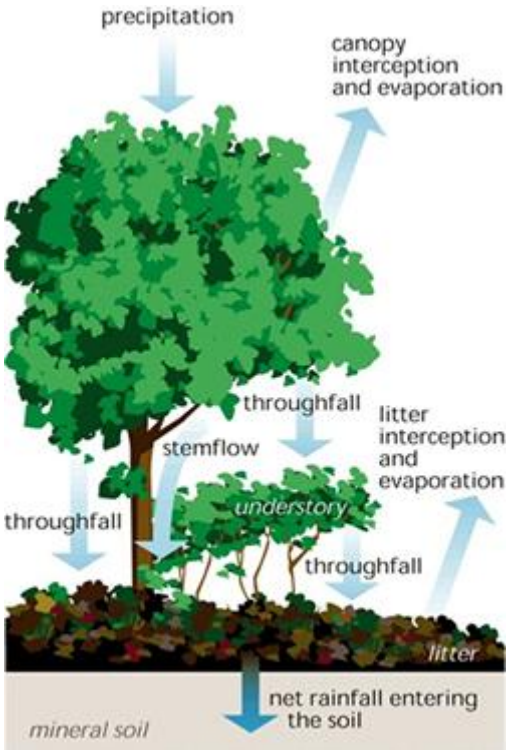

Figure 2.6. The process of the interception (URL11)

2.8. Evapotranspiration

In practice the different time-steps actual or potential evapotranspiration estimation are needed in many situations (such as: rainfall-runoff modeling, small irrigation areas or for irrigated crops within a large irrigation district, deep lakes, post-mining voids, shallow lakes or dams, and of course catchment water balance studies) (*McMahon* et al., 2013).

The potential evapotranspiration can be defined as the amount of water that can be evaporated and transpired, when soil water is sufficient to meet atmospheric demand (*Allen* et al., 1998). Another definition of PET with more details by *Dingman* (2002): potential evapotranspiration is the rate at which evapotranspiration would occur from a large area that is uniformly and completely covered with growing vegetation that has access to an unlimited supply of soil water, without advection or heat storage effect.

However, the latter definition requires an area that covered by homogeneous vegetation, but several characteristics of a vegetative surface can be modified highly the evapotranspiration rate, such as:

- Surface's albedo that determines the net radiation.
- Maximum leaf conductance. This is a function of the number of stoma per unit area (e.g. stomatal density) as well as the size of the stomatal openings (depends on the species). Plants however; can control the size of their stomatal openings, and thus the leaf conductance as well.
- Atmospheric conductance that is largely influenced by plants height. Conductance increases with the horizontal wind speed and for a given wind speed the conductance is higher for higher type of plants. Furthermore, the higher the vegetation, the larger is

the roughness, so the more turbulent is the flow, consequently the more efficient the upward transfer of water vapor.

- Presence or absence of intercepted water (*Dingman*, 2002).

Considering the mentioned modifying facts, *Penman* (1956) redefined potential evapotranspiration as "the amount of water transpired (…) by a short green crop, completely shading the ground of uniform height and never short of water". This term named to reference-crop evapotranspiration.

The amount of PET, which is regularly calculated from meteorological data gathered under conditions in which actual evapotranspiration rate is less than PET rate; however, if evapotranspiration had been occurring at the potential rate the air temperature and humidity (as well as the latent- and sensible-heat exchange between the atmosphere and the surface) would have been significantly different (*Dingman*, 2002). This fact makes another concern about the definition of PET.

Actual evaporation is assumed to occur when water becomes a limitating factor (*Mingteh*, 2006)

The determination of evapotranspiration is important, particularly in the case of arid and semi-arid regions. On these regions water stress is usually assumed to occur, since the high percentage of low and periodical precipitation is returned to the atmosphere via evapotranspiration. The insufficient water supply constrained the plant species to adapt to the water stress in their own way; therefore the process of evapotranspiration is very dynamic over time and variable in space (*Nebo and Sumaya*, 2012).

The main determining factors of ET are:

- Weather conditions
- Water availability
    - temperature
    - solar radiation
    - wind speed
    - vapor pressure
- Vegetation characteristics
- Management
- Environmental constraints (*Nebo and Sumaya*, 2012)

The albedo, ground cover, root density and the type and development stage of vegetation, its structure plus roughness as well as its adaptation to drought are also influencing the ET rates. The management has a huge affection on ET as well, where the different tillage practices, the establishment of windbreaks, different planting densities, thinning of vegetation are the main factors. In the case of the latest, a reduced evaporation (localized irrigation targeting the root zone or mulching) and a reduced transpiration (herbicides or anti-transpirants with stomata closing properties) occur. Furthermore, water stress may induce other type of environmental stresses, such as pests, diseases, nutrient shortages, exposure to toxic substances and salinization, by ET rate and plant growth reduction (*Nebo and Sumaya*, 2012).

The main categories of ET estimations can be summarized as follows:

- Atmospheric measurements
  - Energy balance and micrometeorological methods. The main concept is the calculation of water fluxes based on measurements of atmospheric variables, thus they are usually seen as direct measurements. The most popular are the following:
    - eddy-correlation,
    - Bowen-ratio,
    - scintillometry.
  - Weather data: calculating ET from weather-data, such as the Penman-Monteith equation for reference grass evapotranspiration.
- Plant measurements
  - Satellite or aircraft based remote sensing measurements: measuring the reflected electromagnetic energy with the help of sensors, which generate multi- or hyper-spectral digital images. The measured data can be transformed into spatial variables like surface temperature, surface reflectance or vegetation indices (such as NDVI).
- Soil measurements
  - Lysimeters
  - Soil water balance for catchment or parcel level

    $ET = P - R - D_W + \Delta S$ eq. 2.10.

    Where: P: precipitation; R: runoff/runon; D_W: drainage; ΔS: the change in soil water content. The latest can be measured manually or continuously with numerous methods, such as: soil water sensors, neutron probe, gravimetric method and so on (*Nebo and Sumaya*, 2012).

In the following, the lysimeters and the satellite based remote sensing measurement type will be presented in more detail, since both have been used for calibration and validation of our models.

2.8.1. Lysimeters

Lysimeters traditionally used to develop, evaluate and validate models (*Allen* et al., 1998, 2006; *Doorenbos and Pruitt*, 1977; *Jensen* et al., 1990; *Nolz* et al., 2016). Lysimeters are primarily constructed by metal vessels (and filled with soil), which allows the control over low and lateral boundaries, thus capillary rise (normally occur in nature), can be controlled and reduced to zero (*Fisher*, 2012; *Lanthaler*, 2004).

Mass changes of surface-soil-vegetation system and therefore changes in soil water content can be estimated using weighing lysimeters (*Baumgartner and Liebscher*, 1990; *Fisher*, 2012; *Nolz* et al., 2011a; *Von Unold and Fank*, 2005). They are reliable and precise instruments to determine soil water balance, but in other hand they are costly and the installations as well as the maintenance are complicated and time-consuming (*Nolz* et al., 2011a; *Lanthaler*, 2004).

Considering that lysimeters give point measurements, the climatic, hydrological, and vegetative representation of a larger surrounding area may be challenging. Irregularities of

water movement and pressure may occur if we interrupt the natural soil profile. Seepage water may differ from the soil outside the vessel, which is highly dependent upon soil characteristics, plant growth and meteorological parameters. Moreover**,** the internal structure of the soil in the vessel must be the same as the natural soil in the surrounding area, and the organic layer of soil must not be mixed with the mineral horizon (*Nolz* et al., 2011a).

I introduce a weighing lysimeter type in detail in the *Chapter 4.1.2*. since it is elemental part one of our study area.

2.8.2. Satellite or aircraft based remote sensing measurements

Accurate, spatially homogeneous data collection of the state of the continuously changing terrain and vegetation (plant cover, type of plant communities, soil moisture content) with high-resolution are required to define evapotranspiration. However, quantifying evapotranspiration from mixed plant covers can be still a challenge because of the heterogeneity of plant species, canopy covers, microclimate, and the costly methodological requirements (*Nouri* et al., 2013).

TERRA and AQUA satellites, which are equipped with MODIS (Moderate Resolution Imaging Spectroradiometer) radiation measurement equipment, provide detailed information of the surface (different soil types, vegetation cover). The resolution of those satellites is large, three-dimensional (250 m, 500 m and 1000 m) and spectrally characterized by 36 different wavelength bands (*URL12*).

Considering that many satellites have been starting to gather data, which were limited before, therefore a great opportunity of the remote sensing based evapotranspiration measurement was established. Nonetheless, almost all water balance calculations for the identification of mass and energy fluxes across a given area requires the accurate spatially distributed evapotranspiration estimations (*Szilágyi* et al., 2011).

Before I introduce CREMAP in detail, some recent studies about the types of the remote sensing based evapotranspiration measurement have to be summarized. *Courault* et al. (2005) and *Calcagno* et al. (2007) categorized the remote sensing methods into 4 groups: empirical direct, residual, inference, and deterministic methods.

Assessment of the energy balance (with evapotranspiration) using some surface properties such as albedo, canopy cover, leaf area index and surface temperature are the basis of the empirical methods. In case of the residual method, empirical and physical relationships are combined to estimate the energy balance components (except evapotranspiration) directly through remote sensing, while ET is calculated as the residual of the energy balance equation. (*Boegh* et al., 1999; *Calcagno* et al., 2007; *Kalma* et al., 2008; *Nouri* et al., 2013; *Su*, 2002). The basis of the inference method is a remote sensing application with the aim of measuring a plant reduction adjustment factor (such as crop factor or landscape factor) to determine the actual evapotranspiration of a specific vegetation cover with the modification of the reference evapotranspiration. Deterministic method is established based on the complex soil, vegetation and atmosphere transfer models. Remote sensing can be employed to either assess energy balance components or to integrate (or calibrate) particular input data (*Nouri* et al., 2013).

2.8.3. Potential evapotranspiration

As being a key step to determine the potential evapotranspiration in our method (details in *Chapter 4.3.*) an independent subchapter has been created for it.

Estimation of the magnitude of the actual evaporation over long term is a challenge, compared with the precipitation or streamflow measurements (*McMahon* et al., 2013). Furthermore, the direct measuring of evapotranspiration is difficult, impractical and expensive. As a result, potential evapotranspiration (PET) based methods are the most popular ways to estimate evapotranspiration (*Zhang* et al., 2004; *Zhou* et al., 2008; *Sun* et al., 2011a). In this way, the first step is to calculate the maximum of actual ET, which is PET, and then to compute the actual ET with the help of soil moisture and leaf area dynamics as constraints. This practice is particularly popular at large scales hydrological modeling and if the availability of climate data is limited; and in addition, if the simulation of water pathways in the soil-plant-atmosphere continuum as a process-based modeling approach is not achievable (*Rao* et al., 2011; *Vörösmarty* et al., 1998; *Wolock and McCabe*, 1999; *Dai* et al., 2010).

PET is usually referred to as drying power of the climate or the ambient meteorological condition (*Dingman*, 2002).

Nonetheless, PET is an essential index of hydrologic budgets at different spatial scales and it is a key variable for understanding regional biological processes. Furthermore, with PET, the environmental energies' availability as well as the ecosystem productivity can be represented (*Lu* et al., 2005).

2.8.3.1. Estimation of potential evapotranspiration

The PET estimations created originally for agricultural purposes. The PET calculation for a forested area has to be corrected to reflect differences in potential water loss (*Lu* et al., 2005, 2009). Nonetheless, the researchers have attempted to estimate directly or with lysimeters the forests' PET or actual evapotranspiration (AET [mm]) values with the help of associated equations (*Harsch* et al., 2009). However, mainly indirect methods have been created either at stand or landscape levels, because of the large size of a tree. Therefore, they indirectly estimate with models that were developed for free water surface or short crops (*Thornthwaite and Mather*, 1955; *Kolka and Wolf*, 1998). Nevertheless, field studies in agricultural and open situations are using air-monitored tents as well as lysimeters to determine actual evapotranspiration, but these practical field methods cannot be used within forest systems, since the measurements of PET in a forest stand is impractical, due to massive extension of trees above and below ground (*Kolka and Wolf*, 1998; *Rao* et al., 2011).

PET can mostly be estimated by theoretical or empirical equations or derived simply by multiplying standard pan evaporation data by a coefficient. Both are indirect ways to assess PET. The direct chance of measuring PET is with lysimeters, eddy covariance, or Bowen ratio (*Lu* et al., 2005).

Hydrology has created approximately 50 methods to calculate PET, which can be categorized in 4 methods category (*Dingman*, 2002; *Rao*, 2011; *Xu and Singh*, 2002).

- Temperature-based: In this case air temperature (often climatic average) and occasionally day-length are used as inputs (e.g., *Thornthwaite*, 1948; *Blaney and Criddle*, 1950; *Hamon*, 1963) (*Dingman*, 2002).
- Radiation-based: Air temperature and net radiation are functioned as inputs. An assumption states that air moving large distances over a homogenous well-watered surface would turn into saturated, therefore the mass transfer term in Penman equation would vanish. Under these conditions the equilibrium potential evapotranspiration occurs. The most popular radiation-based method is found by *Priestley and Taylor* (1972). In their approach PET depends only on net radiation and temperature (*Dingman*, 2002). The radiation term dominates over the advection term, by a factor of 1.26, therefore it is applicable in large forest catchments and humid environments (*Nebo and Sumaya*, 2012).
- Combination methods: Based on Penman combination equation, which originally developed for free-water evaporation – these methods using air temperature, net radiation, wind speed as well as relative humidity (*Dingman*, 2002). Nonetheless, in combination equations water advection and heat storage for evaporation from vegetation are negligible. In this case the elimination of the sensible heat exchange (estimated by explicitly) can be also possible. Thus, the net incoming radiation remains the major energy term to be assessed. Loss of heat to the ground with conduction is often negligible (*McMahon* et al., 2013).
- Pan based methods: Based on pan evaporation, but with a modification influenced by temperature, wind speed and humidity. The potential evapotranspiration for short vegetation is regularly quite similar to free-water evaporation (*Dingman*, 2002).

The PET models give inconsistent values, because of their different assumptions plus input data requirements or the fact they were made for specific climatic regions. Consequently, the different estimations may provide significantly different results (*Federer* et al., 1996; *Vörösmarty* et al., 1998).

The most popular PET approach is the Penman-Monteith method, which is recommended by United Nations Food and Agricultural Organization (FAO). The model was adapted to a hypothetical grass reference surface (crop) with adjusted height, surface resistance and albedo. The method requires temperature, solar radiation, wind speed and vapor pressure. Consequently, the weak point of the FAO PM is also that the applications of canopy and air resistance parameters are difficult, and they are unknown for numerous plant species as well as the parameter measurements are complex (*Nebo and Sumaya*, 2012).

If the availability of weather data is limited, *Oudin* et al. (2005) and *Lu* et al. (2005) recommend to use temperature-based ET models at catchment level (*Nebo and Sumaya*, 2012). Nonetheless, the most useful amongst the PET methods, which provide similar results for a given study area for regional scale studies, is what requires the least input parameters (*Lu* et al., 2005).

Hydrology separates PET methods into two categories in another aspect as well. The reference surface methods (such as: Thornthwaite, Hamon, Turc, etc.) and surface dependent PET estimations (Priestley-Taylor, Penman-Monteith, Shuttleworth-Wallace) (*Lu* et al.,

2005). *Federer* et al. (1996) define the reference surface as the evapotranspiration that would occur from a land surface called "reference crop" in designated weather conditions if plant surfaces were externally dry and soil water was at field capacity. They defined also the surface dependent PET as: evapotranspiration that would occur from a designated land surface in designated weather conditions if all surfaces were externally wetted, as by rain.

Federer et al. (1996) have compared 9 methods and found that the general magnitude of those methods were similar on annual temporal scale over wide range of climates, but hundreds of millimeters of deviation (even 700 mm in hot and dry areas) occur for a particular location or cover types. However, *Lu* et al. (2005) found 500 mm · $year^{-1}$ deviations. They found that generally, the Priestly Taylor, Turc and Hamon estimations performed better among the six compared methods. They recommended those three methods in regional scale (however in southeastern United States), but exactly the Priestley-Taylor if the radiation data are available, but in other case the Hamon.

Vörösmarty et al. (1998) extended Federer's point-level comparison study. They compared 11 potential evapotranspiration methods (also distinguished reference surface methods and surface-dependent models) in a global-scale water balance model. This comparison is aimed at finding out the adequacy and suitability of the various evapotranspiration models. Areas of the continental United States were used for the comparison (679 sites). The type of the sites can be divided into mainly two major groups: cultivated and non-cultivated (e.g. grassland, broadleaf forests etc.) surfaces. Each potential evapotranspiration algorithm was compared with the difference between grid precipitation (P) [mm· $year^{-1}$] and mean measured runoff (Q_m) [mm· $year^{-1}$]. To determine annual values for bias, they used the $\beta_e = E_s - (P - Q_m)$ equation where β_e [mm· $year^{-1}$] is the mean annual bias, E_s [mm· $year^{-1}$] is the simulated evapotranspiration.

The overall bias range across all surface dependent methods is approximately 90 mm · $year^{-1}$, whereas for reference surface methods this range is over 200 mm · $year^{-1}$.

Consequently, the surface dependent methods should respond better to physiological and meteorological changes and they can be related to CO_2 exchange models through the canopy resistance and leaf area index terms. However, surface dependent PET models can be better in the context of physiological and meteorological changes, – and thus they are attractive in theoretical grounds – but in practice the gathering of necessary input data may be a challenge (potential inaccuracies in and inconsistencies among, the several climatic forcing fields used by these methods). The Hamon model shows underestimations as bias and demonstrates generally unbiased results for cultivated land as well as for broadleaf cover type. Nevertheless, amongst the tested reference surface methods, Hamon model has the smallest bias (i.e. gave a proper empirical response to the interaction of vegetation type and climate) (*Vörösmarty* et al., 1998).

Nevertheless, in forests Hamon approach particularly underestimates the PET values (*Alkaeed* et al., 2006; *Xu and Singh*, 2002). However, *Rao* et al. (2011) concluded that this underestimation assumed to occur only in humid environment with high rainfall. Nevertheless, in semi-arid regions in Europe it was recommended to use by *Xystrakis and Matzarakis*, (2010, 2011).

2.9. Impact of climate changes on the hydrological cycle: results of water balance models

Considering the overall objective of my dissertation - reveal the impacts of climate change on water-cycle, I introduce studies about water balance models' impact analysis in this subchapter.

Granier et al. (1999) established a daily lumped water balance model for forest stands with the aim of quantifying drought intensity and duration in different region of France from 1951 to 1991. Their model is robust, since they used only potential evapotranspiration (Penman-Monteith instead of Hamon), precipitation (climate data), and leaf area index as well as maximum extractable water (site and stand parameters) as inputs. The model computed stand transpiration, interception, and soil water content. *Granier* et al. (1999) regarded soil profile as several horizontal layers. Sap flow measurements of stand transpiration were completed for calibration, while validation was performed by the comparison of measured and simulated soil water in weekly frequency. They mentioned some values for $SOIL_{MAX}$ (they signed with EW_M (maximum extractable water)): 180 mm (coniferous stand with deep soil), 185 mm (broad-leaved stands with deep soil), and 72 mm (broad-leaved stands with shallow soil). Nevertheless, they did not mention any further information about the soil characteristic and its origin in their research. According to their figures, relative extractable water (REW) values did not drop below the 0.4 threshold in the wettest years in the case of deep soils, not even in the months, when the lowest values occurred (mainly in August and September). However, REW values drop below 0.4 in the driest years, not just in the areas with shallow soils, but also in the areas with deep soil.

Remrová and Císleřová (2010) have done a study with the primary objective to demonstrate the impacts of climate change on a grass covered experimental catchments water-balance, namely Uhlířska, which can be found in the Czech Republic. The determination of potential evapotranspiration was done by means of the Penman-Monteith (FAO) method, Hargreaves model and Penman-Monteith (original) approach. The calculation of the water flow of the soil profile (soil moisture) was performed using S1D deterministic model. This model simulates one dimensional isothermal flow in variably saturated media. They have also run projections to reveal the impacts of climate change for the 2071-2100 period using one regional climate models temperature and precipitation values as input. Furthermore, they have done water stress analyses by the comparison of calculated potential evapotranspiration and the simulated evapotranspiration. The difference between the values of those parameters means water stress and moreover insufficient supply of water for transpiration. The experimental site is a very humid mountainous location with more than 1200 mm annual average precipitation and 8.1 °C annual air temperature. The area has shallow – 75 cm deep – soil profile, which is based on crystalline bedrock. The rooting depth of the grass is shallow (20 cm). According to their applied RCM's simulation results (HIRHAM/HadCM3, follow SREC A2 scenario), the temperature likely increase, and the precipitation may decrease. In their impact analyses, they found a 10-years-long period between 2071-2100 which has to be further evaluated, since dry periods i.e. extremely low precipitations and high temperatures were expected on these 10-years. The longest period of water stress (6 days) is assumed to occur in 2095, due to the low seasonal precipitation (517 mm). In context of the simulated actual evapotranspiration, there

is an increase during the 2073-2100 period from 400 mm to 420 mm (+5%) (means cumulative simulated actual evapotranspiration values). This mountainous study area with high precipitation and low annual temperature is generally not affected by water stress.

Lutz et al. (2010) aimed to describe distributions for the most abundant tree species with respect to water-balance variables, and to evaluate the changes of the water balance affection on species ranges by mid-century in the Yosemite National Park (USA) (*Lutz* et al., 2010). They determined climatic envelopes of tree species over broad ranges of environmental gradients. *Lutz* et al. (2010) established a water balance model using a modified Thornthwaite-type method (*Dingman*, 2002) on monthly step, with Hamon PET approach. They used climate proxies and climate projections to model actual evapotranspiration (AET) and deficit (PET-AET) for past and future climate. Values for AET and deficit refer to the annual sum of the monthly values. The water-balance of the current species (ranges in North America) was compared with the modelled future water balance in Yosemite. In their study, the soil water-holding capacity showed a range of 310 mm which was varying basically with elevation. Mean minimum temperatures range from -13.7 °C to 1.2 °C in January. Mean maximum temperatures range from 13.5 °C to 34.6 °C in July, and annual rainfall was 918 mm. Tree species means were distinguished by AET and deficit, and at higher levels of deficit, species means were increasingly differentiated. In lower montane coniferous forests, the annual trend in AET followed soil water availability: highest from October to June. From June, available soil water decreased, deficit increased, AET was lower and soils were always below field capacity from July to September. In upper montane coniferous forests, mean monthly temperatures were below 0 °C, AET was zero during the cold months, and soil water was available and usable from March to November. However, soil moisture decreased also in the summer, but not as rapidly as in warmer sites. In the future there is an average modelled increase in AET of 10% across all plots. Projected increases in deficit between present and future (2020-2049) were 23% across all plots, as a consequence of the increases in temperature plus PET and decreased snowpack. Generally, higher levels of deficit were associated with lower elevation. Nevertheless, soil water-holding capacity was an important differentiating factor. Their results indicate that recent past changes in forest structure and composition may accelerate in the future, and species respond individualistically to further decreases in water availability. They concluded that, at higher levels of AET and deficit, AET demonstrated less variation, but the deficit became relatively more significant differentiating factor amongst the species (*Lutz* et al. 2010).

Keables and Mehta (2010) presented a soil water climatology at the soil unit level for Kansas using a monthly step Thornthwaite water balance approach. Monthly observations of temperature and precipitation for the period 1950–2006 are used to calculate PET (Hamon type), AET, soil water utilization recharge, and runoff. Observations of stream discharge were compared to model estimates of runoff as a means of validating the performance of the model. Regional climate models project that summers may become increasingly dry during the next 100 years in the Great Plains, therefore raising concern about the availability of water resources may occur. However, the impact of climate change on water availability at the local scale will depend basically on the soils and their water storing ability during dry periods (*Keables and Mehta*, 2010). Their results indicate that winter is the driest season, and

precipitation in the western half of the state is circa 50% of that which falls at the eastern half during December and February. January is the driest month in most parts of the state, when the total monthly precipitation is less than 20 mm. Therefore, AET rates are small during the winter in response to reduced precipitation and lower temperatures, but increases equivalently across Kansas from the spring with temperature and available water, due to the increased amount of rainfall. The precipitation maximum occurs during June. AET also reaching its maximum during summer, but its peaks appear in July with 151-175 mm as highest values for most part of their study area. Nonetheless, summer rainfall is frequently unable to balance the high AET rates. After the summer peak, AET rates decrease throughout the fall and into winter. Soil water utilization is the greatest during summer in eastern Kansas, but soil water deficit are common year-round in the western part of the state in response to less precipitation and increased actual evapotranspiration during the summer, and soils with low field capacities also represent a deficit during the summer months. However, majority of the High Plains are characterized by high field capacities. Soil water recharge is greatest in the spring in central Kansas and during the fall in eastern Kansas, when sufficient water is available from precipitation and when evapotranspiration rates are less severe. *Keables and Mehta* (2010) validated their model with the help of observed stream discharge. Nevertheless, they have not done projections, however mentioned the tendency of the expected temperature values, projected by RCMs.

Mohammed et al. (2012) established a monthly step Thornthwaite-type water balance model for 12 rice-growing districts in Bangladesh for the period 1986 to 2006, with the aim of better understanding the response of crops to moisture variation, since climate change may have a significant effect on soil moisture. Moreover, drought is a common event in Bangladesh and almost every dryland farming crop is affected by water shortage. Thus, information about the soil moisture is essential to determine the optimal water release from a reservoir in accordance with the demand. Potential evapotranspiration (PET), (estimated using the Hamon equation), soil moisture storage, actual evapotranspiration (AET), water deficiency, and water surplus were used to calculate water balance, for three different seasons, as well as evaluate interannual variability (*Mohammed* et al., 2012). When AET < PET, the calculated water deficiency equal to PET – AET. (Furthermore, when the soil storage becomes larger than the soil storage capacity, the excess water becomes water surplus and is eventually available for runoff). They have done projections based on several GCMs outputs, for different part of the study sites, depending on the resolution and availability of projection data. Their study indicates that Bangladesh has a humid, warm, tropical climate, and four climatic seasons. Winter (December to February) is relatively cooler and drier (10 °C – 27.5 °C avg. temperature). Pre-monsoon (March to May) is hot (avg. maximum is 36.7 °C). Monsoon (June to early October) is both hot and humid and brings heavy torrential rainfall. Post-monsoon (late October to November) is a short-lived season characterized by withdrawal of rainfall and gradual lowering of minimum temperature. The mean annual rainfall is 2300 mm, and it makes the single input, since 36-40% of the cultivated land is non-irrigated, plus drought is a common event in Bangladesh. Consequently, water deficiency is one of the main climatic factors limiting crop production, especially in the dry season. Estimation of the average water deficiency of 178 mm $\cdot$ year^{-1} in northern Bangladesh indicated that this region

was subject to the greatest degree of water deficiency and winter is the most crucial season in determining water scarcity. Most of the studied locations have a soil-water storage capacity ($SOIL_{MAX}$) of 200 mm · m^{-1} during the period July to September at all the stations (but they did not mention any information about the rooting depth, which may the consequence of the lot study sites). The soil-water storage began to decrease in November and reached the most negative value in April. Soil moisture values were the lowest in winter in all the regions. They used GCMs as basis of their projections. It was found that all the studied regions in Bangladesh would suffer from water scarcity in future, which might result in a high percentage of crop loss. Compared to the annual soil moisture (1575 mm) during their reference period (1986-2006), there is 21% reduction combined both for the year 2050 and 2100, but individually, the latter would be more critical for moisture loss. The average annual values of highest AET were 1138 mm·$year^{-1}$ (northern part of the country) and 1204 mm·$year^{-1}$ (central). During the pre-monsoon season, the monthly mean AET ranged from 89 to 106 mm·$month^{-1}$ and the central region suffered from the highest water loss. In the monsoon season, the AET and PET values were very similar at all stations. Nevertheless, during the monsoon the core rainy period brings heavy torrential rainfall, causing a huge water surplus, in country-wide. During the post-monsoon season (October and November), the highest monthly average of AET was 89 mm·$month^{-1}$. In winter (December-February), a monthly maximum of AET value was 38 mm (*Mohammed* et al., 2012).

Zamfir (2014) used a program to analyze the impact of climate changes on water balance in western Romania for a period of 30 years (from 1980 to 2012). Their analysis based on also the Thornthwaite method, and was made on a 5 years step. The PET is calculated with Hamon equation (*Zamfir*, 2014). If P for a month is less then PET, then AET is equal to P plus the amount of soil moisture that can be withdrawn from storage of the soil. Soil-moisture storage withdrawal linearly decreases with soil moisture storage, therefore soil becomes drier, and less water is available for AET. If P plus soil-moisture storage withdrawal is less than PET, then a water deficit is calculated as PET minus AET. If P exceeds PET, then AET is equal to PET and the water in excess of PET replenishes soil moisture storage. When soil-moisture storage is greater than soil-moisture storage capacity, the excess water becomes surplus and is finally available for runoff. The climate of the Timiş County (Western Romania), can be characterized by a moderated continental temperate climate with Mediterranean influences, and with periods in which the climate in unpredictable. 4 major regional climates were identified as follows: low plain regional climate, high plain regional climate, hills regional climate and mountains regional climate. The annual average temperatures range from 4 ºC – 7 ºC (in mountain areas) to 10 ºC – 11 ºC. Climate is classified under temperate continental climate with mild winters and considerable amounts of precipitation. The summer is characteristically defined by unstable weather with showers and thunderstorms. He concluded that climate changes impact on water balance of western Romania can be divided in two periods: one between 1985 and 2005, when they had climate conditions with aridization and the second period, started after 2005 with high temperatures but also with significant precipitations bringing additional support in covering the necessary water volumes (*Zamfir*, 2014).

2.10. Discussion and research need

The recent studies, introduced in *Chapter 2*, are discussed and required researches are pointed out in this subchapter.

Consensus emerged on the statistically significant warming in all seasons over Europe (*Christensen* et al., 2007; *Jacob* et al., 2008; *Linden van der and Mitchell*, 2009).

In the Carpathian Basin (located at the transition zone in Europe) the climate projections also indicate increase of temperature (expected in all of the seasons) and of climatic aridity for the 21st century; however the projected value of the change can be between 2-5 °C depending on the applied climate model and emission scenario (*Nováky and Bálint*, 2013; *Pongrácz* et al., 2011).

Warming has also an effect on the hydrological cycle through the precipitation intensity (*Kjellström* et al., 2011); *Pongrácz* et al., 2014). The Carpathian Basin, where a northward shift of the transition zone in summer resulting in a decrease of the precipitation amount, while the southward shift of the transition zone in winter may results in increase of precipitation (*Gálos* et al., 2015; *Nováky and Bálint*, 2013).

Generally, the water cycle has been becoming more intense, therefore the atmosphere contains more water at the same time and/or the retention time of the water vapor in atmosphere will be shorter. Consequently, the most significant effect of climate change is its impact on the water cycle through modifying precipitation patterns and the evapotranspiration processes at multiple scales (*Pongrácz* et al., 2014; *Sun* et al., 2011a). Thus, the climate change can cause changes in the water balance equations structure (*Keve and Nováky*, 2010).

In Hungary, 90% of the fallen precipitation is evapotranspired and 10% is runoff (*Kovács*, 2011). Therefore, mainly evapotranspiration is influencing the water availability at land surfaces and controls the large scale distribution of plant communities as well as the primary production. This large percentage of influence on water cycle makes it necessary of the modeling and attaining a quantitative understanding of the evapotranspiration process (*Vörösmarty*, 1998).

The results of the introduced studies about impact analysis of water balance models (*Granier* et al., 1999; *Remrová and Císleřová,* 2010; *Lutz* et al. 2010; *Keables and Mehta*, 2010; *Mohammed* et al., 2012; *Zamfir*, 2014) demonstrate that the evapotranspiration may increase, but the soil water content may decrease in the future due to the presumably increasing temperature and the decreasing precipitation, thus the occurrence of water scarcity may more common towards the end of the 21st century. However, the tendencies differ regionally.

It can be also said, there are quite a few studies with the aim of evaluating the water-balance components and determining the future development of them, respectively, and which are using an easily adaptable model with only few parameters as requirement at the same time. Nonetheless, *there are only a few studies with the purpose to reveal the impacts of climate change on water-cycle for the agrarian and forestry sectors in the 21st century, regarding the Carpathian Basin's special climatic attributes*.

My work is being a part of a bigger ongoing project (*AgroClimate.2 VKSZ_12-1-2013-0034*), therefore a robust water-balance model is needed that requires few parameters as input, which then can be extended to a larger spatial scale (country-wide) as well as can be applied for future projections based on inputs of climate models.

3. Objectives and research questions

On the basis of the main purpose of the dissertation (*Chapter 1.1.*), 5 key objectives were determined:

- Robust water balance model has to be established, which uses only temperature and precipitation data as inputs, and produces actual evapotranspiration and soil water content as outputs. The robustness is essential in order to assure the easy extendibility of the model, which is crucial, since this water balance model makes the base of *AgroClimate.2* project's hydrological module. As a basis, a modified Thornthwaite-type monthly step water balance method has to be upgraded.
- The upgraded model has to be calibrated and validated with measured actual evapotranspiration data (remote-sensing based actual evapotranspiration maps, and weighting lysimeter's actual evapotranspiration data) for the 3 chosen study areas, which represent three different surface covers in the North-western part of the Carpathian basin. During the calibration of the simulated actual evapotranspiration, the storage capacity of the soil has to be defined. In addition, the rooting depth can be also determined as a practical aspect of the modeling.
- On the basis of the calibrated and validated models, projections for the 21st century on the actual evapotranspiration and soil water content have to be done with the help of the precipitation and temperature results of 4 bias corrected regional climate model, as inputs.
- Different kinds of water stress indices have to be determined to quantify the impacts of climate change on the vegetation, with the help of the relative extractable water and soil water deficit.
- Further investigations are required in the context of water stress, where it is relevant, with the assumption of increased rooting depth of the plants as a possibility of adaptation. This assumption means an entire model re-run with increased value of soil storage capacity. Nevertheless, potential water stress determination for the monthly values needs to be done.

4. Data and methods

4.1. Databases for calibration and validation

4.1.1. CREMAP

CREMAP model is a modified, upgraded version of the ET estimation technique of *Szilágyi and Józsa* (2009). CREMAP applies the MODIS surface temperature data. The time-resolution of the model is monthly step; therefore, it is ideal for regional hydrologic modeling purposes. It only needs a minimum amount of easily accessible and freely available data, and work at watershed level or regional scale. Nevertheless, CREMAP is calibration free (*Szilágyi* et al. 2011).

The monthly and annual ET maps with 1 km spatial resolution are novelty in Hungary (as well as in the world for such a long period) and provide finer spatial details, instead of greatly generalized ET maps, which were previously available.

4.1.1.1. Complementary theory

Here, the complementary theory must be introduced, since it makes the theoretical base of the CREMAP model.

Under constant available energy at the surface (Q_n) [mm · day^{-1}], the regionally representative (ET) [mm] and potential evapotranspiration (PET) [mm] rates are complementary, and this called complementary relationship (*Bouchet*, 1963).

The equation is the following:

$$ET = 2ET_W - PET \qquad \text{(eq. 4.1.)}$$

Where:

ET_W is the wet environment evaporation [mm] (*Bouchet*, 1963).

The main difference between the PET and ET_W is that the latter requires a large (a few km^2), wet surface, with continuously good water supplies, which can already influence the environment variables. The ET_W was described by Priestley-Taylor equation (Priestley and Taylor, 1972).

$$ET_w = c\frac{\delta}{\delta+Y}Q_n \qquad \text{(eq. 4.2.)}$$

The potential evaporation was determined with the Penman-equation (*Penman*, 1948).

$$ET_P = \frac{\delta}{\delta+Y}Q_n + \frac{Y}{\delta+Y}f(u)(e^* - e) \qquad \text{(eq. 4.3.)}$$

Where:

c: Priestley-Taylor constant (typical values from 1.20 to 1.32)

δ: The slope of the saturation vapor pressure curve at the temperature of the air [hPa · °C^{-1}]

Y: (~0.67 hPaK^{-1}) the psychrometric constant [hPa · °C^{-1}]

e & e*: the actual and saturation vapor pressure at the temperature of the air [hPa]

f(u): wind function [mm · day^{-1} · hPa^{-1}]

$$f(u) = 0.26(1 + 0.54u^2) \quad \text{(eq. 4.4.)}$$

Where:

u^2: the mean horizontal wind velocity, measured at 2 m height above the ground [m · s^{-1}] (*Szilágyi* et al., 2011).

Morton et al. (1985) in their WREVAP model specify PET and ET_w slightly differently, but it remained valid (*Szilágyi and Józsa*, 2008). They suggest (eq. 2.10.) to be employed for time-periods equal or longer than about a week to ensure accuracy, because the complementary relationship is based on an assumed equilibrium state of the atmosphere and the underlying land. In their approach the evaluation of PET (with an iterative method) does not require information of the mean wind speed. WREVAP is applied in case of CREMAP for obtaining the regionally representative areal evapotranspiration rate (*Szilágyi and Kovács*, 2010).

4.1.1.2. The CREMAP model structure

The spatial disaggregation of the regionally representative ET rates can be achieved with a linear transformation of 8 days composited MODIS daytime surface temperature (T_s), into actual ET rates. This transformation requires two anchor points in the T_s-ET plane (*Figure 4.1.*). The first anchor point can be determined by the spatially averaged daytime surface temperature, (T_s), and the ET values. The second anchor point results from a spatial averaging of the coldest pixel values (T_{sw}), assuming that the coldest pixels are the wettest as well, and evaporating at the wet environment evapotranspiration rate ET_w. The two anchor points then specify the linear transformation of the T_s pixel values into ET rates for each month by applying monthly means. It should be noted: this linear transformation is valid while Q_n – and therefore the surface albedo – as well as the aerodynamic resistance (r_a) are circa constant among the pixels (*Szilágyi and Kovács*, 2011).

The 1 km MODIS pixel-size is sufficient, since it is enough large to the albedo and r_a changes remain negligible between the cells. Nevertheless, the resolution is small enough to offer satisfying spatial resolution at the watershed scale (*Szilágyi and Józsa*, 2009).

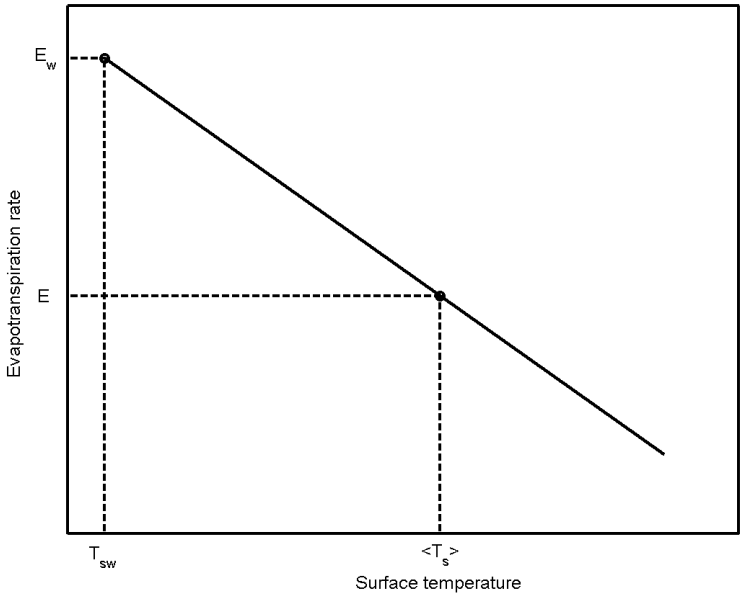

Figure 4.1. Schematic representation of the linear transformation of the MODIS daytime surface temperature values into ET rates (Szilágyi et al., 2011)

4.1.1.3. Application of the CREMAP model

To determine the anchor points of transformation several metrological data were used:

- 0.1° (~7.6 km west-east and ~1.1 km north-south) gridded mean monthly air temperature.
- Specific humidity - provided by the OMSZ (Hungarian Meteorological Service).
- Sunshine duration for the 2000–2008 periods - provided by VITUKI (Environment and Water Management Research Institute Nonprofit Ltd.) (*Szilágyi and Kovács*, 2010).

MODIS daytime surface temperature data (8-days composited) were averaged for each month in the modeling period, therefore the dataset contains 1 averaged surface temperature value per month per pixel (*Szilágyi and Józsa*, 2009).

Hungary was divided into three elevation zones because of the changes in T_s by elevation (<200 m; 200 m-500 m; 500 m<). ET_w was evaluated with the 30–50 coldest T_s points for each month in all three zones (30 in the highest region). In the middle elevation zone the wettest points were taken from the 300 – 400 m strip and in the highest zone from the 550–650 m one. There were no restrictions applied for the lowest zone, due to the small changes in elevation there. The Q_n value for ET_w was evaluated by WREVAP from the zonal means of the 0.1-degree gridded sunshine duration values. The other anchor point was obtained by averaging the MODIS T_s values for each zone and calculating the corresponding ET by WREVAP from the spatial mean of air temperature, specific humidity and sunshine duration values within the zone (*Szilágyi and Kovács*, 2011).

Evaporation values may show sharp jumps at the boundaries of the zones. To avoid these irregularities, the transformation equation was allowed to change linearly with pixel-elevation

(z) between the limiting equations of the upper (u) and the lower (l) zones. The equation is the following (*Szilágyi and Kovács, 2010*):

$$ET(z) = \frac{(z_u - z)[a_l T_s(z) + b_l] + (z - z_l)[a_u T_s(z) + b_u]}{z_u - z_t} \quad \text{(eq. 4.5.)}$$

Where: a and b are the parameters of the linear transformations by zone, obtained with the help of the anchor points. z_u or z_t: reference elevations are taken at 100, 350, and 600 m.

The linear transformations have been neglected in the winter months (from December to February) due to the fact that the ground may have patchy snow cover, or the mountainous areas have snow layer, whereas the lower grounds do not have at the same time. This deviation impedes the constant Q_n assumption, because the snow's albedo is completely different from the albedo of land surface. This restriction is not limiting so much the general applicability of the model, considering that the temperate climates evapotranspiration is significantly limited in the winter months (*Szilágyi* et al., 2011).

4.1.1.4. CREMAP's result

As we can see on *Figure 4.2.*, the ET is relatively uniform and low in the dormant season. The saturation deficit becomes greater with the air temperature rising in April till June. This greater saturation deficit enhances the extent and spatial differences of evaporation. The areal evaporation max is in June because of the favorable soil moisture conditions (due to the within-year peak of precipitation). However, the hottest months are July and August (*Szilágyi and Kovács*, 2010).

The spatial variance of ET is resulted from a combination of land cover, rain and access to groundwater. Higher rates appear in forested mountainous regions of northern Hungary with 100-200 mm higher annual precipitation than the average (600 mm), and the south-western region of Hungary, where precipitation excess the average more than 200 mm. Furthermore, ET is likewise quite high, where there is a constant shallow groundwater-supply, especially in the floodplains along the Tisza and Danube Rivers. The lowest overall ET and precipitation was found in the Great Hungarian, where the grass surface cover and cropland are dominated. This is particularly prevalent for the sandy inter-fluvial plateau between the Danube and the Tisza River where the groundwater table has continuously diminished over the past several decades (*Szilágyi and Kovács*, 2010).

Validation of the results was performed with the help of three eddy-covariance sites and five catchment-scale water-balance closure data (*Szilágyi* et al., 2011). The validation covers nearly three orders of magnitude in spatial scale and showed a beneficial match between estimated ET and observed ET. On a monthly basis the estimated ET indicated an R^2 value of 0.8 – 0.9. The overall strong correspondence between measured ET and estimated ET are basically maintained at annual and multi-annual level, where effects of seasonality are eliminated. The typical R^2 values were between 0.7 – 0.8 on annual and multi-year basis. Nevertheless, the mean annual ET estimates remain well within 10% of the measured values (*Szilágyi* et al., 2011).

Kisfaludi et al. (2015) compared the 9-year average ET values of the CREMAP method with the MODIS Global Evapotranspiration Project (MOD16). The ET of nine watersheds (with

known water balance) provided better results by the CREMAP method (RMSE=17.20 mm/y) than by the MOD16 (RMSE=34.12 mm/y). Furthermore, CREMAP presented ET data for the whole area of Hungary, but MOD16 ET data was unavailable at water bodies and urban areas.

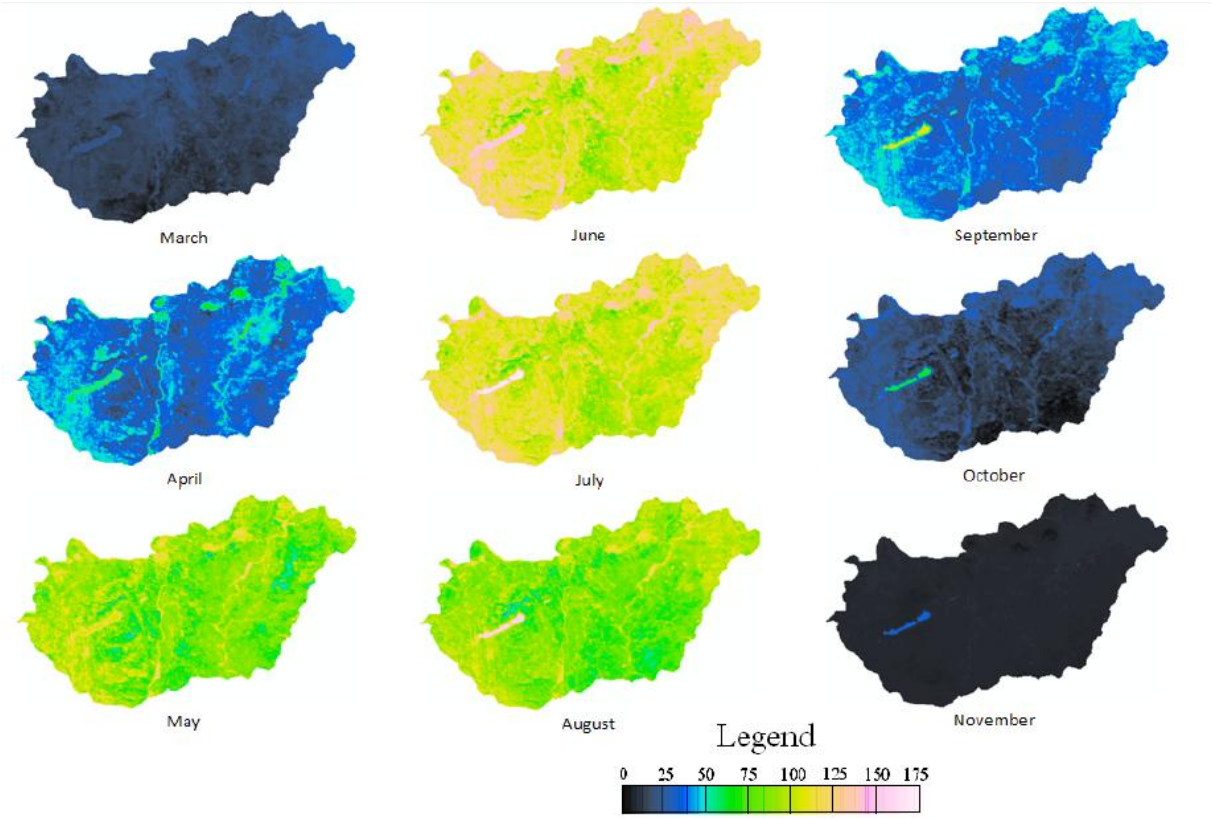

Figure 4.2. Nine years averaged (2000-2008) mean monthly ET rates (mm) (Szilágyi and Kovács, 2010)

4.1.2. Weighing lysimeter

An introduction is presented in *Chapter 2.8.1.* about the lysimeters. As an important part of my study, with providing data for calibration and validation, I give a detailed description about the two large weighing lysimeters in this subchapter, which located at Marchfeld (Groß-Enzersdorf). The scheme of the lysimeter facility is represented by *Figure 4.3.*

The lysimeters were installed in 1983 to study evapotranspiration at the surface, water content in the soil profile, and drainage water at the bottom outlet of the lysimeters (*Neuwirth and Mottl*, 1983). This facility was installed by the Swiss company "Compagnie Industrielle Radioelectrique" (*Neuwirth and Mottl*, 1983), and managed as well as maintained by the Institute of Hydraulics and Rural Water-Management at the University of Life Sciences (BOKU) in Vienna (*Neuwirth and Mottl*, 1983; *Nolz* et al., 2011a).

The cylindrical vessels have an inner diameter of 1.9 m, a resulting surface area of 2.85 m^2, and a hemispherical bottom with a maximum depth of 2.5 m. A typical soil profile was created by re-packing soil in layers as follows:

- sandy loam soil (0–140 cm) (30 % sand, 50 % silt, 20 % clay; porosity: 43 %),
- gravel (140–250 cm) (only macropores with low water holding capacity).

In the past years, one lysimeter and the surrounding area were permanently covered by grass and maintained in order to represent reference conditions for determination of reference evapotranspiration (*Allen* et al., 1998). Accordingly, the lysimeter and its surroundings were frequently cut (about twice a month during the vegetation period), irrigated (about twice a week during summer) and fertilized (twice a year) to guarantee uniform distribution and dynamic growth (*Nolz* et. al., 2016).

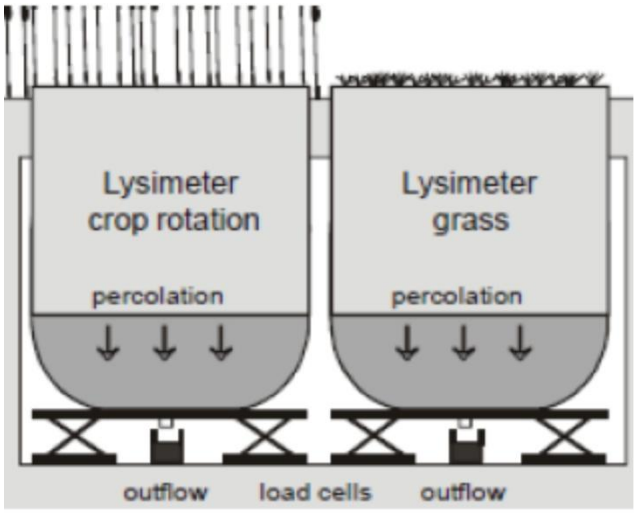

Figure 4.3. Scheme of the lysimeter facility in Groß-Enzersdorf (Nolz and Cepuder, 2008)

The soil water changes, which measured by the capacitance EnviroSCAN® measuring system, developed by the Australian company Sentek. The major components of the EnviroSCAN® sensors are the top cap, the access tube, the sensor electrodes, the sensors and the cable (*Paltineanu and Starr*, 1997; *Sentek*, 2003).

The access tube was installed directly in the lysimeter profile and that provide good contact between tube and soil. The tube is equipped with sensors in 10 cm-intervals from 10 to 160 cm with the aim of measure the changes of water content in different depth of the soil (*Nolz and Cepuder*, 2012).

EnviroSCAN® sensors were not able to evaluate soil water content (θ %) in the first centimeters of the soil profile and over the surface, since the zone of influence is about 10 cm in length along the axis of the probe. In addition, during the experiment in Groß-Enzersdorf, the last 90 cm (between 160 and 250 cm), created by gravel, were not detected (*Nolz and Cepuder*, 2012). Measurements of the sensor in 20 cm depth (θ_{20}) were assumed to represent the water content within the rooting zone (*Nolz* et al., 2016).

Figure 4.4. represents the schema how the lysimeter weighing facility is working.

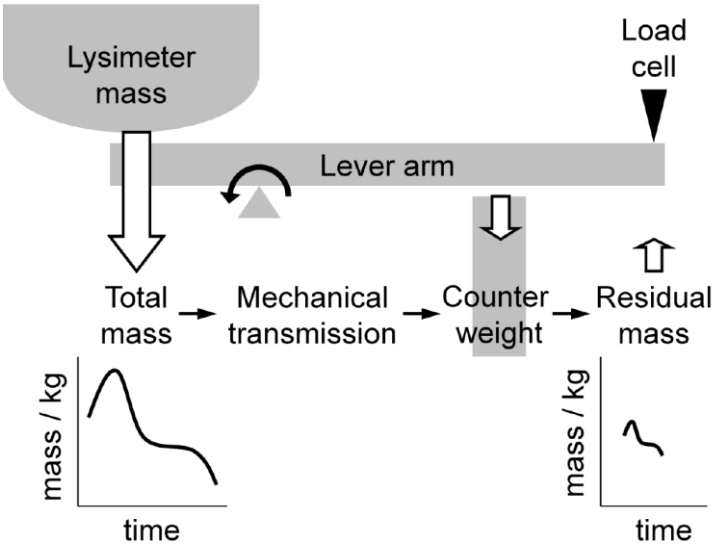

Figure 4.4. Lysimeter weighing facility: a small fraction of the total mass is transmitted to an electronic load cell via a lever-arm mechanism with a counterbalance (measuring accuracy is ±0.18 kg.) (Nolz et al., 2013)

The determination of water balance can be achieved using the lysimeter with

- a tipping bucket to measure percolating water (W_{drain}),
- a lever-arm-counterbalance weighing system to detect changes of mass (= water content) (W_{lys}) and determine fluxes at the soil-atmosphere interface. These fluxes were assumed to be positive due to precipitation and negative because of evapotranspiration. This technique requires short measuring intervals, accurate data, and a suitable data management as well.

To see how the actual ET_{LYS} was determined from the lysimeter data, I have to introduce the water balance equation that demonstrates the correlation between measured (W_{lys}, W_{drain}) and unknown (P_{lys}, I_{lys}, ET_{lys}) components. The equation represents a daily changes Δ of the analyzed components.

The water balance equation is the following according to *Nolz* et al. (2016):

$$\Delta W_{lys} + \Delta W_{drain} = \Delta P_{lys} + \Delta I_{lys} - \Delta ET_{lys} \quad \text{(eq. 4.6.)}$$

ΔW_{lys}: soil water [mm · day^{-1}],
ΔW_{drain}: drainage water [mm · day^{-1}],
ΔP_{lys}: precipitation [mm · day^{-1}],
ΔI_{lys}: irrigation [mm · day^{-1}].
ΔET_{lys}: evapotranspiration [mm · day^{-1}],

The fluxes across the upper boundary of the lysimeter is represented by the right-hand side of the equation.

The weighing facility measures the mass changes, which is equal with changes of soil water (ΔW_{lys}): a mechanical lever arm counterweight system transmitted a fractional amount of lysimeter weight to an electronic load cell with a measuring accuracy of ±0.18 kg.

At the bottom of the lysimeter at a free drainage outlet there is a tipping bucket, which measures the drainage water quantity (ΔW_{drain}) flows through on this bucket.

Weighing data from lysimeters and data of the tipping bucket were measured every few seconds and stored every 10 minutes and collected on Excel sheets (*Nolz* et al., 2011b). The processed output signal of the load cell was registered every few seconds, averaged, and stored on a local server. Storage intervals were 15 min from 2005 to 2007 and 10 min from 2007 to 2010, respectively.

Weighing data and raw data of cumulated outflow were stored together (*Nolz* et al. 2011b). Collected raw data were transformed into physical quantities using calibration factors and divided by the surface area and the density of water with the purpose of obtaining ΔW_{lys} and ΔW_{drain} with a dimension of length (*Nolz* et al., 2013).

Noisy data as well as outliers were processed byway of smoothing operations using a natural cubic approximation spline with discontinuities for rainfall and irrigation and manually adjusted smoothing factors (*Nolz* et al., 2016).

ΔP_{lys} as well as ΔI_{lys} were calculated from increasing ΔW ($=\Delta W_{lys} + \Delta W_{drain}$), but ΔET_{lys} was recorded if ΔW was decreasing. ΔI_{lys} was separated obviously, because the dates were known from record keeping. Ordinarily, this technique provides more credible values of ΔET_{lys}, than the ordinary method with rain gauge data (P), which often shows deviations to the increase of ΔW that resulting in unlikely, negative ΔET_{lys} (*Nolz* et al., 2016).

4.2. Study areas

To test my water balance model, I used three study areas on the Carpathian Basin, namely: forested area, mixed parcel and Marchfeld. The first two situated in the Western part of the Transdanubian Region of Hungary, while the third in the eastern part of Austria next to Vienna (*Figure 4.5.*).

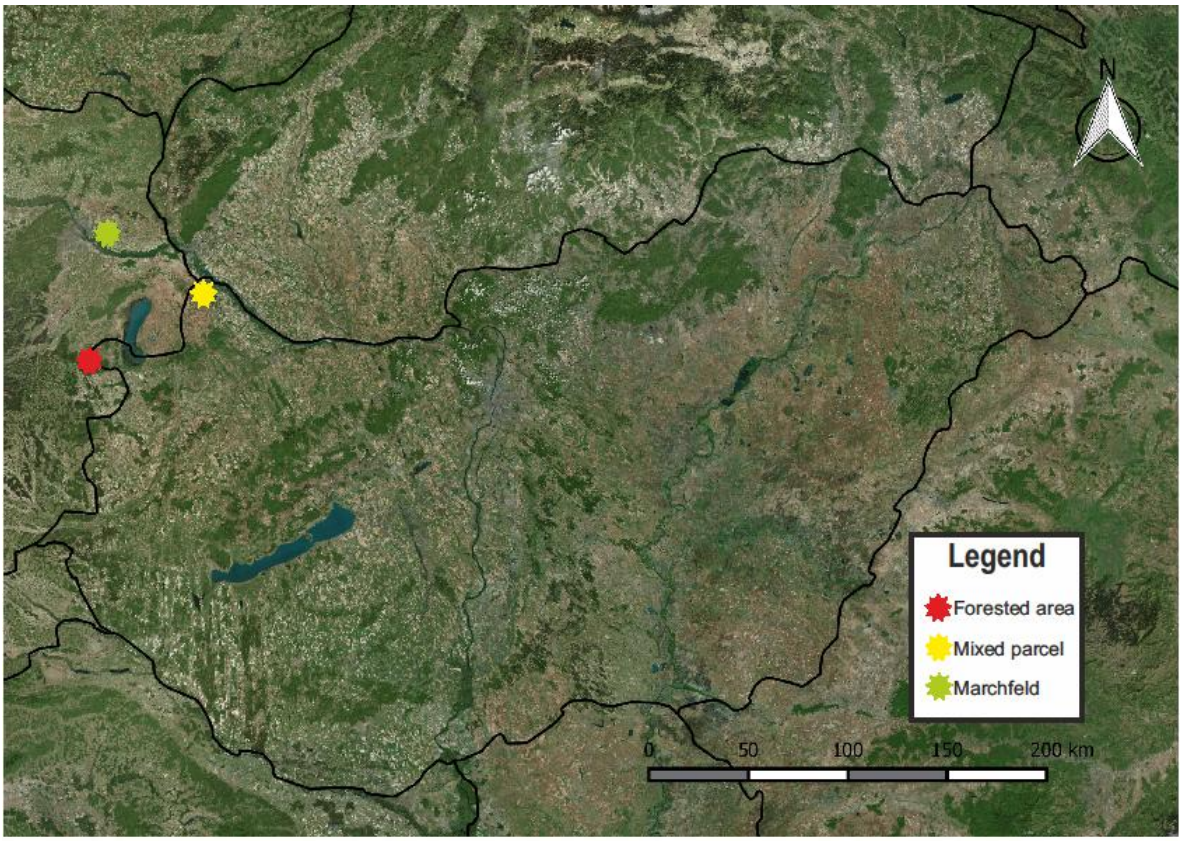

Figure 4.5. The location of study areas

4.2.1. Forested area

The forested area is an experimental catchment at the eastern foothills of the Alps near the city of Sopron.

The climate of this area is subalpine. The average annual temperature is 8.5 °C. The annual precipitation is 700-750 mm. The driest season is autumn, while the wettest part of the year is late spring and early summer (*Dövényi*, 2010).

The geological basis of the catchment is fluvial sediments, deposited in five distinct layers in the tertiary (Miocene) period on crystalline bedrock. A finer-grained layer appears in the valley bottom, which is a good aquifer, giving rise to perennial streams (*Kisházi and Ivancsics*, 1985). The soil texture of this area is loam. The dominant vegetation in the catchment comprises alder (Alnus glutinosa) in the bottom of the valley, spruce (Picea abies) and beech (Fagus sylvatica) on the northern slopes, whereas sessile oak (Quercus petraea) and beech (Fagus sylvatica) on the southern slopes.

Considering that the total area of this catchment is approximately 6 km^2, and the scale of the EOV maps, which contain the input parameters for my model, are in 1 km^2 resolution, I have to create a grid and put it to this study area, and then weight the involved grid cells to establish the input database for my models.

The first step was the creation of a 5x4 km^2 area and put it to the study area applying the DigiTerra Map software (*Czimber and Nyull*, 2004). This 20 km^2 area was divided into 1 km^2 grid cells.

Using the previously described 20 km^2 area and the area of Hidegvíz Valley, I could create my topology. These two layers cut define the proportions of the catchments area that being covered each 1 km^2 square (*Figure 4.6.*). As a result, I could weight the contribution of each pixel.

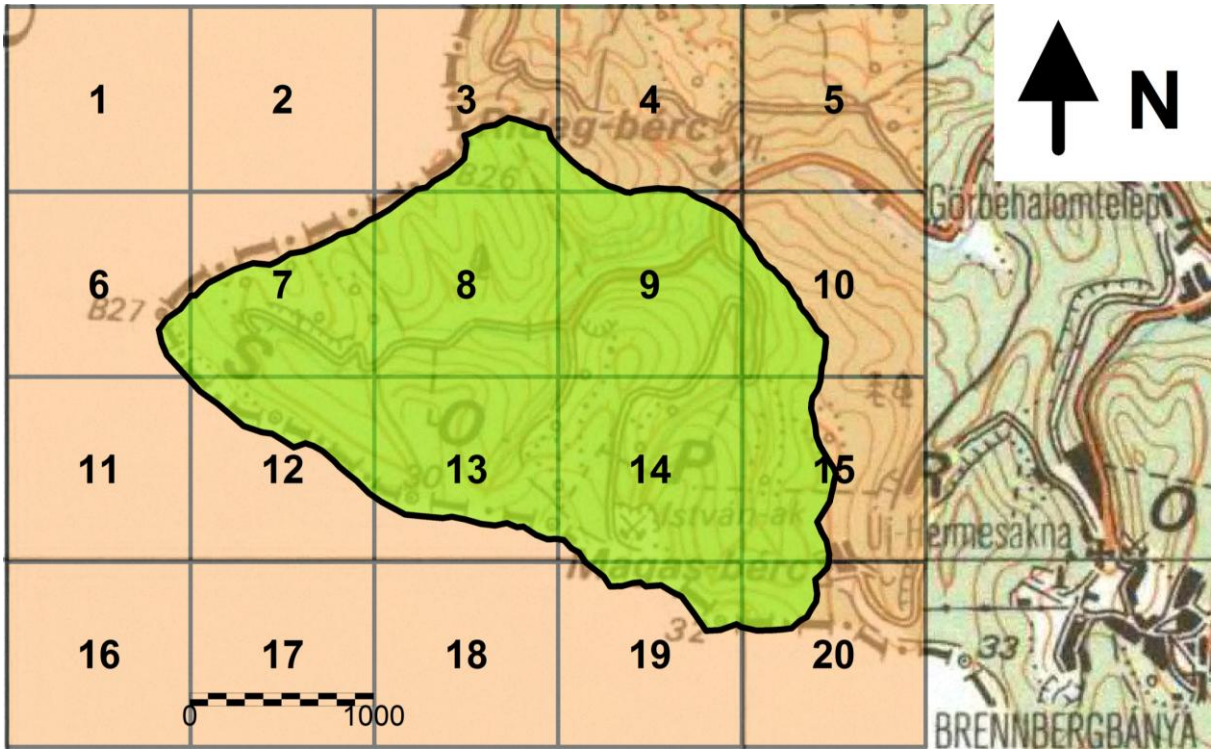

Figure 4.6. Forested area with the grid cells

The identification numbers (ID) of the grid cells over Hungary with the involved areas can be found on *Annex 1*.

Finally, from the involved (and weighted) pixels, I could gather mean monthly temperature (T_M) and monthly summed precipitation (P_M) values as inputs for the forested area and nevertheless measured (remote-sensing based) actual evapotranspiration values (ET_{CREMAP}) (details in *Chapter 4.1.1.*) for calibration and validation. The investigation period was from 01.2000 to 12.2008 due to the availability of the data.

Annex 3 contains the input database of forested area. The data originated from the *AgroClimate.2* project.

4.2.2. Mixed parcel

The mixed parcel is basically used as an agricultural plot and has been primarily a cornfield except during the period between 2003 and 2007 when it was used to grow barley and in 2004 when it was used for wheat. However, poplar species can also be found on this area, and that is why I use the term mixed parcel rather than cornfield for this study area. Nonetheless, it has a total area of about 1 km^2.

The selected parcel is located in the Mosoni-sík microregion that is situated in Győr-Moson-Sopron County. It is basically (73.5%) plough-land. This natural microregion is an alluvial

plain as a whole. In the context of geology, the area is the southern accumulation slope of the transported sediment of the Danube that was built on the sinking recess of the Little Hungarian Plain. In the north-western part of the natural microregion, the surface is covered by recent fluvial silt, and fluvial cobble at the two sides of the Lajta, but south and southeast from that, the surface is covered by muddy-loessal sedimentary cover (*Dövényi*, 2010).

The climate is continental. There is a temperature difference between the western and eastern part of the natural microregion. The average annual temperature is 9.7 °C. The annual precipitation is 560 mm. (*Dövényi*, 2010).

The 71% of the natural microregion is covered by chernozem soil, the 20% of it is covered by alluvial meadow, and the remained 10% is covered by marshland. Hydromorphic soil - evolved on cobble - characterizes the natural microregion. The ratio of the plantation of hybrid poplar (Populus × canadensis) is significant in the natural microregion (*Dövényi*, 2010).

The investigation period was from 01.2000 to 12.2008, the same as for the forested area.

Considering that the extension of the area is only 1 km^2 and it corresponds with the EOV maps topology, I did not create a grid as in case of the forested area. The input dataset contain mean monthly temperature (T_M) and monthly summed precipitation (P_M) values as well as measured (remote-sensing) actual evapotranspiration values (ET_{CREMAP}) for calibration and validation.

Annex 3 contains the input database of mixed parcel. The data originated from the *AgroClimate.2* project.

4.2.3. Marchfeld

The Marchfeld is an area of about 1000 km^2 in the eastern part of Austria, between Vienna and the border to Slovakia (*Figure 4.7.*). It is characterized by a subhumid climate with a mean annual temperature and precipitation of approximately 10 °C and 550 mm, respectively. Typical summers are hot and dry, winters are mainly cold with severe frost and limited snow cover (*Götz,* 2000). About 1900 hours of sunshine represent a large energy input for biomass production. A typical soil type is Chernozem, a black-colored fertile soil with high percentages of humus, phosphoric acids, phosphorous and ammonia matter (*Götz*, 2000). The favorable environmental conditions supported the development of large areas (650 km^2) of intensive production of various crops in the past decades. However, the region is prone to water deficit stress and heat stress. Irrigation has a long tradition and is expected to become even more important due to climate change effects (*Nachtnebel* et al., 2014).

The required data for this study were obtained at a representative location at the south-western boundary of the Marchfeld, namely in Groß-Enzersdorf (*Figure 4.7*). The village comprises an experimental farm of the University of Natural Resources and Life Sciences of Vienna (BOKU). At this site (48°12'N, 16°34'E; 157 m) exist a reference weather station of the Austrian "Zentralanstalt für Meteorologie und Geodynamic (ZAMG)" and a lysimeter station. Monitored meteorological data include air temperature, precipitation, relative humidity,

global radiation, and wind velocity in 10 m height. The mean wind velocity is considerable and the prevailing wind direction is from North-West (*Nolz* et al., 2016).

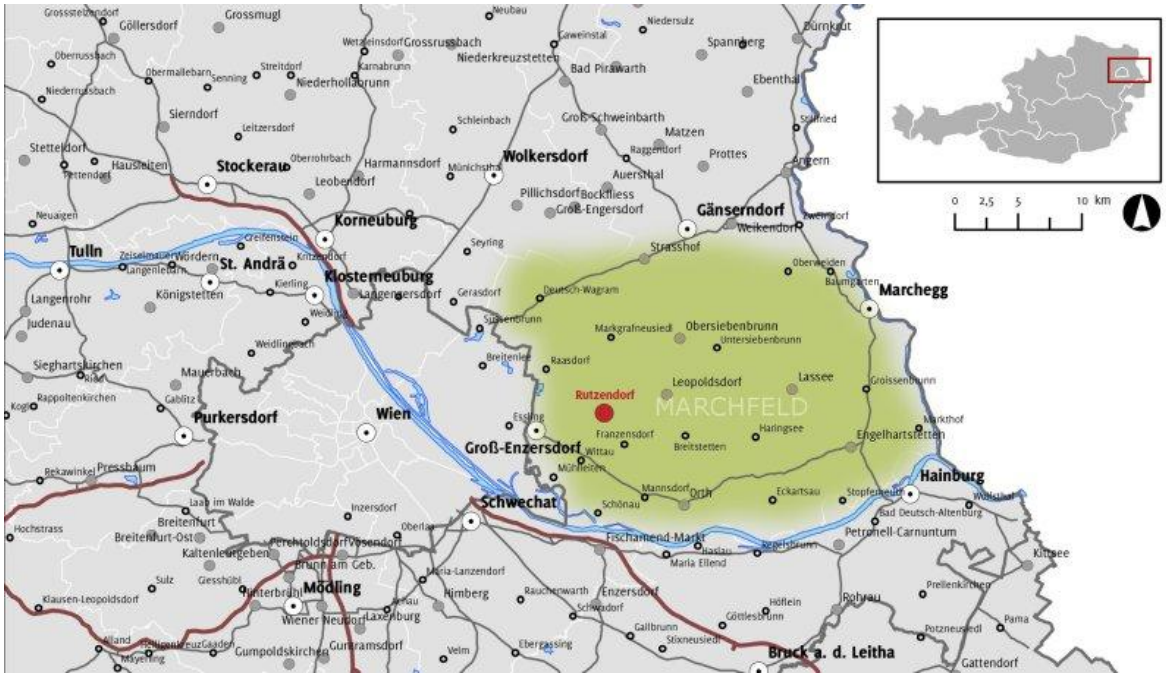

Figure 4.7. Location of the Marchfeld and the experimental site of BOKU in Groß-Enzersdorf (URL12)

Mean monthly temperature (T_M) and summed monthly precipitation (P_M) values make the input dataset and actual evapotranspiration values ($ET_{LYSIMETER}$) for calibration and validation. Nevertheless, all input data refer to the experimental site in Groβ-Enzersdorf. In the given case, the irrigation and the precipitation make the input parameter.

Annex 3 contains the input database for Marchfeld.

4.3. The Thornthwaite-type hydrological model description

Hydrologists use Thornthwaite-type water balance models for steady-state seasonal (climatic average) simulations and also to study the continuous values of watershed or regional water input, snowpack, soil moisture, and evapotranspiration. The model represents a 1-D system, considering only vertical fluxes. In Thornthwaite-type models all water quantities are defined in depths of liquid water (volumes per unit area). Input values are monthly precipitation (P_M) [mm] and temperature (T_M) [°C]. In case of continuous simulations, inputs mean actual monthly averages, where $_M = 1, 2, \ldots 12 \cdot N$, and N means the number of years of record. It has to be noted that the original model considers the effects of snow (*Dingman*, 2002). I did not take into consideration the accumulation and melting effect of the snow, since the temperature and the melting will probably increase in the future. Consequently, the chances of having permanent (stable) snow cover (remaining continuously for at least a month) will likely decrease in Hungary. The details about the original model in context of the input can be found in *Annex 2*.

To run the Thornthwaite-type water balance model, I have chosen the "R" statistical software (*R Core Team*, 2012). It is a programing language and a fully planned and coherent system namely an environment for statistical computing and graphics with wide variety of techniques of them (linear and nonlinear modeling, classical statistical tests, time-series analysis, classification etc.). Furthermore, "R" allows users to add further functionality by defining new functions. This program can be freely downloaded and upgraded by many additional packages from the CRAN family. "R" permits of the creation of publication-quality plots, as well as mathematical symbols and formulae (*R Core Team*, 2012).

The full script of my method can be found in *Annex 4*.

First of all, I have to determine the values of declination (σ). The angle between a horizontal (tangent) plane and the solar beam is determined by latitude (φ) of the plane and the declination of the sun. The sun's declination is the latitude at which the sun is directly overhead at noon; due to the 23.5° tilt of the earth's rotational axis. This latitude changes regularly between +23.5° and -23.5° as the earth revolves around the sun (*Dingman*, 2002).

The equation for declination is the following:

$$\sigma = \frac{180}{\pi} \cdot [0.0006918 - 0.399912 \cdot \cos(\Gamma) + 0.070257 \cdot \sin(\Gamma) - 0.006758 \cdot \cos(2 \cdot \Gamma) + 0.000907 \cdot \sin(2 \cdot \Gamma) - 0.002697 \cdot \cos(3 \cdot \Gamma) + 0.00148 \cdot \sin(3 \cdot \Gamma)] \quad \text{(eq. 4.7.)}$$

Where:

σ: declination [°]
Γ: day angle [°]

The Thornthwaite model applies the standard unit of declination (°), which has to be converted into radian (*Dingman*, 2002). The conversion mathematically:

$$\frac{\sigma}{360} \cdot 2 \cdot \pi \quad \text{(eq. 4.8.)}$$

After that I have to identify the daylenght (D) [hr].

$$D = \frac{2 \cdot \arccos[-\tan(\sigma)) \cdot \tan(\varphi)]}{0.2618} \quad \text{(eq. 4.9.)}$$

Where:

φ: latitude (°).

Note that one has to specify the latitude of the area being examined. It must be converted into radian as well (*Dingman*, 2002).

The next step in setting up the model was the calculation of the potential evapotranspiration (PET). In this study, a temperature-based PET-model after *Hamon* (1963) was applied. Generally, other approaches can also be used to estimate PET in Thornthwaite-type water balance model (*Dingman*, 2002). The calculation of potential evapotranspiration after Hamon (PET_H) is explained through the following equations:

$$PET_H = 29{,}8 \cdot D \frac{e_m^*}{T_M + 273{,}2} \quad \text{(eq. 4.10.)}$$

$$e_m{}^* = 0{,}611 \cdot \exp\left(\frac{17{,}3 \cdot T_M}{T_M + 237{,}3}\right) \quad \text{(eq. 4.11.)}$$

Where:

D: day length [hr]
T_M: the average monthly temperature [°C]
e_m*: saturation vapor pressure [kPa].

The next step was a condition:

If:

$$P_M \geq PET_M \quad \text{(eq. 4.12.)}$$

then

$$ET_M = PET_M \quad \text{(eq. 4.13.)}$$

$$SOIL_M = \min\{[(P_M - ET_M) + SOIL_{M-1}], SOIL_{MAX}\} \quad \text{(eq. 4.14.)}$$

Where PET_M is the calibrated monthly potential evapotranspiration [mm]. Determination of PET_M is part of the calibration, which will be presented in the next subchapter.

ET_M [mm] is the monthly actual evapotranspiration, and $SOIL_M$ [mm] is the monthly soil moisture, which representing the amount of soil water that is available for the vegetation (not the total amount of soil water, as might be expected). Both ET_M and $SOIL_M$ denote the key components of this dissertation.

For the simulation procedure, the first $SOIL_{M-1}$ value was set to a maximum value that corresponded with the soil-water storage capacity ($SOIL_{MAX}$) [mm]. The basic assumption was that soil-water storages is saturated before the vegetative period starts. $SOIL_{MAX}$ was introduced using unsaturated hydraulic parameters of the study areas' soil types with a standard setting of rooting depth (1 m):

$$SOIL_{MAX} = (\theta_{fc} - \theta_{pwp}) * z_{rz} \quad \text{(eq. 4.15.)}$$

Where:

θ_{fc}: water content at field capacity [dimensionless],
θ_{pwp}: water content at permanent wilting point [dimensionless],
z_{rz}: rooting depth (vertical extent of root zone [mm]).

The following procedure explains how soil-water storage is considered as reservoir for evapotranspiration:

If precipitation is less than (calibrated) potential evapotranspiration in a certain month:

$$P_M < PET_M \quad \text{(eq. 4.16.)}$$

then:

$$ET_M = P_M + SOIL_{M-1} - SOIL_M = P_M + \Delta SOIL \quad \text{(eq. 4.17.)}$$

Where:

$$\Delta SOIL = SOIL_{M-1} - SOIL_M = SOIL_{M-1} * \left(1 - \exp\left(-\frac{PET_M - P_M}{SOIL_{MAX}}\right)\right) \quad \text{(eq. 4.18.)}$$

ΔSOIL: decrease in soil-water storage [mm].

4.4. Model calibration and validation

Remote sensing based (for forested area and mixed parcel) and grass-covered lysimeters (for Marchfeld) actual evapotranspiration data served as basis for calibration and validation. The available time series for forested area as well as for mixed parcel (2000-2008) was divided into two parts. The first part is used for calibration from 2000 to 2005, whereas the second is for validation from 2006 to 2008. In case of Marchfeld (2004–2011) time series was also divided into two parts, the first is from 2004 to 2008, the second is from 2009 to 2011. The former period is for calibration and the latter is for validation as well. It is important to note that the difference between the time series of the study areas is due to the availability of the input data.

The calibration datasets was further divided into two parts considering both potential and actual evapotranspiration. The results of calibration and validation are methodical result of the dissertation; therefore I introduce them in *Chapter 5.1*.

Figure 4.8. represents schematically the functioning of the model and the relationships between the applied parameters in the modelling process for forested area and mixed parcel.

Parameters of the calibration and the input data (temperature and precipitation) of the validation period (2009–2011 for Marchfeld; 2006-2008 for forested areas as well as mixed parcel) were used for the validation.

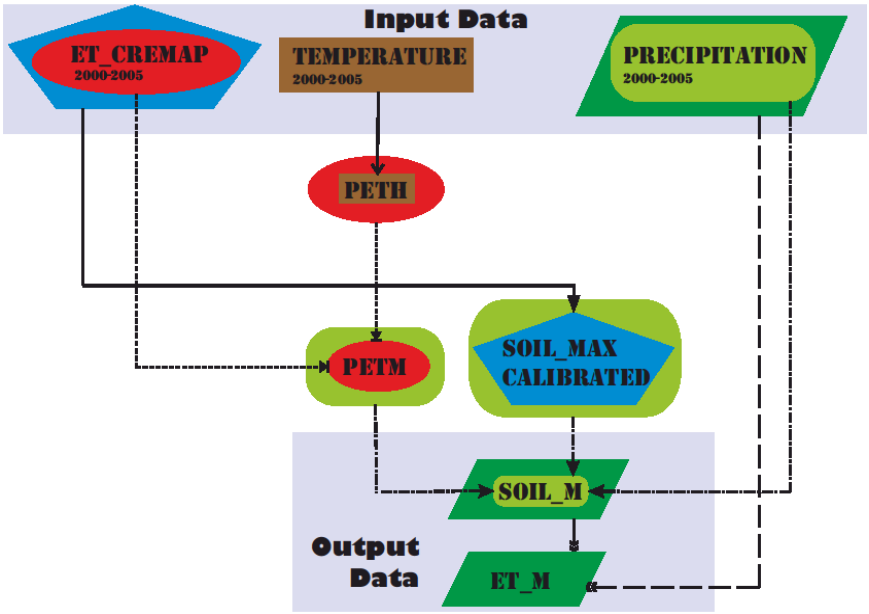

Figure 4.8. Graphical representation of the model of forested area and mixed parcel. (Parameters: ET_CREMAP is the measured actual evapotranspiration; PETH is the Hamon type potential evapotranspiration; PETM is the calibrated potential evapotranspiration; ET_M is the actual evapotranspiration, SOIL_MAX CALIBRATED is the calibrated soil-water storage capacity, and SOIL_M is the soil moisture. The different shapes with the different type of arrows illustrate the connections amongst the used parameters during the model workflow.)

4.5. Projection procedure

4.5.1. FORESEE database

For the bias correction *Dobor* et al. 2012 chose the period from 1951 to 2009 as a reference. The daily E-OBS database (1951-2009) (established within the framework of the ENSEMBLES FP6 project; *Haylock* et al., 2008) and the monthly CRU TS 1.2 (Climatic Research Unit, University of East Anglia, UK; *Mitchell* et al. 2004) high resolution gridded dataset were used for the past. *Dobor* et al. (2012) have compared the regional climate model results and the observation based datasets for the reference period (1951-2009). It should be noted that each of the used RCMs' data are based on the A1B greenhouse gas emission scenario (a balanced emphasis on all energy sources; *IPCC* 2000). Based on monthly comparison, correction factors were determined, which were applied to the daily climate model results for the past as well as for the future. In case of precipitation the correction means multiplication, whereas in case of temperature the correction means shifting. The correction of precipitation is a more difficult process, since in a given month, precipitation is characterized not only by the sum, but also by the frequency (number of wet days). Nonetheless, the systematic errors affect not only the amount of precipitation. Therefore to perform an appropriate bias correction on it, the correction was done for the frequency of precipitation as well (*Ines and Hansen*, 2006; *Déqué*, 2007).

The bias correction is based on the cumulative density function (cdf) fitting technique (also known as quantile mapping/fitting or histogram equalization). The first part of the bias correction is the fitting of the monthly number of wet days (when the precipitation is not less than 0.1 mm/day). Monthly ratios were determined between the observed and the modeled monthly wet days based on the 1951-2009 period pixel by pixel. The second step is the correction of the amount, what is accomplished by cdf fitting. Quantile functions were defined also month by month using 1000 partitions for the corrected E-OBS database and for the climate model results pixel by pixel as well (*Dobor* et al., 2014).

The name of the final database is: Open Database FOR ClimatE Change Related Impact Studies in Central Europe. The bias adjusted database contains daily meteorological data (min./max. temperature and precipitation) based on the simulation results of ten RCMs for 2010-2100, and observation based data for the period 1951-2009 interpolated to 1/6·1/6 degree spatial (horizontal) resolution grid (using inverse distance interpolation technique). Furthermore, all of the time series were converted to a 365-day calendar (*Dobor* et al., 2013).

The domain of the FORESEE database can be found on *Figure 4.9.*

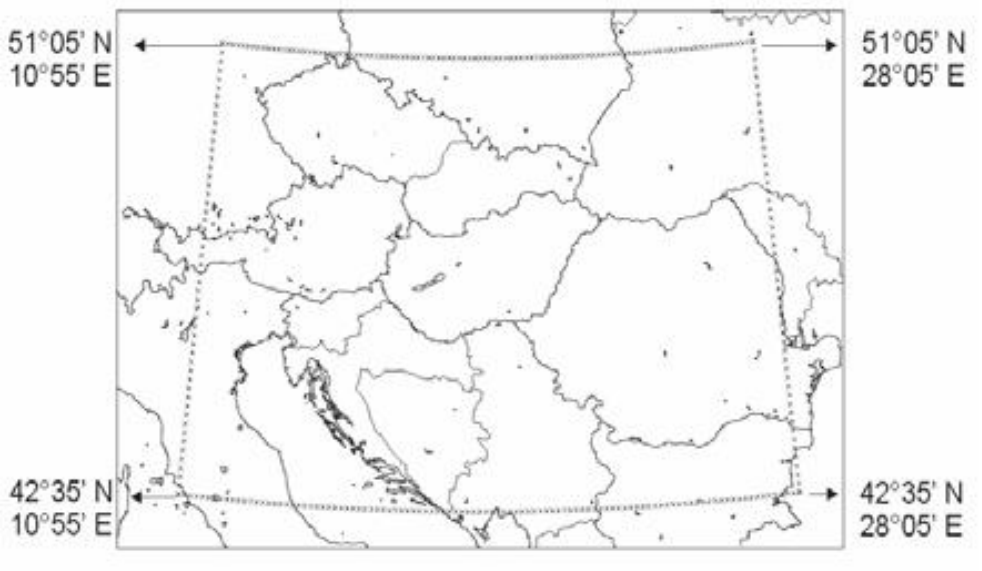

Figure 4.9. The domain of the FORESEE database (dotted rectangle) containing climatic data for the period 1951-2100. The data are distributed in 5,408 (104·52) grid cells organized in 1/6·1/6° regular grid (Dobor et al. 2012)

4.5.2. Regional Climate Models

As basis for the projection procedure, the water balance model was re-calibrated for each study area using all available data (2000-2008 for forested area, mixed parcel and 2004–2011 for Marchfeld). This was done, because calibrating the model with as much data as possible was assumed to deliver the best possible calibration relation. (Furthermore, validation already delivered proper results, but this will be addressed in *Chapter 5*).

Inputs for predicting future developments of actual evapotranspiration (ET_M), soil moisture ($SOIL_M$) and the 10th Percentile of soil moisture ($SOIL_{M\_10Percentile}$) (this parameter means the average of the values below the 10th percentile of the soil moisture) were the equations of the broken line regression, the calibrated $SOIL_{MAX}$ values, and projected temperature and precipitation values. The latter two originate from four grid-based, bias-corrected regional climate models (RCMs) (the data are based on the A1B greenhouse gas emission scenario (*IPCC*, 2000)). Those four different RCMs illustrate the uncertainties, because all climate projections have uncertainties inherently (*URL14*). Data were extracted from nearest pixel to the study sites coordinates. The main properties of the RCMs can be found in *Table 4.1*.

Table 4.1. The applied RCMs (Jacob, 2001; Jacob et al., 2007; Christensen and van Meijgaard, 1992; Christensen et al., 1996; Jones et al., 2004)

Model ID	Research Institute	Regional climate model	Driving general circulation model	Emission scenario	Spatial resolution
1	Max-Planck-Institute for Meteorology (MPI)	REMO	ECHAM5	A1B	25km
2	Sweden's Meteorological and	RCA	ECHAM5-r3	A1B	25km

	Hydrological Institute (SMHI)				
3	Danish Meteorological Institute (DMI)	HIRHAM5	ECHAM5	A1B	25km
4	Royal Netherlands Meteorological Institute (KNMI)	RACMO2	ECHAM5-r3	A1B	25km

In the following, I refer to each model as their model ID (first column of *Table 4.1.*)

The RCMs' time scale covers a range from 2015 to 2100. Each of them contains temperature and precipitation data in monthly time intervals. To evaluate the results for the 21st century, four main investigation periods were designated: 1985–2015 (01.01.1985 – 01.01.2015), 2015–2045 (01.01.2015 – 01.01.2045), 2045–2075 (01.01.2045 – 01.01.2075), and 2070–2100 (01.01.2070 – 01.01.2100). The results of the first investigation period (1985–2015) are based on observation-based data, which represented by model ID '0' in the following. As mentioned before the FORESEE results for the RCMs were available from 2015, therefore I had to shift the investigation periods with 5 years compare to the *AgroClimate.2* project's investigation periods. With the data at hand, these 30-year-blocks with a 5-years overlap in the last two periods seemed the best partitioning. The overlap in the last part of the 21st century was necessary, because only 25 years of data were available.

The graphical representation of the projection phase of the model can be found on *Figure 4.10.*

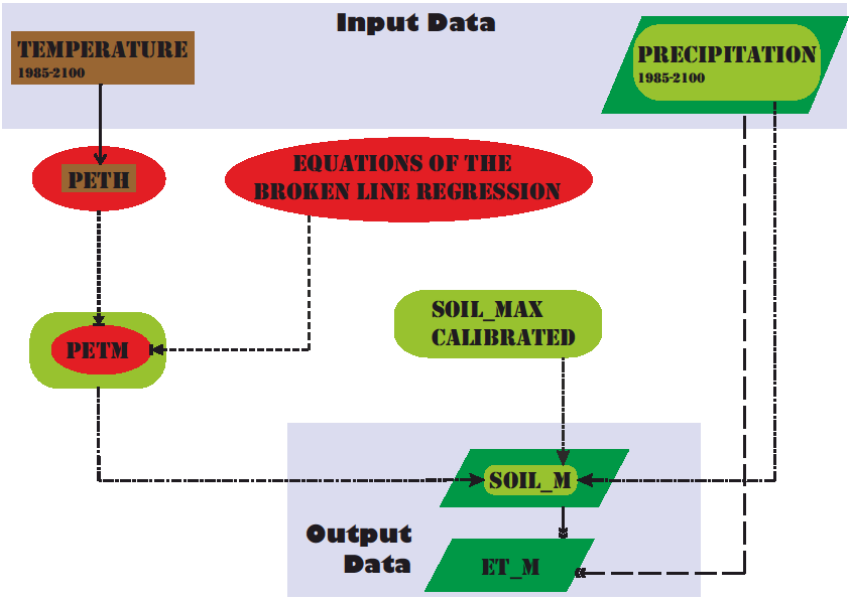

Figure 4.10. Graphical representation of the projection phase of the model. (Parameters: PETH is the Hamon type potential evapotranspiration; PETM is the calibrated potential evapotranspiration; ET_M is the actual evapotranspiration, SOIL_MAX CALIBRATED is the calibrated soil-water storage capacity, SOIL_M is the soil moisture, and equation of the broken line regression, which can be found on Table 5.1. The different shapes with the different type of arrows illustrate the connections amongst the used parameters during the model workflow.)

4.6. Water stress

Different kinds of water stress indexes were determined using the developed water balance model.

An appropriate, simple way to assess water stress is the calculation of the relative extractable water (REW) using the following equation (*Granier* et al., 1999).

$$\mathrm{REW} = \frac{\mathrm{SOIL_M}}{\mathrm{SOIL_{MAX}}} \qquad \text{(eq. 4.19.)}$$

Where:

REW: relative extractable water [dimensionless],

When REW drops below 50% of $SOIL_{MAX}$, the transpiration is progressively reduced (because of stomatal closure); hence, water stress assumed to occur.

$SOIL_{MAX}$ parameter is the maximal amount of water available to plants, and therefore it means maximum extractable water in the soil. The average soil moisture ($SOIL_M$) is the extractable water in the different investigational periods.

$$\mathrm{SWD} = \mathrm{SOIL_{MAX}} \cdot 0.5 - \mathrm{SOIL_M} \qquad \text{(eq. 4.20.)}$$

Where:

SWD: soil water deficit [mm],

If: $SOIL_M < 0.5 \cdot SOIL_{MAX}$ and for that very reason SWD values are positive, then water stress is assumed to occur.

4.7. Evaluating model performance

Model performance was tested using the coefficient of determination (R^2) and the Nash-Sutcliffe model efficiency coefficient (R^2_{NS}). The latter is a criterium that has been used in calibration as well as in validation of hydrologic models. The Nash-Sutcliffe criterium is proper for models that simulate continuous time series of different time-period (*Dingman*, 2002).

$$\mathrm{R^2_{NS}} = 1 - \frac{\sum_{i=1}^{N}(\mathrm{ET_{MSR\_i}} - \mathrm{ET_{SIM\_i}})^2}{\sum_{i=1}^{N}(\mathrm{ET_{MSR\_i}} - \mathrm{m_{MSR\_i}})^2} \qquad \text{(eq. 4.21.)}$$

ET_{MSR_i}: time series of measured values,
ET_{SIM_i}: time series of simulated values,
m_{MSR_i}: average value for the period being measured.

4.8. Rooting depth parameterisation of the Marchfeld

Rooting depth parameterization refers to plant water uptake and water deficit stress. For the simulations two basic conditions (runs) were distinguished with respect to the rooting zone.

The first run was based on a rooting depth corresponding to the characteristics of the lysimeter that was used for the calibration and validation procedure (static rooting depth of

the plants). The second run was that plants are able to adapt to water stress conditions by increasing their rooting depth in order to suffice their needs from a larger soil water reservoir (extended rooting depth of the plants). At the Marchfeld, the bottom of the sandy loam layer within the lysimeter was at 1.4 m depth. Below there is a gravel layer with low water holding capacity. Consequently, for the second run, I set the rooting depth to the physically possible maximum, i.e., to 1.4 m, which then modified the soil storage capacity ($SOIL_{MAX}$) as well (eq. 4.15.).

In such a way, potential stress conditions were determined for both static and extended rooting depth. (Differences arising from varying soil characteristics were not considered in the dissertation).

4.9. Summary of objectives and methods

With the help of *Table 4.2.* I summarize the 6 main task of my dissertation with the utilized methods.

Table 4.2. The tasks of the dissertation based on the main objective with the used methods

Tasks	Methods
Establishment of water balance models for the study areas with components of actual evapotranspiration and soil water content as outputs.	Upgrade a modified Thornthwaite-type monthly step water balance method.
Calibration of the base models potential evapotranspiration and the actual evapotranspiration values and comparison of the results of the three study sites.	Application of the measured actual evapotranspiration datasets to determine the storage capacity of the soil and use broken line and linear regressions. Use coefficient of determination and Nash-Sutcliffe coefficient to evaluate the models' performance.
Validation of the calibrated model and comparison of the results of the three study sites.	Application of the measured actual evapotranspiration data. Use of coefficient of determination and Nash-Sutcliffe coefficient.
Projection of soil moisture and evapotranspiration as water balance components for the 21st century and comparison of the results of the study sites	Utilization of the calibrated and validated model parameters based on the simulation results of 4 regional climate models as input.
Analysis of the future development of water stress in the 21st century and comparison of the results of the study sites.	Determination of the relative extractable water and soil water deficit.
Further investigations in the context of water stress where it is relevant, with the assumption of increased rooting depth of the plants as a possibility of adaptation.	Entire model re-run with increased value of soil storage capacity. Monthly potential water stress determination.

5. Results

5.1. Methodical results

5.1.1. Calibration of the potential evapotranspiration

The first step of calibration considered potential evapotranspiration for actual land cover using ET_{CREMAP}-values (for forested area and mixed parcel) and ET_{lys}-values (for Marchfeld) at well-watered conditions. The latter were assumed to occur when precipitation exceeded potential evapotranspiration or actual evapotranspiration (ET_{CREMAP} or ET_{lys}) exceeded potential evapotranspiration (PET_H).

$$P_M > PET_H \text{ or } ET_{lys}/ET_{CREMAP} > PET_H \quad \text{(eq. 5.1.)}$$

The ET_{lys}/ET_{CREMAP} values selected in such a way are denoted PET_{lys}/PET_{CREMAP}. Measured (PET_{lys}/PET_{CREMAP}) and calculated (PET_H) values were correlated with the second variable as the explanatory one. As PET is known to be different between growing and dormancy, because of the variable state of the vegetation, therefore different relationships had to be established for the two parts (*Rao* et al., 2011). For this purpose, a software package named 'segmented' of 'R' software environment was applied (*R Core Team*, 2012). The bases are the so-called broken-line or segmented models that create a piecewise linear relationship between the response and one or more of the explanatory variables. This linear relationship is represented by two or more straight lines connected at unknown values called breakpoints (*Muggeo*, 2008). A segmented relationship between the mean response $\mu = E[Y]$ and the variable Z, for observation i = 1, 2, …, n is modeled by adding the following terms to the linear predictor:

$$\beta_1 z_i + \beta_2 (z_i - \psi)+ \quad \text{(eq. 5.2.)}$$

Where:

$(z_i - \psi)+ = (z_i - \psi) \cdot I(z_i > \psi)$ and $I(\cdot)$ is the indicator function equal to one when the statement is true.

β_1 is the left slope, β_2 is the difference-in-slopes and Ψ is the breakpoint (*Muggeo*, 2008).

5.1.2. Calibration of the actual evapotranspiration

As the second step of the calibration, I calibrated the calculated actual evapotranspiration (ET_M) with the help of $SOIL_{MAX}$ as calibration parameter. In this case, the initially estimated $SOIL_{MAX}$ parameter had to be adjusted in order to reach a maximal correlation between ET_{lys}/ET_{CREMAP} and ET_M. To achieve this maximum correlation, the 'optim' function of the mentioned 'R' software was applied. With the value of $SOIL_{MAX}$ after the calibration, the vertical extent of the root zone (and the maximum depth of tilth) can be calculated using soil texture data (if they are available).

5.2. Results of calibration of potential evapotranspiration

I compared the 3 study areas in the context of PET calibration. Correlation between PET_H and $PET_{CREMAP/LYS}$ during the period of dormancy is illustrated by the section on the left of the vertical dotted line (broken-line approach) (*Figure 5.1.*). The main attributes of the slopes of the segments can be found in *Table 5.1.* This comparison revealed that each of them separately have high correlation between $PET_{CREMAP/LYS}$ and PET_H, which can be expressed with the coefficient of determination (R^2). The values R^2 were equally 0.98 in each case.

The 1:1 dotted lines exposed overestimations in case of forested area (*Figure 5.1.a*) and mixed parcel (*Figure 5.1.b*), but only in the dormancy. Therefore, the globally calibrated, calculated Hamon type PET has higher values, than the measured PET in the winter seasons and that is why the lines of the first segment appeared under the 1:1 lines. Unlike the former ones, Marchfeld provides proper estimations for the dormant season, which means greater PET_H values as well. However, only two values of lysimeter data (red triangles) could be related to this period, thus little conclusion can be drawn from that (*Figure 5.1.c*).

As mentioned in the *Chapter 5.1.1.*, the calibration of PET_H uses only the well watered months. Mixed parcel has more well watered values (months) than the other two in the dormant season (*Figure 5.1.b*).

The breakpoint value of forested area (24.3 mm) is a smaller than the two others (mixed parcel: 39.1 mm; Marchfeld: 36.9 mm). The reason is the presence of conifer species in the forested area, therefore the growing season starts (mathematically) earlier. Nevertheless, the value of albedo is also smaller in the case of forests; consequently the absorbed energy is higher, which can be manifested in higher evapotranspiration.

In contrary, on the growing season each study area expresses more or less underestimation (i.e., the calculated PET_H shows lower values than the measured), particularly toward the higher values (*Figure 5.1.*). The highest underestimation occurred in the Marchfeld during the growing season. However, the measured PET ($PET_{CREMAP/LYS}$) removes the underestimations during the calibration of the calculated PET (PET_H), because I accepted the measured PET as real data. Therefore, the measured PET ($PET_{CREMAP/LYS}$) makes the calculated PET (PET_H) surface dependent.

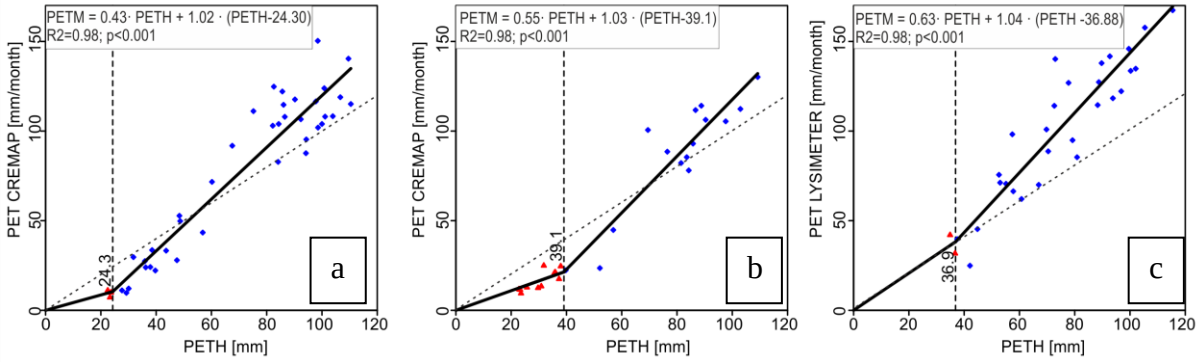

Figure 5.1. Relationship between $PET_{CREMAP}/PET_{LYSIMETER}$ and PET_H in growing and dormant seasons with a 1:1 line (dotted), at forested area (a), at mixed parcel (b), at Marchfeld (c) (i.e., the calibration of PET_H). The triangles represent the values of the dormancy, while the

dots represent the values of the growing season. The reason of vertical dotted line is the separation of the two characteristically different state of the vegetation

Table 5.1. Broken-line regressions results of the 3 study areas

Study area	Slopes	Estimate	Std. Error	t value	Pr(>|t|)
Forested area	Slope of the first segment	0.4283	0.3553	1.206	0.235
	Slope of the second segment	1.0164	0.3652	2.783	NA
Mixed parcel	Slope of the first segment	0.5470	0.1004	5.448	1.55e-05
	Slope of the second segment	1.0164	0.1765	5.850	NA
Marchfeld	Slope of the first segment	0.6340	0.3089	1.877	NA
	Slope of the second segment	1.0357	0.3379	3.353	0.000231

The reason for the 'NA' of the 'Pr (>|t|)'in *Table 5.1.* is that the standard asymptotics do not apply.

5.3. Results of the calibration of actual evapotranspiration

Figure 5.2. illustrate the results of calibration of actual evapotranspiration.

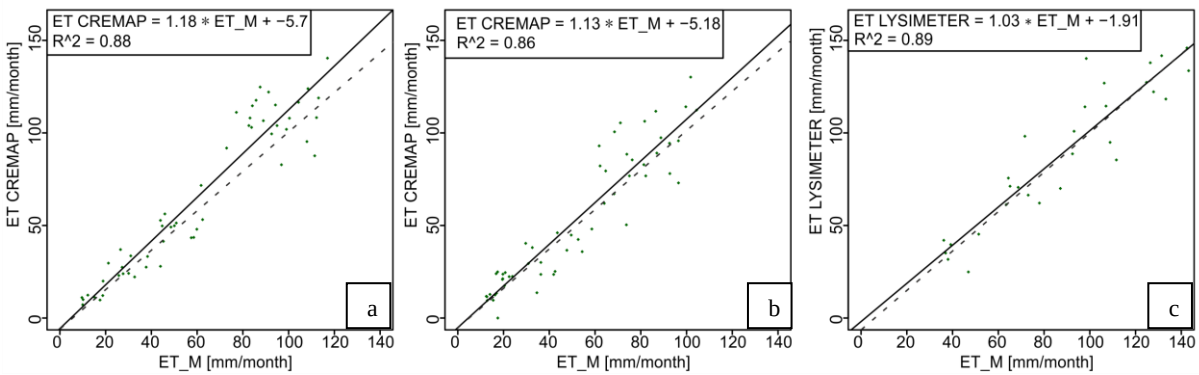

Figure 5.2. Relationship between the calculated ET_M and the measured ET_{CREMAP}/$ET_{LYSIMETER}$; i.e., the calibrated model of forested area (a), mixed parcel (b), Marchfeld (c)

The Nash-Sutcliffe coefficient (R^2_{NS}) of the calibrated models were the following: 0.85 (forested area), 0.88 (mixed parcel) and 0.88 (Marchfeld). Nonetheless, the R^2 were 0.88 (forested area), 0.86 (mixed parcel), 0.89 (Marchfeld). Consequently, the most accurate calibrated model was for Marchfeld. The reason is the more homogenous and continuously similar surface cover, which means permanently grass cover that maintained a reference conditions. However, there were not significant differences between the calibrated models. Accordingly, my model calibration and for that very reason the performance of my model is reliable.

5.4. Results of validation

Figure 5.3. represents the results of the validation. In the interests of clarity it should be noted again that the validation period differs in study areas (2009-2011 for Marchfeld, while 2006-2008 for the other two sites) due to the difference in the availability of the input data.

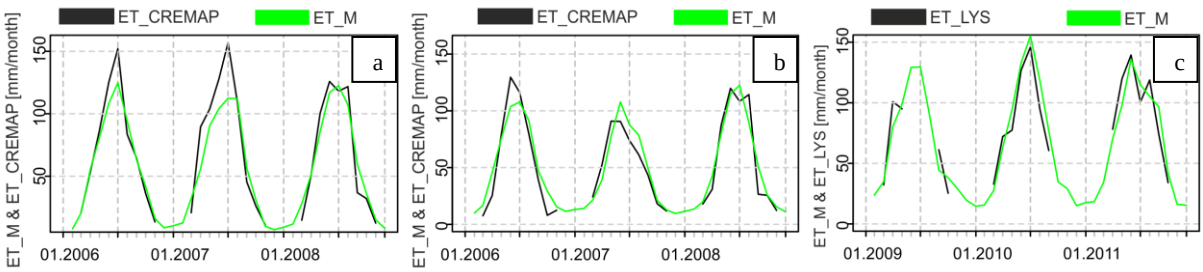

Figure 5.3. Correlation between the measured ET_{CREMAP}/$ET_{LYSIMETER}$ and calculated ET_M values (i.e., the validation of forested area (a), mixed parcel (b), Marchfeld (c)

Calculated ET_M using the weather data of the validation period (forested area and mixed parcel: 2006–2008; Marchfeld: 2009–2011) reflected good accordance with the measured data (ET_{LYS}/ET_{CREMAP}). Therefore, the R^2_{NS} values were equal with 0.88 (forested area); 0.89 (mixed parcel); 0.85 (Marchfeld), consequently each model were accurate.

In the case of forested area, greater difference has been found between the measured ET_{CREMAP} and the calculated ET_M values, particularly in the summer of 2007 (*Figure 5.3.*). The reason of the greater difference is likely due to the interception, because the model does not take this item into consideration. Nevertheless, there were larger sums of small precipitation at forested area in the months of June and July in 2007, which results in higher interception. Therefore there is an underestimation of the calculated actual evapotranspiration that causes the higher difference particularly in July 2007 at the forested area.

Although, visually the curves of the Marchfeld model fit each other the best, but in the context of Nash-Sutcliffe coefficient this model performed the "worst", due to the data loss, because of a thunderstorm in the summer of 2009.

5.5. Results of the model adjustments

As introduced the reason in *Chapter 4.5.* the model was re-calibrated for each study area using all available data as basis for the projection procedure.

Here I show the parameters of the re-calibrated models for the study sites, since those will be used in the projection phase (*Table 5.2.*).

Table 5.2. Results of the adjusted, re-calibrated model parameters for the study sites

Study sites	Re-calibrated PET parameter	Re-calibrated AET parameter
Forested area	$PET_M = 0.42 \cdot PET_H + 1.09 \cdot (PET_H - 26.04)$ $R^2 = 0.98$	$ET_{CREMAP} = 1.14 \cdot ET_M - 4.79$ $R^2 = 0.89$ and $R^2_{NS} = 0.88$
Mixed parcel	$PET_M = 0.50 \cdot PET_H + 1.05 \cdot (PET_H - 37.13)$ $R^2 = 0.98$	$ET_{CREMAP} = 1.08 \cdot ET_M - 4.31$ $R^2 = 0.87$ and $R^2_{NS} = 0.88$
Marchfeld	$PET_M = 0.54 \cdot PET_H + 1.04 \cdot (PET_H - 36.79)$ $R^2 = 0.98$	$ET_{LYS} = 1.04 \cdot ET_M - 2.36$ $R^2 = 0.88$ and $R^2_{NS} = 0.88$

Comparing the adjusted, re-calibrated and the calibrated parameters, it can be said the R^2 and R^2_{NS} values more satisfactorily in the case of re-calibrated models. However, there are not significant differences between them.

Table 5.3. demonstrates the $SOIL_{MAX}$ values after re-calibration with the calculated rooting depth as well as soil types with their field capacity and permanent wilting point, and it illustrates also a key difference between the 3 study areas. Much higher soil-water storage capacity ($SOIL_{MAX}$) was calculated for forested area due to the presence of trees (nearly 100% forest covered area), which also mean higher rooting depth and larger soil water reservoir as well. As I explained in *Chapter 4*, mixed parcel can be seen as a transition between a forest and an agricultural field, because of the presence of the poplar species. Therefore, the circa 2.5 m rooting depth is acceptable. (Note that, one can determine the rooting depth with the help of the calibrated $SOIL_{MAX}$ and soil sampling results).

Table 5.3. Soil types, values of field capacity, permanent wilting point, re-calibrated $SOIL_{MAX}$ and re-calibrated rooting depth in the study areas. Soil types were determined using the available data in the AgroClimate.2 project (forested area), soil sampling from borehole (mixed parcel). Field capacity and permanent wilting point values of forested area and mixed parcel were used in accordance with Maidment (1993)

Study sites	**Soil type**	**Field capacity [dimensionless]**	**Permanent wilting point [dimensionless]**	**$SOIL_{MAX}$ [mm]**	**Vertical extent of root zone [mm]**
Forested area	sandy loam	0.207	0.095	502.4	4486
Mixed parcel	sandy loam			276.9	2472
Marchfeld	sandy loam	-	-	142.4	890

I have used another method to determine the rooting depth in case of the Marchfeld, since θ_{fc} as well as θ_{pwp} parameters of the soil texture and plant available water (PAW) were available (*Table 5.4.*).

Table 5.4. Main properties of the soil profile in the lysimeter. Unit [$l \cdot m^{-2}$] is equal with [mm] (after personal communication with Reinhard Nolz)

Depth [cm]	**θ_{fc} [vol-%]**	**θ_{pwp} [vol-%]**	**PAW [vol-%]**	**PAW [$l \cdot m^{-2}$]**
0-20	30.1	14.9	15.2	30.4
20-40	32.7	17.2	15.5	61.4
40-60	30.4	14.7	15.7	92.8
60-80	30.2	13.5	16.7	126.2
80-100	29.7	12.3	17.4	161
100-140	30.0	11.9	18.1	233.4
140-250	1.7	0.8	0.9	-

The rooting depth (z_{rz}) was 890 mm for the first run (basic rooting depth) (*Table 5.3.*). The exact value of the rooting depth was determined using iteration between PAW values of 126.2 mm and 161.0 mm (*Table 5.4.*).

The $SOIL_{MAX}$ value for the second run (extended rooting depth) was 233.4 mm (*Table 5.4.*). The PAW value of the 100–140 cm soil profile was considered as $SOIL_{MAX}$, because the maximum possible rooting depth was set to 140 cm (as mentioned before).

Table 5.5. Results of the models after adjustment for forested area and mixed parcel (2000-2008) and Marchfeld (2004-2011) ($SOIL_{M\_MIN}$ means the lowest value of soil moisture)

Study area	ET_M [mm]	$SOIL_M$ [mm]	$SOIL_{M\_Min}$ [mm]	$SOIL_{M\_10Percentile}$ [mm]
Forested area	51	405	232	309
Mixed parcel	44	197	78	116
Marchfeld	66	112	32	71

Table 5.5. shows that the mean soil moisture values ($SOIL_M$) of each study sites – especially at Marchfeld and forested area – are usually close to the $SOIL_{MAX}$ value (both ~80%); therefore, they are usually at field capacity (i.e., at well-watered condition).

It should be noted that Marchfeld results were based on input data in which the irrigation was added to the precipitation. This is the reason why ET_M value is the highest amongst the study areas.

Nonetheless, when I did not add the irrigation amount to the precipitation the results were the following in the 2004-2011 periods: ET_M: 50 mm, $SOIL_M$: 86 mm, and the $SOIL_{M\_MIN}$ = 17 mm occurred in September.

5.6. Results and tendencies of the Regional Climate Models

Figure 5.4. represents temperature averages for study areas, while *Figure 5.5.* represents the precipitation values during the 21st century.

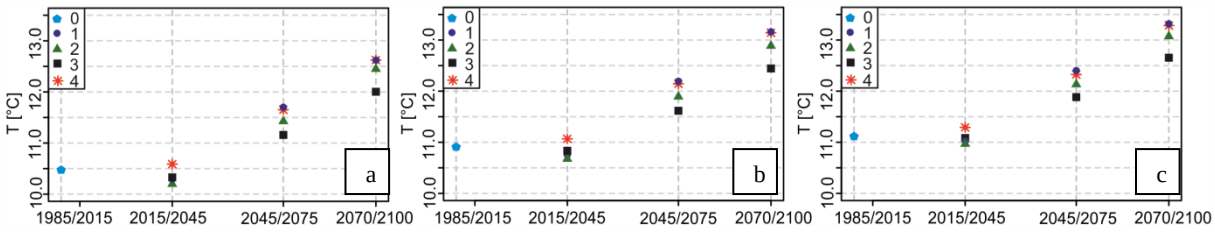

Figure 5.4. Temperature averages for forested area (a), mixed parcel (b), and Marchfeld (c) during the 21st century (Model ID '0' represents observation-based data and the regional climate model's IDs listed in Table 4.1.)

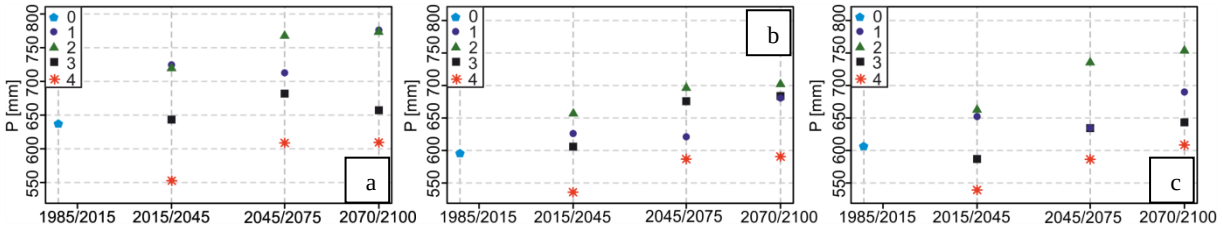

Figure 5.5. Precipitation averages for forested area (a), mixed parcel (b), and Marchfeld (c) area during the 21st century (Model ID '0' represents the observation-based data and the regional climate model's IDs listed in Table 4.1.)

Annex 5. illustrates numerically the development of temperature and precipitation according to the 4 applied RCMs during the 21st century, in case of the 3 study areas.

The annual temperature mean and the annual precipitation sum show an increasing tendency towards the end of 21st century for each study site. According to the RCMs' projection, the rate of increases in the 2070/2100 period (compared to the 1985/2015 reference period) are 1.9 °C (forested area), 1.9 °C (mixed parcel), 1.9 °C (Marchfeld); while for precipitation: 68 mm (forested area); 69 mm (mixed parcel); 71 mm (Marchfeld). The rates of the expected temperature and precipitation increase are equivalent for the 3 study areas.

The range amongst the 4 RCMs may increase towards the end of the 21st century in context of the temperature with 0.3 °C (from 0.4 °C to 0.7 °C) as the highest range at each study sites.

The value of projected temperature given by ID '2' RCM showed the lowest discrepancy from the averaged value among the 4 RCMs for temperature, whereas '3' showed for precipitation in each study sites.

The different RCMs provide different results; therefore as a basis of my projections, those differences influence the parameters (outputs) of the water balance. Comparing to the averages of the RCMs, the model with higher precipitation may indicate higher available water, while the greater temperature may cause greater potential evapotranspiration.

5.7. Results of the projections for the 21st century

Table 5.6. contains the results (means with standard deviations) of projections for the 4 investigation period.

Figure 5.6. demonstrates how the actual evapotranspiration (ET_M) is expected to change towards the end of the 21st century. Furthermore, *Figure 5.7.* illustrates the tendencies of 10th percentiles of soil moistures ($SOIL_{M\_10Percentile}$).

Table 5.6. ET_M, $SOIL_M$ and $SOIL_{M\_10Percentile}$ values (30-year means of mean values of the RCMs) with standard deviations (30-year means of standard deviations' means of the individual RCMs) in parentheses; i.e. the results of the projection for the study areas

Study sites	Parameters	1985/2015	2015/2045	2045/2075	2070/2100
Forested area	ET_M [mm · month^{-1}]	48 (38)	48 (37)	51 (39)	52 (40)
	$SOIL_M$ [mm]	417 (92)	416 (74)	415 (76)	394 (86)
	$SOIL_{M\_10Percentile}$ [mm]	208 (59)	270 (32)	271 (25)	234 (37)
Mixed parcel	ET_M [mm · month^{-1}]	43 (35)	43 (33)	45 (35)	46 (35)
	$SOIL_M$ [mm]	215 (57)	210 (61)	211 (63)	199 (69)
	$SOIL_{M\_10Percentile}$ [mm]	109 (20)	96 (15)	96 (14)	77 (21)
Marchfeld	ET_M [mm · month^{-1}]	49 (34)	49 (33)	52 (34)	53 (35)
	$SOIL_M$ [mm]	58 (40)	65 (43)	66 (44)	67 (48)
	$SOIL_{M\_10Percentile}$ [mm]	8 (3)	7 (2)	6 (3)	5 (3)

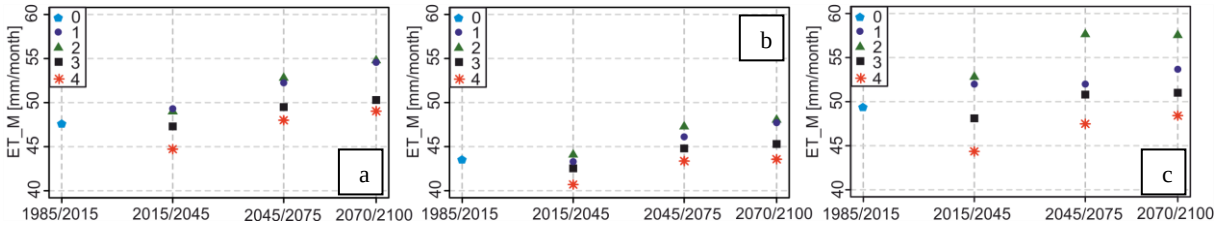

Figure 5.6. The projected means of evapotranspiration for the study areas (forested area (a), mixed parcel (b), Marchfeld (c)) between 1985/2100 on the basis of the projected temperature and precipitations derived from the 4 RCMs (Model ID '0' represents the observation-based data and the regional climate model's IDs listed in Table 4.1.)

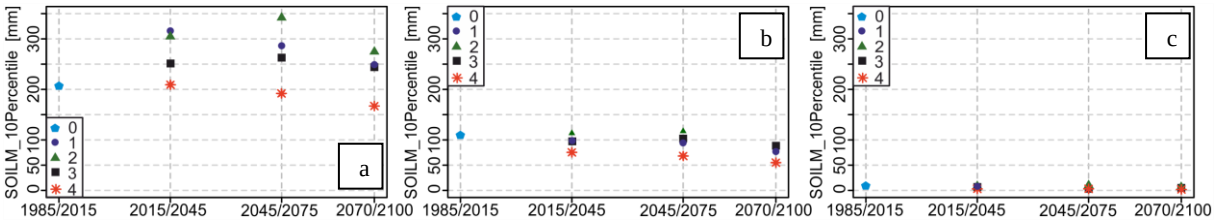

Figure 5.7. The projected 10th percentile values of soil moisture for the study areas (forested area (a), mixed parcel (b), Marchfeld (c)) between 1985/2100 on the basis of the projected temperature and precipitations derived from the 4 RCMs (Model ID '0' represents the observation-based data and the regional climate model's IDs listed in Table 4.1.)

The mean values of actual evapotranspiration (ET_M) will increase slightly at the end of the 21st century at each study site. However, it has to be noted that standard deviation of ET_M was large. This indicates a large uncertainty that is inherent to modeled data, particularly as four different RCMs were used. The rates of increase are +8%; (+4 mm·month^{-1}) in case of forested area (*Figure 5.6. a*), +8% (+4 mm·month^{-1}) at Marchfeld (*Figure 5.6. b*) and +7% (+3 mm·month^{-1}) at mixed parcel (*Figure 5.6. c*) at the end of the 21st century. The highest absolute values of ET_M were represented by Marchfeld due to the fact that RCMs project the highest temperature for the grass covered surface amongst the study areas. During the 2015/2045 period the ET_M values stagnate. However, it has to be noted that model '3' and '4' project decreasing, whereas model '1' and '2' project increasing tendencies during this 2014/2045 period. The reason of the stagnancy can be found on the temperature projections (*Figure 5.4.*), which demonstrate -0.2 °C decrease for forested area, -0.1 °C for mixed parcel and 0 °C for Marchfeld on the 2015/2045 period. Unlike the first part of the 21st century, there is a typical increasing tendency on the second part of the century at each study area. Furthermore, the most considerable upward rate appears in the 2045/2075 period. Amongst the 4 RCMs, model '4' demonstrates the lowest values of ET_M with stagnancy or even a little decrease, whereas model '2' shows the highest values as well as the greatest increase. Unsurprisingly, model '4' has the lowest precipitation values, while the latter has the highest (nearly 100 mm larger precipitation values for the 2045/75 period than the average), as mentioned before. ET_M values derived from the '3' model are the closest to the average values from the 4 RCMs in each study area. The range of the ET_M values amongst the 4 RCMs may increase at the end of the 21st century with 1.5-2.5 mm. The values of the range

are 6 mm at the forested area, 4.5 mm at the mixed parcel and 9.5 mm at the Marchfeld increase at the end of the 21st century.

Contrary to the tendencies of ET_M values, there are larger differences amongst the study sites in context of the mean values of soil moisture ($SOIL_M$) (*Table 5.6.*), because of the larger differences in the $SOIL_{MAX}$ values. Therefore, forested area has the highest and Marchfeld has the lowest soil moisture mean values. I found decreases for the forested area (-6%; -23 mm) and mixed parcel (-7%; -16 mm), but increases for Marchfeld (+12%; +9 mm) at the end of the 21st century.

With regard to plant water uptake, the minimal available soil water might be of interest (*Figure 5.7.*). Therefore, minimum soil moisture values were calculated as 10th percentile minimums ($SOIL_{M\_10Percentile}$). Nevertheless, the percentile analyses offers key information in context of water stress representing different results, than $SOIL_M$ values. In one hand, forested area has increasing $SOIL_{M\_10Percentile}$ values (+11%; +26 mm) at the end of 21st century (compared the 2070/2100 period to the 1985/2015 reference period). This can be explained through the deep root zone (~4.5 m) and for that very reason the great $SOIL_{MAX}$, which means more amount of available water for the plants (larger soil moisture reservoir). There is significant increasing (+23%; +62 mm) in the 2015/2045 period, stagnancy (+1%; +1 mm) in the 2045/2075 period but significant decreasing (-16%; -37 mm) in the 2070/2100 period. On the other hand, there is significant decreasing tendency at the mixed parcel (-29%; -32 mm) and for Marchfeld (-37%; -3 mm). It should be noted, that $SOIL_{M\_10Percentile}$ percentile values of Marchfeld are really close to zero (*Figure 5.7. c*) due to the lowest vertical extent of the root zone as well as lowest $SOIL_{MAX}$ value amongst the 3 study sites. Furthermore, a nearly equal drop rates occur at mixed parcel (-12%; -13 mm) and Marchfeld (-13%; -1 mm) in the 2015/2045 period. Stagnancy has been found in the 2045/2075 period at mixed parcel (0%; 0 mm), but decreasing at Marchfeld (-14%; -1 mm), while a bit more considerable downward trend can be observed at the end of the 21st century at mixed parcel (-29%; -19 mm); however nearly equal decreasing rates at Marchfeld (-17%; -1 mm). The range of the $SOIL_{M\_10Percentile}$ values amongst the 4 RCMs may stagnate at the end of the 21st century, but basically increase in the 2045/2075 period. The highest values of range were found in case of the forested area.

The previous analyses are based on annual mean values, which were applied to compute the average values for the four 30-year-long investigation periods. These analyses however, do not point out the monthly development of output parameters of the models; consequently another research is needed, which focuses on the 30-year monthly mean of ET_M plus $SOIL_M$.

Figures 5.8., 5.9. and *5.10.* emphasize the changes in the 30-year monthly means of ET_M, while *Figures 5.11., 5.12.* and *5.13.* highlight the seasonal periodicity in context of $SOIL_M$. Unlike the previous analyses, those figures demonstrate only the mean changes of the water balance outputs in the different investigation periods for the mean of the 4 RCM_S.

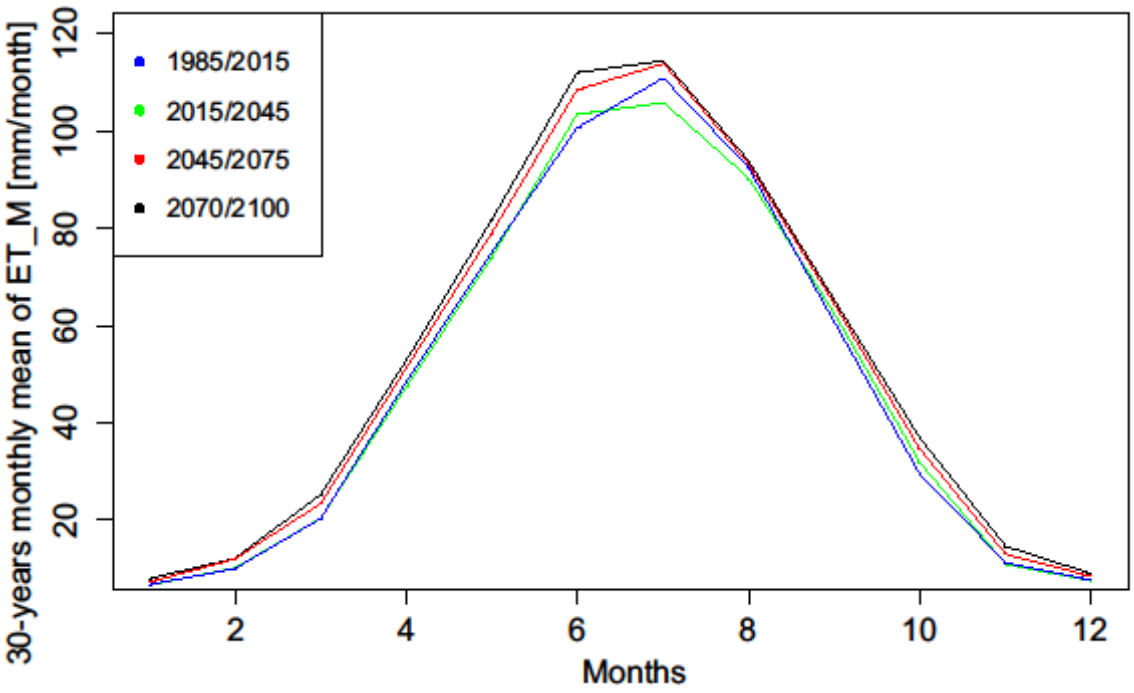

Figure 5.8. Monthly values of ET_M in the case of forested area for the investigated 30-year means

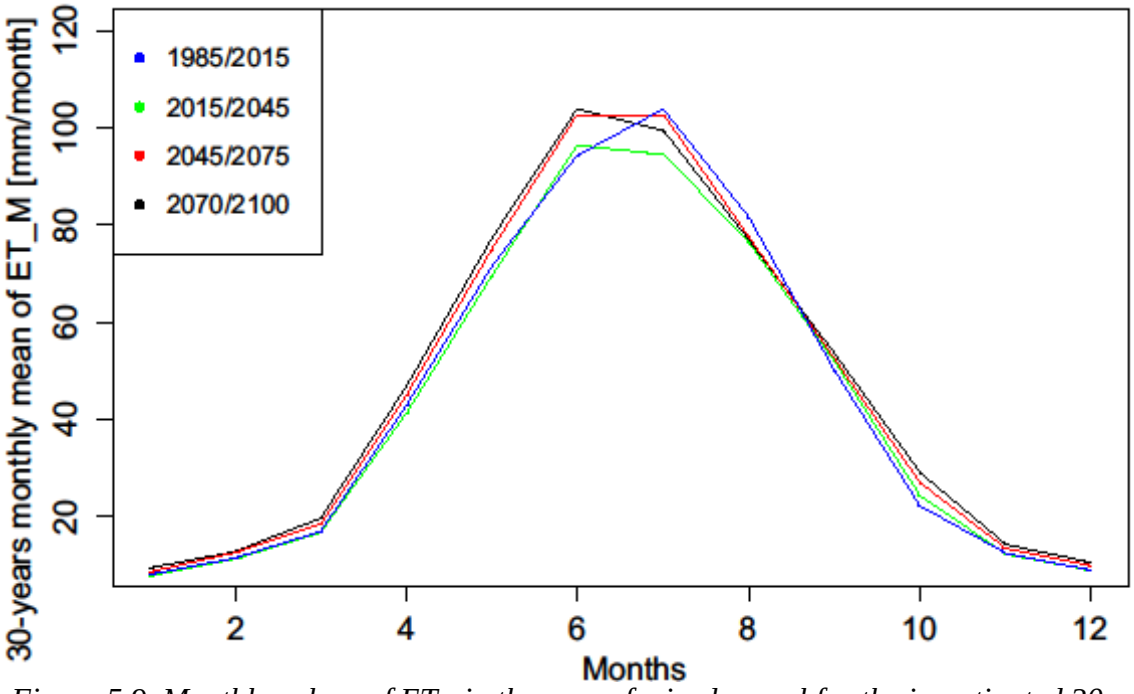

Figure 5.9. Monthly values of ET_M in the case of mixed parcel for the investigated 30-year means

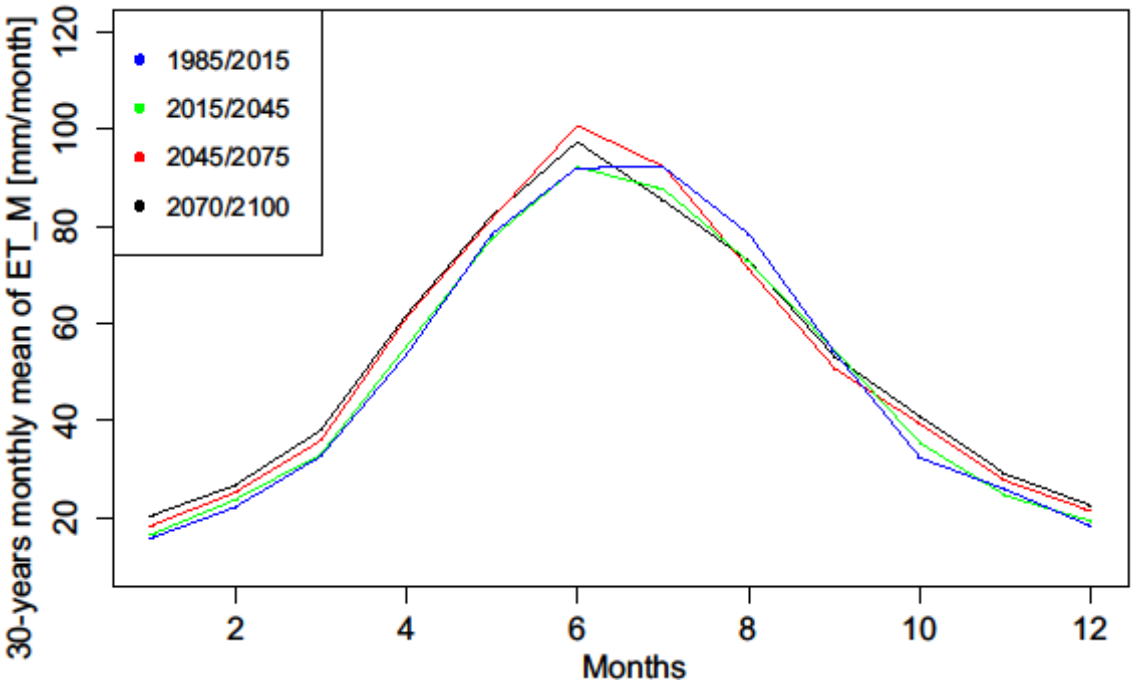

Figure 5.10. Monthly values of ET_M in the case of Marchfeld for the investigated 30-year means

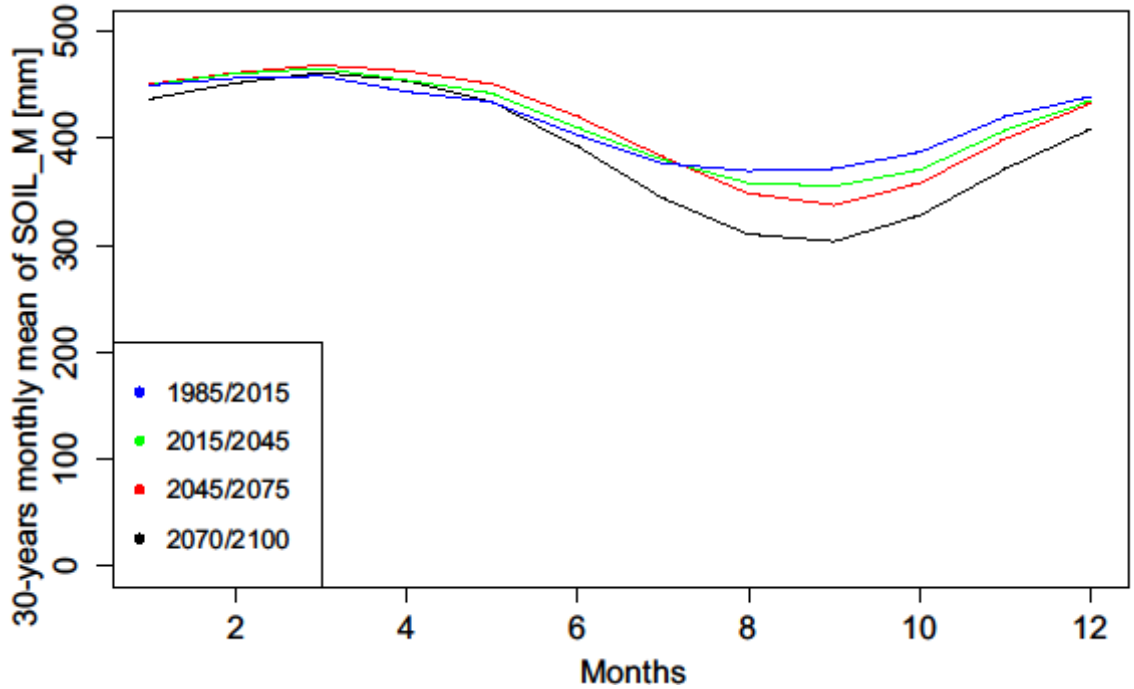

Figure 5.11. Monthly values of $SOIL_M$ in the case of forested area for the investigated 30-year means

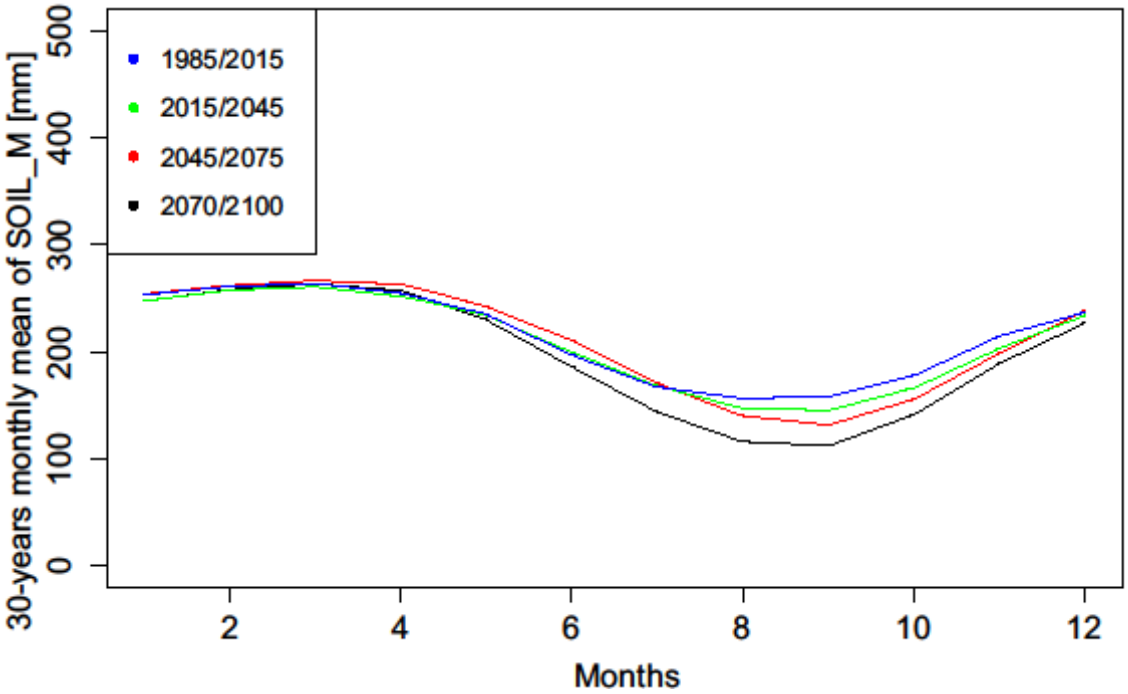

Figure 5.12. Monthly values of $SOIL_M$ in the case of mixed parcel for the investigated 30-year means

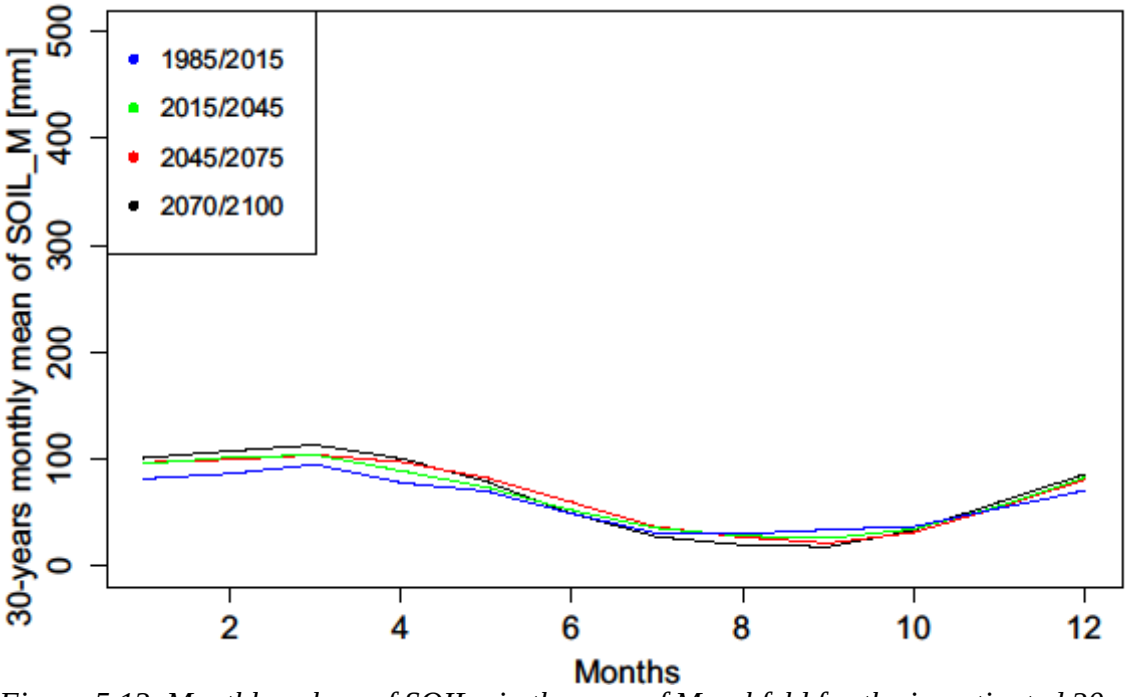

Figure 5.13. Monthly values of $SOIL_M$ in the case of Marchfeld for the investigated 30-year means

Considering the 30-year monthly mean of ET_M, the greatest values occur in June and July, whereas the smallest in December and January at each study site. It can be explained through the greater transpiration in summer period that generates higher evapotranspiration values in the growing season. In addition, a quick jump illustrates the starting of the biological activity of plants from April (*Figure 5.8.*, *5.9.* and *5.10.*). The values of ET_M generally increase towards the end of 21st century, particularly in summer period (10-15 mm · month^{-1}) which

means 10-13% upward rates and therefore it is significant. The reason of the increasing is the intensifying evapotranspiration constraint towards the end of the 21st century, which caused by the likewise intensifying temperatures in summer period. However, in case of Marchfeld the largest values appear in the 2045/2075 period. Nevertheless, the greatest differences occur amongst the investigation periods in summer as well. Similarly to the annual averages, the 1985/2015 period shows larger ET_M values, than the 2015/2045 period. Although, in the context of annual averages, the Marchfeld has the highest values of ET_M, but the calculation of 30-year monthly mean of ET_M reveals that the forested area and even the mixed parcel have higher ET_M maximum values in the summer period (as well as greater jump of values from the starts of growing season). Hence, the shape of the curves of Marchfeld (*Figure 5.10.*) is more flat than the other two, with higher values on winter, but lower values in summer. The reason of the higher values at Marchfeld in the dormancy is that in the case of grass surface the growing season starts earlier. In addition, the grass can transpire even in winter periods contrary to forests (as can be seen the higher values in winter at Marchfeld (*Figure 5.10.*)), which basically means deciduous species in the case of forested area. The maximums of ET_M in summer are the following: 115 $mm \cdot month^{-1}$ (forested area); 105 $mm \cdot month^{-1}$ (mixed parcel); 100 $mm \cdot month^{-1}$ (Marchfeld). The reason is the higher leaf area index of the forests, which leads to higher evaporative surface, characteristically in the growing seasons.

The 30-year monthly mean of $SOIL_M$ demonstrate a slightly increase from January to March, when the soil is saturated, and the values of $SOIL_M$ are the closest to the water storage capacity ($SOIL_{MAX}$). From March to September there is an intensifying decrease of the soil moisture due to the rising evapotranspiration, which consume the soil moisture. Consequently, the minimum values occur in early autumn. The minimums appear exactly in September for each study area (*Figure 5.11., 5.12.* and *5.13.*). At least, from September intensifying increases happens because of the transition to the dormant season.

Comparing the 3 study sites, the difference is more significant concerning the 30-year monthly mean of $SOIL_M$ values than of ET_M values. The highest $SOIL_M$ and ET_M values are observed at the forested area. Forested area and mixed parcel shows equal annual fluctuation (~150 mm), whereas the lowest values of ET_M and $SOIL_M$ and smallest fluctuation of $SOIL_M$ (~90 mm) are revealed at Marchfeld. The rates of the annual soil moisture fluctuations and soil moisture storage capacity ($SOIL_{MAX}$) are lowest in case of the forested area (30%) but highest at Marchfeld (63%). *Figure 5.11., 5.12.* and *5.13.* confirm that the highest $SOIL_M$ values appear at the beginning of the investigation period, but lowest values occur at the end of the 21st century, consequently there is a decreasing tendency. Furthermore, the greatest differences between the investigation periods appear in case of the forested area.

The previously written facts reveal that the water stress probability may increase towards the end of the 21st century; therefore water stress should be analyzed in detail.

5.8. Results of the water stress analyses

The first part of the water stress analysis means the evaluation of relative extractable water (REW; *eq. 4.19.*) and soil water deficit (SWD; *eq. 4.20.*).

Figure 5.14., 5.15. and *5.16.* illustrate the development of the relative extractable water in the 21st century, with the defined 50% threshold for each study sites. *Table 5.7.* summarizes the values of REW derived from the four applied RCMs for each investigation period. For the 1985/2015 period, each study area has one value, since the FORESEE database contains one observation based on the time series of this period. The REW values of this period are the following: 0.83 (forested area); 0.78 (mixed parcel) and 0.42 (Marchfeld). As can be seen, the values decrease under the 50% threshold only at Marchfeld, which means water stress assumed to occur only at Marchfeld.

Table 5.7. The values of relative extractable water (REW) in the 21st century for the study areas

Study area	Model ID	2015/45	2045/75	2070/2100
Forested area	1	0.89	0.85	0.83
	2	0.89	0.91	0.85
	3	0.83	0.83	0.78
	4	0.69	0.71	0.65
	Avg.	0.83	0.82	0.78
Mixed parcel	1	0.78	0.76	0.73
	2	0.81	0.81	0.75
	3	0.77	0.79	0.76
	4	0.67	0.69	0.62
	Avg.	0.76	0.76	0.71
Marchfeld	1	0.51	0.43	0.46
	2	0.51	0.57	0.54
	3	0.42	0.47	0.48
	4	0.38	0.38	0.38
	Avg.	0.46	0.46	0.46

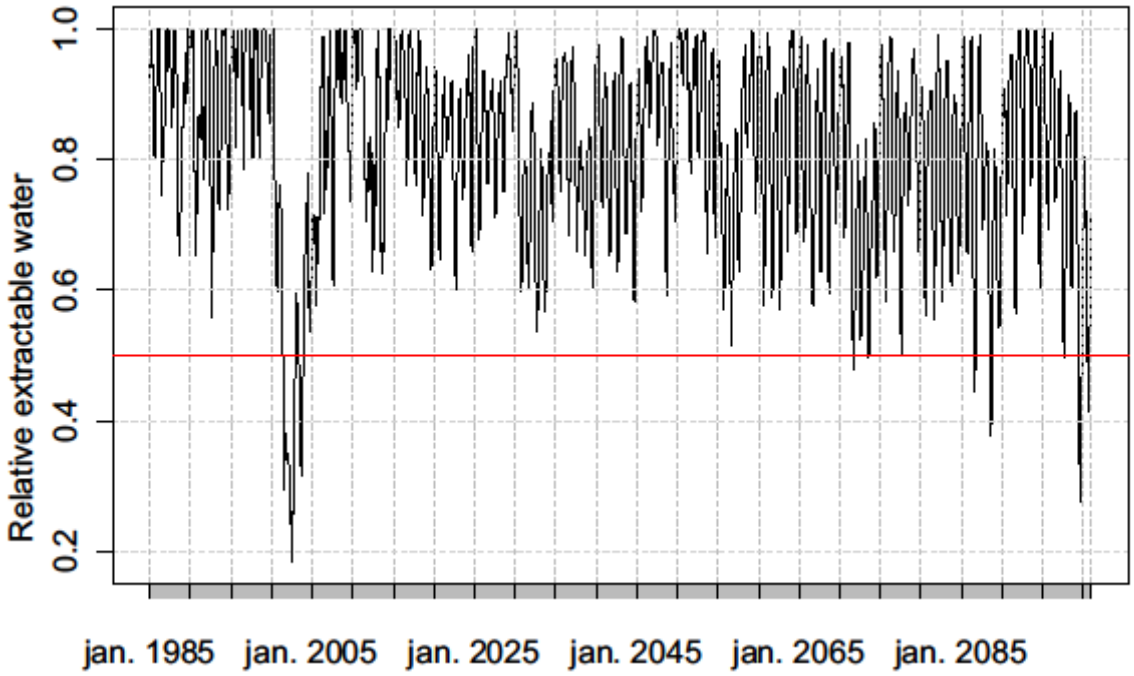

Figure 5.14. Relative extractable water in the case of the forested area

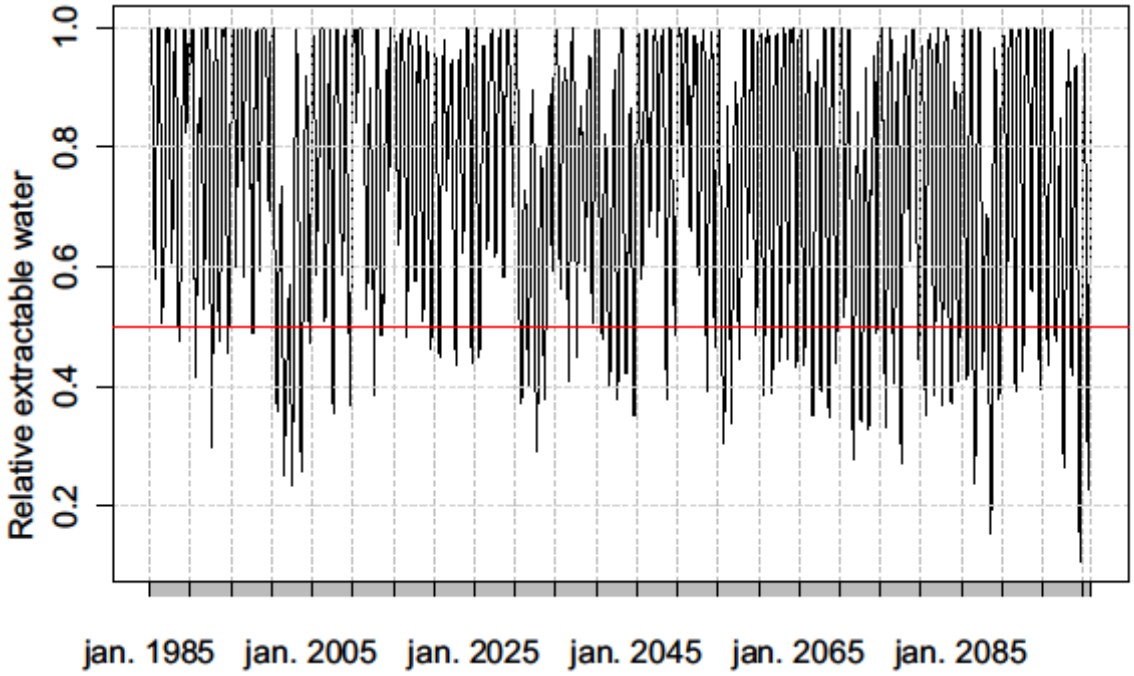

Figure 5.15. Relative extractable water in the case of the mixed parcel

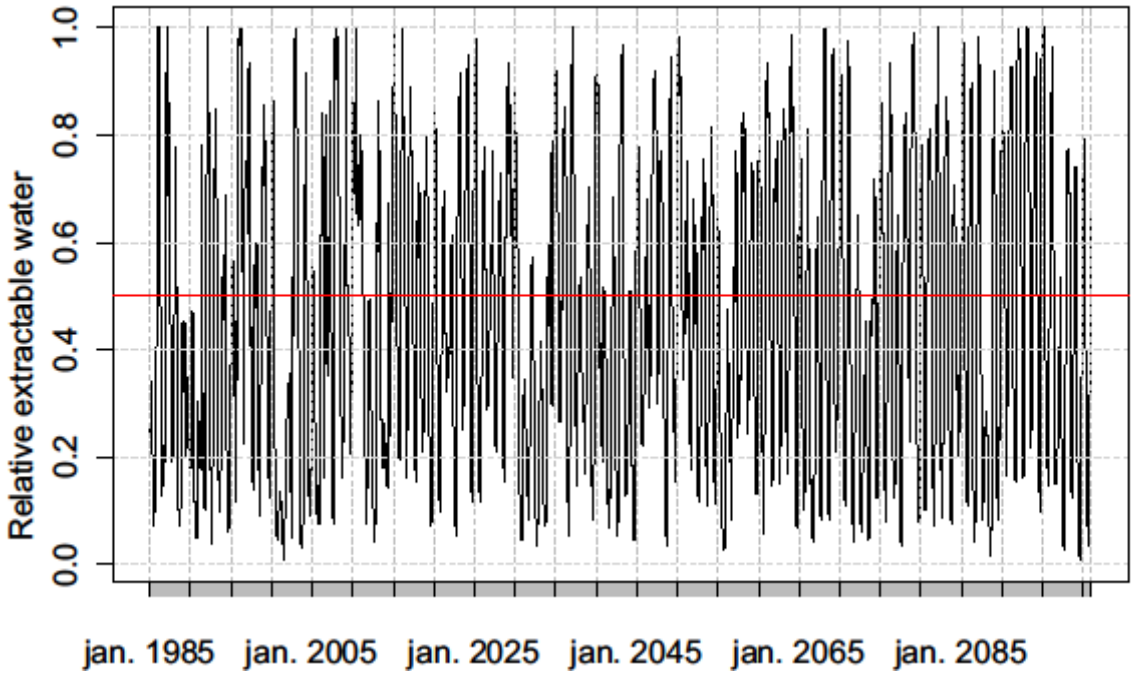

Figure 5.16. Relative extractable water in the case of the Marchfeld

There is a decreasing tendency of REW values towards the end of the 21st century, in case of forested area and mixed parcel. However, the average REW values do not approach the 50% threshold (forested area: from 83% to 78%; mixed parcel: from 78% to 71%). Furthermore, REW values at the Marchfeld decrease below under the 50% threshold more frequently, consequently water stress is assumed to occur. However, there is an increasing tendency of REW values at Marchfeld (from 42% to 46%).

The soil water deficit (SWD) values of the 1985/2015 period are: 0.07 (forested area); 0.11 (mixed parcel); 0.64 (Marchfeld). The results of SWD calculations based on the RCM's results can be found on *Table 5.8. Figure 5.17.*, *5.18.* and *5.19.* demonstrate the tendencies of SWD values towards to the 21st century in absolute values.

Table 5.8. The values of soil water deficit (SWD) in the 21st century for the study areas

Study area	Model	2015/2045 [%]	2045/2075 [%]	2070/2100 [%]
Forested area	1	0	0.01	0.05
	2	0.01	0	0.02
	3	0.04	0.04	0.05
	4	0.15	0.16	0.24
	Avg.	0.05	0.05	0.09
Mixed parcel	1	0.14	0.17	0.22
	2	0.11	0.11	0.20
	3	0.19	0.14	0.17
	4	0.28	0.27	0.39
	Avg.	0.18	0.17	0.24
Marchfeld	1	0.51	0.61	0.59
	2	0.49	0.44	0.49
	3	0.65	0.58	0.55
	4	0.68	0.69	0.69

	Avg.	0.58	0.58	0.58

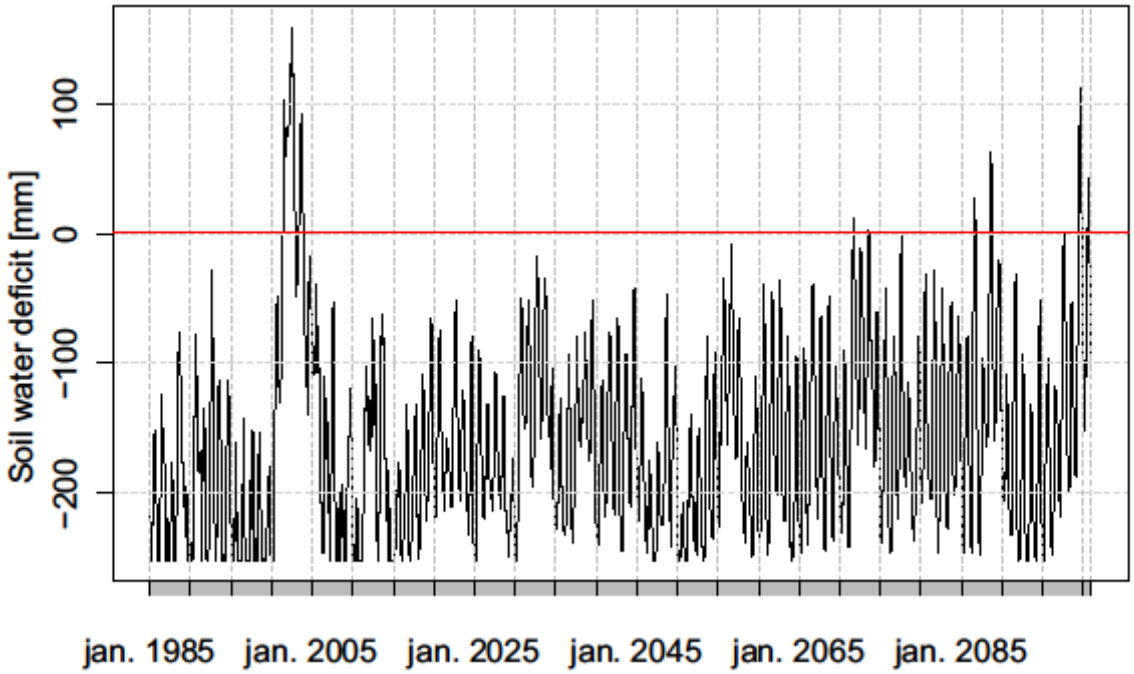

Figure 5.17. Soil water deficit (SWD) values of forested area

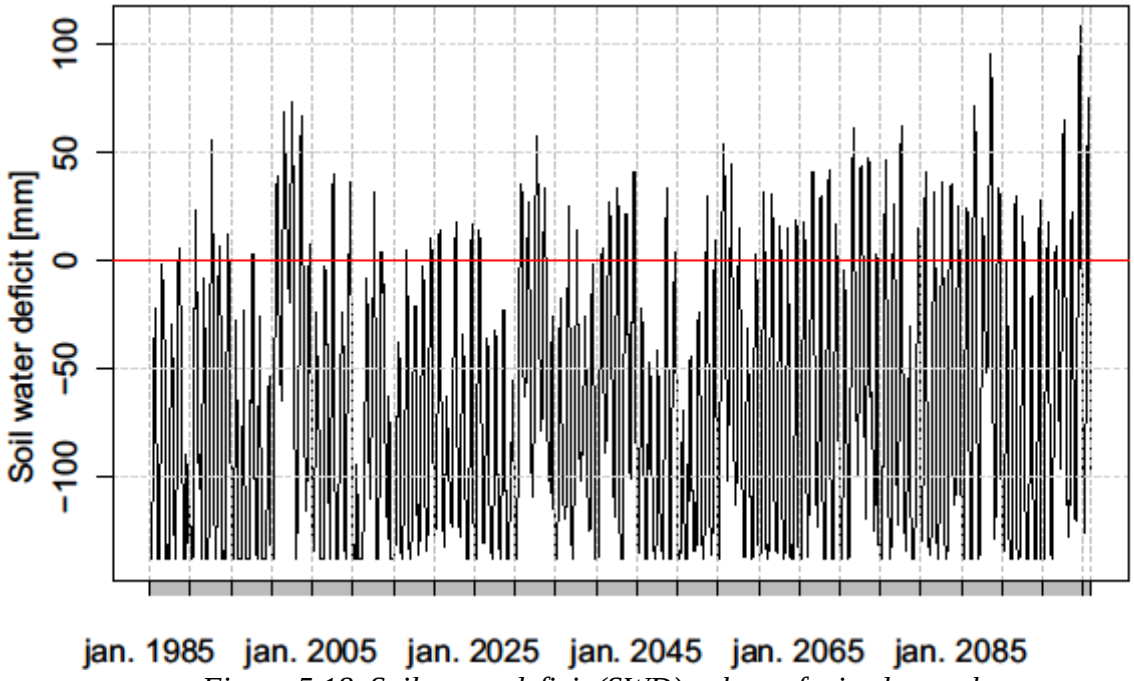

Figure 5.18. Soil water deficit (SWD) values of mixed parcel

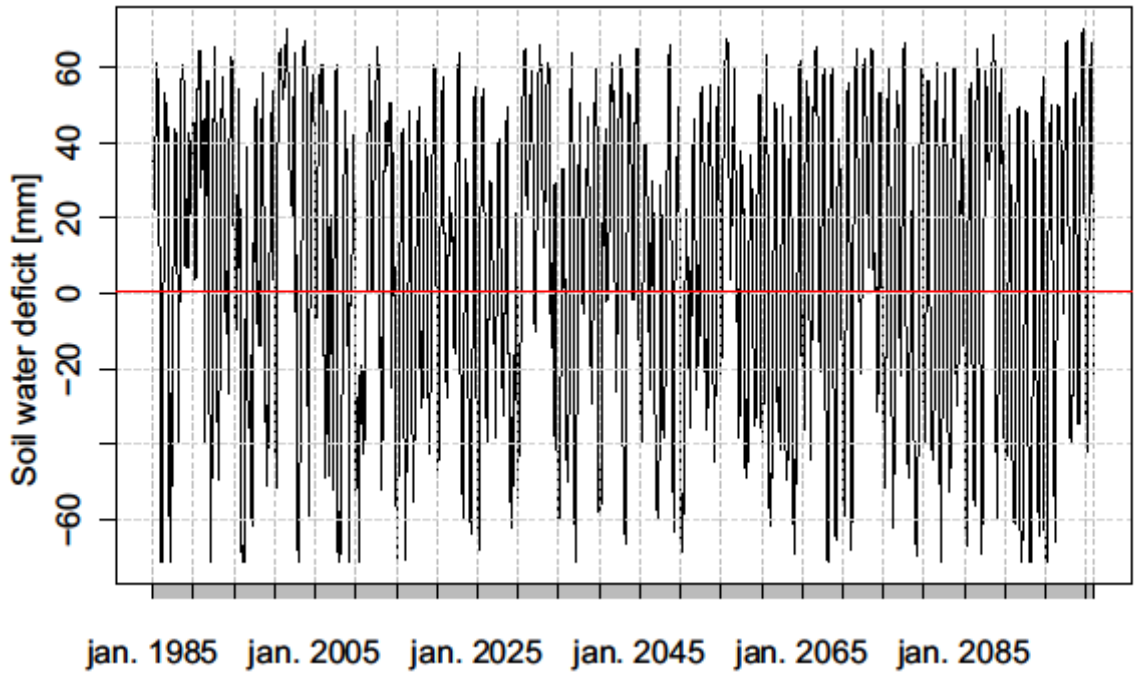

Figure 5.19. Soil water deficit (SWD) values of Marchfeld

The higher SWD values (both absolute and percentile form) mean higher water stress, since the term expresses deficit (i.e., higher value is equal to higher deficit).

Similarly to the REW values, the forested area as well as mixed parcel show negative tendency towards the end of 21st century. Nonetheless, the monthly rates, wherein water stress assumed to occur, are insignificant even at the end of the 21st century (forested area: 9%; mixed parcel: 24%). At Marchfeld, however there are not significant changes towards to the 21st century (stagnate in 58%), but the monthly SWD values exceed the 50% threshold in each investigation period.

To summarize the previous result, it can be concluded that Marchfeld area is where significant water stress can occur in the future. However, water stress also significant in the 'present' (1985/2015 reference investigation period) at Marchfeld. This is mainly the consequence of the relatively small $SOIL_{MAX}$ value of this grass covered area. The small $SOIL_{MAX}$ value leads to small rooting depth as well as smaller soil moisture reservoir. Consequently, the mean soil moisture values ($SOIL_M$) and particularly the $SOIL_{M\_10Percentile}$ values are also small, which can be very close to 0 (wilting point).

5.9. Comparison of the static rooting depth and the adaptive rooting depth of the plants at Marchfeld

I compared two basic conditions regarding the rooting zone. The first simulation (first run) was based on a rooting depth corresponding to the characteristics of the lysimeter that was used for the calibration/validation procedure (static rooting depth of the plants). This condition, has been evaluated in the previous (5.7.) subchapter.

The assumption of the second simulation (second run) was that the plants can adapt to water stress conditions by increasing their rooting depth in order to meet their water demand using a larger soil water reservoir (extended rooting depth of the plants).

In this subchapter I present the results of the first and second runs, respectively (*Table 5.9.*, *Figure 5.20.* and *5.21.*).

Table 5.9. Comparison of the ET_M, $SOIL_M$ and $SOIL_{M\_10Percentile}$ values of static and extended rooting depths at the Marchfeld

Parameters	1985/2015 [mm]	2015/2045 [mm]	2045/2075 [mm]	2070/2100 [mm]
$ET_{M\ [static\ rooting\ depth]}$	49 (34)	49 (33)	52 (34)	53 (35)
$ET_{M\ [extended\ rooting\ depth]}$	50 (33)	51 (32)	53 (33)	55 (33)
$SOIL_{M\ [static\ rooting\ depth]}$	58 (40)	65 (43)	66 (44)	67 (48)
$SOIL_{M\ [extended\ rooting\ depth]}$	92 (51)	105 (57)	105 (58)	108 (64)
$SOIL_{M\_10Percentile\ [static\ rooting\ depth]}$	8 (3)	7 (2)	6 (3)	5 (3)
$SOIL_{M\_10Percentile\ [extended\ rooting\ depth]}$	26 (6)	24 (7)	22 (6)	19 (7)

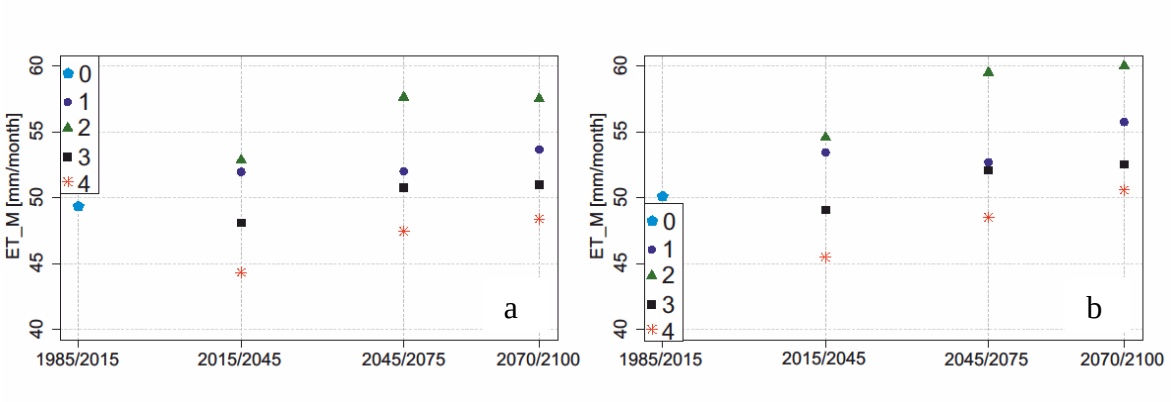

Figure 5.20. The projected ET_M values between 1985-2100; a: first run, and b: second run

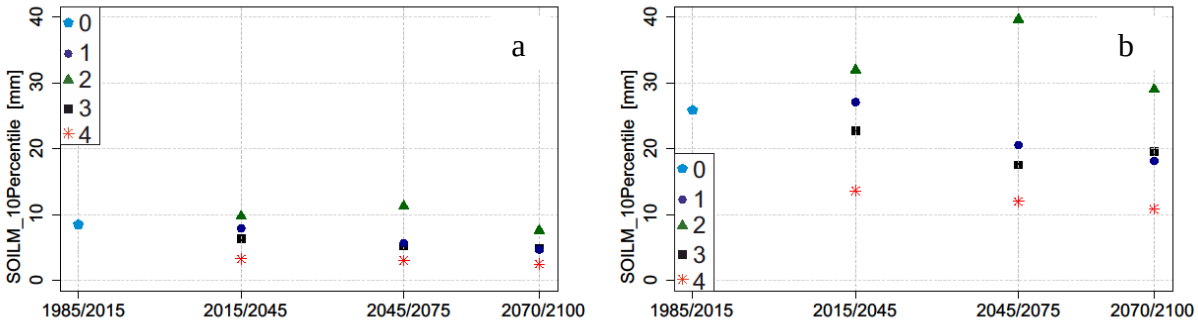

Figure 5.21. The projected 10^{th} percentile minimum values of soil moisture between 1985-2100; a: first run, and b: second run

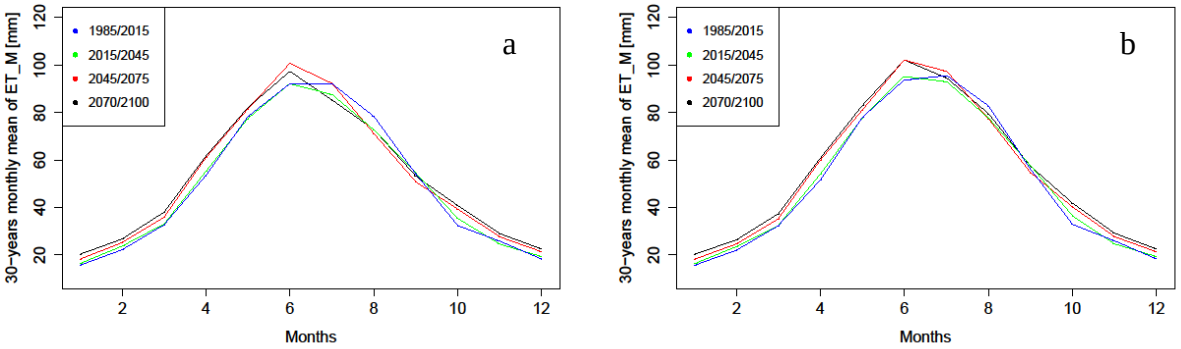

Figure 5.22. Monthly values of ET_M in the projection periods; a: first run, and b: second run

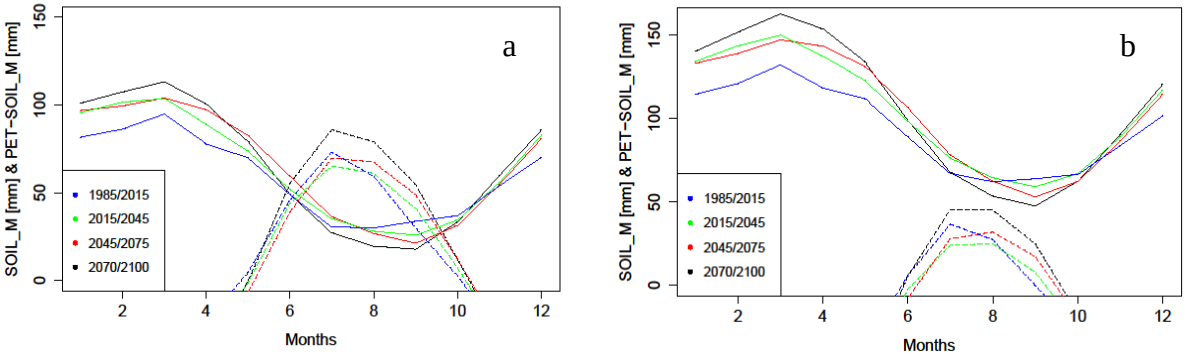

Figure 5.23. Monthly values of $SOIL_M$ in the projection periods (solid lines) and estimated soil water deficit calculated as potential ET minus $SOIL_M$ (dashed lines); first run (a) and second run (b)

Comparing the first run (*Figure 5.20.a*) with the second run (*Figure 5.20.b*), minor differences are revealed, which can be associated to the simulated availability of soil water. Availability of soil water, represented by averaged $SOIL_M$ values, followed an upward tendency (*Table 5.9.),* mainly because of the underlying increasing precipitation. With regard to the plant water uptake, the minimal available soil water might be of interest. Therefore, the minimum soil moisture values were calculated as the 10th percentile minimums ($SOIL_{M\_10Percentile}$). The general trend of the respective $SOIL_{M\_10Percentile}$ values was decreasing as mentioned before, but there are remarkably larger values for the second run (*Figure 5.21.b*). The difference between the averages of the first and second run is 16 mm in average, during the investigation period. It is evident that the larger soil-water storage capacity, as assumed for second run, provided better conditions for plant growth. The four RCMs' evapotranspiration (ET_M) values showed similarity to each other during the entire 21st century (*Figure 5.20.*).

In order to analyze the tendencies of the 30-year monthly means, the corresponding values of ET_M and $SOIL_M$ are illustrated in *Figure 5.22.* and *Figure 5.23.*, respectively. The largest values of ET_M appeared in June (95-100 mm for basic rooting depth; 98-105 mm for extended rooting depth). Smallest $SOIL_M$ can be found in September (12.5-25 mm for static rooting depth; 50-60 mm for extended rooting depth), which is typical after summer and at the end of

the vegetation period. The largest values of $SOIL_M$ appeared in March (115 mm and 165 mm) – at the end of the dormancy and after winter precipitation. Consequently, also the decrease of soil moisture from April to August can be typically explained by plant water uptake (*Figure 23.*).

Beside the evident seasonal trend, *Figure 5.23.* illustrates a shift of soil moisture between summer and winter. While $SOIL_M$ values predicted for the period 2070/2100 are largest in winter (in relation to the other projections), $SOIL_M$ are the smallest during the summer. The reason may be the higher precipitation amount, which will provide the replenishment of soil moisture in the dormancy, while the increasing temperature can lead to larger evapotranspiration and consequently higher rate of water consumption by the plants in the growing season.

In order to estimate periods with potential water stress, a simple water balance was established. The resulting values – calculated as PET_H minus $SOIL_M$ – are illustrated in *Figure 5.23.* If those values are positive and it exceeding soil moisture values, then potential water stress will occur. With respect to the basic rooting depth as considered for the first run, potential water stress was pronounced from June to September with the largest deficit in July, when ET_M is at maximum and $SOIL_M$ is low (*Figure 5.23. a.*). Comparing the projection periods, the deficit is assumed to increase in future. For the 2070/2100 period, the deficit was approximately 50 mm in the first run, for instance. Consequently, periods of water stress are assumed to occur more often and the shortage of the available water is assumed to increase, although more soil water might be available in total (*Table 5.9.*).

The larger $SOIL_{MAX}$ value of the second run implied larger $SOIL_M$ values (*Figure 5.23. b*). As a consequence, water stress did not occur under these simulation preconditions (second run).

6. Discussion and Conclusions

In this study, a Thornthwaite-type water balance model was adapted and applied to assess the future development of evapotranspiration (ET_M) and soil moisture ($SOIL_M$) in the western part of the Carpathian Basin. The input data for the water balance model originated from the *AgroClimate.2* project, in the case of forested area and mixed parcel. For Marchfeld, the meteorological parameters were measured by a reference weather station of the World Meteorological Organization (WMO) standard while the quality and integrity of meteorological data of the period 2004–2010 were verified by the Central Institute for Meteorology and Geodynamics, Austria (ZAMG). Consequently, I utilized the best input data, since another more accurate were not available. PET was calculated using the approach of Hamon. As this part of the model has a substantial impact on the determination of all other water balance components, a certain focus was set on the calibration and validation. For this purpose, a correlation was computed between calculated data (ET_M) and measured data from a remote-sensed AET maps (ET_{CREMAP}) and a weighing lysimeter (ET_{LYS}), which were representative for the study sites. Subsequently, the determined relationship was tested on a validation data set, and it proved to be reliable. Validation of the results of ET_{CREMAP} was performed with the help of three eddy-covariance sites and five catchment-scale water-balance closure data (*Szilágyi* et al., 2011). The overall strong correspondence between the measured and the estimated evapotranspiration with typical R^2 values at annual level, which were between 0.7 – 0.8), while on the monthly basis the ET estimates resulted in an R^2 value of 0.8 – 0.9 (*Szilágyi* et al., 2011). Nevertheless, the comparison of the 9-years average ET values of the CREMAP method with the MODIS Global Evapotranspiration Project (MOD16) revealed that the CREMAP method (RMSE=17.20 mm/y) provided better results than the MOD16 (RMSE=34.12 mm/y) (*Kisfaludi* et al., 2015). They applied the ET of nine watersheds (with known water balance) as reference. The weighing lysimeter (ET_{lys})) (measured data) at the Marchfeld were compared with calculated reference ET between 2005 and 2010, which means the standardized form of the popular FAO Penman-Monteith equation. The validation's results proved a good accordance between measured and calculated values. In one hand, the total mean deviation was 0.01 mm with an average root mean square error (RMSE) of 0.55 mm. On the other hand, the average of the R^2 was 0.92 (*Nolz* et al., 2016).

ET_M and $SOIL_M$ were simulated for three periods of the 21st century (2015–2045; 2045–2075; 2070–2100). Input data were obtained from four different RCMs (and those data are based on the A1B greenhouse gas emission scenario (*IPCC*, 2000)) to illustrate the uncertainties (the bandwidth of simulation results) of the projections resulted from the choice of the RCM. All climate projections have uncertainties inherently, which related to the future path of emissions considering the climate change as well as associated impacts. The future path of emissions, determined by the total effect of global development of technology, energy consumption, world population, as well as many other socio-economic factors. Moreover, the limitation in climate models needs to be taken into account as well. The reason of this limitation is because of our understanding of the climate system (i.e. the complexity (involves processes at many spatial and temporal scales) and/or randomness of the processes and systems) therefore

simplifications are required in the climate models (*URL14*). I applied bias-corrected models; however, they does not give exact prediction for the future. Mean of the simulation results were calculated for further interpretations. My study indicates an increasing tendency of actual evapotranspiration towards the end of the 21st century, with higher annual fluctuation as well as with greater peaks for summer. The soil moisture monthly average values, however, show no clear trend, or even a little increase during this century, whereas the 10th percentile minimums show decreasing tendency and greater annual fluctuation (particularly in the early autumn, when the lowest values are occurred) towards the end of the 21st century. The analyses revealed that significant water stress is assumed to occur only in case of the grass covered surface (Marchfeld). However, the possibly maximum of rooting depth, which can be extended by the plants, may compensate or even save them from water stress. The results also indicate that increasing soil-water storage capacity can be an adequate adaption strategy to mitigate climate change effects in the investigated area. Furthermore, intensified and optimized irrigation strategies might become necessary during summer months, and modern water harvesting systems might help transferring water from relative moist months to dry periods in summer. However, the presented simulations only provide some basic investigations, where a relatively straightforward model approach was adapted and applied to regional conditions. On this basis, further research should address and consider for example different soil and crop characteristics.

The introduced studies about the impact analysis of water balance models (*Chapter 2.9.*) applied mainly Thornthwaite-type, monthly-step water balance model, but basically evaluate their results annually, instead of monthly or seasonal scale as in this dissertation have been done.

Comparing *Granier* et al. (1999) results to my results, I have relatively deep soils i.e. 4.5 m (forested area), 2.4 m (mixed parcel), 0.9 m (Marchfeld) as rooting depths. Contrary to *Granier* et al. (1999), I used only one soil layer, however; they stated that soil profile can be considered as one layer if there is not enough available information about its characteristic. As a consequence of the deep soils, much higher $SOIL_{MAX}$ values, 502.4 mm (forested area); 276.9 mm (mixed parcel) and 142.4 mm (Marchfeld) have been found, than in their study: 180 mm (coniferous stand with deep soil), 185 mm (broad-leaved stands with deep soil), and 72 mm (broad-leaved stands with shallow soil). Unlike *Granier* et al. (1999), I used a more general 0.5 (50%) value, instead of 0.4 (40%) as threshold. I found an increasing tendency towards the end of the 21st century, when monthly REW values decrease below the 50% threshold in case of forested area and mixed parcel. However, the average REW values do not approach the threshold (forested area: 78%, as lowest rate; mixed parcel: 71%). Furthermore, the REW values of Marchfeld decrease below under the 50% threshold more frequently, but show even an increasing tendency (from 42% to 46%). According to *Granier* et al. (1999), the REW values did not drop below the 0.4 threshold in the wettest years in the case of deep soils, not even in the months, when the lowest values occurred (mainly in August and September). Nevertheless, REW values drop below 0.4 in the driest years, not just in the areas with shallow soils, but also in the areas with deep soil.

In *Remrová and Císleřová* (2010) study, the vertical extent of root zone was lower (and the soil profile was also shallower) than in my sites. However, I could only compare their grass

covered study area with my likewise grass covered surface (Marchfeld). The Marchfeld has 69 cm greater rooting depth compared to the grass covered area of Remrová and Císleřová (2010). Generally, the greater rooting depth is due to the lesser soil storage, which causes lesser water stress. However, the climate of their study area is more humid (1200 mm annual average precipitation) as well as colder (8.1 °C annual air temperature), consequently they found insignificant water stress (with only 6 days in the summer period of 2095). It has to be noted that they used other climate scenario (A2), which projections are more pessimistic particularly at the end of the 21st century, than A1B scenario (applied in this dissertation). They applied only one RCM (HIRHAM driven by the global model HADCM3), whereas I utilized 4 models, therefore my work may provide a better approach considering the uncertainties of the climate model projections. Nevertheless, I take the entire 21st century into consideration instead of only the last part (2071-2100) of it. However, I have similar (2070-2100) investigation period. Therefore, I could compare easily the results of those periods. My annual AET increased from 594 mm·year^{-1} to 628 mm·year^{-1} (+5%) in case of the grass covered surface (Marchfeld), which lower than the 400 mm to 450 (+12%) in the study of *Remrová and Císleřová* (2010). Furthermore, the absolute values of actual evapotranspiration (AET) in *Remrová and Císleřová* (2010) study are lower, due to the mentioned temperature difference.

In *Lutz* et al. (2010) study there is an average modelled increase in AET of 10% across all plots in the 2020-2049 period, while I have found stagnancy ~0% for forested area (from 572 mm·year^{-1} to 572 mm·year^{-1}); -2% for mixed parcel (from 524 mm·year^{-1} to 514 mm·year^{-1}) and +1% for Marchfeld (from 603 mm·year^{-1} to 609 mm·year^{-1}) as changes in the annual AET. The reason of the stagnancy can be found in the temperature values of RCMs, which demonstrate stagnancy in that period as well. Similarly to *Lutz* et al. (2010) results the AET peaks in my case also occur in July, but with lower 100-115 mm·month^{-1} as highest values. In case of my study sites in the 2020-2049 period, the deficit (PET-AET) is shifted from 88 mm to 73 mm (-21%) at the forested area, from 96 mm to 100 mm (+4%) at the Marchfeld and from 127 mm to 134 mm (+6%) in case of the mixed parcel. However, at the end of the century, higher levels of deficit were related with lower elevation, therefore Marchfeld area is the most affected by water stress. In *Lutz* et al. (2010) study, the projected increases in deficit between present and future (2020-2049) were 23% across all plots, as a consequence of the increases in temperature plus PET and decreased snowpack.

Our results agree with *Keables and Mehta* (2010) in context of the AET rates annual tendencies. This similarity means that AET rates are small during the winter in response to reduced precipitation and lower temperatures, but increases equivalently from the spring with temperature and available water, due to the increased amount of rainfall. AET also reaching its maximum during summer, but its peaks appear in July with 151-175 mm·month^{-1} as highest values for most part of their study area. In my case basically June has the highest AET values with 100-115 mm·month^{-1}. AET rates decrease throughout the fall and into winter. Consequently, soil water utilization is the greatest during summer in my case as well as in eastern Kansas. Soil water shortage are common year-round in the western part of Kansas in response to less precipitation and increased actual evapotranspiration during the summer, and soils with low field capacities also represent a deficit during the summer months. Similarly to

Keables and Mehta (2010) results the potential water deficit also occurs in the summer period (highest values in July and August). Soil water recharge is greatest in the spring in central Kansas and during the fall in eastern Kansas, when sufficient water is available from precipitation and when evapotranspiration rates are less severe. *Keables and Mehta* (2010) validated their model with the help of observed stream discharge, whereas I applied measured actual evapotranspiration data for validation. Nevertheless, they have not done projections, however mentioned the main tendency of the expected temperature values, projected by RCMs (summers in the Great Plains may become increasingly dry during this century).

Contrary to *Mohammed* et al. (2012) I have used RCMs, because of their finer scale, but their applied GCMs due to the demand for larger spatial scale (HadCM3; CGCM 2.3.2a; CM2.1. CGCM3.1). They utilized 20 years (1986-2006) as a base of comparison to their projections, but I used 30 years block. In *Mohammed* et al. (2012) study the monthly mean AET ranged from 89 to 106 mm·month^{-1} (in march to may) as highest values, while in my study, there is 100-115 mm·month^{-1} maximum values (in June or July) for AET. However, it has to be said only the 100 mm·month^{-1} AET value (Marchfeld) can be compared with the results of Mohammed et al. (2012) from the rice-fields, since my another two study areas represent much more different surface covers. The mixed parcel, but especially the forested area has higher AET values (during growing season) due to the presence of greater evaporative surface of the woods. Nevertheless, in the Carpathian Basin the AET values are close to zero (maximum 20-30 mm·month^{-1}) in the winter months (from November to March), while the lowest AET values (38 mm·month^{-1}) was found in the December-February period in the study of *Mohammed* et al. (2012). The reason is the different climate zone in which lower temperatures is characteristic. Therefore I have 627 mm·year^{-1} (Marchfeld) 550 mm·year^{-1} (mixed parcel), 620 mm·year^{-1} (forested area) as annual values for AET in the 2050-2100 period. It is important to note that the only reason to determine annual AET values for the 2050-2100 period is due to the comparability of the two studies. Those annual values are much greater in the study of *Mohammed* et al. (2012) (1138 mm·year^{-1} for the northern part and 1204 mm·year^{-1} for the central, as mentioned before). They determined the deficit using the PET–AET equation (when PET>AET), but I calculated as PET-$SOIL_M$ for Marchfeld. Unlike *Mohammed* et al. (2012), the critical months – when water stress is assumed to occur – is not appeared on winter, but on late summer and early autumn, after the high water consumption (as well as high transpiration) of the plants. Consequently, water stress occurs between June and October, with 50 mm as highest value in July. I calculated the deficit (PET-AET) for the 2050-2100 period and compared its result with the reference period (1985-2015) for my study areas. In case of Marchfeld it is from 96 mm to 118 mm (+19%).

In *Zamfir* (2014) study there is not any concrete data, modeling results just tendencies, therefore it is hard to compare it with my study.

The main advantage of my model is the robustness, therefore it requires only temperature and precipitation as input data and it has to be calibrated (with for example: measured actual evapotranspiration data).

A basic disadvantage in the context of the usage is that the model does not take into consideration more soil layers. The present phase of this water balance model does not take

into consideration the interception, which is depend on the leaf area index (LAI) and can be highly uncertain for the future. Nevertheless, I did not take into consideration the effect of snow, since it is not likely longer lasting snow cover than a whole month, therefore may not cause any inaccuracy on the chosen monthly step. However, one of the most important barrier is that, it cannot be applied on areas with shallow groundwater, where the water uptake is characteristic from the groundwater. Therefore, as a requirement of the adaptation and spatial extension of the model is that, the study area has to be recharge area.

To sum up, the applied data and methods were suitable considering the availability, and satisfactory to achieve the aim of the dissertation.

In a nutshell, neither of the discussed studies analyzed the entire 21st century in context of the development of the water balances components. Most of them used the Hamon approach to PET, but only *Keables and Mehta* (2010) validated it. However, the globally calibrated Hamon method generally underestimates the rate of PET under many regional conditions. Some of those studies (*Mohammed* et al., 2012; *Lutz* et al., 2010) apply GCMs, instead of RCMs, since they evaluated a much larger spatial scale, such as Bangladesh. It also has to be noted that I have not found studies, which are exactly comparable to my work.

To summarize the role of my study in this scientific field, it was the first step to the establishment of a monthly-step water balance model, which can be extended to a country-wide spatial scale as well as utilized for projection of soil moisture and evapotranspiration, and therefore it can provide a basis of a decision support system like *AgroClimate.2 VKSZ_12-1-2013-0034 EU-national joint founded research project*.

7. Outlook

In this study a modified Thornthwaite-type, monthly step water balance model was chosen (Dingman, 2002) as a basis. I upgraded this model for my own purposes i.e., it was calibrated as well as validated for 3 different cover types and then their calibration parameters and 4 RCMs' database inputs were utilized to project evapotranspiration and soil moisture values.

The developed water balance model makes the basis of the hydrological module of the *AgroClimate.2* as a practical application of it. Nevertheless, the determination of the rooting depth is also possible with the model. Furthermore, the spatial extension of the model assures an easy way of water stress parameters' calculation, since this water balance model is simple as well.

However, further researches may be required:

- Upgrade the model to take into account the impact of interception on the evapotranspiration. Note that, the interception can be 10-40% of the gross precipitation in forest surface covers. As can be seen in *Chapter 6* I observed too high soil moisture reservoir, compare to the other studies (Lutz et al., 2010; Keables and Mehta 2010). The interception components will change the water balance, with higher evapotranspiration, but lower soil moisture values.
- Run projections with all available more regional climate simulations (with different emission and radiative forcing scenarios) as input, therefore the uncertainty of this modeling phase can be more reliably quantified considering the climate models uncertainties of prediction.
- Extend the water balance model to country-wide spatial scale that can be useful, since many country-wide analyses require water balance results data.
- Apply the model runs to the discharge area. My model is for the recharge zones, which are generally located in topographically higher areas, where the water table is found deeper. However, in the discharge areas the aquifers can take water from the groundwater system as well.

8. Theses of the dissertation

1. A new simplified Thornthwaite-type monthly step water balance model has been developed for regional usage, with components of actual evapotranspiration and soil moisture as output parameters. The developed water balance model was calibrated locally, with the help of measured actual evapotranspiration data, for three different surface cover types (forested area; mixed parcel, agricultural field) (*Herceg* et al., 2016a).

2. Using measured actual evapotranspiration data, the developed water balance model has been validated. The calculated actual evapotranspiration using the weather data of the validation periods reflected good accordance with the measured data (nash-sutcliffe model efficiency coefficient were 0.88 (forested area); 0.89 (mixed parcel); 0.85 (agricultural field)) (*Herceg* et al., 2016b).

3. Based on the simulation results of 4 bias-corrected regional climate models (IPCC SRES A1B emission scenario), the hydrological impacts of the climate change has been evaluated during the 21st century for the three study sites. The comparison of the study areas showed that the water availability for plants is expected to be the most favorable in the forested area, whereas the most unfavorable conditions can be in the agricultural field (*Herceg* et al., 2016b).

- The actual evapotranspiration mean values may increase slightly at the end of the 21st century (compared the 2070/2100 period to the 1985/2015 reference period) in each study site. The rates of increase are 6–9%.
- In case of mean soil moisture, small decreases can occur for the forested area (-6%) and mixed parcel (-8%), whereas there might be an increase for the agricultural field (+13%) at the end of 21st century.
- The 10th percentile minimums of soil moisture show an increase for forested area (+11%). Whereas significant decreasing tendency is projected for mixed parcel (-29%) and for Marchfeld (-42%) at the end of 21st century.

4. The changes of 30-year monthly means of actual evapotranspiration and of soil moisture values were analyzed during the 21st century at each study areas (*Herceg* et al., 2016b).

- The 30-year monthly mean values of actual evapotranspiration is likely increasing towards the end of 21st century at each study site, but significant shift of the values (10-15 mm · month^{-1} increases, which may occur in the 2070/2100 period) can only be found in the summer period, particularly in June and July.
- Regarding to the 30-year monthly mean values of soil moistures, there might be a decrease during the growing season, but no clear tendency in the dormancy towards the end of the 21st century. The lowest soil moisture values may occur in September at each study areas. The rates of the annual soil moisture fluctuations (difference between the month with the highest and the month with the lowest soil moisture

values) and soil moisture storage capacity are lowest in case of the forested area (30%) but highest at the agricultural field (63%) at the end of 21st century.

5. Based on the results of water stress analyses (with the determination of relative extractable water and soil water deficit), significant water stress can be assumed to occur only in case of the agricultural field (*Herceg* et al., 2016b).

- In context of the relative extractable water (REW), the projections for the 2070/2100 period were: 78% (forested area), 71% (mixed parcel) and 46% (agricultural field) at the end of the 21st century. Therefore, the values of REW were under the 50% threshold for 79 month at forested area, for 104 months at mixed parcel, and for 194 months at Marchfeld during the 30 years (360 month) long period.
- In case of soil water deficit (SWD), where the water stress assumed to occur when the rates are over 50%, the projections for the 2070/2100 period were 9% (forested area), 24% (mixed parcel) and 58% (agricultural field). Hence, the values of SWD were above the 50% threshold for 34 month at forested area, for 91 months at mixed parcel, and for 215 months at Marchfeld during the 30 years (360 month) long period.

6. Using potential water stress analysis, it has been pointed out that the vegetation of the agricultural field can successfully adapt to the water scarcity by growing their roots to the possibly maximum (1.4 m). Comparison of the static and extended rooting depth of the plants showed the following results:

- In case of static rooting depth, the potential water stress was occurred from June to September, and nevertheless, it is assumed that the potential water stress is likely to increase towards the end of the 21st century. The peak values of potential water stress are increased from approximately 40 mm to 60 mm, and it is shifted from August to July.
- In case of extended rooting depth, the potential water stress is not expected to occur at all during the 21st century.

10.13147/SOE.2018.004

Acknowledgement

First of all, I would like to thank to the Almighty ‘his’ guidance, who lead my way and let me meet with my supervisor Zoltán Gribovszki. He is generous and gentle person and I wish to thank him all his selfless assistance during and beyond my entire studies.

Here I want to express my special thanks to Péter Kalicz, whose helpfulness and expertise in programming as well as in water-balance modeling was the root of my work.

I am also very grateful to Reinhard Nolz from University of Natural Resources and Life Sciences, Vienna, who supported my work with his careful attitude and helped me very much with his useful advices.

I would like to thank the reviewers of this dissertation – Dr. Borbála Gálos, Dr. Norbert Móricz and Dr. Péter Csáfordi – for their useful comments, helpful suggestions.

Hereby I would like to thank the help of Balázs Kisfaludi in geoinformatics at the very beginning of my studies. Warm thanks for Péter Primusz and his sincere encouragement even in the hard times and with whom a good friendship has been formed as well.

I also would like to thank to Péter Csáki and Renáta Szita their presence with whom a respectable society was created.

Many thanks for András Klis, who checked many part of this dissertation in context of wording.

Nevertheless, I would like to thank for my all other colleagues their friendly attitude in the Institute of Geomatics and Civil Engineering, which have been made a peaceful atmosphere as well as a bedrock for the successful work.

My researches have been supported by *AgroClimate.2 (VKSZ_12-1-2013-0034)* EU-national joint founded research project.

References

ALKAEED, O., CLARIZA, F., KENJI, J., ATSUSHI, T. (2006): Comparison of Several Reference Evapotranspiration Methods for Itoshima Peninsula Area, Fukuoka, Japan. Memoirs of the Faculty of Engineering, Kyushu University, Vol.66, No.1, pp.1-14.

ALLEN, R.G., PEREIRA, L.S., RAES, D., SMITH, M. (1998): Crop evapotranspiration: guidelines for computing crop water requirements. In: FAO (ed) Irrigation and drainage paper 56. Food and agriculture organization of the United Nations, Rome.

ALLEN, D. M., MACKIE, D. C., WEI, M. (2004): Groundwater and climate change: A sensitivity analysis for the Grand Forks aquifer, southern Brit-ish Columbia, Canada, Hydrogeol. J., 12(3), 270–290.

ALLEN, R.G., PRUITT, W.O., WRIGHT, J.L., HOWELL, T.A., VENTURA, F., SNYDER, R., ITENFISU, D., STEDUTO, P., BERENGENA, J., BASELGA, YRISARRY, J., SMITH, M., PEREIRA, L.S., RAES, D., PERRIER, A., ALVES, I., WALTER, I., ELLIOTT, R. (2006): A recommendation on standardized surface resistance for hourly calculation of reference ETo by the FAO56 Penman–Monteith method. Agric Water Manag 81:1–22. doi:10.1016/j.agwat.2005.03.007

BAIRD, A. J., WILBY, R. L. (1999): Eco-Hydrology: plants and water in terrestrial and aquatic environment, Routledge, New York.

BARTHOLY, J., PONGRÁCZ, R. (2006): Magyarország múlt éghajlatának jellemzése különös tekintetel a szélsőségekre. Kutatási részjelentés a 2005.07.01.-2006.06.30. időszakban véegzett kutatásokról NKFP-3A/0082/2004 számú pályázat

BARTHOLY, J., BOZÓ, L., HASZPRA, L. (2011): Klímaváltozás – 2011, Klímaszcenáriók a Kárpát-medence térségére, Magyar Tudományos Akadémia; Eötvös Loránd Tudományegyetem Meteorológiai Tanszék, ISBN 978-963-284-232-5. [Climate change – 2011, Climate scenarios onto the area of Carpathian basin]

BATES, B.C., KUNDZEWICZ, Z. W., WU, S., PALUTIKOF, J. P. EDS. (2008): Climate Change and Water. Technical Paper of the Intergovernmental Panel on Climate Change, IPCC Secretariat, Geneva, 210 pp.

BAUMGARTNER, A., LIEBSCHER, H. J. (1990): Allgemeine Hydrologie, Quantitative Hydrologie, Lehrbuche der Hydrologie, Band 1., Berlin, Stuttgart.

BEAR, J., CHENG, H. D. (1999): Seawater Intrusion in Coastal Aquifers – Concepts, Methods and Practices. Kluwer Academic Publisher, Dordrecht, Boston, London, 625 pp.

BENISTON, M., STEPHENSON, D. B. (2004): Extreme climatic events and their evolution under changing climatic conditions. Glob Planet Change 44:1−9

BENISTON, M., STEPHENSON, D. B., CHRISTENSEN, O. B., FERRO, C. A. T., FREI, C., GOYETTE, S., HALSNAES, K., HOLT, T., JYLHÄ, K., KOFFI, B., PALUTIKOF, J., SCHÖLL, R., SEMMLER, T., WOTH, K. (2007): Future extreme events in European climate: an exploration of regional climate model projections, Climatic Change (2007) 81:71−95 DOI 10.1007/s10584-006-9226-z

BLANEY, H. F., AND CRIDDLE, W. D. (1950): Determining water requirements in irrigated areas from climatological data and irrigation data. SCS Technical Paper 96. Washington, D.C.: USDA Soil Conservation Service.

BERKI, I., RASZTOVITS, E., MÓRICZ, N., MÁTYÁS, CS. (2009): Determination of the drought tolerance limit of beech forests and forecasting their future distribution in Hungary. Cereal Research Communations, 37: 613-616.

BOEGH, E., SOEGAARD, H., HANAN, N., KABAT, P., AND LESCH, L. (1999): A remote sensing study of the NDVI–Ts relationship and the transpiration from sparse vegetation in the Sahel based on high-resolution satellite data, Remote Sens. Environ., 69, 224–240, doi:10.1016/S00344257(99)00025-5.

BONAN, G. B. (2004): Biogeophysical feedbacks between land cover and climate. In: R.S. DeFries, G.P. Asner, and R.A. Houghton (eds) Ecosystems and Land Use Change. Geophysical Monograph 153: 61-72, American Geophysical Union, Washington, D.C.

BOUCHET, R.J. (1963): Evapotranspiration reelle, evapotranspiration potentielle, et production agricole. Annal. Agronom. 14, 543–824.

BUONOMO, E., JONES, R. G., HUNTINGFORD, C., HANNAFORD, J. (2007): On the robustness of changes in extreme precipitation over Europe from two high resolution climate change simulations, Q. J. R. Meteorol. Soc., 133, 65–81.

BUYTAERT, W., VUILLE, M., DEWULF, A., URRUTIA, R., KARMALKAR, A., CÉLLERI, R. (2010): Uncertainties in climate change projections and regional downscaling in the tropical Andes: implications for water resources management, Hydrol. Earth Syst. Sci., 14, 1247–1258, doi:10.5194/hess-14-1247-2010.

BOWEN, I. S. (1926): The Ratio of Heat Losses by Conduction and By Evaporation From Any Water Surface, Physical review 27; 777-787.

BROUYE`RE, S., CARABIN, G., DASSARGUES, A. (2004): Climate change impacts on groundwater resources: Modelled deficits in a chalky aquifer,Geer basin, Belgium, Hydrogeol. J., 12, 123–134.

CALCAGNO, G., MENDICINO, G., MONACELLI, G., SENATORE, A., AND VERSACE, P. (2007): Distributed estimation of actual evapotranspiration through remote sensing techniques, in: Methods and Tools for Drought Analysis and Management, edited by: Rossi, G., Vega, T., and Bonaccorso, B., 62, Springer, Series: Water Science and Technology Library, 124–147.

CHEN, Z., GRASBY, S. E., OSADETZ, K. G. (2002): Predicting average an-nual groundwater levels from climatic variables: An empirical model, J.Hydrol., 260, 102–117.

CHEN, Z., GRASBY, S. E., OSADETZ, K. G. (2004): Relation between climate variability and groundwater levels in the upper carbonate aquifer, southern Manitoba, Canada: Journal of Hydrology, v. 290, no. 1–2, p. 43–62.

CHEN, J., BRISSETTE, F. P. POULIN, A., LECONTE, R. (2011a): Overall uncertainty study of the hydrological impacts of climate change for a Canadian watershed, Water Resour. Res., 47,W12509, doi:10.1029/2011WR010602.

CHEN, J., BRISSETTE, F. P., LECONTE, R. (2011b): Uncertainty of downscaling method in quantifying the impact of climate change on hydrology, J. Hydrol., 401, 190–202.

CHEN, J., BRISSETTE, F. P., CHAUMONT, D., BRAUN, M. (2013): Finding appropriate bias correction methods in downscaling precipitation for hydrologic impact studies over North America, Water Resour. Res., 49, 4187–4205, doi:10.1002/wrcr.20331.

CHRISTENSEN, J. H., CHRISTENSEN, O.B., LOPEZ, P., VAN MEIJGAARD, E., BOTZET, M. (1996): The HIRHAM4 regional atmospheric climate model, DMI Technical Report 96-4. Available from DMI, Lyngbyvej 100, Copenhagen Ø.

CHRISTENSEN, J. H., CHRISTENSEN, O. B. (2003): Severe summertime flooding in Europe. Nature 421:805–806

CHRISTENSEN, J. H., CHRISTENSEN, O.B. (2007): A summary of the PRUDENCE model projections of changes in European climate by the end of this century, Climatic Change 81:7–30 DOI 10.1007/s10584-006-9210-7

CHRISTENSEN, J.H., VAN MEIJGAARD, E. (1992): On the construction of a regional atmospheric climate model, DMI Technical Report 92-14. Available from DMI, Lyngbyvej 100, Copenhagen Ø.

CHRISTENSEN, J.H., CARTER, T.R., RUMMUKAINEN, M., AMANATIDIS G. (2007): Evaluating the performance and utility of regional climate models: the PRUDENCE project. Clim. Change 81, 1–6.

CHRISTENSEN, J.H., BOBERG, F., CHRISTENSEN, O.B., LUCAS-PICHER, P. (2008): On the need for bias correction of regional climate change projections of temperature and precipitation. Geophys. Res. Lett., 35. L20709. http://dx.doi.org/10.1029/2008GL035694.

CSÁKI, P., KALICZ, P., BROLLY, G. B., CSÓKA, G., CZIMBER, K., GRIBOVSZKI, Z. (2014): Hydrological impacts of various land cover types in the context of climate change for Zala County. Acta Silv. Lign. Hung., Vol. 10, Nr. 2 (2014) 117–131. [DOI: 10.2478/aslh-2014-0009]

COURAULT, D., SEGUIN, B., OLIOSO, A. (2005): Review on estimation of evapotranspiration from remote sensing data: from empirical to numerical modeling approaches, Irrig. Drain. Syst., 19,30 223–249, 233-249.

CZIMBER, K., NYULL, B. (2004) DigiTerra térinformatikai szoftverfejlesztések In: Márkus B (szerk.) Térinformatika, 280 p. Székesfehérvár: Nyugat-magyarországi Egyetem Geoinformatikai Főiskolai Kar, 2004. pp. 1 11. (ISBN:963 9364 45 2)

CZÚCZ, B., GÁLHIDY, L., MÁTYÁS, CS. (2010): Limiting climating factors and potential future distribution of beech (Fagus sylvatica L.) and sessile oak (Quercus petraea (Mattuschka) Liebl.) forests near their low altitude - xeric limit in Central Europe. Annales of Forest Science, 68: 99-108.

DAI, Z., LI, C., TRETTIN, C., SUN, G., AMATYA, D., LI, H. (2010): Bi-criteria evaluation of the MIKE SHE model for a forested watershed on the South Carolina coastal plain. Hydrol. Earth Syst. Sci. 14(1): 1–14.

DELFS, I. (1955): Die Niederschlagzurückhaltung im Walde /Interzeption/. Mitteilungen des Arbeitskreises "Wald und Wasser", Nr.2.Koblenz: 54p.

DÉQUÉ, M. (2007): Frequency of precipitation and temperature extremes over France in an anthropogenic scenario: Model results and statistical correction according to observed values. Glob. Plan. Change, 57, 16-26., doi:10.1016/j.gloplacha.2006.11.030.

DINGMAN, S. L. (2002): Physical Hydrology (2nd edition), Prentice Hall, 272-324p.

DOBOR, L., BARCZA, Z., HAVASI, Á., HLÁSNY, T. (2012): Construction of a daily meteorological database for climate change related impact studies. In: Proceedings, The

Atmosphere as risk and resource (eds.: Mika, J. et al.). 23 November, 2012, Eger, Hungary. CD-ROM

DOBOR, L., BARCZA, Z., HLÁSNY, T., HAVASI, Á. (2013): Creation of the FORESEE database to support climate change related impact studies, International Scientific Conference for PhD Students, March 19-20, 2013, Gyõr, Hungary.

DOBOR, L., BARCZA, Z., HLÁSNY, T., HAVASI, Á., HORVÁTH, F., ITTZÉS, P., BARTHOLY, J. (2014): Bridging the gap between climate models and impact studies: The FORESEE Database, Geosci Data J 2:1-11. doi:10.1002/gdj3.22

DOORENBOS, J., PRUITT, W. O. (1977): Guidelines for predicting crop water requirements. In: FAO (ed) Irrigation and drainage paper 24. Food and agriculture organization of the United Nations, Rome, 175 pp.

DÖVÉNYI, Z. (2010): Magyarország kistájainak katasztere - második, átdolgozott és bővített kiadás, MTA [Inventory of microregions in Hungary].

ELGUINDI, N., SOMOT, S., DÉQUÉ, M., LUDWIG, W. (2011): Climate change evolution of the hydrological balance of the Mediterranean, Black and Caspian Seas: impact of climate model resolution, Clim. Dynam., 36, 205–228.

FEDERER, C. A., VÖRÖSMARTY, C., FEKETE, B. (1996): Intercomparison of methods for calculating potential evaporation in regional global water balance models, Water Resour. Res. 32, 2315–2321.

FEDDERSEN, H., ANDERSEN, U. (2005): A method for statistical downscaling of seasonal ensemble predictions, Tellus, Ser. A, 57, 398–408.

FINCH, J., CALVER, A. (2008): Methods for the quantification of evaporation from lakes; prepared for the World Meteorological Organization's Commission for Hydrology.

FISHER, D.K. (2012): Simple weighing lysimeters for measuring evapotranspiration and developing crop coefficients. Int. J. Agric. & Biol. Eng. 5(3), 35-43. Division ASCE 108(3): 212–222.

FOWLER, H. J., BLENKINSOP, S., TEBALDI, C. (2007): Linking climate change modelling to impacts studies: recent advances in downscaling techniques for hydrological modelling. Int. J. Climatol. 27 (12), 1547–1578. http://dx.doi.org/10.1002/joc.1556.

FREI, C., CHRISTENSEN, J. H., DEQUE, M., JACOB, D., JONES, R. G., VIDALE, P. L. (2003), Daily precipitation statistics in regional climate models: evaluation and intercomparison for the European Alps, J. Geophys. Res., 108(D3), 4124, doi:10.1029/2002JD002287.

FREI, C., SCHOLL, R., FUKUTOME, S., SCHMIDLI, J., VIDALE, P. L. (2006): Future change of precipitation extremes in Europe: Intercomparison of scenarios from regional climate models, J. Geophys. Res., 111, D06105, doi:10.1029/2005JD005965.

FÜHRER, E. (1995): Az időjárás változásának hatása az erdők fatermőképességére és egészségi állapotára. „Az erdők egészségi állapotának változása" című konferencia kiadványa, pp. 38-45. [The effect of the weather changes onto the tree growth and vitality of forests]

GÁLOS, B., LORENZ, PH., JACOB D. (2007): Will dry events occur more often in Hungary in the future? Environ. Res. Lett. 2. 034006.

GÁLOS, B., MÁTYÁS, CS., JACOB, D. (2012): Az erdőtelepítés szerepe a klímaváltozás hatásának mérséklésében, Erdészettudományi Közlemények 2. évfolyam 1. szám 2012, 35–45 oldal. [The role of the afforestation in context of the mitigation of the climate changes impact]

GÁLOS, B., FÜHRER, E., CZIMBER, K., GULYÁS, K., BIDLÓ, A., HÄNSLER, A., JACOB, D., MÁTYÁS, CS. (2015): Climatic threats determining future adaptive forest management – a case study of Zala County, IDŐJÁRÁS, Quarterly Journal of the Hungarian Meteorological Service Vol. 119, No. 4, October – December, 2015, pp. 425–441.

GASH, J. H. C., MORTON, A. J. (1978): An application of the Rutter model to the estimation of the interception loss from Thetford Forest, Journal of Hydrology, 38: 49-58.

GIORGI, F. (1990): Simulation of regional climate using a limited area model nested in general circulation model, J. Clim., 3, 941–963.

GLOSSARY OF SOIL SCIENCE TERMS (2008) doi:10.2136/2008.glossarysoilscienceterms, Glossary of Soil Science Terms 2008, 1-82.

GODERNIAUX, P., BROUYE`RE, S., FOWLER, H. J., BLENKINSOP, S., THERRIEN, R., ORBAN, P., DASSARGUES, A. (2009a): How can large scale integrated sur-face-subsurface hydrological model be used to evaluate long term climate change impact on groundwater reserves, Calibration and Reliability in Groundwater Modeling: Managing Groundwater and the Environment, pp. 137–140, China Univ. Geosciences, Wuhan.

GODERNIAUX, P., BROUYE`RE, S., FOWLER, H. J., BLENKINSOP, S., THERRIEN, R., ORBAN, P., DASSARGUES, A. (2009b): Large scale surface-subsurface hydrological model to assess climate change impacts on groundwater reserves, J. Hydrol., 373(1–2), 122–138.

GÖTZ, B., HADATSCH, S., KRATOCHVIL, R., VABITSCH, A., FREYER, B. (2000): Biologische Landwirtschaft im Marchfeld. Potenziale zur Entlastung des Natur- und Landschaftshaushaltes. Umweltbundesamt GmbH, Vienna.

GOYETTE, S., BRASSEUR, O., BENISTON, M. (2003): Application of a new wind gust parameterisation; multi-scale case studies performed with the Canadian RCM. J Geophys Res 108:4371−4389

GRANIER, A., BREDA, N., BIRON, P., VILLETTE, S., (1999): A lumped water balance model to evaluate duration and intensity of drought constraints in forest stands, Ecological Modelling 116 (1999) 269 – 283.

GRIBOVSZKI, Z., KALICZ, P., KUCSARA, M. (2006): Streamflow Characteristics of Two Forested Catchments in Sopron Hills. Acta Silv. Lign. Hung., Vol. 2. p. 81-92.

GROTCH, S. L., MACCRACKEN, M. C. (1991): The use of general circulation models to predict regional climatic change. J. Clim. 4 (3). http://dx.doi.org/10.1175/1520-0442(1991)004<0286:TUOGCM>2.0.CO;2.

HAERTER, J. O., BERG, P., HAGEMANN, S. (2010): Heavy rain intensity distributions on varying time scales and at different temperatures, J. Geophys. Res., 115, D17102, doi:10.1029/2009JD013384

HAERTER, J. O., HAGEMANN, S. MOSELEY, C., PIANI, C. (2011): Climate model bias correction and the role of timescales, Hydrol. Earth Syst. Sci., 15, 1065–1079.

HAMON, W. R. (1963): Computation of direct runoff amounts from storm rainfall. Intl. Assoc. Scientific Hydrol. Publ. 63: 52-62.

HANSEN, J., CHALLINOR, A., INES, A., WHEELER, T., AND MORONET, V. (2006): Translating forecasts into agricultural terms: advances and challenges, Clim. Res., 33, 27–41.

HARSCH, N., BRANDENBURG, M., KLEMM, O. (2009): Large-scale lysimeter site St. Arnold, Germany: analysis of 40 years of precipitation, leachate and evapotranspiration, Hydrol. Earth Syst. Sci., 13, 305–317, www.hydrol-earth-syst-sci.net/13/305/2009/

HAYLOCK, M. R., HOFSTRA, N., KLEIN, T., A. M. G., KLOK, E. J., JONES, P. D., NEW, M., (2008): A European daily high-resolution gridded data set of surface temperature and precipitation for 1950–2006. J. Geophys Res., 113. D20119.

HERCEG, A., KALICZ, P., KISFALUDI, B., GRIBOVSZKI, Z. (2016a): A Monthly-Step Water Balance Model to Evaluate the Hydrological Effects of Climate Change on a Regional Scale for Irrigation Design, Slovak Journal of Civil Engineering, Vol. 24, 2016, No. 4, 27 – 35, DOI: 10.1515/sjce-2016-0019

HERCEG, A., KALICZ, P., NOLZ, R., GRIBOVSZKI, Z. (2016b): Present and future seasonal water balance of three different surface cover types, In: Zoltán Gribovszki, Kamila Hlavčová, Péter Kalicz, Silvia Kohnová, Gemma Carr (szerk.) HydroCarpath-2016, Catchment Processes in Regional Hydrology: from plot to regional scales – monitoring catchment processes and hydrological modelling, Konferencia helye, ideje: Bécs, Ausztria, 2016.10.27. ISBN 978-963-334-296-1.

HOLMAN, I. P. (2006): Climate change impacts on ground-water recharge—Uncertainty, shortcomings, and the way forward? Hydrogeology Journal, v. 14, no. 5, p. 637–647.

INES, A., HANSEN, J. (2006): Bias correction of daily GCM rainfall for crop simulation studies. Agric. For. Meteorol., 138, 44-53. http://dx.doi.org/10.1016/j.agrformet.2006.03.009.

INTERGOVERNMENTAL PANEL ON CLIMATE CHANGE (2007), Climate Change 2007. The Physical Science Basis. Contribution of Working Group I to the Fourth Assessment Report of the Intergovernmental Panel on Climate Change, edited by S. Solomon et al., 996 pp., Cambridge Univ. Press, Cambridge, U. K.

IPCC (2000): Emissions scenarios. In: Nebojsa Nakicenovic and Rob Swart (eds.) Contribution of Working Group III to the Special Report of the Intergovernmental Panel on Climate Change. Cambridge University Press, Cambridge, United Kingdom. 570 pp.

IPCC (2007): Climate change 2007: Impacts, adaptation and vulnerability. In: M.L. Parry, O.F. Canziani, J.P. Palutikof, P.J. van der Linden and C.E. Hanson (eds.) Contribution of Working Group II to the Fourth Assessment Report of the Intergovernmental Panel on Climate Change. Cambridge University Press, Cambridge, United Kingdom and New York, NY, USA. 976 pp.

IPCC (2012): Summary for Policymakers. In: Managing the Risks of Extreme Events and Disasters to Advance Climate Change Adaptation [Field, C.B., V. Barros, T.F. Stocker, D. Qin, D.J. Dokken, K.L. Ebi, M.D. Mastrandrea, K.J. Mach, G.-K. Plattner, S.K. Allen, M. Tignor, and P.M. Midgley (eds.)]. A Special Report of Working Groups I and II of the Intergovernmental Panel on Climate Change. Cambridge University Press, Cambridge, UK, and New York, NY, USA, pp. 1-19.

IPCC (2014): Climate Change 2014: Synthesis Report. Contribution of Working Groups I, II and III to the Fifth Assessment Report of the Intergovernmental Panel on Climate Change [Core Writing Team, R.K. Pachauri and L.A. Meyer (eds.)]. IPCC, Geneva, Switzerland, 151 pp.

ITURBE, I. R., PORPORATO, A. (2004): Ecohydrology of Water Controlled Ecosystems, Cambridge University Press.

IIZUMI, T., NISHIMORI, M., DAIRAKU, K., ADACHI, S. A., YOKOZAWA, M. (2011): Evaluation and intercomparison of downscaled daily precipitation indices over Japan in present-day

climate: Strengths and weaknesses of dynamical and bias correction-type statistical downscaling methods, J. Geophys. Res., 116, D01111, doi:10.1029/2010JD014513.

JACOB, D. (2001): A note to the simulation of the annual and inter-annual variability of the water budget over the Baltic Sea drainage basin. Meteorol Atmos Phys 77:61-73.

JACOB, D., BARRING, L., CHRISTENSEN, O.B., CHRISTENSEN, J.H., CASTRO, M., DEUE, M., GIORGI, F., HAGEMANN, S., HIRSCHI, M., JONES, R., KJELLSTRÖM, E., LENDERINK, G., ROCKEL, B., SANCHEZ, E., SCHAR, C., SENEVIRATNE, S.I., SOMOT, S., VAN ULDEN, A., VAN DEN HURK, B. (2007): An inter-comparison of regional climate models for Europe: model performance in present-day climate. Clim Change, 81:31-52, doi: 10.1007/s 10584-006-9213-4.

JACOB, D., KOTOVA, L., LORENZ, P., MOSELEY, CH., PFEIFER, S. (2008): Regional climate modeling activities in relation to the CLAVIER project. Időjárás 112, 141–153.

JENSEN, M. E., BURMAN, R.D., ALLEN, R.G. (1990): Evapotranspiration and irrigation water requirements, New York, 1990.

JONES, C. G., ULLERSTIG, A., WILLEN, U., HANSSON, U. (2004): The Rossby Centre regional atmospheric climate model (RCA). Part I: model climatology and performance characteristics for present climate over Europe. Ambio 33 (4-5): 199-210.

KALMA, J., MCVICAR, T., MCCABE, M. (2008): Estimating land surface evaporation: a review of methods using remotely sensed surface temperature data, Surv. Geophys., 29, 421–469, doi:10.1007/s10712-008-9037-z.

KEABLES, M.J., MEHTA, S. (2010): A soil water climatology for Kansas, Great Plains Research: A Journal of Natural and Social Sciences. Paper 1124.

KEVE, G., NOVÁKY, B. (2010): Klímaváltozás hatásának vizsgálata a Bácsbokodi-Kígyós csatorna vízgyűjtőjén Budyko-modell alkalmazásával. A Magyar Hidrológiai Társaság XXVIII. Országos Vándorgyűlése. Sopron 2010. július 7-9. ISBN 978-963-8172-25-9.

KISFALUDI, B., CSÁKI, P., PRIMUSZ, P., PÉTERFALVI, J., GRIBOVSZKI, Z. (2015): Comparison of CREMAP and MODIS MOD16 evapotranspiration, International conference: Catchment processes in regional hydrology: Linking experiments and modelling in Carpathian drainage basins

KISHÁZI, P., IVANCSICS, J. (1985): Sopron Környéki Üledékek Összefoglaló Földtani Értékelése [Geological Assessement of Sediments in the Neighbourhood of Sopron]. Manuscript, Sopron, 48 pp. (in Hungarian)

KJELLSTRÖM, E., NIKULIN, G., HANSSON, U., STRANDBERG, G., ULLERSTIG, A. (2011): 21st century changes in the European climate: uncertainties derived from an ensemble of regional climate model simulations. Tellus 63A, 24–40.

KOLKA, R. K., WOLF, A. T. N. (1998): Estimating Actual Evapotranspiration for Forested Sites: Modifications to the Thornthwaite Model, United States Department of Agriculture, Forest Service, Southern Research station.

KOVÁCS, Á. (2011): Tó- és területi párolgás becslésének pontosítása és magyarországi alkalmazásai. PhD értekezés. Budapesti Műszaki és Gazdaságtudományi Egyetem [Specifying lake and areal evapotranspiration rates in Hungary]

KUNDZEWICZ, Z. W., SZAMALEK. K., KOWALCZAK, P. (1999): The great flood of 1997 in Poland. Hydrol Sci J 44:855–870

LAFON, T., DADSON, S., BUYS, G., PRUDHOMME, C. (2012): Bias correction of daily precipitation simulated by a regional climate model: A comparison of methods, Int. J. Climatol., 33, 1367–1381, doi:10.1002/joc.3518.

LAKATOS, M., SZÉPSZÓ, G., BIHARI, Z., KRÜZSELYI, I., SZABÓ, P., BARTHOLY, J., PONGRÁCZ, R., PIECZKA, I., TORMA, CS. (szerk.) (2012): HREX jelentés: Éghajlati szélsőségek változásai Magyarországon: Közelmúlt és jövő. http://www.met.hu/doc/IPCC_jelentes/HREX_jelentes-2012.pdf [Climate extreme changes in Hungary: recent past and future.]

LANDSBERG, H. E. (1982): Climatic aspects of drought. Bull Am Meteorol Soc 63:593–596.

LANTHALER, C. (2004): Lysimeter Stations and Soil Hydrology Measuring Sites in Europe-Purpose, Equipment, Research Results, Future Developments . Diploma thesis. School of Natural Sciences, Karl-Franzens-University, Graz.

LENDERINK, G., BUISHAND, A., VAN DEURSEN, W. (2007): Estimates of future discharges of the river Rhine using two scenario methodologies: direct versus delta approach, Hydrol. Earth Syst. Sci., 11, 1145–1159, doi:10.5194/hess-11-1145-2007.

LEITH, R. M. M., WHITFIELD, P. H. (1998): Evidence of climate change effects on the hydrology of streams in south-central B.C. Can. Water Resour. J. 23 (3), 219–230.

LINDEN VAN DER, P., MITCHELL, J.F.B., EDS. (2009): ENSEMBLES: Climate Change and its Impacts: Summary of research and results from the ENSEMBLES project. Met Office Hadley Centre, FitzRoy Road, Exeter EX1 3PB, UK.

LIU, L. HONG, Y., BEDNARCZYK, N.C., YONG, B., HOCKER, J.E., SHAFER, M.A. (2011): Hydro-climatological Drought Analyses and Projection Using Meteorological and Hydrological Drought Indices: A Case Study in Blue River Basin, Oklahoma, Science and Technology Infusion Climate Bulletin NOAA's National Weather Service 36th NOAA Annual Climate Diagnostics and Prediction Workshop Fort Worth, TX, 3-6 October 2011.

LOA´ICIGA, H. A., MAIDMENT, D. R., VALDES, J. B. (2000): Climate-change impacts in a regional karst aquifer, Texas, USA, J. Hydrol., 267, 173–194.

LOA´ICIGA, H. A. (2003): Clim. Change and Ground Water, Ann. Assoc. Am.Geograph., 93(1), 30–41.

LU, J., SUN, G., MCNULTY, S.G., AMATYA, D.M. (2005): A comparison of six potential evapotranspiration methods for regional use in the southeastern united states, Journal of the American water resources association, pp 621-633.

LUTZ, J.A., WAGTENDONK, J.W., FRANKLIN, J.F. (2010): Climatic water deficit, tree species ranges, and climate change in Yosemite National Park, Journal of Biogeography, 37, 936-950.

MAIDMENT, D.R. (1993): Handbook of Hydrology, McGraw-Hill Education; 1 edition (February 1, 1993).

MANNINGER, M. (2004): Erdei fák éves és korszaki növekedésmenete és kapcsolódása egyes ökológiai tényezőkhöz. In: Mátyás Cs. és Vig P. (eds): Erdô és klíma IV. Nyugat-Magyarországi Egyetem, Sopron. 151–162. [The annual and periodic growth process of forests trees and its involvement in certain ecological factors]

MARAUN, D. (2012): Nonstationarities of regional climate model biases in European seasonal mean temperature and precipitation sums, Geophys. Res. Lett., 39, L06706.

MÁTYÁS, CS. (2010): Forecasts needed for retreating forests (opinion). Nature, 464: 1271

MÁTYÁS, CS., CZIMBER, K. (2000): A magyarországi zonális erdőövek mezoklímatikus meghatározottsága: számítógépes elemzés első eredményei. Ökol. Kongresszus, Debrecen, Absztrakt kötet. [The mezzo climatic determination of Hungarian zonal forest belts: the first results of computer analysis]

MÁTYÁS, CS., CZIMBER, K. (2004): A zonális erdőhatár klímaérzékenysége Magyarországon – előzetes eredmények. In: Erdő és Klíma IV. (szerk.: Mátyás Cs. Víg P.). Nyme, Sopron, pp. 35–44. [The sensitivity of xercic limit in Hungary]

MÁTYÁS, CS., FÜHRER, E., BERKI, I., CSÓKA, GY., DRÜSZLER Á., LAKATOS, F., MÓRICZ, N., RASZTOVITS, E., SOMOGYI, Z., VEPERDI, G., VIG, P., GÁLOS, B. (2010): Erdők a szárazsági határon. „KLÍMA-21" Füzetek. 61: 84-97. [Forests in xeric limit]

MCMAHON, T.A., PEEL, M.C., LOWE, L., SRIKANTHAN, R., MCVICAE, T. R. (2013): Estimating actual, potential, reference crop and pan evaporation using standard meteorological data: pragmatic synthesis, Hydrol. Earth Syst. Sci., 17 1331.1363, 2013, www.hydrol-earth-syst-sci.net/17/1331/2013/ doi: 10.5194/hess-17-1331-2013.

MIKA, J., (1999): Climate scenarios for the development of the national strategy in water management. In: Somlyo ´ dy, L. (ed.) Strategy of National Water Management. The Hungarian Academy of Science, Budapest (in Hungarian).

MINGTEH, CS. (2006): Forest Hydrology: An introduction to water and forests (second edition), Stephen F. Austin State University, Texas, U.S.A., 181 pp.

MITCHELL, T., CARTER, T. R., JONES, P. D., HULME, M., NEW, M. (2004): A comprehensive set of high resolution grids of monthly climate for Europe and the globe: the observed record (1901-2000) and 16 scenarios (2001-2100). Tyndall Centre. Working Paper 55.

MOHAMMED, R. K., MAMORU, I., MOTOYOSHI, I. (2012): Modeling of seasonal water balance for crop production in Bangladesh with implications for future projection, Italian Journal of Agronomy 2012; volume 7:e21.

MOORE, B., ALLARD, G. (2008): Climate change impacts on forest health, Forestry Department Food and Agriculture Organization of the United Nations, Forest health & Biosecurity working papers, FBS/34E.

MOLNÁR, M., LAKATOS, F. (2007): A bükk tömeges pusztulása Zala megyében. In: Lakatos F., Varga D. (szerk.): Erdészeti Tudományos Konferencia 2007. december 11. Poszter p:45, Sopron [Mass decay of beech in Zala county]

MONTEITH, J. L. (1991): Weather and water in the Sudano-Sahelian zone. Soil Water Balance in the Sudano-Sahelian Zone, Proceedings of the Niamey Workshop, February 1991, International Association of Hydrological Sciences Publication, 11–28, 1991.

MÓRICZ, N., MÁTYÁS, C., BERKI, I., RASZTOVITS, E., VEKERDY, Z., GRIBOVSZKI, Z. (2012): Comparative water balance study of forest and fallow plots. iForest 5: 188-196 [online 2012-08-02] URL: http://www.sisef.it/iforest/contents?id=ifor0624-005

MORTON, F.I., (1983): Operational estimates of areal evapotranspiration and their significance to the science and practice of hydrology. J. Hydrol. 66, 1–76.

MORTON, F.I., RICARD, F., FOGARASI, S. (1985): Operational estimates of areal evapotranspiration and lake evaporation – Program WREVAP. National Hydrological Research Institute Paper #24, Ottawa, Ontario, Canada.

MPELASOKA, F. S., CHIEW, F. H. S. (2009): Influence of rainfall scenario construction methods on runoff projections, J. Hydrometeorol., 10, 1168–1183.

MUGGEO, V.M.R. (2008): Segmented: An R Package to Fit Regression Models with Broken-Line Relationships, R News, The Newsletter of the R Project, Volume 8/1, May 2008.

NACHTNEBEL, H.P., DOKULIL, M., KUHN, M., LOISKANDL, W., SAILER, R., SCHÖNER, W. (2014): Influence of climate change on the hydrosphere. In: Austrian Panel on Climate Change (APCC) Austrian Assessment Report Climate Change 2014 (AAR14). Austrian Academy of Sciences Press, Vienna, pp 411–466.

NAMIAS, J. (1966): Nature and possible causes of the northeastern United States Drought during 1962–1965. Mon Weather Rev 94(9):543–557.

NOURI, H., BEECHAM, S., KAZEMI, F., HASSANLI, A. M., AND ANDERSON, S. (2013): Remote sensing techniques for predicting evapotranspiration from mixed vegetated surfaces, Hydrol. Earth Syst. Sci. Discuss., 10, 3897-3925, doi:10.5194/hessd-10-3897-2013.

NEBO, J., SUMAYA, I. (2012): Critical Review of Methods for the Estimation of Actual Evapotranspiration in Hydrological Models, Evapotranspiration - Remote Sensing and Modeling, Dr. Ayse Irmak (Ed.), In Tech, DOI: 10.5772/21279. Available from: http://www.intechopen.com/books/evapotranspiration-remote-sensing-and-modeling/critical-review-of-methods-for-the-estimation-of-actual-evapotranspiration-in-hydrological-models

NEUWIRTH, F., MOTTL, W. (1983): Errichtung einer Lysimeteranlage an der agrar-meteorologischen Station in Groß-Enzersdorf. „Wetter und Leben“. 35, 48-53.

NOLZ, R., CEPUDER, P., (2008): Water balance in Marchfeld as measured by a Lysimeter. International workshop and course for decision makers on the effective use of water in agricultural crop production. Jois, Austria, October 6-8.

NOLZ, R., CEPUDER, P., KAMMERER, G. (2011a): Determining soil water-balance components using an irrigated grass lysimeter in NE Austria. J. Plant Nutr. Soil Sci. 000, 1-8.

NOLZ, R., KAMMERER, G., CEPUDER,. P. (2011b): Datenmanagement der wägbaren Lysimeter in Groß-Enzersdorf. In: LFZ Raumberg-Gumpenstein (ed.): Proc. 14th Lysimeter Conf., Gumpenstein, Austria, May 3-4, 2011, 33-38.

NOLZ, R., CEPUDER, P. (2012): Evapotranspiration of spring barley on lysimeter- and field scale. International Symposium on Managing Soils for Food Security and Climate Change Adaptation and Mitigation, CN-191 Joint FAO/IAEA Programme, Vienna, Austria, July 23-27.

NOLZ, R., CEPUDER, P., EITZINGER, J. (2016): Comparison of lysimeter based and calculated ASCE reference evapotranspiration in a subhumid climate, Theor Appl Climatol 124: 315-324. doi:10.1007/s00704-015-1417-y.

NOLZ, R., KAMMERER, G., CEPUDER, P. (2013): Interpretation of lysimeter weighing data affected by wind. J. Plant Nutr. Soil Sci, 176, 200–208.

NOVÁKY, B., BÁLINT, G., (2013): Shifts and Modification of the Hydrological Regime Under Climate Change in Hungary; http://dx.doi.org/10.5772/54768

OKI, T., KANAE, S. (2006): Global hydrological cycles and world water resources, Science, 313, 1068–1072.

OLSSON, J., BERG, P., KAWAMURA, A. (2014): Impact of RCM Spatial Resolution on the Reproduction of Local, Subdaily Precipitation; Journal of Hydrometeorology, DOI: http://dx.doi.org/10.1175/JHM-D-14-0007.1

OUDIN, L., HERVIEU, F., MICHEL, C., PERRIN, C., ANDREASSIAN, V., ANCTIL, F., LOUMAGNE, C. (2005): Which potential evapotranspiration input for a lumped rainfall–runoff model? Part 2 – Towards a simple and efficient potential evapotranspiration model for rainfall–runoff modelling, J. Hydrol., 303, 290–306.

PALMER, W. C. (1965): Meteorological drought. Research Paper No. 45. U.S. Weather Bureau

PALTINEANU, I. C., STARR, J. L., (1997): Real-time soil water dynamics over large areas using multisensor capacitance probes: Laboratory Calibration. Soil Science Society of America. Journal 61 (6), 1576–1585.

PENMAN, H. L. (1948): Natural evaporation from open water, bare soil, and grass, Proceedings of the Royal Society London A193, 120–146.

PENMAN, H. L. (1956): Evaporation: An introductory survey, Neth. J. Agr. Sci., 4, 9–29.

PONGRÁCZ, R., BARTHOLY, J., MIKLÓS, E. (2011): Analysis of projected climate change for Hungary using ENSEMBLES simulations. Applied Ecology and Environmental Research, 9(4), 387-398.

PONGRÁCZ, R., BARTHOLY, J., KIS, A., (2014): Estimation of future precipitation conditions for Hungary with special focus on dry periods, IDŐJÁRÁS Quarterly Journal of the Hungarian Meteorological Service Vol. 118, No. 4, October – December, 2014, pp. 305–321.

PIANI, C., HAERTER O., CORPOLA, E. (2010): Statistical bias correction for daily precipitation in regional climate models over Europe, Theor. Appl. Climatol., 99, 187–192.

PRIESTLEY, C. H. B., TAYLOR, R. J. (1972): On the assessment of surface heat flux and evaporation using large-scale parameters, Monthly Weather Review 100, 81–92.

RAO, L.Y., SUN, G., FORD, C. R., VOSE, J. M. (2011): Modeling potential evapotranspiration of two forested watersheds in the southern Appalachians, Soil & Water Division of ASABE, Vol. 54(6): 2067-2078 2011 American Society of Agricultural and Biological Engineers ISSN 2151-0032.

REMROVÁ, M., CÍSLEŘOVÁ, M. (2010): Analysis of climate change effects on evapotranspiration in the watershed Uhlírská in the Jizera mountains. Soil & Water resources, 5, 2010 (1): 28-38.

RIEBSAME, W.E., CHANGNON, S.A., KARL, T.R (1991): Drought and natural resources management in the United States: Impacts and implications of the 1987–89 Drought. Westview Press, 174pp.

R CORE TEAM, (2012): R: A language and environment for statistical computing. R Foundation for Statistical Computing, Vienna, Austria. ISBN 3-900051-07-0, URL http://www.R-project.org/

RYU, J. H., PALMER, R. N., WILEY, M. W., JEONG, S. (2009): Midrange streamflow forecasts based on climate modeling-statistical correction and evaluation, J. Am. Water Resour. Assoc., 45(2), 355–368.

SALATHÉ JR., E. P. (2003): Comparison of various precipitation downscaling methods for the simulation of streamflow in a rainshadow river basin. Int. J. Climatol. 23 (8), 887–901. http://dx.doi.org/10.1002/joc.922.

SCHÄR, C., VIDALE, P. L., LÜTHI, D., FREI, C., HÄBERLI, C., LINIGER, M., APPENZELLER, C. (2004): The role of increasing temperature variability in European summer heatwaves. Nature 427:332–336

SCHMIDLI, J., FREI, C., VIDALE, P. L. (2006): Downscaling from GC precipitation: A benchmark for dynamical and statistical downscaling methods, Int. J. Climatol., 26, 679–689, doi:10.1002/joc.1287.

SALVI, K., KANNAN, S., GHOSH, S. (2011): Statistical downscaling and bias correction for projections of Indian rainfall and temperature in climate change studies, in 2011 International Conference on Environmental and Computer Science, vol. 19, pp. 7–11, IACSIT Press, Singapore.

SCIBEK, J., ALLEN, D. M. (2006a): Comparing modelled responses of two high-permeability, unconfined aquifers to predicted climate change, Global Planet. Change, 50(1–2), 50–62.

SCIBEK, J., ALLEN, D. M. (2006b): Modeled impacts of predicted climate change on recharge and groundwater levels, Water Resour. Res., 42, W11405, doi:10.1029/2005WR004742.

SCIBEK, J., ALLEN, D. M., CANNON, A. J., WHITfiELD, P. H. (2007): Ground-water-surface water interaction under scenarios of climate change using a high-resolution transient groundwater model, J. Hydrol., 333(2–4), 165–181

SOLYMOS, R. (2009): A klímaváltozás hatása az erdők fanövedékére. „Klíma-21" Füzetek, 56: 43–47. [The impacts of the climate change on the tree growth of the forests]

SOMOGYI, Z. (2009): A klíma, a klímaváltozás és a fanövekedés néhány összefüggése. „Klíma-21" Füzetek, 56: 48–56. [Climate, climate change and tree growth in some context]

SENEVIRATNE, S. I., CORTI, T., DAVIN, E. L., HIRSCHI, M., JAEGER, E. B., LEHNER, I., ORLOWSKY, B., TEULING, A. J. (2010): Investigating soil moisture–climate interactions in a changing climate: A review, Earth-Science Reviews 99, 125–161.

SENTEK PTY LTD, (2003): Access Tube Installation, Guide Version 1.0. Stepney.

SERRAT-CAPDEVILA, A., VALDE´S, J. B. PE´REZ, J. G., BAIRD, K., MATA, L. J., MADDOCK, T. (2007): Modeling climate change impacts and uncertainty—on the hydrology of a riparian system: The San Pedro Basin (Arizona/Sonora), J. Hydrol., 347(1–2), 48–66.

SHARMA, D., DAS GUPTA, A., BABEL, M. S. (2007): Spatial disaggregation of bias-corrected GCM precipitation for improved hydrologic simulation: Ping River Basin, Thailand, Hydrol. Earth Syst. Sci., 11, 1373–1390, doi:10.5194/hess-11-1373-2007.

SIMONFFY, Z. (2003): Szélsőséges meteorológiai események hatása a vízkészletekre. Vízügyi Közlemények, 2003. 4. füzet, 582-598.

SOMLYÓDY, L., NOVÁKY, B., SIMONFFY, Z. (2010): Éghajlatváltozás, szélsőségek és víz-gazdálkodás. „Klíma-21" Füzetek (Klímaváltozás – Hatások – Válaszok), (2010/61): 15-32. [Climate change, extremes and water management]

SOMMER, J. H., KREFT, H., KIER, G., JETZ, MUTKE, J., BARTHLOTT, W. (2010): Projected impacts of climate change on regional capacities for global plant species richness, Proceedings of the Royal Society B: Biological Sciences 277(1692):2271-80 · March 2010.

SU, Z. (2002): The Surface Energy Balance System (SEBS) for estimation of turbulent heat fluxes, Hydrol. Earth Syst. Sci., 6, 85–100, doi:10.5194/hess-6-85-2002.

SUN, G. K., ALSTAD, J., CHEN, S., CHEN, C. R., FORD, G., LIN, C., LIU, N., LU, S. G., MCNULTY, H., MIAO, A., NOORMETS, J. M., VOSE, B., WILSKE, M., ZEPPEL, Y., ZHANG Z. (2011a): A general projective model for estimating monthly ecosystem evapotranspiration. Ecohydrol. 4(2): 245-255.

SUN, F., RODERICK, M. L., LIM, W. H., FARQUHAR, G. D. (2011b): Hydroclimatic projections for the Murray-Darling Basin based on an ensemble derived from Intergovernmental Panel on Climate Change AR4 climate models, Water Resour. Res., 47, W00G02, doi:10.1029/2010wr009829.

SZALAI, S. (2011): The hydro-climatic characteristics of Hungary (in Hungarian). "CLIMA - 21" Brochures. Climate change – impact – responses. No.65, 2011, pp. 17-28. ISSN 1789-428X

SZILÁGYI, J., JÓZSA, J. (2008): New findings about the complementary relationship based evaporation estimation methods. J. Hydrol., 354, 171-186.

SZILÁGYI, J., JÓZSA, J. (2009): Estimating spatially distributed monthly evapotranspiration rates by linear transformations of MODIS daytime landsurface temperature data. Hydrol. EarthSystem Sci. 13(5), 629–-637.

SZILÁGYI, J. KOVÁCS, Á. (2010): Complementary-relationship-based evapotranspiration mapping (CREMAP) technique for Hungary, Periodica Polytechnica - Civil Engineering, 54(2), 95-100.

SZILÁGYI J., KOVÁCS, Á. (2011): A calibration-free evapotranspiration mapping technique for spatially-distributed regionalscale hydrologic modelling, J. Hydrol. Hydromech., 59, 2011, 2, 118–130 DOI: 10.2478/v10098-011-0010-z.

SZILÁGYI, J., KOVACS, A., JÓZSA, J., (2011): A calibration-free evapotranspiration mapping (CREMAP) technique, in Evaporation, INTECH, Rijeka, Croatia, ISBN 978-953-307-251-7.

TEUTSCHBEIN, C., SEIBERT, J. (2010): Regional climate models for hydrological impact studies at the catchment scale: a review of recent modeling strategies. Geogr. Compass 4 (7), 834–860. http://dx.doi.org/10.1111/j.17498198.2010.00357.x.

TEUTSCHBEIN, C., SEIBERT, J. (2012): Bias correction of regional climate model simulations for hydrological climate-change impact studies: Review and evaluation of different methods, J. Hydrol., 456, 12–29, doi:10.1016/j.jhydrol.2012.05.052.

TERINK, W., HURKMANS, R. T. W. L., TORFS, P. J. J. F., UIJLENHOET, R. (2010): Evaluation of a bias correction method applied to downscaled precipitation and temperature reanalysis data for the Rhine basin, Hydrol. Earth Syst. Sci., 14, 687–703, doi:10.5194/hess-14-687- 2010.

THEMESSL, M. J., GOBIET, A., HEINRICH, G. (2012): Empirical-statistical downscaling and error correction of regional climate models and its impact on the climate change signal, Clim. Change, 112, 449–468.

THORNTHWAITE, C.W. (1948): An Approach toward a Rational Classification of Climate, Geographical Review, Vol. 38, No. 1. (Jan., 1948), pp. 55-94.

THORNTHWAITE, C.W., MATHER, J.R. (1955): The water balance. Phiadelphia, PA: Drexel Institue of technology, climatological laboratory publication 8.

ULBRICH, U., FINK, A. H., KLAWA, M., PINTO, J. G. (2000): Three extreme storms over Europe in December 1999. Weather 56

VAN ROOSMALEN, L., SONNENBORG, T. O., JENSEN, K. H. (2009): Impact of climate and land use change on the hydrology of a large-scale agricultural catchment, Water Resour. Res., 45, W00A15, doi:10.1029/2007WR006760

VARIS, O., KAJANDER, T., LEMMELÄ, R. (2004): Climate and water: from climate models to water resources management and vice versa. Clim. Change 66 (3), 321–344. http://dx.doi.org/10.1023/B:CLIM.0000044622.42657.d4.

VAUTARD, R., GOBIET, A., SOBOLOWSKI, S., KJELLSTRÖM, E., STEGEHUIS, A., WATKISS, P., MENDLIK, T., LANDGREN, O., NIKULIN, G., TEICHMANN, C., JACOB, D. (2014): The European climate under a 2 °C global warming, Environ. Res. Lett. 9 034006 (11pp), doi:10.1088/1748-9326/9/3/034006

VON UNOLD, G., FANK, J. (2005): Mechanic Cultivated, Weighable Monolithic Lysimeters. 11th Gumpensteiner Lysimeter Conference, Irdning.

VÖRÖSMARTY, C. J., FEDERER, C. A., SCHLOSS, A. L. (1998): Potential evaporation functions compared on US watersheds: Possible implications for global-scale water balance and terrestrial ecosystem modeling, Journal of Hydrology 207(3-4): 147-169.

VÖRÖSMARTY, C. J., GREEN, P., SALISBURY, J., LAMMERS, R. B. (2000): Global water resources: vulnerability from climate change and population growth, Science, 289, 547.

WANG, J., RICH, P. M., PRICE, K. P. (2003): Temporal responses of NDVI to precipitation and temperature in the central Great Plains, USA. Int J Remote Sens 24:2345–2364.

WILCKE, R. A. I., MENDLIK, T., GOBIET, A. (2013): Multi-variable error correction of regional climate models, Clim. Change, 120, 871–887.

WILSON, B.N., BROWN J. W. (1992): Development and evaluation of dimensionless unit hydrograph, Water Resource Bulletin: 28: 397-408.

WINTER, T. C. (1983): The interaction of lakes with variably saturated porous media. Water Resour. Res. 19 (5), 1203–1218.

WOLDEAMLAK, S., BATELAAN, O., DE SMEDT, F. (2007): Effects of climate change on the groundwater system in the Grote-Nete catchment, Belgium, Hydrogeol. J., 15(5), 891–901.

WOLOCK, D.M., MCCABE, G.J. (1999): Estimates of runoff using water balance and atmospheric general circulation models. JAWRA 35(6): 1341-1349.

XU, C.Y., SINGH, V.P. (2002): Cross-comparison of empirical equations for calculating potential evapotranspiration with data from Switzerland. Water Resources Mgmt. 16(3): 197-219.

XYSTRAKIS, F., MATZARAKIS, A. (2010): The importance of meteorological variables in the bias of potential evapotranspiration estimates in Crete, southern Greece. In Proc.7th Conf. on Biometeorology 20: 96-100. A. Matzarakis, H.Mayer, and F. M. Chmielewski, eds. Freiburg, Germany: University of Freiburg Meteorological Institute.

XYSTRAKIS, F., MATZARAKIS, A. (2011): Evaluation of 13 empirical reference potential evapotranspiration equations on the island of Crete in southern Greece. J. Irrig. Drain. Eng.137(4): 211-222.

YUSOFF, I., HISCOCK, K. M., CONWAY, D. (2002): Simulation of the impacts of climate change on groundwater resources in eastern England, Geol. Soc. London Spec. Pub., 193(1), 325–344.

ZAMFIR, R.H.C. (2014): The impact of climate changes on water balance from western Romania using computer tools, Recent Advances in Energy, Environment, Biology and Ecology, ISBN: 978-960-474-358-2.

ZEKTSER, I. S., LOAICIGA, H. A. (1993): Groundwater fluxes in the global hydrologic cycle: Past, present and future. J. Hydrol. 144 (1–4), 405–427

ZHANG L., K. HICKEL, AND DAWES W. R. (2004): A rational function approach for estimating mean annual evapotranspiration. Water Resources Res. 40: W02502.

ZHOU G. Y., SUN G., WANG, X., ZHOU, C.Y., MCNULTY, S.G., VOSE, J.M,, AMATYA, D.M.. (2008): Estimating forest ecosystem evapotranspiration at multiple temporal scale.

URL1: http://klimabarat.hu/node/96 (Access date: 01.31. 2014)
URL2: http://www.wmo.int/pages/themes/climate/climate_models.php (Access date: 10.01.2015)
URL3: http://www.climateprojection.net/climate-science/climate-modelling/regional-models/ (Access date: 10.03.2015)
URL4: http://www.wmo.int/pages/themes/climate/climate_models.php (Access date: 11.03.2016)
URL5: http://link.springer.com/referenceworkentry/10.1007%2F978-90-481-3585-1_58 (Access date: 13.01.2016)
URL6: https://nrcca.cals.cornell.edu/soil/CA2/CA0212.1-3.php (Access date: 20.01.2016)
URL7: http://www.virginiaplaces.org/watersheds/graphics/groundh20.png (Access date: 20.01.2016)
URL8: http://www.ontariograinfarmer.ca/Portals/1/Issues/2013/January%202013/Water.jpg (Access date: 12.10.2015)
URL9: https://svs.gsfc.nasa.gov/vis/a030000/a030500/a030580/water_cycle.png (Access date: 15.04.2015)
URL10:http://www.fao.org/docrep/X0490E/x0490e07.htm#latent%20heat%20of%20vaporization%20(l) (Access date: 17.11.2015)
URL11: http://www.fs.fed.us/t-d/atv_trails_site/images/interception.png (Access date: 11.11.2015)
URL12: https://modis.gsfc.nasa.gov/data/ (Access date: 28.05.2015)
URL13: http://mubil.boku.ac.at/?page_id=5 (Access date: 10.06.2015)
URL14:https://climate4impact.eu/impactportal/documentation/backgroundandtopics.jsp?q=Uncertainties (Access date: 10.08.2017)

List of figures

Figure 2.1. The saturated and the unsaturated zones (URL7)
Figure 2.2. The available water in the different case of physical soil types (URL8)
Figure 2.3. Actual yield/maximum yield (Nebo and Sumaya, 2012)
Figure 2.4. The water-cycle (URL10)
Figure 2.5. The effect of advected air that passing from dryland over an irrigated land (McMahon et al., 2013)
Figure 2.6. The process of the interception (URL11)

Figure 4.1. Schematic representation of the linear transformation of the MODIS daytime surface temperature values into ET rates (Szilágyi et al., 2011)
Figure 4.2. Nine years averaged (2000-2008) mean monthly ET rates (mm) (Szilágyi and Kovács, 2010)
Figure 4.3. Scheme of the lysimeter facility in Groß-Enzersdorf (Nolz and Cepuder, 2008)
Figure 4.4. Lysimeter weighing facility: a small fraction of the total mass is transmitted to an electronic load cell via a lever-arm mechanism with a counterbalance (measuring accuracy is ±0.18 kg.) (Nolz et al., 2013)
Figure 4.5. The location of study areas
Figure 4.6. Forested area with the grid cells
Figure 4.7. Location of the Marchfeld and the experimental site of BOKU in Groß-Enzersdorf (URL12)
Figure 4.8. Graphical representation of the model of forested area and mixed parcel. (Parameters: ET_CREMAP is the measured actual evapotranspiration; PETH is the Hamon type potential evapotranspiration; PETM is the calibrated potential evapotranspiration; ET_M is the actual evapotranspiration, SOIL_MAX CALIBRATED is the calibrated soil-water storage capacity, and SOIL_M is the soil moisture. The different shapes with the different type of arrows illustrate the connections amongst the used parameters during the model workflow.)
Figure 4.9. The domain of the FORESEE database (dotted rectangle) containing climatic data for the period 1951-2100. The data are distributed in 5,408 (104·52) grid cells organized in 1/6·1/6° regular grid (Dobor et al. 2012)
Figure 4.10. Graphical representation of the projection phase of the model. (Parameters: PETH is the Hamon type potential evapotranspiration; PETM is the calibrated potential evapotranspiration; ET_M is the actual evapotranspiration, SOIL_MAX CALIBRATED is the calibrated soil-water storage capacity, SOIL_M is the soil moisture, and equation of the broken line regression, which can be found on Table 5.1. The different shapes with the different type of arrows illustrate the connections amongst the used parameters during the model workflow.)

Figure 5.1. Relationship between $PET_{CREMAP}/PET_{LYSIMETER}$ and PET_H in growing and dormant seasons with a 1:1 line (dotted), at forested area (a), at mixed parcel (b), at Marchfeld (c) (i.e., the calibration of PET_H). The triangles represent the values of the dormancy, while

the dots represent the values of the growing season. The reason of vertical dotted line is the separation of the two characteristically different state of the vegetation
Figure 5.2. Relationship between the calculated ET_M and the measured ET_{CREMAP}; i.e., the calibrated model of forested area (a), mixed parcel (b), Marchfeld (c)
Figure 5.3. Correlation between the measured $ET_{CREMAP}/ET_{LYSIMETER}$ and calculated ET_M values (i.e., the validation of forested area (a), mixed parcel (b), Marchfeld (c)
Figure 5.4. Temperature averages for forested area (a), mixed parcel (b), and Marchfeld (c) during the 21st century (Model ID '0' represents observation-based data and the regional climate model's IDs listed in Table 4.1)
Figure 5.5. Precipitation averages for forested area (a), mixed parcel (b), and Marchfeld (c) area during the 21st century (Model ID '0' represents observation-based data and the regional climate model's IDs listed in Table 4.1)
Figure 5.6. The projected means of evapotranspiration for the study areas (forested area (a), mixed parcel (b), Marchfeld (c)) between 1985/2100 on the basis of the projected temperature and precipitations derived from the 4 RCMs (Model ID '0' represents observation-based data and the regional climate model's IDs listed in Table 4.1)
Figure 5.7. The projected 10th percentile values of soil moisture for the study areas (forested area (a), mixed parcel (b), Marchfeld (c)) between 1985/2100 on the basis of the projected temperature and precipitations derived from the 4 RCMs (Model ID '0' represents observation-based data and the regional climate model's IDs listed in Table 4.1)
Figure 5.8. Monthly values of ET_M in the case of forested area for the investigated 30-year means
Figure 5.9. Monthly values of ET_M in the case of mixed parcel for the investigated 30-year means
Figure 5.10. Monthly values of ET_M in the case of Marchfeld for the investigated 30-year means
Figure 5.11. Monthly values of $SOIL_M$ in the case of forested area for the investigated 30-year means
Figure 5.12. Monthly values of $SOIL_M$ in the case of mixed parcel for the investigated 30-year means
Figure 5.13. Monthly values of $SOIL_M$ in the case of Marchfeld for the investigated 30-year means
Figure 5.14. Relative extractable water in the case of the forested area
Figure 5.15. Relative extractable water in the case of the mixed parcel
Figure 5.16. Relative extractable water in the case of the Marchfeld
Figure 5.17. Soil water deficit (SWD) values of forested area
Figure 5.18. Soil water deficit (SWD) values of mixed parcel
Figure 5.19. Soil water deficit (SWD) values of Marchfeld
Figure 5.20. The projected ET_M values between 1985-2100; a: first run, and b: second run
Figure 5.21. The projected 10th percentile minimum values of soil moisture between 1985-2100; a: first run, and b: second run
Figure 5.22. Monthly values of ET_M in the projection periods; a: first run, and b: second run

10.13147/SOE.2018.004

Figure 5.23. Monthly values of $SOIL_M$ in the projection periods (solid lines) and estimated soil water deficit calculated as potential ET minus $SOIL_M$ (dashed lines); first run (a) and second run (b)

10.13147/SOE.2018.004

List of tables

Table 2.1. Types of evapotranspirations and their main properties (after Dingman (2002; pp. 276, table 7.1)

Table 4.1. The applied RCMs (Jacob, 2001; Jacob et al., 2007; Christensen and van Meijgaard, 1992; Christensen et al., 1996; Jones et al., 2004)
Table 4.2. The tasks of the dissertation based on the main objective with the used methods

Table 5.1. Broken-line regressions results of the 3 study areas
Table 5.2. Results of the adjusted, re-calibrated model parameters for the study sites
Table 5.3. Soil types, values of field capacity, permanent wilting point, re-calibrated $SOIL_{MAX}$ and re-calibrated rooting depth in the study areas. Soil types were determined using the available data in the AgroClimate.2 project (forested area), soil sampling from borehole (mixed parcel). Field capacity and permanent wilting point values of forested area and mixed parcel were used in accordance with Maidment (1993)
Table 5.4. Main properties of the soil profile in the lysimeter. Unit [$l \cdot m^{-2}$] is equal with [mm] (after personal communication with Reinhard Nolz)
Table 5.5. Results of the models after adjustment for forested area and mixed parcel (2000-2008) and Marchfeld (2004-2011) ($SOIL_{M\_MIN}$ means the lowest value of soil moisture)
Table 5.6. ET_M, $SOIL_M$ and $SOIL_{M\_10Percentile}$ values (30-year means of mean values of the RCMs) with standard deviations (30-year means of standard deviations' means of the individual RCMs) in parentheses; i.e. the results of the projection for the study areas
Table 5.7. The values of relative extractable water (REW) in the 21st century for the study areas
Table 5.8. The values of soil water deficit (SWD) in the 21st century for the study areas
Table 5.9. Comparison of the ET_M, $SOIL_M$ and $SOIL_{M\_10Percentile}$ values of static and extended rooting depths at the Marchfeld

Annex

Annex 1. The identification numbers (ID) of the grid cells over Hungary with the involved areas (The IDs are illustrated on Figure 4.6.)

Grid cell ID	Area [%]
3	19.91
4	4.23
8	98.47
9	97.38
7	65.6
10	22.56
6	4.61
12	33.4
13	77.81
11	0.04
15	44.43
14	98.88
20	15.7
19	17.21

10.13147/SOE.2018.004

Annex 2. The original model with snowpacks and snowmelts

Monthly precipitation must be divided into snow $SNOW_M$ and rain $RAIN_M$ (Dingman, 2002).

$$RAIN_M = F_m \cdot P_m$$

$$SNOW_m = (1 - F_m) \cdot P_m$$

F_m: melt factor

If: $T_m \leq 0$ °C $\rightarrow F_m = 0$

If: 0 °C $\leq T_m \leq 6$ °C $\rightarrow F_m = 0.167 \cdot T_m$

If: $T_m \geq 6$ °C $F_m = 1$

$$MELT_M = F_m(PACK_{m-1} + SNOW_m)$$

$PACK_{m-1}$: snowpack water equivalent at the end of month m^{-1}.

$$PACK_m = (1 - F_m)^2 \cdot P_m + (1 - F_m) \cdot PACK_{m-1}$$

$$W_m = RAIN_m + MELT_m$$

W_m: water input

Annex 3. Input and results databases of study areas for present

Input data of forested area

Date	ET.CREMAP [mm]	P [mm]	T [°C]
15.01.1999	NA	11.9	0.0
15.02.1999	NA	34.3	1.1
15.03.1999	NA	28.0	7.9
15.04.1999	NA	85.3	12.4
15.05.1999	NA	76.5	16.1
15.06.1999	NA	85.4	18.6
15.07.1999	NA	119.5	21.5
15.08.1999	NA	94.3	19.8
15.09.1999	NA	58.8	18.6
15.10.1999	NA	20.9	11.6
15.11.1999	11.1	67.8	3.6
15.12.1999	NA	58.8	0.5
15.01.2000	NA	28.6	-1.4
15.02.2000	NA	14.6	4.8
15.03.2000	23.9	78.4	7.0
15.04.2000	71.7	39.8	14.3
15.05.2000	124.8	31.7	17.7
15.06.2000	150.3	31.9	20.7
15.07.2000	95.3	100.6	19.7
15.08.2000	101.9	67.2	22.3
15.09.2000	48.0	52.9	16.3
15.10.2000	27.9	87.9	13.6
15.11.2000	12.1	57.1	8.7
15.12.2000	NA	47.8	1.9
15.01.2001	NA	10.5	0.8
15.02.2001	NA	14.5	3.9
15.03.2001	33.6	56.8	8.1
15.04.2001	49.8	34.7	10.4
15.05.2001	103.0	29.7	17.6
15.06.2001	114.6	41.4	18.1
15.07.2001	108.3	86.7	21.6
15.08.2001	108.1	32.1	22.8
15.09.2001	43.4	126.2	14.7
15.10.2001	27.5	21.8	14.2
15.11.2001	10.0	31.5	4.5
15.12.2001	NA	33.3	-2.7

15.01.2002	NA	4.3	1.0
15.02.2002	NA	21.4	1.0
15.03.2002	24.1	69.7	7.8
15.04.2002	41.4	40.7	10.5
15.05.2002	104.0	30.3	18.1
15.06.2002	104.0	44.8	21.0
15.07.2002	115.1	43.4	22.8
15.08.2002	87.6	143.2	21.4
15.09.2002	43.6	55.2	15.5
15.10.2002	22.2	94.1	10.3
15.11.2002	9.7	52.6	8.2
15.12.2002	NA	53.5	-0.7
15.01.2003	NA	36.0	-0.8
15.02.2003	NA	2.8	-1.5
15.03.2003	23.0	8.3	6.9
15.04.2003	52.7	33.8	10.3
15.05.2003	122.1	52.5	18.4
15.06.2003	140.4	70.5	22.8
15.07.2003	118.9	82.6	22.1
15.08.2003	99.5	39.0	24.6
15.09.2003	56.2	26.9	16.7
15.10.2003	27.4	73.0	8.5
15.11.2003	11.1	28.5	7.2
15.12.2003	NA	31.4	0.8
15.01.2004	NA	34.7	-1.3
15.02.2004	NA	56.6	2.6
15.03.2004	29.7	50.8	4.7
15.04.2004	51.3	51.8	11.7
15.05.2004	91.8	83.9	13.9
15.06.2004	107.9	125.6	18.2
15.07.2004	116.5	25.8	20.4
15.08.2004	106.6	37.7	21.0
15.09.2004	49.1	23.2	15.9
15.10.2004	33.3	52.9	12.0
15.11.2004	12.4	23.7	5.8
15.12.2004	NA	25.6	0.6
15.01.2005	NA	18.9	1.3
15.02.2005	NA	35.7	-1.8
15.03.2005	20.0	16.8	4.0
15.04.2005	49.8	48.5	11.6
15.05.2005	111.1	55.4	15.9

15.06.2005	117.6	41.8	19.0
15.07.2005	123.9	88.1	21.0
15.08.2005	82.8	159.2	19.2
15.09.2005	53.2	45.6	17.2
15.10.2005	37.0	3.9	11.8
15.11.2005	7.2	50.3	4.2
15.12.2005	NA	61.3	0.6
15.01.2006	NA	43.6	-3.3
15.02.2006	NA	25.9	-0.1
15.03.2006	20.9	38.1	4.4
15.04.2006	53.5	72.6	12.8
15.05.2006	86.5	74.5	15.4
15.06.2006	125.2	101.6	19.4
15.07.2006	152.0	23.3	23.7
15.08.2006	83.5	149.9	18.8
15.09.2006	64.5	15.3	18.2
15.10.2006	36.3	35.3	13.6
15.11.2006	13.4	30.4	7.6
15.12.2006	NA	11.16	3.0
15.01.2007	NA	47.1	5.3
15.02.2007	NA	34.2	5.6
15.03.2007	20.8	89.7	8.5
15.04.2007	89.6	0.3	13.7
15.05.2007	103.7	78.3	17.2
15.06.2007	128.1	36.5	21.6
15.07.2007	157.0	71.6	22.6
15.08.2007	109.0	112.3	21.5
15.09.2007	45.6	171.8	14.5
15.10.2007	26.2	74.0	9.8
15.11.2007	11.1	37.1	4.3
15.12.2007	NA	48.3	-0.1
15.01.2008	NA	17.4	3.1
15.02.2008	NA	3.5	4.6
15.03.2008	14.8	55.4	7.1
15.04.2008	50.8	48.5	11.8
15.05.2008	100.5	38.9	16.7
15.06.2008	125.8	231.6	20.6
15.07.2008	118.1	136.5	21.2
15.08.2008	121.7	79.3	20.9
15.09.2008	36.9	43.7	15.5
15.10.2008	32.2	26.1	11.8

15.11.2008	12.5	39.4	7.2
15.12.2008	NA	51.4	2.2

Model results of forested area

Date	ET_M [mm]	SOIL_M [mm]
15.01.1999	NA	502.4
15.02.1999	8.4	502.4
15.03.1999	29.3	501.1
15.04.1999	53.8	502.4
15.05.1999	86.4	492.5
15.06.1999	104.5	473.4
15.07.1999	127.5	465.3
15.08.1999	102.2	457.5
15.09.1999	75.4	440.9
15.10.1999	34.1	427.8
15.11.1999	9.5	486.1
15.12.1999	7.4	502.4
15.01.2000	6.9	502.4
15.02.2000	10.8	502.4
15.03.2000	26.4	502.4
15.04.2000	62.2	480.0
15.05.2000	89.8	421.9
15.06.2000	100.2	353.6
15.07.2000	110.1	344.1
15.08.2000	102.0	309.3
15.09.2000	60.4	301.8
15.10.2000	43.5	346.2
15.11.2000	17.1	386.2
15.12.2000	8.1	425.9
15.01.2001	7.9	428.5
15.02.2001	9.9	433.1
15.03.2001	29.9	459.9
15.04.2001	44.3	450.3
15.05.2001	85.3	394.7
15.06.2001	86.2	350.0
15.07.2001	114.8	321.8
15.08.2001	86.2	267.7
15.09.2001	57.6	336.2
15.10.2001	37.5	320.5
15.11.2001	10.0	342.0

15.12.2001	6.1	369.2
15.01.2002	7.0	366.5
15.02.2002	8.4	379.5
15.03.2002	29.0	420.3
15.04.2002	44.9	416.1
15.05.2002	83.6	362.8
15.06.2002	97.0	310.6
15.07.2002	97.0	256.9
15.08.2002	114.1	286.0
15.09.2002	58.7	282.5
15.10.2002	31.7	344.9
15.11.2002	15.9	381.6
15.12.2002	6.9	428.2
15.01.2003	7.2	457.0
15.02.2003	6.8	453.0
15.03.2003	24.1	437.3
15.04.2003	43.3	427.8
15.05.2003	92.0	388.2
15.06.2003	118.9	339.8
15.07.2003	115.0	307.4
15.08.2003	94.5	251.9
15.09.2003	46.3	232.4
15.10.2003	26.0	279.4
15.11.2003	13.4	294.5
15.12.2003	7.6	318.3
15.01.2004	7.0	346.0
15.02.2004	9.5	393.1
15.03.2004	19.7	424.1
15.04.2004	50.8	425.1
15.05.2004	73.8	435.2
15.06.2004	102.6	458.3
15.07.2004	103.8	380.3
15.08.2004	89.5	328.4
15.09.2004	48.5	303.2
15.10.2004	37.6	318.5
15.11.2004	10.8	331.4
15.12.2004	7.5	349.5
15.01.2005	8.2	360.3
15.02.2005	7.1	388.9
15.03.2005	17.6	388.2
15.04.2005	49.9	386.8

15.05.2005	77.8	364.3
15.06.2005	86.8	319.3
15.07.2005	110.2	297.2
15.08.2005	98.9	357.5
15.09.2005	62.4	340.6
15.10.2005	25.5	319.0
15.11.2005	9.9	359.4
15.12.2005	7.5	413.3
15.01.2006	6.2	450.6
15.02.2006	7.8	468.7
15.03.2006	18.9	487.9
15.04.2006	55.7	502.4
15.05.2006	82.3	494.7
15.06.2006	110.7	485.5
15.07.2006	128.8	380.0
15.08.2006	96.2	433.6
15.09.2006	64.0	385.0
15.10.2006	41.5	378.7
15.11.2006	14.4	394.7
15.12.2006	8.6	397.3
15.01.2007	10.3	434.1
15.02.2007	10.9	457.4
15.03.2007	31.3	502.4
15.04.2007	56.4	446.3
15.05.2007	91.9	432.7
15.06.2007	108.2	361.0
15.07.2007	116.2	316.5
15.08.2007	113.9	314.9
15.09.2007	56.7	430.0
15.10.2007	30.1	473.9
15.11.2007	9.9	501.1
15.12.2007	7.2	502.4
15.01.2008	9.1	502.4
15.02.2008	10.6	495.3
15.03.2008	26.7	502.4
15.04.2008	51.2	499.7
15.05.2008	87.4	451.2
15.06.2008	119.8	502.4
15.07.2008	125.7	502.4
15.08.2008	109.6	472.2
15.09.2008	60.0	455.8

15.10.2008	35.8	446.2
15.11.2008	13.4	472.1
15.12.2008	8.2	502.4

Input data of mixed parcel

Date	ET.CREMAP [mm]	P [mm]	T [°C]
15.01.1999	NA	12.3	0.2
15.02.1999	NA	53.6	0.9
15.03.1999	NA	18.2	7.7
15.04.1999	NA	61.4	12.0
15.05.1999	NA	47.9	16.3
15.06.1999	NA	97.3	19.0
15.07.1999	NA	74.2	21.8
15.08.1999	NA	64.3	19.8
15.09.1999	NA	24.5	19.0
15.10.1999	NA	26.9	11.6
15.11.1999	11.7	63.1	3.8
15.12.1999	NA	50.8	0.9
15.01.2000	NA	46.7	1.9
15.02.2000	NA	23.9	4.5
15.03.2000	20.9	86.4	6.7
15.04.2000	42.4	20.0	14.3
15.05.2000	85.4	20.3	17.9
15.06.2000	105.4	11.5	20.5
15.07.2000	89.1	69.0	19.7
15.08.2000	62.0	34.2	22.3
15.09.2000	36.6	43.3	16.3
15.10.2000	23.6	44.4	14.0
15.11.2000	13.4	54.5	9.2
15.12.2000	NA	45.0	2.2
15.01.2001	NA	13.2	0.7
15.02.2001	NA	16.2	3.8
15.03.2001	24.6	53.5	7.8
15.04.2001	38.1	25.9	10.1
15.05.2001	82.2	19.9	17.4
15.06.2001	93.0	29.8	18.0
15.07.2001	97.4	65.7	21.6
15.08.2001	79.5	41.1	22.4
15.09.2001	44.8	121.1	14.7
15.10.2001	22.5	10.6	14.2

15.11.2001	11.5	38.2	4.1
15.12.2001	NA	35.0	3.6
15.01.2002	NA	13.7	0.6
15.02.2002	NA	26.4	5.7
15.03.2002	17.5	47.6	7.5
15.04.2002	30.0	32.2	10.6
15.05.2002	76.8	27.6	18.5
15.06.2002	76.8	40.2	21.0
15.07.2002	82.9	44.0	23.1
15.08.2002	73.0	89.5	21.7
15.09.2002	35.9	54.9	15.7
15.10.2002	22.4	80.4	10.3
15.11.2002	12.5	53.2	8.5
15.12.2002	NA	60.4	-0.6
15.01.2003	NA	43.0	-1.3
15.02.2003	NA	1.1	1.3
15.03.2003	0.0	3.2	6.5
15.04.2003	13.7	23.8	10.4
15.05.2003	111.7	53.5	18.6
15.06.2003	130.2	52.2	22.7
15.07.2003	95.7	67.1	22.0
15.08.2003	50.4	40.1	24.0
15.09.2003	29.5	18.8	16.6
15.10.2003	21.2	57.9	8.5
15.11.2003	9.6	22.8	7.6
15.12.2003	NA	22.8	1.2
15.01.2004	NA	41.3	1.9
15.02.2004	NA	47.0	2.4
15.03.2004	24.9	68.7	4.7
15.04.2004	46.1	48.4	12.0
15.05.2004	100.6	61.4	14.4
15.06.2004	114.1	98.3	18.7
15.07.2004	94.4	25.1	20.5
15.08.2004	67.1	19.9	21.3
15.09.2004	25.2	31.1	16.1
15.10.2004	40.4	41.6	12.3
15.11.2004	12.8	40.3	5.9
15.12.2004	NA	19.2	1.1
15.01.2005	NA	37.2	0.9
15.02.2005	NA	46.1	1.7
15.03.2005	24.0	27.3	4.0

15.04.2005	23.5	55.3	11.6
15.05.2005	88.5	40.9	16.2
15.06.2005	106.3	34.9	19.0
15.07.2005	112.3	80.5	21.4
15.08.2005	78.1	159.0	19.2
15.09.2005	48.1	44.9	17.4
15.10.2005	23.7	2.7	11.7
15.11.2005	9.5	42.9	4.4
15.12.2005	NA	76.0	0.7
15.01.2006	NA	61.2	-3.0
15.02.2006	NA	33.9	-0.4
15.03.2006	7.6	39.6	4.0
15.04.2006	25.4	78.6	12.4
15.05.2006	78.9	88.6	15.4
15.06.2006	129.6	63.9	19.6
15.07.2006	116.3	24.4	23.7
15.08.2006	79.3	107.4	19.0
15.09.2006	39.5	18.6	18.3
15.10.2006	8.0	23.7	13.6
15.11.2006	12.4	33.3	7.6
15.12.2006	NA	14.0	3.5
15.01.2007	NA	29.7	5.0
15.02.2007	NA	38.7	5.6
15.03.2007	24.2	72.4	8.3
15.04.2007	52.8	0.0	12.8
15.05.2007	90.9	45.3	17.8
15.06.2007	90.7	80.3	22.0
15.07.2007	73.9	45.4	22.8
15.08.2007	61.3	59.1	21.8
15.09.2007	43.2	156.8	14.6
15.10.2007	18.3	62.1	9.9
15.11.2007	11.8	49.6	4.3
15.12.2007	NA	29.7	0.4
15.01.2008	NA	35.6	2.7
15.02.2008	NA	8.7	4.2
15.03.2008	17.9	64.1	7.1
15.04.2008	30.9	31.3	11.8
15.05.2008	87.5	45.2	16.8
15.06.2008	119.8	95.7	21.2
15.07.2008	108.4	131.8	21.4
15.08.2008	114.3	48.6	20.9

15.09.2008	26.5	43.3	15.9
15.10.2008	25.6	21.6	11.9
15.11.2008	12.3	35.5	7.6
15.12.2008	NA	55.7	2.9

Model results of mixed parcel

Date	ET_M [mm]	SOIL_M [mm]
15.01.1999	NA	276.9
15.02.1999	9.8	276.9
15.03.1999	19.5	275.6
15.04.1999	43.3	276.9
15.05.1999	78.1	246.6
15.06.1999	100.1	243.8
15.07.1999	113.9	204.1
15.08.1999	86.0	182.4
15.09.1999	52.8	154.1
15.10.1999	27.0	154.0
15.11.1999	11.4	205.8
15.12.1999	9.0	247.7
15.01.2000	10.0	276.9
15.02.2000	12.5	276.9
15.03.2000	17.8	276.9
15.04.2000	52.0	244.8
15.05.2000	74.9	190.2
15.06.2000	69.4	132.4
15.07.2000	86.0	115.3
15.08.2000	62.9	86.7
15.09.2000	47.4	82.5
15.10.2000	36.1	90.8
15.11.2000	15.4	129.9
15.12.2000	9.7	165.3
15.01.2001	9.2	169.2
15.02.2001	11.6	173.8
15.03.2001	19.8	207.6
15.04.2001	32.8	200.7
15.05.2001	63.1	157.5
15.06.2001	62.2	125.1
15.07.2001	88.7	102.1
15.08.2001	64.8	78.3
15.09.2001	49.1	150.3

15.10.2001	24.3	136.7
15.11.2001	11.6	163.3
15.12.2001	10.5	187.7
15.01.2002	9.2	192.2
15.02.2002	13.0	205.6
15.03.2002	18.8	234.3
15.04.2002	36.4	230.2
15.05.2002	76.8	180.9
15.06.2002	83.5	137.6
15.07.2002	82.3	99.3
15.08.2002	96.2	92.5
15.09.2002	53.8	93.7
15.10.2002	22.6	151.5
15.11.2002	14.8	189.9
15.12.2002	8.2	242.1
15.01.2003	8.2	276.9
15.02.2003	9.9	268.1
15.03.2003	16.8	254.5
15.04.2003	35.1	243.3
15.05.2003	87.4	209.4
15.06.2003	103.4	158.2
15.07.2003	97.1	128.2
15.08.2003	74.8	93.5
15.09.2003	31.3	81.1
15.10.2003	17.9	121.0
15.11.2003	14.1	129.7
15.12.2003	9.1	143.4
15.01.2004	10.0	174.7
15.02.2004	11.1	210.6
15.03.2004	15.8	263.4
15.04.2004	43.2	268.6
15.05.2004	68.2	261.9
15.06.2004	98.3	261.9
15.07.2004	96.4	190.6
15.08.2004	70.9	139.6
15.09.2004	43.0	127.6
15.10.2004	29.6	139.6
15.11.2004	12.8	167.0
15.12.2004	9.1	177.2
15.01.2005	9.4	205.0
15.02.2005	10.3	240.8

15.03.2005	15.3	252.8
15.04.2005	41.6	266.5
15.05.2005	75.4	232.0
15.06.2005	84.0	182.9
15.07.2005	104.9	158.5
15.08.2005	91.3	226.3
15.09.2005	58.9	212.2
15.10.2005	20.9	194.0
15.11.2005	11.7	225.2
15.12.2005	8.9	276.9
15.01.2006	7.4	276.9
15.02.2006	9.1	276.9
15.03.2006	15.2	276.9
15.04.2006	45.2	276.9
15.05.2006	74.4	276.9
15.06.2006	102.2	238.5
15.07.2006	105.8	157.1
15.08.2006	89.8	174.7
15.09.2006	46.9	146.4
15.10.2006	29.3	140.8
15.11.2006	14.1	160.0
15.12.2006	10.4	163.6
15.01.2007	11.9	181.3
15.02.2007	12.9	207.2
15.03.2007	21.5	258.1
15.04.2007	40.3	217.8
15.05.2007	77.4	185.7
15.06.2007	107.4	158.6
15.07.2007	87.8	116.1
15.08.2007	78.5	96.7
15.09.2007	48.7	204.8
15.10.2007	21.1	245.8
15.11.2007	11.7	276.9
15.12.2007	8.7	276.9
15.01.2008	10.4	276.9
15.02.2008	12.3	273.2
15.03.2008	18.1	276.9
15.04.2008	42.1	266.1
15.05.2008	79.2	232.0
15.06.2008	113.2	214.5
15.07.2008	120.4	226.0

15.08.2008	88.9	185.7
15.09.2008	50.8	178.2
15.10.2008	25.9	173.9
15.11.2008	14.1	195.4
15.12.2008	10.1	241.0

Input data of Marchfeld

Index	ET.LYSIMETER [mm]	P [mm]	T [°C]
31.01.2004	NA	42.4	-1.6
29.02.2004	NA	54.8	3.4
31.03.2004	NA	55.3	4.5
30.04.2004	NA	45.9	12.0
31.05.2004	NA	52.2	14.4
30.06.2004	NA	167.2	18.1
31.07.2004	122.2	89.9	20.2
31.08.2004	127.3	132.8	20.8
30.09.2004	61.3	38.8	15.8
31.10.2004	24.9	48.1	11.9
30.11.2004	NA	29.3	6.3
31.12.2004	NA	9.5	1.3
31.01.2005	NA	30.0	1.9
28.02.2005	NA	31.7	-1.1
31.03.2005	NA	18.6	4.0
30.04.2005	71.2	82.7	11.3
31.05.2005	114.1	110.4	15.8
30.06.2005	141.7	155.5	18.9
31.07.2005	134.8	162.6	21.2
31.08.2005	85.4	188.2	19.0
30.09.2005	70.0	70.6	17.1
31.10.2005	35.1	15.5	11.1
30.11.2005	NA	34.5	4.4
31.12.2005	NA	17.1	0.7
31.01.2006	NA	34.6	-3.9
28.02.2006	NA	18.7	-0.2
31.03.2006	NA	46.2	3.8
30.04.2006	70.6	98.4	12.0
31.05.2006	100.9	118.8	15.1
30.06.2006	118.3	132.3	19.1
31.07.2006	167.4	132.7	23.6
31.08.2006	94.9	158.7	18.6

30.09.2006	88.7	73.5	18.1
31.10.2006	45.3	58.2	13.1
30.11.2006	NA	25.6	8.0
31.12.2006	NA	13.3	3.8
31.01.2007	NA	34.2	5.9
28.02.2007	NA	44.5	5.5
31.03.2007	39.7	82.7	8.2
30.04.2007	98.2	58.0	12.8
31.05.2007	126.9	105.2	17.1
30.06.2007	157.7	156.0	21.4
31.07.2007	175.6	144.5	22.5
31.08.2007	137.9	164.1	21.1
30.09.2007	66.4	176.5	14.4
31.10.2007	31.7	79.1	9.4
30.11.2007	NA	30.6	4.1
31.12.2007	NA	44.2	0.8
31.01.2008	NA	26.4	3.4
29.02.2008	NA	5.9	4.5
31.03.2008	42.0	47.9	6.9
30.04.2008	75.6	63.7	11.2
31.05.2008	140.2	145.9	15.9
30.06.2008	145.9	132.9	20.2
31.07.2008	133.6	136.9	20.9
31.08.2008	114.5	69.9	20.7
30.09.2008	62.1	77.9	15.3
31.10.2008	NA	27.7	11.2
30.11.2008	NA	34.2	7.6
31.12.2008	NA	25.1	2.7
31.01.2009	NA	22.2	-1.7
28.02.2009	NA	30.4	1.7
31.03.2009	32.2	81.4	6.3
30.04.2009	100.9	65.7	14.4
31.05.2009	95.0	87.1	16.4
30.06.2009	NA	190.5	18.6
31.07.2009	NA	72.0	21.8
31.08.2009	NA	61.9	22.1
30.09.2009	61.2	31.6	18.3
31.10.2009	25.4	37.4	10.7
30.11.2009	NA	42.9	7.0
31.12.2009	NA	22.2	1.6
31.01.2010	NA	42.6	-2.3

28.02.2010	NA	8.2	1.2
31.03.2010	32.8	21.5	6.4
30.04.2010	72.1	87.1	10.9
31.05.2010	77.4	116.3	15.3
30.06.2010	126.7	127.4	19.2
31.07.2010	146.0	144.7	22.6
31.08.2010	95.3	168.7	20.0
30.09.2010	60.6	73.2	15.1
31.10.2010	NA	24.4	8.3
30.11.2010	NA	21.2	7.9
31.12.2010	NA	19.1	-2.7
31.01.2011	NA	20.7	0.9
28.02.2011	NA	2.2	0.8
31.03.2011	NA	32.7	6.3
30.04.2011	78.2	60.1	13.3
31.05.2011	119.8	108.5	15.9
30.06.2011	139.4	122.9	20.2
31.07.2011	100.5	91.7	20.2
31.08.2011	118.8	92.5	21.5
30.09.2011	74.3	96.8	18.6
31.10.2011	34.1	63.7	10.6
30.11.2011	NA	9.8	3.7
31.12.2011	NA	10.7	4.0

Model results of Marchfeld

Date	ET_M [mm]	SOIL_M [mm]
31.01.2004	NA	142.4
29.02.2004	26.4	142.4
31.03.2004	32.0	142.4
30.04.2004	65.8	122.5
31.05.2004	78.8	95.8
30.06.2004	121.6	141.4
31.07.2004	127.6	103.7
31.08.2004	121.2	115.3
30.09.2004	67.4	86.7
31.10.2004	47.0	87.8
30.11.2004	28.4	88.7
31.12.2004	15.4	82.7
31.01.2005	18.9	93.8
28.02.2005	20.3	105.2

31.03.2005	27.3	96.4
30.04.2005	64.4	114.8
31.05.2005	95.5	129.6
30.06.2005	127.5	142.4
31.07.2005	142.4	142.4
31.08.2005	108.6	142.4
30.09.2005	85.7	127.3
31.10.2005	38.6	104.2
30.11.2005	25.6	113.1
31.12.2005	18.3	111.9
31.01.2006	13.4	133.1
28.02.2006	21.2	130.5
31.03.2006	30.6	142.4
30.04.2006	67.7	142.4
31.05.2006	91.0	142.4
30.06.2006	129.2	142.4
31.07.2006	160.5	114.6
31.08.2006	106.0	142.4
30.09.2006	90.9	125.0
31.10.2006	51.3	131.9
30.11.2006	30.8	126.7
31.12.2006	21.1	118.9
31.01.2007	23.9	129.2
28.02.2007	29.8	142.4
31.03.2007	39.7	142.4
30.04.2007	70.8	129.6
31.05.2007	103.7	131.1
30.06.2007	147.6	139.5
31.07.2007	153.1	130.9
31.08.2007	122.8	142.4
30.09.2007	71.9	142.4
31.10.2007	38.5	142.4
30.11.2007	25.1	142.4
31.12.2007	18.8	142.4
31.01.2008	21.4	142.4
29.02.2008	26.5	121.8
31.03.2008	36.6	133.1
30.04.2008	63.7	133.1
31.05.2008	96.1	142.4
30.06.2008	138.3	137.0
31.07.2008	139.3	134.6

31.08.2008	110.1	94.3
30.09.2008	76.7	95.6
31.10.2008	38.3	85.0
30.11.2008	30.7	88.5
31.12.2008	21.0	92.7
31.01.2009	15.3	99.6
28.02.2009	24.0	106.0
31.03.2009	35.4	142.4
30.04.2009	78.9	129.1
31.05.2009	97.4	118.8
30.06.2009	125.4	142.4
31.07.2009	130.4	83.9
31.08.2009	94.0	51.9
30.09.2009	49.8	33.7
31.10.2009	38.6	32.4
30.11.2009	29.7	45.6
31.12.2009	19.6	48.2
31.01.2010	14.8	76.0
28.02.2010	15.8	68.4
31.03.2010	27.9	62.0
30.04.2010	62.4	86.7
31.05.2010	92.1	110.8
30.06.2010	129.5	108.8
31.07.2010	151.6	101.9
31.08.2010	115.6	142.4
30.09.2010	75.5	140.1
31.10.2010	35.4	129.1
30.11.2010	29.9	120.4
31.12.2010	15.2	124.3
31.01.2011	17.8	127.2
28.02.2011	19.3	110.1
31.03.2011	34.8	108.0
30.04.2011	70.2	97.9
31.05.2011	95.7	110.8
30.06.2011	134.1	99.5
31.07.2011	117.3	73.9
31.08.2011	107.9	58.5
30.09.2011	94.9	60.4
31.10.2011	42.2	81.9
30.11.2011	17.9	73.8
31.12.2011	16.6	67.9

Annex 4. The script of the model

Present; 'Base model'

```
###Open the required package
library(et.proj)

###Create the input database
raw = read.csv2("raw.csv", stringsAsFactors= FALSE)
raw.xts <- xts(raw[-1] , order.by = as.Date(raw$Index,"%Y-%m-%d"))

###Generate PET values
PETH.xts <- PETH.gen(raw.xts$t)

forsegment.df <- df.segmentit.gen(raw.xts[,1], PETH.xts, raw.xts$P)

###Initial linear regression
lm.fit <- lm(CREMAP ~ PETH - 1 , data=forsegment.df)
###Segmented regression based lm.fit
seg.result <- segmented(lm.fit, seg.Z= ~PETH, psi=40)

###A graphical test; segmented regression
plot(forsegment.df,xlim=c(0,max(forsegment.df$PETH)*1.05),ylim=c(0,max(forsegment.df$CREMAP)*1.05),
type="n", xlab="PETH [mm]",ylab="ET CREMAP [mm/month]", xaxs="i", yaxs="i")
points(forsegment.df[forsegment.df$PETH < seg.result$psi[2],], col="red", pch=24, bg="red")
points(forsegment.df[forsegment.df$PETH >= seg.result$psi[2],], col="blue", pch=23, bg="blue")
plot(seg.result,add=T, rug=F, lwd=2)
# slope(seg.result)
curve(slope(seg.result)$PETH[1,1]*x,from=0,to=seg.result$psi[2],add=T, lwd=2)
axis(1,seg.result$psi[2], tck=1, lty="dotted", lab=F)
text(seg.result$psi[2], 0.5, lab=round(seg.result$psi[2],1), srt=90, adj=c(0, -0.3))

PET.proj <- predict.PETH(seg.result, PETH.xts)

###Calibrate SOILMAX
SOIL.MAX <- optimize(et.test, interval=c(100,10000), temp = raw.xts$t, prec=raw.xts$P, pet.real=PET.proj,
cremap=raw.xts$ET.CREMAP)$minimum

###Calculate the results of base model
Present = et.calc(SOIL_MAX=SOIL.MAX,Temp = raw.xts$t, Prec=raw.xts$P, PET.real=PET.proj)

###Nash coefficient for the full period
LYSALL_ETMALL=(raw.xts$ET.CREMAP)-(Present$ET_M)
LYSCAL_LYS_ALL_Mean=(raw$ET.CREMAP)-(mean(raw$ET.CREMAP, na.rm=TRUE))

1-(sum(LYSALL_ETMALL^2, na.rm = TRUE) / (sum(LYSCAL_LYS_ALL_Mean^2, na.rm = TRUE)))

mean(Present$ET_M, na.rm=TRUE)
mean(Present$SOIL_M, na.rm=TRUE)
min(Present$SOIL_M, na.rm=TRUE)

qtl.Present = quantile(Present$SOIL_M, c(.10))
TENPercentile.Present = Present$SOIL_M[Present$SOIL_M < qtl.Present]

## Plot the calibrated AET
plot(coredata(raw.xts$ET.CREMAP) ~ coredata(Present$ET_M), pch=18,col="darkgreen", xlab="ET_M",
ylab="ET LYSIMETER", xlim = c(0,140), ylim=c(0,160))
Tttmp.lm <- lm(coredata(raw.xts$ET.CREMAP) ~ coredata(Present$ET_M))
Tttmp.sum <- summary(Tttmp.lm)
```

```
abline(Tttmp.lm)
legend("topleft",c(paste("ET CREMAP =",round(coef(Tttmp.lm)[2],2) ,"* ET_M
+",round(coef(Tttmp.lm)[1],2)),paste("R^2 =",round(Tttmp.sum$r.squared,2))))

###Plot precipitation with temperature
plot.prectemp <- function(temp, prec , xaxt = "s") {
  ## plot temp.
  temp.min = -10
  temp.max = 35
  plot(temp, main="", ylim=c(temp.min, temp.max), xaxs= "i", yaxs = "i", xaxt = xaxt)
  par( new=TRUE)
  ## plot prec.
  prec.max = 350
  plot(prec, type="h", ylim=c(prec.max, 0), main="", axes=FALSE, xaxs= "i", yaxs = "i")
  axis(4)
}

par(mfrow = c(3,1), mar=c(0, 4.1, 0, 4.1), oma = c(4.4, 0, 0.5, 0), las=1)
plot.prectemp(raw.xts$t, raw.xts$P, xaxt = "n")

plot(raw.xts$ET.CREMAP, main="", xaxs= "i")
lines(Present$ET_M, col="green")

plot(Present$SOIL_M, main ="", xaxs= "i")
```

Projection phase; Future

```
###Create inputs for projections based on RCMs nc files
remo.echam_RAW = read.csv2("remo.echam.csv", stringsAsFactors= FALSE)
dmi.echam_RAW = read.csv2("dmi.echam.csv", stringsAsFactors= FALSE)
knmi.racmo2_RAW = read.csv2("knmi.racmo2.csv", stringsAsFactors= FALSE)
smhirca.bcm_RAW = read.csv2("smhirca.bcm.csv", stringsAsFactors= FALSE)
present.foresee_RAW = read.csv2("present.foresee.csv", stringsAsFactors= FALSE)

remo.echam=xts(remo.echam_RAW[c("p","t")],as.POSIXct(as.character(remo.echam_RAW$Index)))
dmi.echam=xts(dmi.echam_RAW[c("p","t")],as.POSIXct(as.character(dmi.echam_RAW$Index)))
knmi.racmo2=xts(knmi.racmo2_RAW[c("p","t")],as.POSIXct(as.character(knmi.racmo2_RAW$Index)))
smhirca.bcm=xts(smhirca.bcm_RAW[c("p","t")],as.POSIXct(as.character(smhirca.bcm_RAW$Index)))

present.foresee = xts(present.foresee_RAW[c("p","t")],as.POSIXct(as.character(present.foresee_RAW$Index)))

## Means & standard deviation of RCMs

dmi.echam.T.Yearly = apply.yearly(dmi.echam$t,sum)
remo.echam.T.Yearly = apply.yearly(remo.echam$t,sum)
knmi.racmo2.T.Yearly = apply.yearly(knmi.racmo2$t,sum)
smhirca.bcm.T.Yearly = apply.yearly(smhirca.bcm$t,sum)
present.foresee.T.Yearly = apply.yearly(present.foresee$t, sum)

remo.echam.T.avg = c(mean(remo.echam$t['2015/2044']), mean(remo.echam$t['2045/2074']),
mean(remo.echam$t['2070/2099']))
knmi.racmo2.T.avg = c(mean(knmi.racmo2$t['2015/2044']), mean(knmi.racmo2$t['2045/2074']),
mean(knmi.racmo2$t['2070/2099']))
smhirca.bcm.T.avg = c(mean(smhirca.bcm$t['2015/2044']), mean(smhirca.bcm$t['2045/2074']),
mean(smhirca.bcm$t['2070/2099']))
dmi.echam.T.avg = c(mean(dmi.echam$t['2015/2044']), mean(dmi.echam$t['2045/2074']),
mean(dmi.echam$t['2070/2099']))
present.foresee.T.avg = mean(present.foresee$t['1985/2014'])

dmi.echam.P.Yearly = apply.yearly(dmi.echam$p,sum)
```

```
remo.echam.P.Yearly = apply.yearly(remo.echam$p,sum)
knmi.racmo2.P.Yearly = apply.yearly(knmi.racmo2$p,sum)
smhirca.bcm.P.Yearly = apply.yearly(smhirca.bcm$p,sum)
present.foresee.P.Yearly = apply.yearly(present.foresee$p, sum)

remo.echam.P.avg = c(mean(remo.echam.P.Yearly$p['2015/2044']),
mean(remo.echam.P.Yearly$p['2045/2074']), mean(remo.echam.P.Yearly$p['2070/2099']))
knmi.racmo2.P.avg = c(mean(knmi.racmo2.P.Yearly$p['2015/2044']),
mean(knmi.racmo2.P.Yearly$p['2045/2074']), mean(knmi.racmo2.P.Yearly$p['2070/2099']))
smhirca.bcm.P.avg = c(mean(smhirca.bcm.P.Yearly$p['2015/2044']),
mean(smhirca.bcm.P.Yearly$p['2045/2074']), mean(smhirca.bcm.P.Yearly$p['2070/2099']))
dmi.echam.P.avg = c(mean(dmi.echam.P.Yearly$p['2015/2044']), mean(dmi.echam.P.Yearly$p['2045/2074']),
mean(dmi.echam.P.Yearly$p['2070/2099']))
present.foresee.P.avg = mean(present.foresee.P.Yearly['1985/2014'])

## SD: temperature
remo.echam.T.SD = c(sd(remo.echam.T.Yearly$t['2015/2044']), sd(remo.echam.T.Yearly $t['2045/2074']),
sd(remo.echam.T.Yearly $t['2070/2099']))
knmi.racmo2.T.SD = c(sd(knmi.racmo2.T.Yearly $t['2015/2044']), sd(knmi.racmo2.T.Yearly $t['2045/2074']),
sd(knmi.racmo2.T.Yearly $t['2070/2099']))
smhirca.bcm.T.SD = c(sd(smhirca.bcm.T.Yearly $t['2015/2044']), sd(smhirca.bcm.T.Yearly $t['2045/2074']),
sd(smhirca.bcm.T.Yearly $t['2070/2099']))
dmi.echam.T.SD = c(sd(dmi.echam.T.Yearly $t['2015/2044']), sd(dmi.echam.T.Yearly $t['2045/2074']),
sd(dmi.echam.T.Yearly $t['2070/2099']))
present.foresee.T.SD = sd(present.foresee.T.Yearly $t['1985/2014'])

## SD: precipitation
remo.echam.P.SD = c(sd(remo.echam.P.Yearly$p['2015/2044']), sd(remo.echam.P.Yearly$p['2045/2074']),
sd(remo.echam.P.Yearly$p['2070/2099']))
knmi.racmo2.P.SD = c(sd(knmi.racmo2.P.Yearly$p['2015/2044']), sd(knmi.racmo2.P.Yearly$p['2045/2074']),
sd(knmi.racmo2.P.Yearly$p['2070/2099']))
smhirca.bcm.P.SD = c(sd(smhirca.bcm.P.Yearly$p['2015/2044']), sd(smhirca.bcm.P.Yearly$p['2045/2074']),
sd(smhirca.bcm.P.Yearly$p['2070/2099']))
dmi.echam.P.SD = c(sd(dmi.echam.P.Yearly$p['2015/2044']), sd(dmi.echam.P.Yearly$p['2045/2074']),
sd(dmi.echam.P.Yearly$p['2070/2099']))
present.foresee.P.SD = sd(present.foresee.P.Yearly['1985/2014'])

## Create monthly means
monthly.T_dmi.echam = apply.monthly(dmi.echam$t,mean)
monthly.P_dmi.echam = apply.monthly(dmi.echam$p,sum)

monthly.T_knmi.racmo2 = apply.monthly(knmi.racmo2$t,mean)
monthly.P_knmi.racmo2 = apply.monthly(knmi.racmo2$p,sum)

monthly.T_remo.echam = apply.monthly(remo.echam$t,mean)
monthly.P_remo.echam = apply.monthly(remo.echam$p,sum)

monthly.T_smhirca.bcm = apply.monthly(smhirca.bcm$t,mean)
monthly.P_smhirca.bcm = apply.monthly(smhirca.bcm$p,sum)

monthly.T_present = apply.monthly(present.foresee$t,mean)
monthly.P_present = apply.monthly(present.foresee$p,sum)

#####################################################
## Figures for temperature and precipitation

## TEMPERATURE

temp.mean.dm <- numeric(4)
temp.mean.sm <- numeric(4)
```

```
temp.mean.knmi <- numeric(4)
temp.mean.remo <- numeric(4)
temp.present.foresee <- numeric(4)

for(tti in 2:length(dat.win.plt)) temp.mean.dm[tti] <- mean(dmi.echam$t[dat.win.plt[tti]],na.rm=T)
for(tti in 2:length(dat.win.plt)) temp.mean.sm[tti] <- mean(smhirca.bcm$t[dat.win.plt[tti]],na.rm=T)
for(tti in 2:length(dat.win.plt)) temp.mean.knmi[tti] <- mean(knmi.racmo2$t[dat.win.plt[tti]],na.rm=T)
for(tti in 2:length(dat.win.plt)) temp.mean.remo[tti] <- mean(remo.echam$t[dat.win.plt[tti]],na.rm=T)
for(tti in 1:length(dat.win.plt)) temp.present.foresee[tti] <- mean(present.foresee$t[dat.win.plt[tti]],na.rm=T)


plot(xts(temp.mean.dm,as.POSIXct(ttpredict.time)),type="p",pch=15,main="", xaxt="n",
ylab=expression(t[mean]*"["*degree*"C]"),ylim=c(10.0,13.5))
axis(1,at=as.POSIXct(c('2005-06-30', '2030-06-15','2060-06-15','2085-06-15')), lab=dat.win.plt)
points(xts(temp.present.foresee,as.POSIXct(ttpredict.time)),pch=15)
points(xts(temp.mean.dm,as.POSIXct(ttpredict.time)),pch=15)
points(xts(temp.mean.sm,as.POSIXct(ttpredict.time)),pch=17,col="darkgreen")
points(xts(temp.mean.remo,as.POSIXct(ttpredict.time)),pch=16,col="darkblue")
points(xts(temp.mean.knmi,as.POSIXct(ttpredict.time)),pch=8,col="red")
lines(xts(temp.mean.allaverages,as.POSIXct(ttpredict.time)),pch=20,col="gold")

legend("topleft", x.intersp =1, y.intersp=0.5, c("remo","smhirca","dm", "knmiracmo2",
"average"),pch=c(16,17,18,15,NA),lwd=c(rep(NA,4),1),col=c("darkblue","darkgreen","black", "red", "gold"),
bg="white")

##  PRECIPITATION

prec.mean.dm <- numeric(4)
prec.mean.sm <- numeric(4)
prec.mean.knmi <- numeric(4)
prec.mean.remo <- numeric(4)
prec.present.foresee <- numeric(4)

for(tti in 2:length(dat.win.plt)) prec.mean.dm[tti] <- mean(dmi.echam.P.Yearly$p[dat.win.plt[tti]],na.rm=T)
for(tti in 2:length(dat.win.plt)) prec.mean.sm[tti] <- mean(smhirca.bcm.P.Yearly$p[dat.win.plt[tti]],na.rm=T)
for(tti in 2:length(dat.win.plt)) prec.mean.knmi[tti] <- mean(knmi.racmo2.P.Yearly$p[dat.win.plt[tti]],na.rm=T)
for(tti in 2:length(dat.win.plt)) prec.mean.remo[tti] <- mean(remo.echam.P.Yearly$p[dat.win.plt[tti]],na.rm=T)
for(tti in 1:length(dat.win.plt)) prec.present.foresee[tti] <-
mean(present.foresee.P.Yearly$p[dat.win.plt[tti]],na.rm=T)

plot(xts(prec.mean.dm,as.POSIXct(ttpredict.time)),type="p",pch=15,main="", xaxt="n",
ylab=expression(p[mean]*"[mm]"),ylim=c(530,760))
axis(1,at=as.POSIXct(c('2005-06-30', '2030-06-15','2060-06-15','2085-06-15')), lab=dat.win.plt)
points(xts(prec.present.foresee,as.POSIXct(ttpredict.time)),pch=15)
points(xts(prec.mean.dm,as.POSIXct(ttpredict.time)),pch=15)
points(xts(prec.mean.sm,as.POSIXct(ttpredict.time)),pch=17,col="darkgreen")
points(xts(prec.mean.remo,as.POSIXct(ttpredict.time)),pch=16,col="darkblue")
points(xts(prec.mean.knmi,as.POSIXct(ttpredict.time)),pch=8,col="red")
lines(xts(prec.mean.allaverages,as.POSIXct(ttpredict.time)),pch=20,col="gold")

legend("topleft", x.intersp =1, y.intersp=0.5, c("remo","smhirca","dm", "knmiracmo2",
"average"),pch=c(16,17,18,15,NA),lwd=c(rep(NA,4),1),col=c("darkblue","darkgreen","black", "red", "gold"),
bg="white")


##############################################################################################
temp.present.monthly <-
tapply(present.foresee$t['1985/2014'],format(index(present.foresee$t['1985/2014']),"%m"),mean, na.rm=TRUE)
```

```
temp.dm.monthly.2015 <-
tapply(dmi.echam$t['2015/2044'],format(index(dmi.echam$t['2015/2044']),"%m"),mean, na.rm=TRUE)
temp.dm.monthly.2045 <-
tapply(dmi.echam$t['2045/2074'],format(index(dmi.echam$t['2045/2074']),"%m"),mean, na.rm=TRUE)
temp.dm.monthly.2070 <-
tapply(dmi.echam$t['2070/2100'],format(index(dmi.echam$t['2070/2100']),"%m"),mean, na.rm=TRUE)

temp.sm.monthly.2015 <-
tapply(smhirca.bcm$t['2015/2044'],format(index(smhirca.bcm$t['2015/2044']),"%m"),mean, na.rm=TRUE)
temp.sm.monthly.2045 <-
tapply(smhirca.bcm$t['2045/2074'],format(index(smhirca.bcm$t['2045/2074']),"%m"),mean, na.rm=TRUE)
temp.sm.monthly.2070 <-
tapply(smhirca.bcm$t['2070/2100'],format(index(smhirca.bcm$t['2070/2100']),"%m"),mean, na.rm=TRUE)

temp.knmi.monthly.2015 <-
tapply(knmi.racmo2$t['2015/2044'],format(index(knmi.racmo2$t['2015/2044']),"%m"),mean, na.rm=TRUE)
temp.knmi.monthly.2045 <-
tapply(knmi.racmo2$t['2045/2074'],format(index(knmi.racmo2$t['2045/2074']),"%m"),mean, na.rm=TRUE)
temp.knmi.monthly.2070 <-
tapply(knmi.racmo2$t['2070/2100'],format(index(knmi.racmo2$t['2070/2100']),"%m"),mean, na.rm=TRUE)

temp.remo.monthly.2015 <-
tapply(remo.echam$t['2015/2044'],format(index(remo.echam$t['2015/2044']),"%m"),mean, na.rm=TRUE)
temp.remo.monthly.2045 <-
tapply(remo.echam$t['2045/2074'],format(index(remo.echam$t['2045/2074']),"%m"),mean, na.rm=TRUE)
temp.remo.monthly.2070 <-
tapply(remo.echam$t['2070/2100'],format(index(remo.echam$t['2070/2100']),"%m"),mean, na.rm=TRUE)

temp.all.monthly.2015 = (temp.remo.monthly.2015 + temp.sm.monthly.2015 + temp.dm.monthly.2015 +
temp.knmi.monthly.2015) / 4
temp.all.monthly.2045 = (temp.remo.monthly.2045 + temp.sm.monthly.2045 + temp.dm.monthly.2045 +
temp.knmi.monthly.2045) / 4
temp.all.monthly.2070 = (temp.remo.monthly.2070 + temp.sm.monthly.2070 + temp.dm.monthly.2070 +
temp.knmi.monthly.2070) / 4

######################

plot(temp.present.monthly, type = "l",ylim = c(0,25) , col="blue", ylab="Seasonal periodicity of temperature
[C])", xlab = "Months")
lines(temp.all.monthly.2015, type = "l", col="green")
lines(temp.all.monthly.2045, type = "l", col="red")
lines(temp.all.monthly.2070, type = "l", col="black")

########################################

prec.present.monthly <-
tapply(monthly.P_present$p['1985/2014'],format(index(monthly.P_present$p['1985/2014']),"%m"),mean,
na.rm=TRUE)

prec.dm.monthly.2015 <-
tapply(monthly.P_dmi.echam$p['2015/2044'],format(index(monthly.P_dmi.echam$p['2015/2044']),"%m"),mean
, na.rm=TRUE)
prec.dm.monthly.2045 <-
tapply(monthly.P_dmi.echam$p['2045/2074'],format(index(monthly.P_dmi.echam$p['2045/2074']),"%m"),mean
, na.rm=TRUE)
prec.dm.monthly.2070 <-
tapply(monthly.P_dmi.echam$p['2070/2100'],format(index(monthly.P_dmi.echam$p['2070/2100']),"%m"),mean
, na.rm=TRUE)
```

```
prec.sm.monthly.2015 <-
tapply(monthly.P_smhirca.bcm$p['2015/2044'],format(index(monthly.P_smhirca.bcm$p['2015/2044']),"%m"),m
ean, na.rm=TRUE)
prec.sm.monthly.2045 <-
tapply(monthly.P_smhirca.bcm$p['2045/2074'],format(index(monthly.P_smhirca.bcm$p['2045/2074']),"%m"),m
ean, na.rm=TRUE)
prec.sm.monthly.2070 <-
tapply(monthly.P_smhirca.bcm$p['2070/2100'],format(index(monthly.P_smhirca.bcm$p['2070/2100']),"%m"),m
ean, na.rm=TRUE)

prec.knmi.monthly.2015 <-
tapply(monthly.P_knmi.racmo2$p['2015/2044'],format(index(monthly.P_knmi.racmo2$p['2015/2044']),"%m"),
mean, na.rm=TRUE)
prec.knmi.monthly.2045 <-
tapply(monthly.P_knmi.racmo2$p['2045/2074'],format(index(monthly.P_knmi.racmo2$p['2045/2074']),"%m"),
mean, na.rm=TRUE)
prec.knmi.monthly.2070 <-
tapply(monthly.P_knmi.racmo2$p['2070/2100'],format(index(monthly.P_knmi.racmo2$p['2070/2100']),"%m"),
mean, na.rm=TRUE)

prec.remo.monthly.2015 <-
tapply(monthly.P_remo.echam$p['2015/2044'],format(index(monthly.P_remo.echam$p['2015/2044']),"%m"),mea
an, na.rm=TRUE)
prec.remo.monthly.2045 <-
tapply(monthly.P_remo.echam$p['2045/2074'],format(index(monthly.P_remo.echam$p['2045/2074']),"%m"),mea
an, na.rm=TRUE)
prec.remo.monthly.2070 <-
tapply(monthly.P_remo.echam$p['2070/2100'],format(index(monthly.P_remo.echam$p['2070/2100']),"%m"),mea
an, na.rm=TRUE)

prec.all.monthly.2015 = (prec.remo.monthly.2015 + prec.sm.monthly.2015 + prec.dm.monthly.2015 +
prec.knmi.monthly.2015) / 4
prec.all.monthly.2045 = (prec.remo.monthly.2045 + prec.sm.monthly.2045 + prec.dm.monthly.2045 +
prec.knmi.monthly.2045) / 4
prec.all.monthly.2070 = (prec.remo.monthly.2070 + prec.sm.monthly.2070 + prec.dm.monthly.2070 +
prec.knmi.monthly.2070) / 4

plot(prec.present.monthly, type = "l",ylim = c(20,80) , col="blue", ylab="Seasonal periodicity of precipitation
[mm])", xlab = "Months")
lines(prec.all.monthly.2015, type = "l", col="green")
lines(prec.all.monthly.2045, type = "l", col="red")
lines(prec.all.monthly.2070, type = "l", col="black")


## Calculate PETH, AETM, SOILM for future

PETHknmi.xts <- PETH.gen(monthly.T_knmi.racmo2)
PET.proj.knmi <- predict.PETH(seg.result, PETHknmi.xts)
Future.knmi <- et.calc(SOIL_MAX=SOIL.MAX,Temp = monthly.T_knmi.racmo2$t,
Prec=monthly.P_knmi.racmo2$p, PET.real=PET.proj.knmi)

PETHdm.xts <- PETH.gen(monthly.T_dmi.echam)
PET.proj.dm <- predict.PETH(seg.result, PETHdm.xts)
Future.dm <- et.calc(SOIL_MAX=SOIL.MAX,Temp = monthly.T_dmi.echam$t,
Prec=monthly.P_dmi.echam$p, PET.real=PET.proj.dm)

PETHsm.xts <- PETH.gen(monthly.T_smhirca.bcm)
PET.proj.sm <- predict.PETH(seg.result, PETHsm.xts)
Future.sm <- et.calc(SOIL_MAX=SOIL.MAX,Temp = monthly.T_smhirca.bcm$t,
Prec=monthly.P_smhirca.bcm$p, PET.real=PET.proj.sm)
```

```
PETHremo.xts <- PETH.gen(monthly.T_remo.echam)
PET.proj.remo <- predict.PETH(seg.result, PETHremo.xts)
Future.remo <- et.calc(SOIL_MAX=SOIL.MAX,Temp = monthly.T_remo.echam$t,
Prec=monthly.P_remo.echam$p, PET.real=PET.proj.remo)

PETHPresent.xts <- PETH.gen(monthly.T_present)
PET.proj.present <- predict.PETH(seg.result, PETHPresent.xts)
Future.Present <- et.calc(SOIL_MAX=SOIL.MAX,Temp = monthly.T_present$t, Prec=monthly.P_present$p,
PET.real=PET.proj.present)

###Create investigation periods & ETM means, SOILM means and min.s for this inv. periods
dat.win <- c('2015/2044','2045/2074','2070/2099')
dat.win.plt <- c('1985/2015', '2015/2045','2045/2075','2070/2100')

et.sum.dm <- numeric(4)
et.sum.dm[1] <- mean(Future.Present$ET_M['1984/2014'])
for(tti in 1:length(dat.win)) {et.sum.dm[tti+1] <- mean(Future.dm$ET_M[dat.win[tti]],na.rm=T)}
ttpredict.time <- c('2000-06-15','2030-06-15','2060-06-15','2085-06-15')
plot(xts(et.sum.dm,as.POSIXct(ttpredict.time)),type="p",pch=18,main="", xaxt="n", ylab="ET_M
[mm/month]")
axis(1,at=as.POSIXct(c('2000-06-15','2030-06-15','2060-06-15','2085-06-15')), lab=dat.win.plt)

soil.sum.dm <- numeric(4)
soil.sum.dm[1] <- mean(Future.Present$SOIL_M['1984/2014'])
for(tti in 1:length(dat.win)) soil.sum.dm[tti+1] <-mean(Future.dm$SOIL_M[dat.win[tti]],na.rm=T)
plot(xts(soil.sum.dm,as.Date(ttpredict.time)),type="p",pch=18,main="", xaxt="n", ylab="SOIL_M
[mm/month]")
axis(1,at=as.POSIXct(c('2000-06-05','2030-06-15','2060-06-15','2085-06-15')), lab=dat.win.plt)

soil.min.dm <- numeric(4)
soil.min.dm[1] <- min(Future.Present$SOIL_M['1984/2014'])
for(tti in 1:length(dat.win)) soil.min.dm[tti+1] <-min(Future.dm$SOIL_M[dat.win[tti]],na.rm=T)
plot(xts(soil.min.dm,as.Date(ttpredict.time)),type="p",pch=18,main="", xaxt="n", ylab="Min. of SOIL_M
[mm/month]")
axis(1,at=as.POSIXct(c('2000-06-15','2030-06-15','2060-06-15','2085-06-15')), lab=dat.win.plt)

et.sum.sm <- numeric(4)
et.sum.sm[1] <- mean(Future.Present$ET_M['1984/2014'])
for(tti in 1:length(dat.win)) et.sum.sm[tti+1] <- mean(Future.sm$ET_M[dat.win[tti]],na.rm=T)
ttpredict.time <- c('2000-06-15','2030-06-15','2060-06-15','2085-06-15')
plot(xts(et.sum.sm,as.POSIXct(ttpredict.time)),type="p",pch=18,main="SMHIRCA models evapotranspiration
prediction", xaxt="n", ylab="ET_M [mm/month]")
axis(1,at=as.POSIXct(c('2000-06-15','2030-06-15','2060-06-15','2085-06-15')), lab=dat.win.plt)

soil.sum.sm <- numeric(4)
soil.sum.sm[1] <- mean(Future.Present$SOIL_M['1984/2014'])
for(tti in 1:length(dat.win)) soil.sum.sm[tti+1] <- mean(Future.sm$SOIL_M[dat.win[tti]],na.rm=T)
plot(xts(soil.sum.sm,as.Date(ttpredict.time)),type="p",pch=18,main="SMHIRCA models soil moisture
prediction", xaxt="n", ylab="SOIL_M [mm/month]")
axis(1,at=as.POSIXct(c('2000-06-15','2030-06-15','2060-06-15','2085-06-15')), lab=dat.win.plt)

soil.min.sm <- numeric(4)
soil.min.sm[1] <- min(Future.Present$SOIL_M['1984/2014'])
for(tti in 1:length(dat.win)) soil.min.sm[tti+1] <-min(Future.sm$SOIL_M[dat.win[tti]],na.rm=T)
plot(xts(soil.min.sm,as.Date(ttpredict.time)),type="p",pch=18,main="", xaxt="n", ylab="Min. of SOIL_M
[mm/month]")
axis(1,at=as.POSIXct(c('2000-06-16','2030-06-15','2060-06-15','2085-06-15')), lab=dat.win.plt)

et.sum.remo <- numeric(4)
```

```
et.sum.remo[1] <- mean(Future.Present$ET_M['1984/2014'])
for(tti in 1:length(dat.win)) et.sum.remo[tti+1] <- mean(Future.remo$ET_M[dat.win[tti]],na.rm=T)
ttpredict.time <- c('2000-06-15','2030-06-15','2060-06-15','2085-06-15')
plot(xts(et.sum.remo,as.POSIXct(ttpredict.time)),type="p",pch=18,main="REMO models evapotranspiration
prediction", xaxt="n", ylab="ET_M [mm/month]")
axis(1,at=as.POSIXct(c('2000-06-15','2030-06-15','2060-06-15','2085-06-15')), lab=dat.win.plt)

soil.sum.remo <- numeric(4)
soil.sum.remo[1] <- mean(Future.Present$SOIL_M['1984/2014'])
for(tti in 1:length(dat.win)) soil.sum.remo[tti+1] <- mean(Future.remo$SOIL_M[dat.win[tti]],na.rm=T)
plot(xts(soil.sum.remo,as.Date(ttpredict.time)),type="p",pch=18,main="Remo models soil moisture prediction",
xaxt="n", ylab="SOIL_M [mm/month]")
axis(1,at=as.POSIXct(c('2000-06-15','2030-06-15','2060-06-15','2085-06-15')), lab=dat.win.plt)

soil.min.remo <- numeric(4)
soil.min.remo[1] <- min(Future.Present$SOIL_M['1984/2014'])
for(tti in 1:length(dat.win)) soil.min.remo[tti+1] <-min(Future.remo$SOIL_M[dat.win[tti]],na.rm=T)
plot(xts(soil.min.remo,as.Date(ttpredict.time)),type="p",pch=18,main="", xaxt="n", ylab="Min. of SOIL_M
[mm/month]")
axis(1,at=as.POSIXct(c('2000-06-15','2030-06-15','2060-06-15','2085-06-15')), lab=dat.win.plt)

et.sum.knmi <- numeric(4)
et.sum.knmi[1] <- mean(Future.Present$ET_M['1984/2014'])
for(tti in 1:length(dat.win)) et.sum.knmi[tti+1] <- mean(Future.knmi$ET_M[dat.win[tti]],na.rm=T)
ttpredict.time <- c('2000-06-05','2030-06-15','2060-06-15','2085-06-15')
plot(xts(et.sum.knmi,as.POSIXct(ttpredict.time)),type="p",pch=18,main="KNMIRACMO2 models
evapotranspiration prediction", xaxt="n", ylab="ET_M [mm/month]")
axis(1,at=as.POSIXct(c('2000-06-15','2030-06-15','2060-06-15','2085-06-15')), lab=dat.win.plt)

soil.sum.knmi <- numeric(4)
soil.sum.knmi[1] <- mean(Future.Present$SOIL_M['1984/2014'])
for(tti in 1:length(dat.win)) soil.sum.knmi[tti+1] <- mean(Future.knmi$SOIL_M[dat.win[tti]],na.rm=T)
plot(xts(soil.sum.knmi,as.Date(ttpredict.time)),type="p",pch=18, main="KNMIRACMO2 models soil moisture
prediction", xaxt="n", ylab="SOIL_M [mm/month]")
axis(1,at=as.POSIXct(c('2000-06-15','2030-06-15','2060-06-15','2085-06-15')), lab=dat.win.plt)

soil.min.knmi <- numeric(4)
soil.min.knmi[1] <- min(Future.Present$SOIL_M['1984/2014'])
for(tti in 1:length(dat.win)) soil.min.knmi[tti+1] <-min(Future.knmi$SOIL_M[dat.win[tti]],na.rm=T)
plot(xts(soil.min.knmi,as.Date(ttpredict.time)),type="p",pch=18,main="", xaxt="n", ylab="Min. of SOIL_M
[mm/month]")
axis(1,at=as.POSIXct(c('2000-06-15','2030-06-15','2060-06-15','2085-06-15')), lab=dat.win.plt)

### Plot the ETM result of RCMs
plot(xts(et.sum.dm,as.POSIXct(ttpredict.time)),type="p",pch=15, cex=1.4 ,main="", xaxt="n", ylab="ET_M
[mm]",ylim=c(40,60))
axis(1,at=as.POSIXct(c('2000-06-15','2030-06-15','2060-06-15','2085-06-15')), lab=dat.win.plt)
points(xts(et.sum.dm,as.POSIXct(ttpredict.time)),pch=15, cex=1.4)
points(xts(et.sum.sm,as.POSIXct(ttpredict.time)),pch=17, cex=1.4, col="darkgreen")
points(xts(et.sum.remo,as.POSIXct(ttpredict.time)),pch=16, cex=1.4, col="darkblue")
points(xts(et.sum.knmi,as.POSIXct(ttpredict.time)),pch=8, cex=1.4, col="red")
et.sum.allavg=(et.sum.dm+et.sum.knmi+et.sum.sm+et.sum.remo)/4
lines(xts(et.sum.allavg,as.POSIXct(ttpredict.time)),pch=19,col="gold")

legend("topleft",c("remo","smhirca","dm",
"knmiracmo2"),pch=c(16,17,15,8),col=c("darkblue","darkgreen","black", "red"), cex=0.8)


###Plot the SOILM result of RCMs
```

```
plot(xts(soil.sum.dm,as.POSIXct(ttpredict.time)),type="p",pch=15, cex=1.4, main="", xaxt="n", ylab="SOIL_M
[mm]",ylim=c(200,450))
axis(1,at=as.POSIXct(c('2000-06-15','2030-06-15','2060-06-15','2085-06-15')), lab=dat.win.plt)
points(xts(soil.sum.dm,as.POSIXct(ttpredict.time)),pch=15, cex=1.4)
points(xts(soil.sum.sm,as.POSIXct(ttpredict.time)),pch=17, cex=1.4, col="darkgreen")
points(xts(soil.sum.remo,as.POSIXct(ttpredict.time)),pch=16, cex=1.4, col="darkblue")
points(xts(soil.sum.knmi,as.POSIXct(ttpredict.time)),pch=8, cex=1.4, col="red")
legend("bottomleft",c("remo","smhirca","dm",
"knmiracmo2"),pch=c(16,17,15,8),col=c("darkblue","darkgreen","black", "red"), cex=0.8)
soil.sum.allavg=(soil.sum.dm+soil.sum.knmi+soil.sum.sm+soil.sum.remo)/4

lines(xts(soil.sum.allavg,as.POSIXct(ttpredict.time)),pch=19,col="gold")


### Plot the SOILM_MIN result of RCMs
plot(xts(soil.min.dm,as.POSIXct(ttpredict.time)),type="p",pch=15, cex=1.4, main="", xaxt="n",
ylab="SOIL_M_MIN [mm]",ylim=c(0,20))
axis(1,at=as.POSIXct(c('2000-06-05','2030-06-15','2060-06-15','2085-06-15')), lab=dat.win.plt)
points(xts(soil.min.dm,as.POSIXct(ttpredict.time)),pch=15, cex=1.4)
points(xts(soil.min.sm,as.POSIXct(ttpredict.time)),pch=17, cex=1.4, col="darkgreen")
points(xts(soil.min.remo,as.POSIXct(ttpredict.time)),pch=16, cex=1.4, col="darkblue")
points(xts(soil.min.knmi,as.POSIXct(ttpredict.time)),pch=8, cex=1.4, col="red")

legend("topleft",c("remo","smhirca","dm",
"knmiracmo2"),pch=c(16,17,15,8),col=c("darkblue","darkgreen","black", "red"), cex=0.6)
soil.min.allavg=(soil.min.dm+soil.min.knmi+soil.min.sm+soil.min.remo)/4
lines(xts(soil.min.allavg,as.POSIXct(ttpredict.time)),pch=19,col="gold")

###Preparation for SOILM_10Percentile calculation
qtl.dm.2070 = quantile(Future.dm$SOIL_M['2070/2099'], c(.10))
qtl.dm.2045 = quantile(Future.dm$SOIL_M['2045/2074'], c(.10))
qtl.dm.2015 = quantile(Future.dm$SOIL_M['2015/2044'], c(.10))

qtl.sm.2015 = quantile(Future.sm$SOIL_M['2015/2044'], c(.10))
qtl.sm.2045 = quantile(Future.sm$SOIL_M['2045/2074'], c(.10))
qtl.sm.2070 = quantile(Future.sm$SOIL_M['2070/2099'], c(.10))

qtl.remo.2015 = quantile(Future.remo$SOIL_M['2015/2044'], c(.10))
qtl.remo.2045 = quantile(Future.remo$SOIL_M['2045/2074'], c(.10))
qtl.remo.2070 = quantile(Future.remo$SOIL_M['2070/2099'], c(.10))

qtl.knmi.2015 = quantile(Future.knmi$SOIL_M['2015/2044'], c(.10))
qtl.knmi.2045 = quantile(Future.knmi$SOIL_M['2045/2074'], c(.10))
qtl.knmi.2070 = quantile(Future.knmi$SOIL_M['2070/2099'], c(.10))

qtl.present.1985 = quantile(Future.Present$SOIL_M['1985/2014'], c(.10))

dm.future.2070 = Future.dm$SOIL_M['2070/2099']
dm.future.2045 = Future.dm$SOIL_M['2045/2074']
dm.future.2015 = Future.dm$SOIL_M['2015/2044']

sm.future.2070 = Future.sm$SOIL_M['2070/2099']
sm.future.2045 = Future.sm$SOIL_M['2045/2074']
sm.future.2015 = Future.sm$SOIL_M['2015/2044']

knmi.future.2070 = Future.knmi$SOIL_M['2070/2099']
knmi.future.2045 = Future.knmi$SOIL_M['2045/2074']
knmi.future.2015 = Future.knmi$SOIL_M['2015/2044']

remo.future.2070 = Future.remo$SOIL_M['2070/2099']
```

```
remo.future.2045 = Future.remo$SOIL_M['2045/2074']
remo.future.2015 = Future.remo$SOIL_M['2015/2044']

present.1985 = Future.Present$SOIL_M['1985/2014']

dm.2070.10Percentile = dm.future.2070[dm.future.2070 < qtl.dm.2070]
dm.2045.10Percentile = dm.future.2045[dm.future.2045 < qtl.dm.2045]
dm.2015.10Percentile = dm.future.2015[dm.future.2015 < qtl.dm.2015]

dm.1980to2100.10Percentile = c(mean(present.1985.10Percentile), mean(dm.2015.10Percentile$SOIL_M,
na.rm=TRUE),mean(dm.2045.10Percentile$SOIL_M, na.rm=TRUE), mean(dm.2070.10Percentile$SOIL_M,
na.rm=TRUE))

sm.2070.10Percentile = sm.future.2070[sm.future.2070 < qtl.sm.2070]
sm.2045.10Percentile = sm.future.2045[sm.future.2045 < qtl.sm.2045]
sm.2015.10Percentile = sm.future.2015[sm.future.2015 < qtl.sm.2015]

sm.1980to2100.10Percentile = c(mean(present.1985.10Percentile), mean(sm.2015.10Percentile$SOIL_M,
na.rm=TRUE),mean(sm.2045.10Percentile$SOIL_M, na.rm=TRUE), mean(sm.2070.10Percentile$SOIL_M,
na.rm=TRUE))

knmi.2070.10Percentile = knmi.future.2070[knmi.future.2070 < qtl.knmi.2070]
knmi.2045.10Percentile = knmi.future.2045[knmi.future.2045 < qtl.knmi.2045]
knmi.2015.10Percentile = knmi.future.2015[knmi.future.2015 < qtl.knmi.2015]

knmi.1980to2100.10Percentile = c(mean(present.1985.10Percentile), mean(knmi.2015.10Percentile$SOIL_M,
na.rm=TRUE),mean(knmi.2045.10Percentile$SOIL_M, na.rm=TRUE),
mean(knmi.2070.10Percentile$SOIL_M, na.rm=TRUE))

remo.2070.10Percentile = remo.future.2070[remo.future.2070 < qtl.remo.2070]
remo.2045.10Percentile = remo.future.2045[remo.future.2045 < qtl.remo.2045]
remo.2015.10Percentile = remo.future.2015[remo.future.2015 < qtl.remo.2015]

remo.1980to2100.10Percentile = c(mean(present.1985.10Percentile), mean(remo.2015.10Percentile$SOIL_M,
na.rm=TRUE),mean(remo.2045.10Percentile$SOIL_M, na.rm=TRUE),
mean(remo.2070.10Percentile$SOIL_M, na.rm=TRUE))

present.1985.10Percentile = present.1985[present.1985 < qtl.present.1985]

###Plot the SOILM_10Percentile result of RCMs
plot(xts(dm.1980to2100.10Percentile,as.POSIXct(ttpredict.time)),type="p",pch=15, cex=1.4, main="", xaxt="n",
ylab="SOIL_M_MIN [mm/month]",ylim=c(0,320))
axis(1,at=as.POSIXct(c('2000-06-05','2030-06-15','2060-06-15','2085-06-15')), lab=dat.win.plt)
points(xts(sm.1980to2100.10Percentile,as.POSIXct(ttpredict.time)),pch=17, cex=1.4, col="darkgreen")
points(xts(remo.1980to2100.10Percentile,as.POSIXct(ttpredict.time)),pch=16, cex=1.4, col="darkblue")
points(xts(knmi.1980to2100.10Percentile,as.POSIXct(ttpredict.time)),pch=8, cex=1.4, col="red")

legend("topleft",c("remo","smhirca","dm",
"knmiracmo2"),pch=c(16,17,15,8),col=c("darkblue","darkgreen","black", "red"), cex=0.8)

all.1980to2100.10Percentile =
(dm.1980to2100.10Percentile+sm.1980to2100.10Percentile+knmi.1980to2100.10Percentile+remo.1980to2100.1
0Percentile)/4

lines(xts(all.1980to2100.10Percentile,as.POSIXct(ttpredict.time)),pch=19,col="gold")

### Standard Deviations of ET_M
sd(Future.Present$ET_M['1985/2015'], na.rm=TRUE)
sd(Future.Present$SOIL_M['1985/2015'], na.rm=TRUE)
```

```
Sd.dm.ETM.21st = c(sd(Future.Present$ET_M['1985/2015'], na.rm=TRUE), sd(Future.dm$ET_M['2015/2045'],
na.rm=TRUE), sd(Future.dm$ET_M['2045/2075'], na.rm=TRUE), sd(Future.dm$ET_M['2070/2100'],
na.rm=TRUE) )

sd(Future.dm$ET_M['2015/2045'], na.rm=TRUE)
sd(Future.dm$ET_M['2045/2075'], na.rm=TRUE)
sd(Future.dm$ET_M['2070/2100'], na.rm=TRUE)

sd(Future.sm$ET_M['2015/2045'], na.rm=TRUE)
sd(Future.sm$ET_M['2045/2075'], na.rm=TRUE)
sd(Future.sm$ET_M['2070/2100'], na.rm=TRUE)

Sd.sm.ETM.21st = c(sd(Future.Present$ET_M['1985/2015'], na.rm=TRUE), sd(Future.sm$ET_M['2015/2045'],
na.rm=TRUE), sd(Future.sm$ET_M['2045/2075'], na.rm=TRUE), sd(Future.sm$ET_M['2070/2100'],
na.rm=TRUE) )

sd(Future.knmi$ET_M['2015/2045'], na.rm=TRUE)
sd(Future.knmi$ET_M['2045/2075'], na.rm=TRUE)
sd(Future.knmi$ET_M['2070/2100'], na.rm=TRUE)

Sd.remo.ETM.21st = c(sd(Future.Present$ET_M['1985/2015'], na.rm=TRUE),
sd(Future.remo$ET_M['2015/2045'], na.rm=TRUE), sd(Future.remo$ET_M['2045/2075'], na.rm=TRUE),
sd(Future.remo$ET_M['2070/2100'], na.rm=TRUE) )

sd(Future.remo$ET_M['2015/2045'], na.rm=TRUE)
sd(Future.remo$ET_M['2045/2075'], na.rm=TRUE)
sd(Future.remo$ET_M['2070/2100'], na.rm=TRUE)

Sd.knmi.ETM.21st = c(sd(Future.Present$ET_M['1985/2015'], na.rm=TRUE),
sd(Future.knmi$ET_M['2015/2045'], na.rm=TRUE), sd(Future.knmi$ET_M['2045/2075'], na.rm=TRUE),
sd(Future.knmi$ET_M['2070/2100'], na.rm=TRUE) )

sd.all.ETM.from1985 = (Sd.knmi.ETM.21st+Sd.remo.ETM.21st+Sd.dm.ETM.21st+Sd.sm.ETM.21st)/4

###Standard Deviations SOIL_M
sd(Future.Present$SOIL_M['1985/2015'], na.rm=TRUE)

Sd.dm.SOILM.21st = c(sd(Future.Present$SOIL_M['1985/2015'], na.rm=TRUE),
sd(Future.dm$SOIL_M['2015/2045'], na.rm=TRUE), sd(Future.dm$SOIL_M['2045/2075'], na.rm=TRUE),
sd(Future.dm$SOIL_M['2070/2100'], na.rm=TRUE) )

sd(Future.dm$SOIL_M['2015/2045'], na.rm=TRUE)
sd(Future.dm$SOIL_M['2045/2075'], na.rm=TRUE)
sd(Future.dm$SOIL_M['2070/2100'], na.rm=TRUE)

sd(Future.sm$SOIL_M['2015/2045'], na.rm=TRUE)
sd(Future.sm$SOIL_M['2045/2075'], na.rm=TRUE)
sd(Future.sm$SOIL_M['2070/2100'], na.rm=TRUE)

Sd.sm.SOILM.21st = c(sd(Future.Present$SOIL_M['1985/2015'], na.rm=TRUE),
sd(Future.sm$SOIL_M['2015/2045'], na.rm=TRUE), sd(Future.sm$SOIL_M['2045/2075'], na.rm=TRUE),
sd(Future.sm$SOIL_M['2070/2100'], na.rm=TRUE) )

sd(Future.knmi$SOIL_M['2015/2045'], na.rm=TRUE)
sd(Future.knmi$SOIL_M['2045/2075'], na.rm=TRUE)
sd(Future.knmi$SOIL_M['2070/2100'], na.rm=TRUE)

Sd.remo.SOILM.21st = c(sd(Future.Present$SOIL_M['1985/2015'], na.rm=TRUE),
sd(Future.remo$SOIL_M['2015/2045'], na.rm=TRUE), sd(Future.remo$SOIL_M['2045/2075'], na.rm=TRUE),
sd(Future.remo$SOIL_M['2070/2100'], na.rm=TRUE) )
```

```
sd(Future.remo$SOIL_M['2015/2045'], na.rm=TRUE)
sd(Future.remo$SOIL_M['2045/2075'], na.rm=TRUE)
sd(Future.remo$SOIL_M['2070/2100'], na.rm=TRUE)

Sd.knmi.SOILM.21st = c(sd(Future.Present$SOIL_M['1985/2015'], na.rm=TRUE),
sd(Future.knmi$SOIL_M['2015/2045'], na.rm=TRUE), sd(Future.knmi$SOIL_M['2045/2075'], na.rm=TRUE),
sd(Future.knmi$SOIL_M['2070/2100'], na.rm=TRUE) )

sd.all.SOILM.from1985 =
(Sd.knmi.SOILM.21st+Sd.remo.SOILM.21st+Sd.dm.SOILM.21st+Sd.sm.SOILM.21st)/4

(sd(remo.2070.10Percentile$SOIL_M) + sd(remo.2045.10Percentile$SOIL_M) +
sd(remo.2015.10Percentile$SOIL_M) + sd(present.1985.10Percentile$SOIL_M)) / 4
(sd(knmi.2070.10Percentile$SOIL_M) + sd(knmi.2045.10Percentile$SOIL_M) +
sd(knmi.2015.10Percentile$SOIL_M) + sd(present.1985.10Percentile$SOIL_M)) / 4
(sd(dm.2070.10Percentile$SOIL_M) + sd(dm.2045.10Percentile$SOIL_M) +
sd(dm.2015.10Percentile$SOIL_M) + sd(present.1985.10Percentile$SOIL_M)) / 4
(sd(sm.2070.10Percentile$SOIL_M) + sd(sm.2045.10Percentile$SOIL_M) +
sd(sm.2015.10Percentile$SOIL_M) + sd(present.1985.10Percentile$SOIL_M)) / 4

(sd(remo.2070.10Percentile$SOIL_M) + sd(sm.2070.10Percentile$SOIL_M) +
sd(dm.2070.10Percentile$SOIL_M) + sd(knmi.2070.10Percentile$SOIL_M))/4
(sd(remo.2045.10Percentile$SOIL_M) + sd(sm.2045.10Percentile$SOIL_M) +
sd(dm.2045.10Percentile$SOIL_M) + sd(knmi.2045.10Percentile$SOIL_M))/4
(sd(remo.2015.10Percentile$SOIL_M) + sd(sm.2015.10Percentile$SOIL_M) +
sd(dm.2015.10Percentile$SOIL_M) + sd(knmi.2015.10Percentile$SOIL_M))/4

###Seasonal Periodicity of ETM and SOILM calculations

###Seasonal Periodicity of ETM
Present.monthly.ET_M_mean <-
tapply(Future.Present$ET_M['1985/2014'],format(index(Future.Present$ET_M['1985/2014']),"%m"),mean,
na.rm=TRUE)
Present.monthly.SOIL_M_mean <-
tapply(Future.Present$SOIL_M['1985/2014'],format(index(Future.Present$SOIL_M['1985/2014']),"%m"),mean,
na.rm=TRUE)

Remo.monthly.ET_M_mean_2015 <-
tapply(Future.remo$ET_M['2015/2044'],format(index(Future.remo$ET_M['2015/2044']),"%m"),mean,
na.rm=TRUE)
Remo.monthly.ET_M_mean_2045 <-
tapply(Future.remo$ET_M['2045/2074'],format(index(Future.remo$ET_M['2045/2074']),"%m"),mean,
na.rm=TRUE)
Remo.monthly.ET_M_mean_2070 <-
tapply(Future.remo$ET_M['2070/2100'],format(index(Future.remo$ET_M['2070/2100']),"%m"),mean,
na.rm=TRUE)

Sm.monthly.ET_M_mean_2015 <-
tapply(Future.sm$ET_M['2015/2044'],format(index(Future.sm$ET_M['2015/2044']),"%m"),mean,
na.rm=TRUE)
Sm.monthly.ET_M_mean_2045 <-
tapply(Future.sm$ET_M['2045/2074'],format(index(Future.sm$ET_M['2045/2074']),"%m"),mean,
na.rm=TRUE)
Sm.monthly.ET_M_mean_2070 <-
tapply(Future.sm$ET_M['2070/2100'],format(index(Future.sm$ET_M['2070/2100']),"%m"),mean,
na.rm=TRUE)
```

```
Dm.monthly.ET_M_mean_2015 <-
tapply(Future.dm$ET_M['2015/2044'],format(index(Future.dm$ET_M['2015/2044']),"%m"),mean,
na.rm=TRUE)
Dm.monthly.ET_M_mean_2045 <-
tapply(Future.dm$ET_M['2045/2074'],format(index(Future.dm$ET_M['2045/2074']),"%m"),mean,
na.rm=TRUE)
Dm.monthly.ET_M_mean_2070 <-
tapply(Future.dm$ET_M['2070/2100'],format(index(Future.dm$ET_M['2070/2100']),"%m"),mean,
na.rm=TRUE)

Knmi.monthly.ET_M_mean_2015 <-
tapply(Future.knmi$ET_M['2015/2044'],format(index(Future.knmi$ET_M['2015/2044']),"%m"),mean,
na.rm=TRUE)
Knmi.monthly.ET_M_mean_2045 <-
tapply(Future.knmi$ET_M['2045/2074'],format(index(Future.knmi$ET_M['2045/2074']),"%m"),mean,
na.rm=TRUE)
Knmi.monthly.ET_M_mean_2070 <-
tapply(Future.knmi$ET_M['2070/2100'],format(index(Future.knmi$ET_M['2070/2100']),"%m"),mean,
na.rm=TRUE)

AllRcm.monthly.ET_M_mean_2015 = (Knmi.monthly.ET_M_mean_2015 + Dm.monthly.ET_M_mean_2015 +
Sm.monthly.ET_M_mean_2015 + Remo.monthly.ET_M_mean_2015)/4
AllRcm.monthly.ET_M_mean_2045 = (Knmi.monthly.ET_M_mean_2045 + Dm.monthly.ET_M_mean_2045 +
Sm.monthly.ET_M_mean_2045 + Remo.monthly.ET_M_mean_2045)/4
AllRcm.monthly.ET_M_mean_2070 = (Knmi.monthly.ET_M_mean_2070 + Dm.monthly.ET_M_mean_2070 +
Sm.monthly.ET_M_mean_2070 + Remo.monthly.ET_M_mean_2070)/4

###Plot the seasonal periodicity of ETM
plot(AllRcm.monthly.ET_M_mean_2070, type="l", ylim=c(10,120), xlab="Months", ylab="Seasonal periodicity
of ET_M [mm]")
lines(AllRcm.monthly.ET_M_mean_2045, col="red")
lines(AllRcm.monthly.ET_M_mean_2015, col="green")
lines(Present.monthly.ET_M_mean, col="blue")
legend("topleft",c("1985/2015","2015/2045","2045/2075",
"2070/2100"),pch=c(16,16,16,16),col=c("blue","green","red", "black"), cex=0.8)

###Seasonal Periodicity of SOILM
Remo.monthly.SOIL_M_mean_2015 <-
tapply(Future.remo$SOIL_M['2015/2044'],format(index(Future.remo$SOIL_M['2015/2044']),"%m"),mean,
na.rm=TRUE)
Remo.monthly.SOIL_M_mean_2045 <-
tapply(Future.remo$SOIL_M['2045/2074'],format(index(Future.remo$SOIL_M['2045/2074']),"%m"),mean,
na.rm=TRUE)
Remo.monthly.SOIL_M_mean_2070 <-
tapply(Future.remo$SOIL_M['2070/2100'],format(index(Future.remo$SOIL_M['2070/2100']),"%m"),mean,
na.rm=TRUE)

Sm.monthly.SOIL_M_mean_2015 <-
tapply(Future.sm$SOIL_M['2015/2044'],format(index(Future.sm$SOIL_M['2015/2044']),"%m"),mean,
na.rm=TRUE)
Sm.monthly.SOIL_M_mean_2045 <-
tapply(Future.sm$SOIL_M['2045/2074'],format(index(Future.sm$SOIL_M['2045/2074']),"%m"),mean,
na.rm=TRUE)
Sm.monthly.SOIL_M_mean_2070 <-
tapply(Future.sm$SOIL_M['2070/2100'],format(index(Future.sm$SOIL_M['2070/2100']),"%m"),mean,
na.rm=TRUE)

Dm.monthly.SOIL_M_mean_2015 <-
tapply(Future.dm$SOIL_M['2015/2044'],format(index(Future.dm$SOIL_M['2015/2044']),"%m"),mean,
na.rm=TRUE)
```

```
Dm.monthly.SOIL_M_mean_2045 <-
tapply(Future.dm$SOIL_M['2045/2074'],format(index(Future.dm$SOIL_M['2045/2074']),"%m"),mean,
na.rm=TRUE)
Dm.monthly.SOIL_M_mean_2070 <-
tapply(Future.dm$SOIL_M['2070/2100'],format(index(Future.dm$SOIL_M['2070/2100']),"%m"),mean,
na.rm=TRUE)

Knmi.monthly.SOIL_M_mean_2015 <-
tapply(Future.knmi$SOIL_M['2015/2044'],format(index(Future.knmi$SOIL_M['2015/2044']),"%m"),mean,
na.rm=TRUE)
Knmi.monthly.SOIL_M_mean_2045 <-
tapply(Future.knmi$SOIL_M['2045/2074'],format(index(Future.knmi$SOIL_M['2045/2074']),"%m"),mean,
na.rm=TRUE)
Knmi.monthly.SOIL_M_mean_2070 <-
tapply(Future.knmi$SOIL_M['2070/2100'],format(index(Future.knmi$SOIL_M['2070/2100']),"%m"),mean,
na.rm=TRUE)

AllRcm.monthly.SOIL_M_mean_2015 = (Knmi.monthly.SOIL_M_mean_2015 +
Dm.monthly.SOIL_M_mean_2015 + Sm.monthly.SOIL_M_mean_2015 +
Remo.monthly.SOIL_M_mean_2015)/4
AllRcm.monthly.SOIL_M_mean_2045 = (Knmi.monthly.SOIL_M_mean_2045 +
Dm.monthly.SOIL_M_mean_2045 + Sm.monthly.SOIL_M_mean_2045 +
Remo.monthly.SOIL_M_mean_2045)/4
AllRcm.monthly.SOIL_M_mean_2070 = (Knmi.monthly.SOIL_M_mean_2070 +
Dm.monthly.SOIL_M_mean_2070 + Sm.monthly.SOIL_M_mean_2070 +
Remo.monthly.SOIL_M_mean_2070)/4

###Plot the seasonal periodicity of SOILM
plot(AllRcm.monthly.SOIL_M_mean_2070, type="l", ylim=c(0,120), xlab="Months", ylab="Seasonal
periodicity of SOIL_M [mm]")
lines(AllRcm.monthly.SOIL_M_mean_2045, col="red")
lines(AllRcm.monthly.SOIL_M_mean_2015, col="green")
lines(Present.monthly.SOIL_M_mean, col="blue")

###Calculation of potential stress
Monthly_PET_SOILM_PRESENT_1985

PET_SOILM_KNMI = PETHknmi.xts$t - Future.knmi$SOIL_M
PET_SOILM_REMO = PETHremo.xts$t - Future.remo$SOIL_M
PET_SOILM_DM = PETHdm.xts$t - Future.dm$SOIL_M
PET_SOILM_SM = PETHsm.xts$t - Future.sm$SOIL_M
PET_SOILM_PRESENT = PETHPresent.xts$t - Future.Present$SOIL_M

Monthly_PET_SOILM_PRESENT_1985 =
tapply(PET_SOILM_PRESENT$t['1985/2014'],format(index(PET_SOILM_PRESENT$t['1985/2014']),"%m"),
mean, na.rm=TRUE)

Monthly_PET_SOILM_KNMI_2015 =
tapply(PET_SOILM_KNMI$t['2015/2044'],format(index(PET_SOILM_KNMI$t['2015/2044']),"%m"),mean,
na.rm=TRUE)
Monthly_PET_SOILM_KNMI_2045 =
tapply(PET_SOILM_KNMI$t['2045/2074'],format(index(PET_SOILM_KNMI$t['2045/2074']),"%m"),mean,
na.rm=TRUE)
Monthly_PET_SOILM_KNMI_2070 =
tapply(PET_SOILM_KNMI$t['2070/2100'],format(index(PET_SOILM_KNMI$t['2070/2100']),"%m"),mean,
na.rm=TRUE)

Monthly_PET_SOILM_REMO_2015 =
tapply(PET_SOILM_REMO$t['2015/2044'],format(index(PET_SOILM_REMO$t['2015/2044']),"%m"),mean,
na.rm=TRUE)
```

```
Monthly_PET_SOILM_REMO_2045 =
tapply(PET_SOILM_REMO$t['2045/2074'],format(index(PET_SOILM_REMO$t['2045/2074']),"%m"),mean,
na.rm=TRUE)
Monthly_PET_SOILM_REMO_2070 =
tapply(PET_SOILM_REMO$t['2070/2100'],format(index(PET_SOILM_REMO$t['2070/2100']),"%m"),mean,
na.rm=TRUE)

Monthly_PET_SOILM_SM_2015 =
tapply(PET_SOILM_SM$t['2015/2044'],format(index(PET_SOILM_SM$t['2015/2044']),"%m"),mean,
na.rm=TRUE)
Monthly_PET_SOILM_SM_2045 =
tapply(PET_SOILM_SM$t['2045/2074'],format(index(PET_SOILM_SM$t['2045/2074']),"%m"),mean,
na.rm=TRUE)
Monthly_PET_SOILM_SM_2070 =
tapply(PET_SOILM_SM$t['2070/2100'],format(index(PET_SOILM_SM$t['2070/2100']),"%m"),mean,
na.rm=TRUE)

Monthly_PET_SOILM_DM_2015 =
tapply(PET_SOILM_DM$t['2015/2044'],format(index(PET_SOILM_DM$t['2015/2044']),"%m"),mean,
na.rm=TRUE)
Monthly_PET_SOILM_DM_2045 =
tapply(PET_SOILM_DM$t['2045/2074'],format(index(PET_SOILM_DM$t['2045/2074']),"%m"),mean,
na.rm=TRUE)
Monthly_PET_SOILM_DM_2070 =
tapply(PET_SOILM_DM$t['2070/2100'],format(index(PET_SOILM_DM$t['2070/2100']),"%m"),mean,
na.rm=TRUE)

Monthly_PET_SOILM_ALLRCM_2015 = (Monthly_PET_SOILM_DM_2015 +
Monthly_PET_SOILM_SM_2015 + Monthly_PET_SOILM_REMO_2015 +
Monthly_PET_SOILM_KNMI_2015) / 4
Monthly_PET_SOILM_ALLRCM_2045 = (Monthly_PET_SOILM_DM_2045 +
Monthly_PET_SOILM_SM_2045 + Monthly_PET_SOILM_REMO_2045 +
Monthly_PET_SOILM_KNMI_2045) / 4
Monthly_PET_SOILM_ALLRCM_2070 = (Monthly_PET_SOILM_DM_2070 +
Monthly_PET_SOILM_SM_2070 + Monthly_PET_SOILM_REMO_2070 +
Monthly_PET_SOILM_KNMI_2070) / 4

###Plot the seasonal periodicity of SOILM with the potential stress

plot(AllRcm.monthly.SOIL_M_mean_2070, type="l", ylim=c(0,150), xlab="Months", ylab="SOIL_M [mm] &
PET-SOIL_M [mm]")
lines(AllRcm.monthly.SOIL_M_mean_2045, col="red")
lines(AllRcm.monthly.SOIL_M_mean_2015, col="green")
lines(Present.monthly.SOIL_M_mean, col="blue")
lines(Monthly_PET_SOILM_ALLRCM_2015, col="green", lty=5) ## test: PET-SOILM monthly tapply
lines(Monthly_PET_SOILM_ALLRCM_2045, col="red", lty=5) ## test: PET-SOILM monthly tapply
lines(Monthly_PET_SOILM_ALLRCM_2070, col="black", lty=5) ## test: PET-SOILM monthly tapply
lines(Monthly_PET_SOILM_PRESENT_1985, col="blue", lty=5)
legend("bottomleft",c("1985/2015","2015/2045","2045/2075",
"2070/2100"),pch=c(16,16,16,16),col=c("blue","green","red", "black"), cex=0.8)
```

Validation

```
rawcalib_Marchfeld = raw.xts['/200812']

PETH.MARCH.xts <- PETH.gen(rawcalib_Marchfeld$t)

forsegment.MARCH.df <- df.segmentit.gen(rawcalib_Marchfeld[,1], PETH.MARCH.xts,
rawcalib_Marchfeld$P)
```

```
## Initial linear regression
lm.fit.MARCH <- lm(CREMAP ~ PETH - 1 , data=forsegment.MARCH.df)
## segmented regression based lm.fit
seg.result.MARCH <- segmented(lm.fit.MARCH, seg.Z= ~PETH, psi=40)

## A graphical test; segmented regression
plot(forsegment.MARCH.df,xlim=c(0,max(forsegment.MARCH.df$PETH)*1.05),ylim=c(0,max(forsegment.M
ARCH.df$CREMAP)*1.05), type="n", xlab="PETH [mm]",ylab="ET CREMAP [mm/month]", xaxs="i",
yaxs="i")
points(forsegment.MARCH.df[forsegment.MARCH.df$PETH < seg.result.MARCH$psi[2],], col="red",
pch=24, bg="red")
points(forsegment.MARCH.df[forsegment.MARCH.df$PETH >= seg.result.MARCH$psi[2],], col="blue",
pch=23, bg="blue")
plot(seg.result.MARCH,add=T, rug=F, lwd=2)
# slope(seg.result)
curve(slope(seg.result.MARCH)$PETH[1,1]*x,from=0,to=seg.result.MARCH$psi[2],add=T, lwd=2)
axis(1,seg.result.MARCH$psi[2], tck=1, lty="dotted", lab=F)
text(seg.result.MARCH$psi[2], 0.5, lab=round(seg.result.MARCH$psi[2],1), srt=90, adj=c(0, -0.3))

PET.proj.MARCH <- predict.PETH(seg.result.MARCH, PETH.MARCH.xts)

SOIL.MAX.MARCH <- optimize(et.test, interval=c(100,10000), temp = rawcalib_Marchfeld$t,
prec=rawcalib_Marchfeld$P, pet.real=PET.proj.MARCH,
cremap=rawcalib_Marchfeld$ET.CREMAP)$minimum

###Calibration
Present.RIPPLEDPeriod = et.calc(SOIL_MAX=SOIL.MAX.MARCH,Temp = raw.xts$t['/200812'],
Prec=raw.xts$P['/200812'], PET.real=PET.proj.MARCH['/200812'])

plot(coredata(raw.xts$ET.CREMAP['/200812']) ~ coredata(Present.RIPPLEDPeriod$ET_M),
pch=18,col="darkgreen", xlab="ET_M", ylab="ET LYSIMETER", xlim = c(0,140), ylim=c(0,160))
Tttmp.lm.RIPPLED <- lm(coredata(raw.xts$ET.CREMAP['/200812']) ~
coredata(Present.RIPPLEDPeriod$ET_M))
Tttmp.sum.RIPPLED <- summary(Tttmp.lm.RIPPLED)
abline(Tttmp.lm.RIPPLED)
legend("topleft",c(paste("ET LYSIMETER =",round(coef(Tttmp.lm.RIPPLED)[2],2) ,"* ET_M
+",round(coef(Tttmp.lm.RIPPLED)[1],2)),paste("R^2 =",round(Tttmp.sum.RIPPLED$r.squared,2))))

### Nash Sutcliffe Coefficient (Calibration test)
1-(sum(LYSCAL_ETMCAL, na.rm = TRUE) / (sum(LYSCAL_LYSCAL_MEAN, na.rm = TRUE)))

##### Run validation ####
rawvalid.MARCH = raw.xts['200901/']

PETHValid.MARCH.xts <- PETH.gen(rawvalid.MARCH$t)  ### LATITUDE-ra figyelni.
PET.proj.Valid.MARCH <- predict.PETH(seg.result.MARCH, PETHValid.MARCH.xts)
Future.Valid.MARCH <- et.calc(SOIL_MAX=SOIL.MAX.MARCH,Temp = rawvalid.MARCH$t,
Prec=rawvalid.MARCH$P, PET.real=PET.proj.Valid.MARCH)

###Plot the result of validation
plot(raw.xts$ET.CREMAP["2009/2011"], ylim=c(0,150))
lines(Future.Valid.MARCH$ET_M, col="green")
lines(raw.xts$ET.CREMAP["2009/2011"], col="green")

### Nash Sutcliffe Coefficient
1-(sum(LYS_ET_M, na.rm = TRUE) / (sum(LYS_LYS_Mean, na.rm = TRUE)))
```

Contents of ET.PROJ package: the functions

```
day.in.month.calc <- function(x) {
   ## The times necessary to endin in 31 days long month
   differences.in.days <- diff(x)
   ## Add the last value and impicitly convert to numeric vector
   c(differences.in.days, 31)
}

 daylength.calc <- function(Latitude = 47.5){
    ## Latitude In degree
    ## Declination is a given value for the month, see Dingman p. 601--602
    Declination <- c(-21.3, -13.3, -2.0, 9.8, 18.9, 23.3, 21.3, 13.7, 3.0, -9.0, -18.6, -23.3)
    ## Convert to radian
    Latitude.rad <- (Latitude/360) * 2 * pi
    Declination.rad <- (Declination/360) * 2*pi
    ## Length of the day,
    ## where omega is the angular velocity
    omega <- 0.2618
    ## doubled because it calculates the sunrise and sufall befor and after noon
    2*acos(-tan(Declination.rad)*tan(Latitude.rad))/omega
 }

df.segmentit.gen <- function(CREMAP, PETH, Prec, as.xts = FALSE){
   require(segmented)
   ## Remove xts and data.frame properties
   if(!as.xts){
      PETH <- as.vector(coredata(PETH))
      CREMAP <- as.vector(coredata(CREMAP))
   }
   Large.CREMAP <- CREMAP > PETH
   Large.Prec <- Prec > PETH
   Available.CREMAP <- !is.na(CREMAP)
   NonLimitedET.idx <- (Large.CREMAP | Large.Prec) & Available.CREMAP
   PETH.nolimit <- PETH[NonLimitedET.idx]
   CREMAP.nolimit <- CREMAP[NonLimitedET.idx]
   data.frame(PETH = PETH.nolimit, CREMAP=CREMAP.nolimit)
}

et.calc <- function(SOIL_MAX, Temp, Prec, PET.real) {
   ## convert xts data to ordinary vector

   ## Make empty data.frame
   TET.df <- data.frame(ET_M = numeric(nrow(Temp)),
                        SOIL_M = numeric(nrow(Temp))
                        )
   ## Set the initial value
   TET.df$SOIL_M[1] <- SOIL_MAX
   ## Set the first value of modelled ET to NA
   TET.df$ET_M[1] <- NA
   for(tti in 2:nrow(Temp)){
      curr.prec <- as.numeric(Prec[tti])
      curr.pet <- as.numeric(PET.real[tti])
      if (curr.prec > curr.pet) {
         TET.df$SOIL_M[tti] <- min(
            c(as.vector(curr.prec - curr.pet + TET.df$SOIL_M[tti-1]),
              SOIL_MAX
              )
         )
         TET.df$ET_M[tti] <- curr.pet
      } else {
```

```
        TET.df$SOIL_M[tti] <- TET.df$SOIL_M[tti-1] *
          exp(-(curr.pet - curr.prec) / SOIL_MAX)
        TET.df$ET_M[tti] <- curr.prec +
          TET.df$SOIL_M[tti-1] -
            TET.df$SOIL_M[tti]
      }
    }
    xts(TET.df, index(Temp))
}

et.test <- function(soil.max, temp, prec, pet.real, cremap) {
      et.pred.prelim <- et.calc(SOIL_MAX = soil.max, Temp = temp, Prec= prec, PET.real=pet.real)
    valid.difference <- na.omit(cremap - et.pred.prelim$ET_M)
    val.diff.sum <- sum(valid.difference^2)
    val.diff.sum +  val.diff.sum/1000 * soil.max^2/1000
}

PETH.gen <- function(Temp, lat = 47.5){
    require(xts)
    ## Temp time series in deg C
    ## Next equation from Hamon_PET_equation.pdf
    SatVaporPress <- 0.6108*exp((17.27*Temp)/(Temp+273.3)) # [kPa]
    Day.length.hour <- daylength.calc(Latitude = lat)
    ## Temp begin in January!
    PETH.daily.average <- 29.8*Day.length.hour*(SatVaporPress/(Temp+273.2)) # [mm/nap]
    days.in.month <- day.in.month.calc(index(Temp))
    PETH.daily.average * days.in.month # [mm/hó]
}

predict.PETH <- function(seg.obj=seg.fit, PETH=PETH.xts){
  require(xts)
  require(segmented)
  PETH.df <- as.data.frame(coredata(PETH))
  names(PETH.df) <- "PETH"
  ## Esetleg az idősorra számolni.
  real <- predict(seg.obj, newdata = PETH.df)
  xts(real,index(PETH))
}
forsegment.df <- df.segmentit.gen(test.meteo.xts[,1], PETH.xts, test.meteo.xts$P)

SOIL.MAX <- optimize(et.test, interval=c(100,10000), temp = test.meteo.xts$t, prec=test.meteo.xts$P,
pet.real=PET.proj, cremap=test.meteo.xts$ET-CREMAP)$minimum

## Visual scanning SOIL.MAX parameter
tempsoilm <- seq(100,1000,50)
tempsoilm.df <- data.frame(soilmax=tempsoilm, RSS=numeric(length(tempsoilm)))
for(tti in 1:nrow(tempsoilm.df)){
  tempsoilm.df[tti,"RSS"] <- et.test(tempsoilm.df[tti,"soilmax"],test.meteo.xts$t, test.meteo.xts$P, PET.proj,
test.meteo.xts$ET.CREMAP)
}
plot(tempsoilm.df, type="p", pch=".", xlab="SOIL_MAX", ylab="RSS")

et.calc(SOIL.MAX,Temp = test.meteo.xts$t, Prec=test.meteo.xts$P, PET.real=PET.proj)
```

REW; SWD; IS calculation

```
rcm.soilm.avg = (Future.knmi['2015/2100','SOIL_M'] + Future.sm['2015/2100','SOIL_M'] +
Future.remo['2015/2100','SOIL_M'] + Future.dm['2015/2100','SOIL_M']) / 4
plot(rcm.soilm.avg, ylim=c(0,250))
axis(2,SOIL.MAX*0.5, lab=F,tck=1,col=2)
```

```
summary(rcm.soilm.avg < SOIL.MAX*0.5)

swd.havi.present = Future.Present[(SOIL.MAX*0.5-Future.Present$SOIL_M) >0,"SOIL_M"]
swd.eves.present = apply.yearly(swd.havi.present,mean)

swd.havi.knmi = Future.knmi[(SOIL.MAX*0.5-Future.knmi$SOIL_M) >0,"SOIL_M"]
plot(swd.havi.knmi,type = "h")

 (SOIL.MAX*0.5-Future.knmi$SOIL_M) >0

swd.eves.knmi=apply.yearly(swd.havi.knmi,mean)
sum(coredata(swd.eves.present['1985/2014']))/SOIL.MAX/30
sum(coredata(swd.eves.knmi['2015/2044']))/SOIL.MAX/30
sum(coredata(swd.eves.knmi['2045/2074']))/SOIL.MAX/30
sum(coredata(swd.eves.knmi['2070/2100']))/SOIL.MAX/30

sum(coredata(swd.havi.knmi['2071']))/SOIL.MAX

swd.havi.dm = Future.dm[(SOIL.MAX*0.5-Future.dm$SOIL_M) >0,"SOIL_M"]
plot(swd.havi.dm,type = "h")
swd.eves.dm=apply.yearly(swd.havi.dm,mean)
sum(coredata(swd.eves.dm['2070/2100']))/SOIL.MAX/30
sum(coredata(swd.eves.dm['2045/2074']))/SOIL.MAX/30
sum(coredata(swd.eves.dm['2015/2044']))/SOIL.MAX/30

swd.havi.sm = Future.sm[(SOIL.MAX*0.5-Future.sm$SOIL_M) >0,"SOIL_M"]
plot(swd.havi.sm,type = "h")
swd.eves.sm=apply.yearly(swd.havi.sm,mean)
sum(coredata(swd.eves.sm['2070/2100']))/SOIL.MAX/30
sum(coredata(swd.eves.sm['2045/2074']))/SOIL.MAX/30
sum(coredata(swd.eves.sm['2015/2044']))/SOIL.MAX/30

swd.havi.remo = Future.remo[(SOIL.MAX*0.5-Future.remo$SOIL_M) >0,"SOIL_M"]
plot(swd.havi.remo,type = "h")
swd.eves.remo=apply.yearly(swd.havi.remo,mean)
sum(coredata(swd.eves.remo['2070/2100']))/SOIL.MAX/30
sum(coredata(swd.eves.remo['2045/2074']))/SOIL.MAX/30
sum(coredata(swd.eves.remo['2015/2044']))/SOIL.MAX/30

summary((SOIL.MAX*0.5-Future.Present$SOIL_M['1985/2014']) >0)
summary((SOIL.MAX*0.5-Future.knmi$SOIL_M['2015/2044']) >0)
summary((SOIL.MAX*0.5-Future.knmi$SOIL_M['2045/2074']) >0)
summary((SOIL.MAX*0.5-Future.knmi$SOIL_M['2070/2100']) >0)
summary((SOIL.MAX*0.5-Future.sm$SOIL_M['2015/2044']) >0)
summary((SOIL.MAX*0.5-Future.sm$SOIL_M['2045/2074']) >0)
summary((SOIL.MAX*0.5-Future.sm$SOIL_M['2070/2100']) >0)
summary((SOIL.MAX*0.5-Future.dm$SOIL_M['2015/2044']) >0)
summary((SOIL.MAX*0.5-Future.dm$SOIL_M['2045/2074']) >0)
summary((SOIL.MAX*0.5-Future.dm$SOIL_M['2070/2100']) >0)
summary((SOIL.MAX*0.5-Future.remo$SOIL_M['2015/2044']) >0)
summary((SOIL.MAX*0.5-Future.remo$SOIL_M['2045/2074']) >0)
summary((SOIL.MAX*0.5-Future.remo$SOIL_M['2070/2100']) >0)

### SWD united
swd.full.all.havi=((SOIL.MAX*0.5-Future.knmi$SOIL_M) + (SOIL.MAX*0.5-Future.sm$SOIL_M) +
(SOIL.MAX*0.5-Future.dm$SOIL_M) + (SOIL.MAX*0.5-Future.remo$SOIL_M))/4
swd.full.all.eves = apply.yearly(swd.full.all.havi, mean)

plot(swd.full.all.havi['2015/2044'])
```

```
plot(swd.full.all.havi['2045/2075'])
plot(swd.full.all.havi['2075/2100'])

plot(swd.full.all.havi)

plot(swd.full.all.eves['2015/2044'])
plot(swd.full.all.eves['2045/2075'])
plot(swd.full.all.eves['2075/2100'])

plot(swd.full.all.eves)

swd.havi.dm = Future.dm[(SOIL.MAX*0.5-Future.dm$SOIL_M) >0,"SOIL_M"]
swd.havi.dm_NOT.stress = Future.dm[(SOIL.MAX*0.5-Future.dm$SOIL_M) <0,"SOIL_M"]

plot(swd.havi.dm)
plot(swd.havi.dm_NOT.stress)

lines(swd.havi.dm_NOT.stress, col="blue")
lines(swd.havi.dm, col="blue")

PresentSWD=SOIL.MAX*0.5-Present$SOIL_M
PresentSWD[PresentSWD >0]

###REW calculation
rew = function(model, soil.max) {
  REW = model/soil.max
  plot(REW)
  #mean.2001= mean(REW['1980/2014'])
  mean.2010= mean(REW['2015/2044'])
  mean.2040= mean(REW['2045/2074'])
  mean.2070= mean(REW['2070/2100'])
  data.frame(mean.2010,mean.2040,mean.2070)
}

axis(at=0.5, side=2, lab=F,tck=1,col=2)
rew(model=Future.remo$SOIL_M,soil.max=SOIL.MAX)

Present$SOIL_M/SOIL.MAX
rewPresent = Present$SOIL_M/SOIL.MAX
plot(rewPresent, ylim=c(0, 1))
```

Annex 5. Annual mean values of temperature and precipitation derived from the regional climate models at the 3 study area from 1985 to 2100 with standard deviations in parentheses

Forested area

In the first investigation period of forested area (1985–2015), the observation-based averaged values (with standard deviations) are 10.5 °C (0.7) and 638 mm (125) for temperature and rainfall, respectively.

Regional climate model's ID	Parameter	2015/2045	2045/2075	2070/2100
1	T [°C]	10.3 (1.0)	11.7 (0.9)	12.6 (0.9)
	P [mm]	726 (135)	714 (101)	777 (142)
2	T [°C]	10.2 (0.9)	11.4 (0.7)	12.4 (0.7)
	P [mm]	720 (126)	775 (99)	770 (119)
3	T [°C]	10.3 (0.8)	11.2 (0.8)	11.9 (0.7)
	P [mm]	645 (127)	683 (140)	664 (124)
4	T [°C]	10.6 (0.7)	11.6 (0.7)	12.6 (0.8)
	P [mm]	555 (113)	603 (132)	609 (117)
Average projection	T [°C]	10.3 (0.8)	11.5 (0.8)	12.4 (0.8)
	P [mm]	661 (125)	694 (118)	705 (125)

Mixed parcel

In the first investigation period of mixed parcel (1985–2015), the observation based averaged values (with standard deviations) are 10.9 °C (0.8) for the temperature and 596 mm (96) for the rainfall.

Regional climate model's ID	Parameter	2015/2045	2045/2075	2070/2100
1	T [°C]	10.7 (1.0)	12.2 (0.9)	13.1 (0.9)
	P [mm]	627 (115)	624 (94)	682 (138)
2	T [°C]	10.7 (0.9)	11.9 (0.6)	12.8 (0.7)
	P [mm]	656 (108)	704 (93)	700 (122)
3	T [°C]	10.8 (0.8)	11.6 (0.9)	12.4 (0.73)

	P [mm]	607 (111)	678 (117)	688 (121)
4	T [°C]	11.1 (0.7)	12.1 (0.8)	13.1 (0.9)
	P [mm]	538 (106)	583 (121)	590 (118)
Average	T [°C]	10.8 (0.8)	11.9 (0.8)	12.8 (0.82)
	P [mm]	607 (110)	647 (106)	665 (125)

Marchfeld

In the first investigation period of Marchfeld (1985–2015), the observation based averaged values (with standard deviations) are 11.1°C (0.76) and 606 mm (98) for temperature and precipitation, respectively.

Regional climate model's ID	Parameter	2015/2045	2045/2075	2070/2100
1	T [°C]	11.0 (0.9)	12.4 (0.9)	13.3 (0.9)
	P [mm]	653 (128)	635 (99)	692 (127)
2	T [°C]	10.9 (0.8)	12.1 (0.6)	13.0 (0.7)
	P [mm]	664 (106)	743 (116)	752 (122)
3	T [°C]	11.1 (0.8)	11.9 (0.9)	12.6 (0.7)
	P [mm]	587 (102)	634 (122)	653 (147)
4	T [°C]	11.3 (0.7)	12.3 (0.7)	13.2 (0.8)
	P [mm]	543 (128)	585 (127)	611 (115)
Average	T [°C]	11.1 (0.8)	12.2 (0.8)	13.0 (0.8)
	P [mm]	612 (116)	649 (117)	677 (128)